Université de Liège
Faculté des Sciences
Département de Mathématique

New Methods for Signal Analysis: Multifractal Formalisms based on Profiles

From Theory to Practice

Dissertation présentée par

Thomas Kleyntssens

en vue de l'obtention du grade de Docteur en Sciences

24 avril 2019

Samuel Nicolay
Université de Liège
Promoteur

Antoine Ayache
Université de Lille

Françoise Bastin
Université de Liège
Secrétaire

Stéphane Jaffard
Université de Paris-Est Créteil
Rapporteur

Jean-Pierre Schneiders
Université de Liège
Président

Herwig Wendt
Université de Toulouse
Rapporteur

“ L’homme n’est pas fait pour travailler, la preuve, c’est que ça le fatigue.”

Georges Courteline

Abstract

Given an irregular signal f, the associated *Hölder exponent* $h_f(x_0)$, characterising the pointwise regularity of f at the point x_0, may change widely from a point to another: the function h_f itself can be irregular and is often hard to compute. It is thus more interesting to estimate the "size" of the set of points which share the same Hölder exponent, i.e. to determine the *Hölder spectrum* of f. In practice, *multifractals formalisms* are used to numerically approximate this spectrum.

In this thesis, we study some multifractal formalisms based on profiles: these are functions allowing to study the histograms of coefficients obtained by the wavelet transform of f. The profile-based formalisms studied here are the *Wavelet Profile Method* (WPM) and the *Leaders Profile Method* (LPM). For the second method, the wavelet coefficients are replaced with the leaders. An advantage of these methods, compared to those that use a Legendre transform on a structure function (as for example the WLM and the MFDFA), lies in the fact that they are able to approximate non-concave spectra.

Let us recall that $h_f(x_0) \leq 1$ is defined as the upper bound of the $h < 1$ such that the quantity

$$||f(x) - f(x_0)||_{L^\infty(B(x_0,2^{-j}))} \tag{1}$$

is upper bounded by $C2^{-hj}$ ($C > 0$ depending on h and x_0). Nothing guarantees that Quantity (1) behaves like $2^{-h_f(x_0)j}$. For example, in the case of the Brownian motion B (which is a monofractal process of exponent $1/2$), the Khintchin law states that, almost surely, Quantity (1) behaves like $2^{-j/2}\sqrt{\log j}$, for almost every $x_0 \in \mathbb{R}$.

In general, the amplitudes of the coefficients obtained by the wavelet transform of a signal f have not necessarily the same asymptotic behaviour as Quantity (1); logarithmic corrections can appear. However, we show here that the Khintchin law is still valid for the asymptotic behaviour of the size of the wavelet leaders of B.

This result also shows the interest of considering a generalisation of the profiles, by replacing the sequences $(2^{-hj})_{j\in\mathbb{N}}$ by an admissible sequence of positive numbers σ. Under some conditions on σ, we show that the spaces $S^{\nu,\sigma^{(\cdot)}}$ associated to these generalised profiles have the same properties as the spaces S^ν and that they are linked to the generalised Besov spaces.

We then present an algorithm implementing these formalisms. We study it in detail on classical examples, such as the fractional Brownian motion, the Lévy process and the Mandelbrot cascades, as well as on processes constructed in this thesis with prescribed pointwise regularity.

Finally, we propose a new method allowing to distinguish between the mono- and the multifractal character of a signal, based on the LPM. It is applied on a practical example: the fractal structure of Mars' topography. The simultaneous use of the LPM and the WLM allows to obtain additional information on the nature of the signals. It is also possible to detect major surface features of Mars in the spatial distribution of the Hölder exponents.

Résumé

Etant donné un signal irrégulier f, l'*exposant de Hölder* associé $h_f(x_0)$, caractérisant la régularité ponctuelle de f en x_0, peut varier d'un point à l'autre : la fonction h_f peut elle-même être irrégulière et est souvent impossible à estimer numériquement. Il est donc préférable de calculer la "taille" des ensembles des points partageant le même exposant, i.e. déterminer le *spectre de Hölder* de f. En pratique, des *formalismes multifractals* sont utilisés pour estimer numériquement ce spectre.

Cette thèse présente des formalismes multifractals basés sur des profils, i.e. des fonctions permettant d'étudier les histogrammes des coefficients relatifs à la transformée en ondelette de f. Ces formalismes sont appelés *Wavelet Profile Method* (WPM) et *Leaders Profile Method* (LPM), selon qu'ils soient basés sur les coefficients d'ondelettes ou les coefficients dominants. Un avantage de ces méthodes, comparées à celles qui utilisent une transformée de Legendre sur une fonction de structure (comme par exemple la WLM et la MFDFA), est de permettre l'approximation des spectres non-concaves.

Rappelons que $h_f(x_0) \leq 1$ est défini comme la borne supérieure des $h < 1$ tels que la quantité

$$||f(x) - f(x_0)||_{L^\infty(B(x_0,2^{-j}))} \tag{2}$$

est majorée par $C2^{-hj}$ ($C > 0$ dépendant de h et x_0). Rien ne garantit cependant que Quantité (2) se comporte comme du $2^{-h_f(x_0)j}$. Par exemple, dans le cas du mouvement Brownien B (processus monofractal d'exposant $1/2$), la loi de Khintchine affirme que, presque sûrement, Quantité (2) se comporte comme du $2^{-j/2}\sqrt{\log j}$, pour presque tout $x_0 \in \mathbb{R}$.

En toute généralité, la taille des coefficients relatifs à la transformée en ondelette d'un signal f n'a pas forcément le même comportement asymptotique que Quantité (2) ; il peut exister une correction logarithmique. Cependant, nous montrons que la loi de Khintchine s'observe à nouveau sur le comportement asymptotique de la taille des coefficients dominants de B.

Ce résultat montre aussi l'intérêt d'une généralisation des profils, en remplaçant la suite $(2^{-hj})_{j\in\mathbb{N}}$ par une suite admissible de nombres strictement positifs σ. Sous certaines conditions sur σ, nous montrons que les espaces $S^{\nu,\sigma^{(\cdot)}}$ associés à ces profils généralisés ont des propriétés similaires à celles des espaces S^ν usuels et qu'ils sont liés aux espaces de Besov généralisés.

Un algorithme permettant de mettre en oeuvre ces formalismes est ensuite présenté. Nous l'étudions en détails sur des exemples classiques, comme le mouvement Brownien fractionnaire, le processus de Lévy et les cascades de Mandelbrot, ainsi que sur des processus construits dans cette thèse où la régularité ponctuelle peut être finement prescrite.

Enfin, nous proposons une nouvelle méthode basée sur la LPM pour faire la distinction entre le caractère mono- et multifractal d'un signal. Elle est appliquée sur un exemple concret : la topographie de la planète Mars. L'utilisation simultanée de la LPM et de la WLM permet d'obtenir des informations supplémentaires sur la nature des signaux. Il est aussi possible de distinguer les principales caractéristiques de la surface de Mars dans la distribution spatiale des exposants de Hölder.

Remerciements

Tout d'abord, je remercie mon promoteur, Samuel Nicolay, de m'avoir lancé dans cette thèse, ainsi que pour son aide précieuse, ses conseils et sa disponibilité durant toutes ces années. Il a été pour moi un excellent chef, collaborateur et ami, qui a toujours su s'adapter aux personnes avec qui il travaille. Je le remercie particulièrement pour son écoute et le soutien qu'il m'a apporté, tant dans le cadre de la thèse, que dans les moments parfois difficiles que j'ai pu traverser, ainsi que pour sa patience et ses conseils pour m'aider à la rédaction des articles et de cette thèse. Je n'oublierais pas non plus l'instauration des "fins de journées" dans les divers bureaux de l'équipe, permettant de se décontracter et de parler de tout. Il a instauré une excellente ambiance de travail dans l'équipe d'analyse. C'est en grande partie grâce à lui que j'ai passé de merveilleuses années dans ce bâtiment.

Autre personne à qui je dois également cette thèse, Céline Esser. Si je ne l'avais pas recroisée à une conférence de philosophie (dont j'ai oublié le nom) en 2011, et qu'elle ne m'avait pas convaincu de reprendre contact avec Samuel, je n'aurais sûrement pas commencé cette thèse. Pour ça, je ne la remercierai jamais assez. Je la remercie également pour sa disponibilité et toute l'aide apportée quand j'avais des questions, ainsi que pour toutes les "pauses 10h". J'ai été ravi que nous ayons pu écrire des articles ensemble, et j'espère que des occasions de collaboration se représenteront.

Je remercie Stéphane Jaffard et Herwig Wendt en qualité de rapporteurs et membres du jury, et pour leurs conseils qui ont permis d'améliorer cette thèse. Je remercie également Stéphane pour les nombreuses discussions qu'on a eu, qui m'ont aidé à avancer dans mes recherches.

Je remercie également Antoine Ayache d'avoir accepté de faire partie du jury et d'avoir pris du temps pour m'aider à trouver une réponse à ma question concernant les coefficients dominants du mouvement Brownien. J'ai été ravi de cette collaboration, qui en plus d'avoir permis d'écrire un article ensemble avec Céline, m'a apporté beaucoup de choses, tant du point de vue mathématique qu'humain. Je le remercie également d'avoir remarqué lors d'un SCAM en janvier 2018 que je n'allais pas bien moralement ; il a pu trouver les mots pour m'aider.

Je remercie Jean-Pierre Schneiders, pour qui j'ai été ravi d'être assistant pendant 6 ans, ainsi que Alain Arneodo et Françoise Bastin d'avoir accepté de faire partie de mon jury, avec une pensée particulière pour Alain.

Je passe à présent aux remerciements à toutes les autres personnes qui sont passées dans l'équipe d'analyse de Samuel durant ma thèse : Adrien Deliège, Laurent Loosveldt, Arman Molla, Laura Reynaerts et Laurent Simons. Ils ont contribué à la bonne ambiance générale de l'équipe. J'ai été ravi d'avoir passer toutes ces années avec eux, dans le cadre de collaborations, de rigolades et de soirées mémorables.

Je voudrais également remercier toute l'équipe des whisteurs (toutes les personnes concernées se reconnaîtront) pour toutes les mémorables parties qui ont eu lieu ces dernières années durant les temps de midi. Et un petit mot pour Loïc : bonjour ! (je suis sur qu'il comprendra ;))

Je remercie également Danielle Bartholoméus pour son aide à remplir la montagne de paperasses liées aux déplacements lors de conférences, ainsi que pour toutes les discussions dans son bureau. Je la remercie également d'avoir toujours remué ciel et terre pour obtenir l'information dont j'avais besoin. Le département sans Danielle, ce n'est plus le département.

Je suis également ravi d'avoir fait ma thèse pendant que Pierre Mathonet était président du département de math. Je le remercie pour son aide financière pour quelques conférences et également pour sa grande capacité d'écoute. Je le remercie aussi de m'avoir "secoué" en première année de bachelier, pour m'inciter à aller plus loin. Un conseil que je continue à me répéter de temps en temps, quand je me repose trop sur mes acquis.

Je remercie également mes parents, qui m'ont toujours soutenu, que ça soit durant mes études ou ma thèse, et surtout d'avoir supporté mon sale caractère pendant toutes ces années.

Je remercie aussi Emilie Clette d'être présente dans ma vie depuis ces 3 dernières années. Même si je ne lui dis pas assez souvent, elle m'a apporté et m'apporte encore beaucoup de bonheur. J'espère que ça va durer encore longtemps et qu'on va continuer à construire notre vie ensemble. Je la remercie également pour la relecture attentive de cette thèse.

Le remerciement qui suit est certainement le plus compliqué de tous. Je souhaite remercier Anthony Corman pour son amitié, son écoute et pour tous les délires qu'on a pu avoir, ainsi que pour toutes les bonnes idées qu'il a eu et qui m'ont permis de me débloquer. J'adorais toutes nos discussions, mathématiques ou autres. Quand tu as décidé de nous quitter définitivement, ça n'a plus jamais été pareil, mais je pense que j'ai compris... La citation de cette thèse vient de lui dans une des cartes postales pour mon anniversaire.

Enfin, je termine en remerciant tous mes amis (Benoît, Damien, Isabelle, Marie, Michel, Renaud, Safia, Sébastien, Sophie et tous les autres), qui ont toujours été là pour moi, dans les bons et mauvais moments. Leur amitié est sans faille. Je vous adore toutes et tous, restez comme vous êtes :)

Contents

Introduction

How to characterise the regularity of a function f on $\mathbb{R}$? There is not a unique answer, but the notions of continuity and differentiability seem to be a first step. It is well-known that differentiability implies continuity, while the reciprocal is not valid: the classical example is the absolute value which is continuous but not differentiable at the origin.

Let us take a more general example: the function $f_h : x \in \mathbb{R} \mapsto |x|^h$ is also continuous but not differentiable at the origin if $h \in (0, 1]$, and f_h is differentiable if $h > 1$. When we look at a representation of the graph of f_h for different values of h (see Figure 1.1), the smaller h is the "less regular" the graph of f_h seems to be around the origin. Knowing only the (non-) continuity and the (non-) differentiability is not sufficient to characterise the regularity of f_h at the origin. The value of h gives an information about this regularity and it seems to be a "transition" between the continuity and the differentiability.

In terms of functional spaces, if we denote by $C^0(x_0)$ (resp. $C^1(x_0)$) the set of continuous (resp. continuously differentiable) functions at x_0, the question is thus: can we define some spaces "between" $C^0(x_0)$ and $C^1(x_0)$? The pointwise Hölder continuity, as introduced more than 130 years ago, allows to obtain a first answer: a function f belongs to the Hölder space $\Lambda^h(x_0)$ ($h \in (0, 1)$) if there exists a constant $C > 0$ such that

$$|f(x) - f(x_0)| \leq C f_h(|x - x_0|) = C|x - x_0|^h, \tag{3}$$

for any x in a neighbourhood of x_0. We can prove that these spaces verify the following property:

$$C^1(x_0) \subset \Lambda^{h_2}(x_0) \subset \Lambda^{h_1}(x_0) \subset C^0(x_0), \quad (0 < h_1 < h_2 < 1).$$

The uniform version Λ^h of the Hölder spaces imposes that Condition (3) holds for any x_0, uniformly in C. It is also possible to define the Hölder spaces for $h \geq 1$, by modifying Condition (3). From the pointwise Hölder spaces embedding, the regularity of f at x_0 can be characterised by the upper bound of $h > 0$ such that $f \in \Lambda^h(x_0)$; this bound is called the *Hölder exponent* of f at x_0 and is denoted by $h_f(x_0)$.

The next question is to know if a function can be "irregular at each point". In the 19th century, mathematicians thought that every continuous function is differentiable except on a set of isolated points [6]. In 1872, the mathematician Karl Weierstraß presented at the Academy of Science in Berlin a family

of functions that are continuous everywhere but nowhere differentiable [134]: these functions are defined as

$$W_{a,b} : x \mapsto \sum_{n=0}^{+\infty} a^n \cos(b^n \pi x),$$

where $a \in (0,1)$, b is any odd integer and $ab > 1 + \frac{3\pi}{2}$. At that time, the scientific community was not ready for this result: the usefulness of such functions was debated and in 1908, even the well-known mathematician Henri Pointcaré qualified these functions of "monsters" and said[1] [117]: "In the past, when a new function was invented, it was with practical perspectives; nowadays, they are invented on purpose to show our ancestors' reasoning is at fault, and we shall never get anything more out of them" .

In 1916, the mathematician Godfrey Harold Hardy extended the result of Weierstraß for any $b > 0$ such that $ab > 1$ and proved that the regularity of the Weierstraß functions is the same at all points [56]; he showed that $h_{W_{a,b}}(x_0) = \frac{-\log a}{\log b}$, for any $x_0 \in \mathbb{R}$.

Another classical example of signal having the same Hölder exponent at each point is, almost surely, a realisation of the *Brownian motion* B, which has been studied during the same period. It is a Gaussian process which was first observed in the random motion of particles suspended in a fluid. Several observations were done in relation with this phenomena, for example by the biologists John Turberville Needham and Jan Ingenhousz in the 18th century, but the discovery is often credited to the biologist Robert Brown in 1827, when he observed pollen grains of the plant Clarkia pulchella suspended in water under a microscope. In 1905, Albert Einstein proposed a physical explanation of this motion [44]. In 1923, Norbert Wiener gave a mathematical construction of B with the help of a probability measure of the space of real continuous functions [137]. In 1933, Paul Lévy presented the necessary and sufficient conditions to obtain a Brownian motion and in 1948, he published the first version of his famous book "Processus stochastiques et mouvement brownien" [93]. Since then, the Brownian motion has been used to model many phenomena (see e.g. [106, 93, 73, 75, 94] and references therein).

Let us recall that, almost surely, B is continuous everywhere and nowhere differentiable; moreover, $h_B(x_0) = 1/2$, for any $x_0 \in \mathbb{R}$ [93]. While $W_{a,b}$ belongs to $\Lambda^{h_{W_{a,b}}(x_0)}(x_0)$ for any $x_0 \in \mathbb{R}$, the Khintchin law [45], established in 1924, implies that B does not belong to $\Lambda^{h_B(x_0)}(x_0)$, for almost every $x_0 \in \mathbb{R}$.

Therefore, the Hölder spaces $\Lambda^h(x_0)$ do not allow to fully characterise the pointwise regularity. For this reason, these spaces have been generalised: the idea is to modify the quantity $f_h(|x - x_0|)$ in Condition (3) by a more general

[1] Originally: "Autrefois, quand on inventait une fonction nouvelle, c'était en vue de quelque but pratique ; aujourd'hui, on les invente tout exprès pour mettre en défaut les raisonnements de nos pères, et on n'en tirera jamais que cela"

expression. There exist two approaches: either to replace the function f_h by a modulus of smoothness [2] w [34], or use admissible sequences of positive numbers[3] σ [84]. The link between these two notions is the following: if w is an modulus of continuity, then $\sigma = (w(2^{-j}))_{j\in\mathbb{N}}$ is an admissible sequence, and if σ is an non-increasing admissible sequence, then there exists a modulus of continuity w such that $\sigma_j = w(2^{-j})$ [82]. In this thesis, we choose the approach using the admissible sequences, which is more natural for the spaces presented in the sequel. The generalised Hölder spaces are denoted by $\Lambda^{\sigma,M}(x_0)$ ($M \in \mathbb{N}$ is a complementary parameter, see Definition 1.6.15). With this notation, the Khintchin law implies that, almost surely, B belongs to $\Lambda^{\sigma,0}(x_0)$ with $\sigma = (2^{-j/2}\sqrt{\log\log 2^j})_{j\in\mathbb{N}}$, for almost every $x_0 \in \mathbb{R}$ [93].

Let us mention that there exist other spaces allowing to study the regularity of functions. For example, the Besov spaces $B^s_{p,q}$, which are a generalisation of the Hölder spaces, have been defined in 1959 by Oleg Vladimirovich Besov [25]. A lot of articles are devoted to their study and their generalisation with the help of modulus of smoothness or admissible sequences ([26, 27, 128, 129, 130, 132, 133, 4, 49] and reference therein). The uniform Hölder spaces have also been generalised with the help of modulus of smoothness in 1996 by Stéphane Jaffard and Yves Meyer [70]. A unified approach is proposed in 2016 by Damien Kreit and Samuel Nicolay by defining generalised uniform Hölder spaces as a particular case of generalised Besov spaces through the use of admissible sequences, to obtain a better understanding of the underlying mechanisms behind such spaces[81].

Now that functional spaces allowing to study the regularity are defined, the next question is to know how this regularity is distributed within the same function. The Weierstraß functions and the Brownian motions have the same Hölder exponent at each point. This kind of function is called a *monofractal function*. If a function has at least two distinct real Hölder exponents, the function is called a *multifractal function*. For such a function, the pointwise regularity may change widely from a point to another: the function h_f can be very irregular and is often impossible to numerically approximate. For this reason, it is more interesting to characterise the "size" of the set of points $E^f(h)$ which share the same Hölder exponent h. Roughly speaking, the information concerning the regularity of a function f is summarised by its *Hölder spectrum*, defined as

$$d_f : [0,+\infty] \mapsto \{-\infty\} \cup [0,n],\ h \mapsto \dim_{\mathcal{H}} E^f(h),$$

where $\dim_{\mathcal{H}}$ is the Hausdorff dimension [48, 47]. This function gives a geometrical idea about the distribution of $E^f(h)$. The Hölder spectrum of a

[2] A non-decreasing function non identically null $w : [0,+\infty) \to [0,+\infty)$ is a *modulus of smoothness*, if $w(0) = 0$ and there exists a constant $C > 0$ such that $w(2t) \leq Cw(t)$ for any $t \geq 0$.

[3] A positive sequence $\sigma = (\sigma_j)_{j\in\mathbb{N}}$ is admissible if σ_{j+1}/σ_j and σ_j/σ_{j+1} are bounded for any $j \in \mathbb{N}$.

multifractal function can have an increasing part and a decreasing part; there also exist concave and non-concave spectra (see Figure 1.2 and Figure 1.3).

The next step is to determine d_f for a given function f. On theoretical examples, it is often possible to deduce the spectrum from a few calculation tricks, but on real-life signals, we need algorithms to numerically approximate the spectrum. These methods are called *multifractal formalisms*.

The first method appeared in physics in the context of turbulence. The mathematician Andreï Kolmogorov introduced in the 1940's a first hypothesis on the linear power-law of the increments of a structure function. While it was false in a general framework, it paved the way for the modern understanding and analysis of turbulent flows. In 1985, Giorgio Parisi and Uriel Frish proposed the first multifractal formalism based on a Legendre transform of a structure function [115]. They used heuristics arguments to show that their methods lead to an approximation of the Hölder spectra. In 1997, Stéphane Jaffard linked this method with the Besov spaces $B^s_{p,q}$ and proved that this method approximates the spectrum of a class of functions[61].

To construct multifractal formalisms, it is necessary to have a tool which is accurate enough to study the pointwise regularity, and which is numerically computable. In this thesis, the notion of *wavelet* is used. To understand where this notion comes from, let us begin with Joseph Fourier. In 1822, he suggested to decompose the function of the propagation of the heat into a weighted sum of a set of simple oscillating functions, namely sines and cosines. This idea gave birth to *Fourier series* and to the basis of the *harmonic analysis*. His technique allows to decompose and reconstruct a signal without loss of information. It also gives a representation in frequency, but loosing the temporal information. In other words, it can detect the presence of different frequencies in the signal, but not the order of appearance of these, which means that it does not allow temporal location of abrupt changes.

In 1946, Dennis Gabor introduced a *time-frequency analysis*, often called the *short-time Fourier transform*, which is optimal in terms of the uncertainty principle[4]. The idea is to use a window function in order to localise the Fourier analysis, then to shift the window to another position [74].

In 1982, Jean Morlet noted several problems with the functions of Gabor: they oscillate too much at high frequencies, which implies a numerical instability in the computation of the coefficients, and too little at low frequencies, which implies that they don't allow a practical reconstruction formula. Morlet has the idea to decompose a function f with the help of coefficients defined as the scalar product of f with some dilatations and discrete translations of a "mother function". The *wavelet transform* was born. In 1984, he worked with Alexander Grossman to obtain some first theoretical results about this

[4]The *Gabor Uncertainty Principle* states that the product of the uncertainties in frequency and time is larger than a fixed constant, and so the accuracy with which one of them can be measured limits the best possible accuracy with which the other can be measured.

transform [53]. In 1986, Pierre Gilles Lemarié and Yves Meyer unified these results and established the first wavelet theory [89]. During the following years, Stéphane Mallat worked on the fast wavelet transform and the multiresolution analysis [97, 96] and Ingrid Daubechies proposed wavelets with compact supports [39]. These progresses allow a fast and efficient numerical computation of the wavelet coefficients of a signal. Let us note that the Daubechies wavelets are used in the standard format of image compression JPEG2000.

The wavelet transform allows a time-frequency analysis. Metaphorically, we can say that the wavelet decomposition is the equivalent of the music sheet of a signal, indicating the musical notes (frequencies) and also when they are played. Yves Meyer says about the wavelets[32][5]: "contrary to what happens for the Fourier series, wavelet coefficients render in a simple, accurate and faithful way the properties of functions, at least the properties that correspond to a discontinuity, an unexpected event".

All the functional spaces cited above can be (quasi-)characterised with the coefficients obtained from the wavelet transform. Moreover, the Hölder exponent is also connected with these coefficients [60, 67]. Consequently, the wavelet transform is a good tool to construct multifractal formalisms.

In 1988, Alain Arneodo et al. suggested a multifractal formalism based on the continuous wavelet transform [9]. Like those of Parisi and Frish, this method cannot approximate the decreasing part of the spectrum. To take care of this problem, Arneodo at al. proposed in 1993 the wavelet transform modulus maxima method (WTMM) [109], using the notion of line of maxima in the wavelet transform. This technique was proved helpful in many practical problems, but its theoretical contribution was limited; in particular, there is no underlying function space. This is why Jaffard replaced the continuous wavelet transform with the discrete one and introduced the *Wavelet Leaders Method* (WLM) [67], based on the oscillation spaces O^s_p, which are a generalisation of the Besov Spaces. When comparing the WTMM with the WLM, numerical results are similar [71].

In these previous methods, the spectrum is obtained with an inverse Legendre transform and so is necessarily concave. To overcome this problem, in 2002, Jaffard introduced a multifractal formalism which is heuristically based on the histogram of the discrete wavelet coefficients [14]. This method relies on the spaces S^ν. If this formalism allows to effectively recover non-concave spectra, the problem met with the first approaches reappears: one cannot access the decreasing part of the spectrum. The idea to solve this issue is to replace the wavelet coefficients in the spaces S^ν with the wavelet leaders. These new spaces are called L^ν and the method related to these spaces can detect non-increasing and non-concave spectra [23, 22].

[5] Originally: "à l'inverse de ce qui sepasse pour les séries de Fourier, les coefficients d'une série d'ondelettes traduisent de façon simple, précise et fidèle les propriétés des fonctions, du moins les propriétés qui correspondent à une discontinuité, un événement imprévu."

The contribution of this thesis on a practical level is directly related to these last methods. We propose an algorithm for these multifractal formalisms based on the spaces S^ν and L^ν. This algorithm is applied and is compared with the WLM on classical examples, as the fractional Brownian motion, the Lévy process and the Mandelbrot cascades, as well as on processes constructed in this thesis with prescribed pointwise regularity. A new method to distinguish the mono- and multifractality of a signal is proposed. This algorithm is used on a practical example: the Mars' topography.

On the theoretical level, the contributions of this thesis can be divided into two parts. First, we propose a new study of the Brownian motion showing that its wavelet leaders allow to get very fine properties concerning its trajectories. Indeed, in general, the amplitudes of the coefficients obtained by the wavelet transform of a signal f have not necessarily the same asymptotic behaviour as $|f(x) - f(x_0)|$: a logarithmic correction can appear [63]. In the case of the Brownian motion, this correction is almost everywhere not present. The suggested approach provides a new way to study fine properties of stochastic processes. We also construct a multifractal process that has a local regularity similar to that of the Brownian motion. The second contribution is a generalisation of the S^ν spaces with the help of the admissible sequences. This generalisation is motivated by the fact that the coefficients related to the wavelet transform of f can describe very precisely the regularity of f. We show that the main properties of the classical S^ν spaces are preserved, and that these new spaces are linked to the generalised Besov spaces.

This thesis is structured as follows. The first chapter presents the mathematical tools and the important notations used throughout the thesis. The useful functional spaces (Besov, Hölder spaces and their generalisation with the help of admissible sequences, as well as the spaces S^ν and L^ν) are defined and their (quasi-)characterisations with the wavelets are presented. The three following multifractal formalisms are presented: the Wavelet Leaders Method (WLM), the Wavelet Profile Method (WPM) and the Leaders Profile Method (LPM).

Chapter 2 studies the Hölderian behaviour of some functions through wavelets. First, the wavelet decomposition is used to construct a function with prescribed Hölder exponents whose wavelet coefficients display a prescribed behaviour. Second, the study of the wavelet leaders of the Brownian motion is given. We prove that the three well-known behaviours of its oscillations (known as ordinary, rapid and slow) are also present in the behaviour of the amplitude of its wavelet leaders. Finally, a multifractal process based on the decomposition of the Brownian motion in the Shauder basis is presented. This is a variant of the multifractional Brownian motion [116, 24].

Chapter 3 presents the spaces $S^{\nu,\sigma^{(\cdot)}}$ which are a generalisation of the S^ν spaces with the help of the admissible sequences. The topological properties holding for the usual S^ν spaces are preserved. The robustness of $S^{\nu,\sigma^{(\cdot)}}$ is also

presented, which implies the independence of the chosen wavelet basis, and finally a link with the generalised Besov spaces is given.

Chapter 4 describes some profile-based multifractal formalisms. A *profile* is a function allowing to study the histograms of coefficients obtained by the wavelet transform of f and which can be related to the spaces S^ν, $S^{\nu,\sigma^{(\cdot)}}$ or L^ν. In particular, an implementation of the WPM and the LPM is presented. These two methods are usually as good as the WLM with monofractal functions and multifractal functions with a concave spectrum. Moreover, these two methods can approximate non-concave spectra, and are generally more robust than the WLM.

Chapter 5 contains numerical applications of the profile-based multifractal formalisms. More precisely, we show the advantages of the LPM compared to the WLM, and the specificities of the LPM are studied to understand some drawbacks of this method. We also answer to the following question: is it possible to detect an admissible sequence appearing in the Hölderian behaviour of a numeric function? To this end, the profile associated to $S^{\nu,\sigma^{(\cdot)}}$ is used.

The last chapter contains a practical application: the study of the fractal structure of Mars' topography with the help of the WLM and the LPM. A complete study at small scales in 1D and 2D is done. We highlight the difficulty of the WLM to distinguish between the mono- and multifractality and a new approach with the LPM is suggested. We also show that the simultaneous use of these two methods allows to obtain additional information on the nature of signals. Finally, we show that it is possible to detect major surface features of Mars in the spatial distribution of the Hölder exponents.

Part I.

Theory

Chapter 1

General Framework: Regularity of Functions

This chapter contains the mathematical tools used throughout this thesis. Some important notions and notations are reviewed. No proof is given; each result is preceded by a reference containing one.

The main notion studied in this chapter is the regularity of functions via the Hölder exponent. The first section precises its general framework. The other sections define the concepts studied throughout the following chapters and give some important results. Functional spaces linked to functions' regularity, namely Besov, Hölder, S^ν and L^ν spaces, are defined, as well as their generalisation with the help of admissible sequences. Their (quasi-)characterisations with the wavelets are also presented. Finally, the three main multifractal formalisms used in this thesis are explained: the Wavelet Leaders Method (WLM), the Wavelet Profile Method (WPM) and the Leaders Profile Method (LPM).

More precisely, this chapter is structured as follows:

1.1 Introduction

It is well-known that the function

$$f_h : x \mapsto |x|^h \quad (h \geq 0)$$

is continuous and if $h \in (0, 1]$, f_h is not differentiable at the origin. Figure 1.1 shows this function for several values of h. The smaller h is the "less regular" the graph of f seems to be around 0. An idea to define the regularity of a function f at a point x_0 consists in comparing f with the function f_h, i.e. to find the "best" h for which there exists a constant $C > 0$ such that

$$|f(x) - f(x_0)| \leq C f_h(x - x_0),$$

for any x in a neighbourhood of x_0. This characterisation is not necessarily relevant if $h > 1$. Indeed, let $f : x \mapsto |x|^{3/2} + x$; the regularity of this function is "similar" to the function $f_{3/2}$ around the origin but f does not satisfy the previous inequality. The constant $f(x_0)$ must be replaced by the polynomial $f(x_0) + f'(x_0)x$. It seems thus natural to replace the constant $f(x_0)$ by a polynomial of degree less than h. We will see in Section 1.6.1 that the case $h \in \mathbb{N}$ is more delicate. For the moment, we only treat the case $h > 0$ and $h \notin \mathbb{N}$.

Definition 1.1.1. Let us set $h > 0$, $h \notin \mathbb{N}$ and let $x_0 \in \mathbb{R}^n$. The *pointwise Hölder space* $\Lambda^h(x_0)$ is the set of locally bounded functions f for which there exist a constant $C > 0$ and a polynomial P_{x_0} of degree less than h such that

$$|f(x) - P_{x_0}(x)| \leq C|x - x_0|^h, \tag{4}$$

for any x in a neighbourhood of x_0. The *uniform Hölder space* Λ^h is the set of functions f such that Condition (4) holds for any $x_0 \in \mathbb{R}^n$ uniformly in C.

A function is said *uniformly Hölder* if $f \in \Lambda^\epsilon$ for some $\epsilon > 0$.

The following proposition gives some basic properties about these spaces.

Proposition 1.1.2.

1. *One has $\Lambda^{h+\epsilon}(x_0) \subset \Lambda^h(x_0)$ and $\Lambda^{h+\epsilon} \subset \Lambda^h$ for any $\epsilon > 0$.*
2. *If $f \in \Lambda^h(x_0)$ for some $h > 0$ then f is continuous at x_0 and, if $h > 1$ then f is differentiable at x_0.*

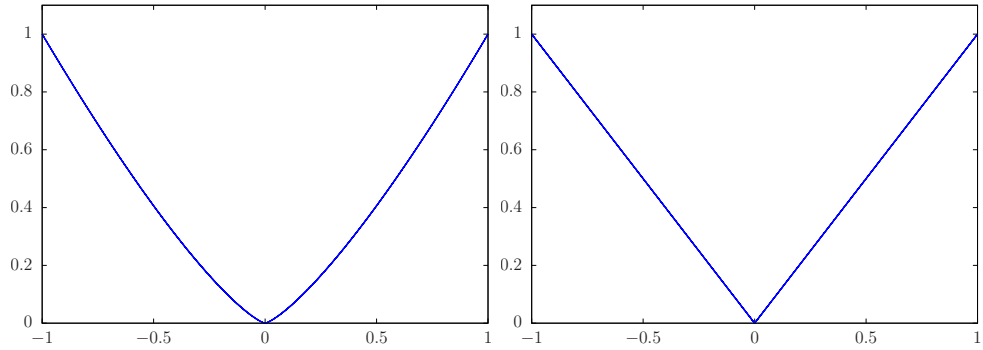

(a) $h = 1.3$ (b) $h = 1$

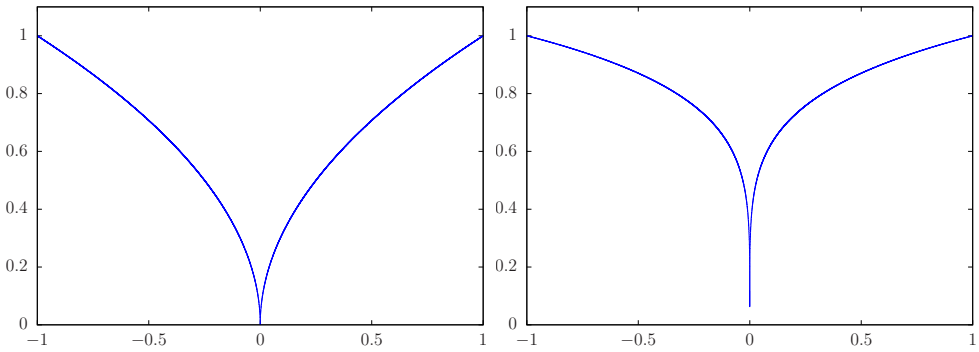

(c) $h = 0.5$ (d) $h = 0.2$

Figure 1.1.: The function $f_h : x \mapsto |x|^h$ around the origin.

3. *If f is differentiable at x_0 then Condition (4) holds for $h = 1$.*

4. *If $f \in \Lambda^{m+\epsilon}(x_0)$ ($m \in \mathbb{N}$ and $\epsilon > 0$) and if f is m-times continuously differentiable in a neighbourhood of x_0 then the polynomial P_{x_0} of Condition (4) is the Taylor polynomial of order m.*

5. *If $f \in \Lambda^{m+\epsilon}$ ($m \in \mathbb{N}$ and $\epsilon > 0$) then f is m-times continuously differentiable.*

Let us note that there exist functions $f \in \Lambda^h(x_0)$ for some $h > 1$ for which f' does not belong to $\Lambda^{h-1}(x_0)$. Take for example the function

$$f : x \in \mathbb{R} \mapsto \begin{cases} |x|^h \sin(x^{-(h+2)}) & \text{if } x \neq 0 \\ 0 & \text{if } x = 0 \end{cases} .$$

This function belongs to $\Lambda^h(0)$ but its derivative is not continuous at the origin.

From the pointwise Hölder spaces embedding, it is natural to consider the following definition.

Definition 1.1.3. The *Hölder exponent* of f at the point x_0 is defined as

$$h_f(x_0) = \sup\{h > 0 : f \in \Lambda^h(x_0)\}.$$

Let us note that this supremum is not necessarily reached. Take for example the function

$$f : x \mapsto \begin{cases} |x|^{1/2} \log |x| & \text{if } x \neq 0 \\ 0 & \text{if } x = 0 \end{cases}.$$

One has directly $f \in \Lambda^h(0)$ for any $h < 1/2$ but $f \notin \Lambda^{1/2}(0)$.

The Hölder exponent $h_f(x_0)$ gives information about the local regularity of f at x_0. The smaller its value, the less regular the function f is around x_0. Moreover, if $h_f(x_0) \in (0, 1)$ then the function is continuous and is not differentiable at the point x_0. For a long time, mathematicians thought that any continuous function is differentiable except on a set of isolated points. The first published example (1872) of a function continuous everywhere and nowhere differentiable is the *Weierstraß function* [134], defined as follow:

$$W_{a,b} : x \mapsto \sum_{n=0}^{+\infty} a^n \cos(b^n \pi x),$$

for $a \in (0, 1)$ and $b > 0$ such that $ab > 1$. Notice that its Hölder exponent is the same at every point. More precisely, we have the following result.

Theorem 1.1.4. *[56] The Weierstraß function $W_{a,b}$ is continuous and nowhere differentiable. Moreover, its Hölder exponent equals $-\log a / \log b$ at every point and $W_{a,b} \in \Lambda^{-\log a/\log b}(x_0)$ for any $x_0 \in \mathbb{R}$.*

For an arbitrary locally bounded function f, the function $x \mapsto h_f(x)$ is not necessarily "simple", as for the Weierstraß function; it can be very erratic and computing h_f can thus be very difficult, if not impossible. Therefore, it is more interesting to characterise the "size" of the set of points $E^f(h)$ which share the same Hölder exponent h. In general, one set $E^f(h)$ has full Lebesgue measure and the others have a vanishing one. Moreover, it appears that the sets $E^f(h)$ are dense in $\mathbb{R}^n$ for the most functions of interest or sample paths of stochastic processes. We thus need of a notion giving a geometrical idea about the distribution of $E^f(h)$.

Definition 1.1.5. The *Hölder spectrum* of a locally bounded function f is defined as

$$d_f : [0, +\infty] \mapsto \{-\infty\} \cup [0, n], \ h \mapsto \dim_{\mathcal{H}} E^f(h),$$

where $\dim_{\mathcal{H}}$ is the Hausdorff dimension[1] and the *iso-Hölder sets* $E^f(h)$ are defined as

$$E^f(h) = \{x \in \mathbb{R}^n : h_f(x) = h\}.$$

[1] This notion is presented in Section 1.2.

If the support of d_f is reduced to one point H, the function f is said *monofractal* of exponent H. If the support of d_f is not reduced to one point, the function f is said *multifractal*.

Figure 1.2 and Figure 1.3 show a few examples of Hölder spectra. In the multifractal case, the Hölder spectrum can have an increasing part and a decreasing part; we also see that there exist concave and non-concave spectra.

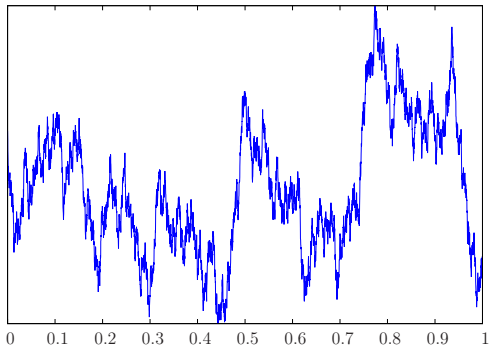

(a) Simulation of a Brownian motion

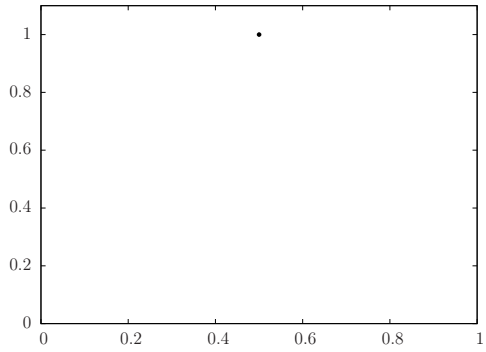

(b) Spectrum of the Brownian motion [73] (monofractal function with an exponent $H = 1/2$)

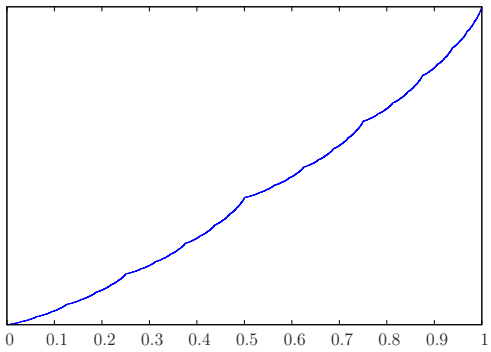

(c) a Binomial cascade

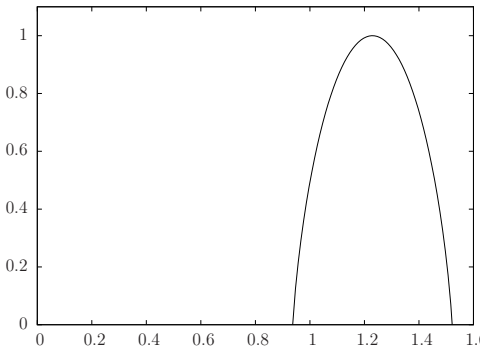

(d) Spectrum of a Binomial cascade [127] (multifractal function with a concave spectrum)

Figure 1.2.: A few examples of signals with their Hölder spectrum (1)

For a real-life signal, to compute the Hölder spectrum directly from its definition is not feasible. For this reason, one uses an indirect way to estimate the spectrum, called *multifractal formalism*. It is a formula, numerically computable, which approximates the spectrum. More precisely, this formula must give an upper bound of the Hölder spectrum for any uniformly Hölder function and it also must give the correct spectrum for some classes of functions. Moreover, a multifractal formalism can also hold for a generic subset of a func-

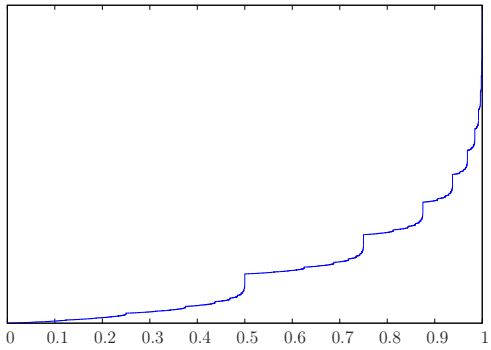

(a) Sum of two binomial cascades

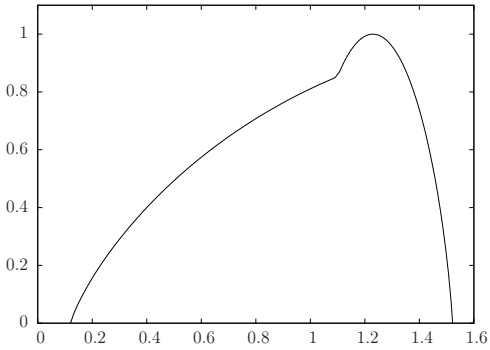

(b) Spectrum of two binomial cascades [78] (multifractal function with a non-concave spectrum)

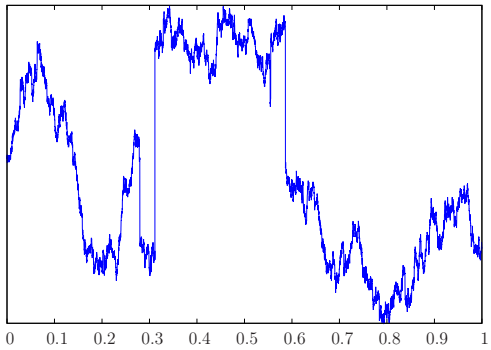

(c) Simulation of a Lévy process with a Brownian part

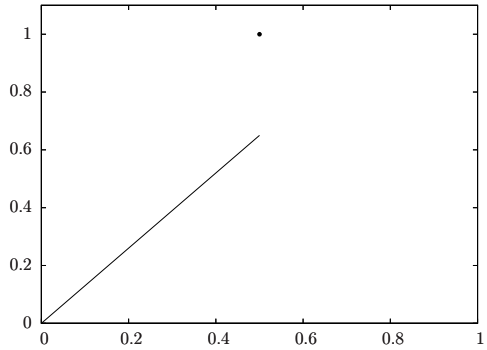

(d) Spectrum of a Lévy process with a Brownian part [64] (multifractal function with a non-concave spectrum without decreasing part)

Figure 1.3.: A few examples of signals with their Hölder spectrum (2)

tion space [67]. The following sections present the tools needed to obtain the multifractal formalisms studied in this thesis.

To finish this section, let us recall some links between multifractal formalisms and functional spaces. The first multifractal formalism was proposed by Parisi and Frish in the context of fully developed turbulence [115]. Later, Arneodo et al. proposed a similar method based on the continuous wavelet transform [9]. These methods are relying on the Besov spaces $B^s_{p,q}$ using the box-counting technique or wavelets [61]. Since the Besov spaces $B^s_{p,q}$ are not defined for negative values of p, the decreasing part of the spectrum cannot be obtained. To take care of this problem, Arneodo at al. proposed the wavelet transform modulus maxima method (WTMM) [109]. However, there is no underlying function space. This is why Jaffard replaced the continuous wavelet

transform with the discrete one and introduced the *Wavelet Leaders Method* (WLM) (see Section 1.7) [67], based on the oscillation spaces O^s_p [68].

However, in these previous methods, the spectrum is obtained with an inverse Legendre transform and so is necessarily concave. To overcome this second problem, Jaffard introduced the spaces S^ν that allow to get a multifractal formalism which is heuristically based on the histogram of (discrete) wavelet coefficients [14]. This formalism is called the *Wavelet Profile Method* (WPM) (see Section 1.8) [78]. If this formalism allows to effectively recover non-concave spectra, the problem met with the first approaches reappears: one cannot access the decreasing part of the spectrum. The idea to take care of this problem is the same that for the WLM: to replace the wavelet coefficients appearing in the spaces S^ν with the wavelet leaders. These news spaces are called the spaces L^ν and allow to construct a multifractal formalism detecting non-increasing and non-concave spectra [22, 23]. This formalism is called the *Leaders Profile Method* (LPM) (see Section 1.9) [46].

1.2 HAUSDORFF DIMENSION

As mentioned in the previous section, the Hausdorff dimension is used to formalise the "size" of the iso-Hölder sets (see Definition 1.1.5). This section presents briefly this notion. For more details, see [48, 47] for example.

In this section, the notation X represents a separable metric space.

Definition 1.2.1. Let $\epsilon, h > 0$. The *Hausdorff outer measure* is defined as

$$\mathcal{H}^h_\epsilon : A \subset X \mapsto \inf\{\sum_{i=1}^{+\infty} \operatorname{diam}^h(A_i) : A \subset \bigcup_{i=1}^{+\infty} A_i,\ \operatorname{diam}(A_i) \leq \epsilon\},$$

where $\operatorname{diam}(B)$ is the diameter of the set B.

Since $\mathcal{H}^h_\epsilon$ is a decreasing function with respect to ϵ, one can define the application

$$\mathcal{H}^h : A \subset X \mapsto \sup_{\epsilon>0} \mathcal{H}^h_\epsilon(A) = \lim_{\epsilon \to 0^+} \mathcal{H}^h_\epsilon(A).$$

This application is an outer measure and its restriction to the $\mathcal{H}^h$-measurable sets is called the *h-dimensional Hausdorff measure.*

By definition, the h-dimensional Hausdorff measure is invariant by translation. In the case $X = \mathbb{R}^n$, the following proposition gives the link between the measure $\mathcal{H}^n$ and the n-dimensional Lebesgue measure $\mathcal{L}^n$.

Proposition 1.2.2. *For any measurable set $A \subset \mathbb{R}^n$, one has*

$$\mathcal{L}^n(A) = c_n \mathcal{H}^n(A), \quad \textit{where} \quad c_n = \frac{\pi^{n/2}}{2^n \Gamma(n/2+1)}.$$

Let us notice that for any $\epsilon > 0$ and any $0 < h_1 < h_2$, one has

$$\mathcal{H}^{h_1}_{\epsilon}(A) \geq \frac{\mathcal{H}^{h_2}_{\epsilon}(A)}{\epsilon^{h_2-h_1}}.$$

One thus obtains the important following proposition.

Proposition 1.2.3. *Let $0 < h_1 < h_2$.*

- *If $\mathcal{H}^{h_1}(A) < +\infty$, then $\mathcal{H}^{h_2}(A) = 0$.*
- *If $\mathcal{H}^{h_1}(A) > 0$, then $\mathcal{H}^{h_2}(A) = +\infty$.*

There thus exists a critical value h_c for which the function $h \mapsto \mathcal{H}^h(A)$ is equal to $+\infty$ for any $h < h_c$ and is equal to 0 for any $h > h_c$. This critical value is called the Hausdorff dimension of A.

Definition 1.2.4. The *Hausdorff dimension* of a set A is defined as

$$\dim_{\mathcal{H}}(A) = \sup\{h > 0 : \mathcal{H}^h(A) = +\infty\}.$$

To conclude this section, let us give some properties of the Hausdorff dimension.

Proposition 1.2.5.

- *If $A \subseteq B$ then $\dim_{\mathcal{H}}(A) \leq \dim_{\mathcal{H}}(B)$.*
- *If A is a countable set, then $\dim_{\mathcal{H}}(A) = 0$.*
- *We have*
$$\dim_{\mathcal{H}}\left(\bigcup_{i\in\mathbb{N}} A_i\right) = \sup_{i\in\mathbb{N}} \dim_{\mathcal{H}}(A_i).$$
- *For $X = \mathbb{R}^n$, we have $\dim_{\mathcal{H}}(A) \leq n$ for any $A \subset \mathbb{R}^n$ and if $\mathcal{L}^n(A) > 0$, then $\dim_{\mathcal{H}}(A) = n$.*

1.3 Admissible Sequences

This section presents the admissible sequences [107]. These sequences are "small modifications" of the sequences $(2^{-hj})_{j\in\mathbb{N}}$. They will allow a finer study of the regularity of functions and a generalisation of some function spaces, such as the Besov spaces (see Section 1.6) and the spaces S^ν (see Chapter 3).

Let us begin with some definitions and notations.

Definition 1.3.1. A sequence $\sigma = (\sigma_j)_{j\in\mathbb{N}}$ of strictly positive real numbers is called *admissible* if there exists a constant $C > 0$ such that

$$C^{-1}\sigma_j \leq \sigma_{j+1} \leq C\sigma_j, \tag{5}$$

for any $j \in \mathbb{N}$.

For example, for any $h \in \mathbb{R}$, the following sequences are admissible:

$$(2^{-hj})_{j\in\mathbb{N}},\ (2^{-hj}j)_{j\in\mathbb{N}},\ (2^{-hj}\sqrt{j})_{j\in\mathbb{N}},\ (2^{-hj}\sqrt{\log j})_{j\in\mathbb{N}}.$$

By contrast, the sequence $(2^{2^j})_{j\in\mathbb{N}}$ is not an admissible sequence. This shows that Condition (5) limits the speed of convergence.

Let us set

$$\underline{\sigma}_j = \inf_{k\in\mathbb{N}} \frac{\sigma_{j+k}}{\sigma_k} \quad \text{and} \quad \overline{\sigma}_j = \sup_{k\in\mathbb{N}} \frac{\sigma_{j+k}}{\sigma_k},$$

for any $j \in \mathbb{N}$. The sequence $(\log_2 \underline{\sigma}_j)_{j\in\mathbb{N}}$ is subadditive and the sequence $(\log_2 \overline{\sigma}_j)_{j\in\mathbb{N}}$ is superadditive. We thus can define the *lower* and *upper Boyd indices* as follows:

$$\underline{s}(\sigma) = \lim_{j\to+\infty} \frac{\log \underline{\sigma}_j}{\log 2^j} \quad \text{and} \quad \overline{s}(\sigma) = \lim_{j\to+\infty} \frac{\log \overline{\sigma}_j}{\log 2^j}.$$

Let us give some properties about these notions.

Proposition 1.3.2. *Let σ be an admissible sequence. We have the following properties:*

- *if $\underline{s}(\sigma) > 0$, then $\sigma_j \to +\infty$ as $j \to +\infty$,*
- *if $\underline{s}(\sigma) < 0$, then $\sigma_j \to 0$ as $j \to +\infty$,*
- *for any $\epsilon > 0$, there exists a positive constant D such that*

$$D^{-1}2^{j(\underline{s}(\sigma)-\epsilon)} \leq \frac{\sigma_{j+k}}{\sigma_k} \leq D2^{j(\overline{s}(\sigma)+\epsilon)},$$

for any $j, k \in \mathbb{N}$.

The following lemma shows how to obtain new admissible sequences from other admissible sequences.

Lemma 1.3.3. *Let σ and γ be two admissible sequences. We have the following properties:*

- *the sequence $\sigma + \gamma$ is admissible,*
- *the sequence $\sigma\gamma$ is admissible and one has*

$$\underline{s}(\sigma\gamma) \geq \underline{s}(\sigma) + \underline{s}(\gamma) \quad \text{and} \quad \overline{s}(\sigma\gamma) \leq \overline{s}(\sigma) + \overline{s}(\gamma),$$

- *for any strictly positive real number r, the sequence $r\sigma$ is admissible and one has $\underline{s}(r\sigma) = \underline{s}(\sigma)$ and $\overline{s}(r\sigma) = \overline{s}(\sigma)$,*
- *the sequence σ^α is admissible ($\alpha \in \mathbb{R}$) and if $\alpha \geq 0$, one has*

$$\underline{s}(\sigma^\alpha) = \alpha\underline{s}(\sigma) \quad \text{and} \quad \overline{s}(\sigma^\alpha) = \alpha\overline{s}(\sigma),$$

and if $\alpha \leq 0$, one has

$$\underline{s}(\sigma^\alpha) = \alpha\overline{s}(\sigma) \quad \text{and} \quad \overline{s}(\sigma^\alpha) = \alpha\underline{s}(\sigma).$$

1.4 Some Notations about the Spaces $L^p(X, \mathcal{A}, \mu)$

This section fixes some classical notations about the spaces $L^p(X, \mathcal{A}, \mu)$, where $(X, \mathcal{A}, \mu)$ is a measured space with μ a σ-finite measure. For more details about the $L^p(X, \mathcal{A}, \mu)$ spaces, see [30, 120] for example.

Definition 1.4.1. Let $p > 0$ or $p = +\infty$, and let f be a complex function defines on X. If $p \neq +\infty$, we set

$$||f||_{L^p(X,\mathcal{A},\mu)} := \left(\int_X |f|^p \, d\mu \right)^{1/p},$$

and if $p = +\infty$, we set

$$||f||_{L^\infty(X,\mathcal{A},\mu)} := \inf\{C \geq 0 : |f| \leq C \ \mu\text{-almost everywhere}\}.$$

Since $f = g$ μ-almost everywhere implies $||f||_{L^p(X,\mathcal{A},\mu)} = ||g||_{L^p(X,\mathcal{A},\mu)}$, the space $L^p(X, \mathcal{A}, \mu)$ is defined as the quotient of the set of functions f for which $||f||_{L^p(X,\mathcal{A},\mu)}$ is finite, by the relation $\sim$ defined as

$$f \sim g \quad \text{ if and only if } \quad f = g \ \mu\text{-almost everywhere.}$$

We have the following proposition.

Proposition 1.4.2.

- *If $1 \leq p \leq +\infty$, then $(L^p(X, \mathcal{A}, \mu), ||.||_{L^p(X,\mathcal{A},\mu)})$ is a Banach space.*
- *If $0 < p < 1$, then $(L^p(X, \mathcal{A}, \mu), d_{L^p(X,\mathcal{A},\mu)})$ is a quasi-Banach space, where*

$$d_{L^p(X,\mathcal{A},\mu)} : L^p(X, \mathcal{A}, \mu) \times L^p(X, \mathcal{A}, \mu) \mapsto [0, +\infty), \ ([f]_\sim, [g]_\sim) \mapsto ||f-g||_p^p.$$

To simplify the notations, a function f is assimilated to its equivalence class $[f]_\sim$. We thus write $f \in L^p(X, \mathcal{A}, \mu)$. Let us distinguish two important cases.

1. If $X \subseteq \mathbb{R}^n$ and $\mathcal{A}$ is the Borel σ-algebra, then the space $L^p(X, \mathcal{A}, \mathcal{L}^n)$ is denoted by $L^p(X)$. If $X = \mathbb{R}^n$, the notation L^p is used.
2. If μ is the counting measure on $\mathbb{N}$, then the sequences space $L^p(\mathbb{N}, \mathcal{P}(\mathbb{N}), \mu)$ is denoted by l^p.

When there is no possible confusion, the application $||.||_{L^p(X,\mathcal{A},\mu)}$ is noted $||\cdot||_p$ and the application $d_{L^p(X,\mathcal{A},\mu)}$ is noted $d_p(\cdot, \cdot)$.

1.5 WAVELETS

The notion of wavelet allows to study the multifractal properties of functions. For example, the Hölder exponent of a function f can be computed directly from the wavelet coefficients of f. Moreover, they allow to have some numerically computable formula to approximate the Hölder spectrum (see Section 1.7). The first orthonormal wavelet basis is due to Haar in 1910 [55]. Lemarié and Meyer showed the existence of wavelet in the Schwartz class in 1986 [89]. A classical way to construct wavelets is based on a multiresolution analysis. This approach was created by Mallat [98] and Meyer [104]. Daubechies used this method to construct compactly supported wavelets with an arbitrary number of vanishing moment [39]. For more details, see [39, 98, 105, 104] for example. From now on, the *inner product of* L^2 is noted by

$$\langle f, g\rangle := \int_{\mathbb{R}^n} f(x)\overline{g(x)}\, dx.$$

This section presents the wavelets and their construction with the help of a multiresolution analysis. The link with the Hölder exponent is also presented.

Definition 1.5.1. Let $(\psi^{(i)})_{1\leq i<2^n}$ be 2^n-1 functions of L^2. For any $1 \leq i < 2^n$, $j \in \mathbb{Z}$ and $k \in \mathbb{Z}^n$, the function $\psi^{(i)}_{j,k}$ is defined as

$$\psi^{(i)}_{j,k} : x \in \mathbb{R}^n \mapsto \psi^{(i)}(2^j x - k).$$

The functions $(\psi^{(i)})_{1\leq i<2^n}$ are called *(mother) wavelets* of the L^2 space if the set

$$\{2^{jn/2}\psi^{(i)}_{j,k} : 1 \leq i < 2^n, j \in \mathbb{Z}, k \in \mathbb{Z}^n\}$$

form an orthonormal basis of L^2.

In other words, we have a basis of L^2 formed of translation and dilation of functions $\psi^{(i)}$. Therefore, any function $f \in L^2$ can be decomposed as

$$f(x) = \sum_{j\in\mathbb{Z}}\sum_{k\in\mathbb{Z}}\sum_{i=1}^{2^n-1} c^{(i)}_{j,k}\psi^{(i)}_{j,k}(x) \quad \text{where} \quad c^{(i)}_{j,k} = 2^{nj}\langle f, \psi^{(i)}_{j,k}\rangle. \tag{6}$$

The values $c^{(i)}_{j,k}$ are called the *wavelet coefficients* of f. The index j is called the *scale* and the index k represents the *position*. Moreover, the index i can be seen as the *direction* to a vector of origin 0 and of end a vertex of the unit cube $[0, 1)^n$; there are thus $2^n - 1$ possible directions. Let us notice that the L^2 normalisation is not chosen, but rather the L^∞ normalisation, which will be more appropriate to the study of the regularity of a function.

1.5.1 Multiresolution Analysis: Generalities

Let us now present how to construct wavelets with the help of a multiresolution analysis. For more details, see [97, 96, 39].

Definition 1.5.2. A *multiresolution analysis* of L^2 is a sequence of closed vector subspaces $(V_j)_{j\in\mathbb{Z}}$ of L^2 satisfying the following properties:

- one has $V_j \subset V_{j+1}$ for any $j \in \mathbb{Z}$,
- one has
$$\bigcap_{j\in\mathbb{Z}} V_j = \{0\} \quad \text{and} \quad \overline{\bigcap_{j\in\mathbb{Z}} V_j} = L^2,$$
- for any $j \in \mathbb{Z}$, the function f belongs to V_j if and only if the function $f(2\cdot)$ belongs to V_{j+1},
- the function f belongs to V_0 if and only if $f(\cdot - k)$ belongs to V_0 for any $k \in \mathbb{Z}^n$,
- there exists a function $\phi \in V_0$ such that the functions $(\phi(\cdot - k))_{k\in\mathbb{Z}^n}$ form an orthonormal basis of V_0.

The function ϕ is called a *scaling function* (or a *father wavelet*).

For any $j \in \mathbb{Z}$ and $k \in \mathbb{Z}^n$, the function $\phi_{j,k}$ is defined as

$$\phi_{j,k} : x \in \mathbb{R}^n \mapsto \phi(2^j x - k).$$

We directly have that the set $\{2^{jn/2}\phi_{j,k} : k \in \mathbb{Z}^n\}$ form a orthonormal basis of V_j. Moreover, if P_j is the projection operator on V_j defined as

$$P_j : L^2 \to V_j,\ f \mapsto \sum_{k\in\mathbb{Z}} a_{j,k}\phi_{j,k}, \quad \text{where} \quad a_{j,k} = 2^{nj}\langle f, \phi_{j,k}\rangle,$$

then we have

$$\lim_{j\to+\infty} P_j(f) = f \quad \text{and} \quad \lim_{j\to-\infty} P_j(f) = 0.$$

The function $P_j(f)$ can be considered as an approximation of the function f. The sequence $(a_{j,k})_{k\in\mathbb{Z}^n}$ is thus called the *approximation coefficients* of f at scale j.

Moreover, since the function ϕ belongs to $V_0 \subset V_1$, we have

$$\phi = 2\sum_{k\in\mathbb{Z}^n} h_k\phi_{1,k} \quad \text{where} \quad h_k = \langle\phi, \phi_{1,k}\rangle.$$

The sequence $h = (h_k)_{k\in\mathbb{Z}}$ is called the *filter*[2] of the multiresolution analysis $(V_j)_{j\in\mathbb{Z}}$ associated to the function ϕ. We will see below that h allows to construct wavelets and to compute the wavelet coefficients of a function $f \in L^2$. Let us first introduce the spaces W_j.

Definition 1.5.3. The space W_j is defined as the orthogonal complement of V_j in V_{j+1}. One thus has

$$V_{j+1} = V_j \oplus W_j.$$

The next theorem gives some properties about these spaces.

Theorem 1.5.4.

- *For any $j \in \mathbb{Z}$, one has $f \in W_j$ if and only if $f(2\cdot) \in W_{j+1}$.*
- *One has*

$$L^2 = \overline{\bigoplus_{j\in\mathbb{Z}} W_j} = \overline{V_0 \oplus \bigoplus_{j\geq 0} W_j}.$$

We still have to find a basis of the spaces W_j. In Section 1.5.2, we construct a basis in the case $L^2(\mathbb{R})$, which allows to build one in the general case $L^2(\mathbb{R}^n)$ with the help of the tensor product in Section 1.5.3.

1.5.2 Multiresolution Analysis: The Case of $L^2(\mathbb{R})$

This section presents the case of $L^2(\mathbb{R})$. For more details, see [97, 96, 39]. The following theorem defines a wavelet of $L^2(\mathbb{R})$ from a multiresolution analysis $(V_j)_{j\in\mathbb{Z}}$ of $L^2(\mathbb{R})$.

Theorem 1.5.5. *Let $(V_j)_{j\in\mathbb{Z}}$ be a multiresolution analysis of $L^2(\mathbb{R})$ and $(h_k)_{k\in\mathbb{Z}}$ the filter of $(V_j)_{j\in\mathbb{Z}}$ associated to ϕ. A wavelet ψ of $L^2(\mathbb{R})$ is given by*

$$\psi = 2\sum_{k\in\mathbb{Z}} g_k \phi_{1,k},$$

where $g_k = (-1)^k \overline{h_{1-k}}$. Moreover, the set $\{2^{j/2}\psi_{j,k} : k \in \mathbb{Z}\}$ form an orthonormal basis of W_j.

The previous theorem combined with Theorem 1.5.4 imply that the set

$$\{\phi(\cdot - k) : k \in \mathbb{Z}\} \cup \{2^{j/2}\psi_{j,k} : j \in \mathbb{N}, k \in \mathbb{Z}\}$$

[2] In the literature, the filter h is sometimes defined as

$$h_k = \sqrt{2}\langle \phi, \phi(2\cdot - k)\rangle.$$

form an orthogonal basis of $L^2(\mathbb{R})$. Any function $f \in L^2(\mathbb{R})$ can thus be decomposed as

$$f(x) = \sum_{k\in\mathbb{Z}} C_k \phi(x-k) + \sum_{j\in\mathbb{N}} \sum_{k\in\mathbb{Z}} c_{j,k}\psi_{j,k}(x), \quad \text{where} \quad C_k = \langle f, \phi(\cdot - k)\rangle. \tag{7}$$

Furthermore, from the approximation coefficients at a scale j, there exists an efficient algorithm to compute the approximation and wavelet coefficients at the scale $j-1$. Let us give a last definition before presenting this algorithm.

Definition 1.5.6. Let $a = (a_k)_{k\in\mathbb{Z}}$ and $b = (b_k)_{k\in\mathbb{Z}}$ be two sequences of complex numbers. The *discrete convolution* between a and b is the sequence $a * b$ defined as

$$(a * b)_k = \sum_{l\in\mathbb{Z}} a_l b_{k-l},$$

for any $k \in \mathbb{Z}$.

Theorem 1.5.7 (Mallat algorithm)**.** *Let $(V_j)_{j\in\mathbb{Z}}$ be a multiresolution analysis of $L^2(\mathbb{R})$, $(h_k)_{k\in\mathbb{Z}}$ the filter of $(V_j)_{j\in\mathbb{Z}}$ associated to ϕ and $(g_k)_{k\in\mathbb{Z}}$ the sequence defined as $g_k = (-1)^k \overline{h_{1-k}}$. Let f be a function of $L^2(\mathbb{R})$ and $(c_{j,k})_{(j,k)\in\mathbb{Z}\times\mathbb{Z}}$ its wavelet coefficients associated to the wavelet ψ given in Theorem 1.5.5. Moreover, let's denote its approximation coefficients at scale j as $a^{(j)} := (a_{j,k})_{k\in\mathbb{Z}}$. We have*

$$a_{j-1,k} = (a^{(j)} * \tilde{h})_{2k} \quad \textit{and} \quad c_{j-1,k} = (a^{(j)} * \tilde{g})_{2k}, \tag{8}$$

where $\tilde{h}_k = \overline{h_{-k}}$ and $\tilde{g}_k = \overline{g_{-k}}$.

In practice, a real-life signal is a finite sequence of real numbers. This sequence is interpreted as the approximation coefficients of a function f at a scale j. The Mallat algorithm allows to compute the wavelet coefficients of the function f at a scale smaller than j. Moreover, let us note that if ψ is a compactly supported wavelet then the filter h is finite, which implies that Formula (8) involves finite sums. For any $r \in \mathbb{N}$, Daubechies has shown that there exists a compactly supported wavelet ψ with its r first moments vanishing, i.e.

$$\int_{\mathbb{R}} x^\alpha \psi(x)\, dx = 0,$$

for any $\alpha \in \{0, \dots, r-1\}$. These wavelets are called the *Daubechies wavelets of order r*. The associated filters are given in [39].

1.5.3 Multiresolution Analysis: The Case of $L^2(\mathbb{R}^n)$

This section uses the tensor product to define a multiresolution analysis of $L^2(\mathbb{R}^n)$ from one of $L^2(\mathbb{R})$. For more details, see [39, 105]. Let us begin with some definitions.

Definition 1.5.8. Let $c^{(i)} = (c_j^{(i)})_{j\in\mathbb{Z}}$ be a sequence of complex numbers $(1 \leq i \leq n)$. The sequence $\bigotimes_{i=1}^n c^{(i)}$ is defined as

$$(\bigotimes_{i=1}^n c^{(i)})_j = \prod_{i=1}^n c_{j_i}^{(i)},$$

for any $j = (j_1, \ldots, j_n) \in \mathbb{Z}^n$.

Definition 1.5.9. Let f_i be a function of $L^2(\mathbb{R})$ $(1 \leq i \leq n)$. The function $\bigotimes_{i=1}^n f_i$ is defined as

$$\bigotimes_{i=1}^n f_i : x = (x_1, \ldots, x_n) \in \mathbb{R}^n \mapsto \prod_{i=1}^n f(x_i).$$

This function belongs to $L^2(\mathbb{R}^n)$ and we have

$$\langle \bigotimes_{i=1}^n f_i, \bigotimes_{i=1}^n g_i \rangle = \prod_{i=1}^n \langle f_i, g_i \rangle. \tag{9}$$

Definition 1.5.10. Let H_i be a vector subspace of $L^2(\mathbb{R})$ $(1 \leq i \leq n)$. The *tensor product* of these subspaces is the vector subspace of $L^2(\mathbb{R}^n)$ defined as the closure of the set of all finite linear combinations of

$$\{\bigotimes_{i=1}^n f_i : f_i \in H_i \text{ for any } 1 \leq i \leq n\}.$$

It is denoted by $\bigotimes_{i=1}^n H_i$.

Let us note that $\bigotimes_{i=1}^n L^2(\mathbb{R}) = L^2(\mathbb{R}^n)$. Let us now define a multiresolution analysis of $L^2(\mathbb{R}^n)$.

Theorem 1.5.11. *Let $(V_j)_{j\in\mathbb{Z}}$ be a multiresolution analysis of $L^2(\mathbb{R})$. The sequence $(V_j^{(n)})_{j\in\mathbb{Z}}$, where the space $V_j^{(n)}$ is defined as*

$$V_j^{(n)} = \bigotimes_{i=1}^n V_j,$$

is a multiresolution analysis of $L^2(\mathbb{R}^n)$. In particular, if ϕ is a scaling function of $(V_j)_{j\in\mathbb{Z}}$, then $\phi^{(n)} := \bigotimes_{i=1}^n \phi$ is a scaling function of $(V_j^{(n)})_{j\in\mathbb{Z}}$.

Let us note that

$$(\phi^{(n)})_{j,k} = \bigotimes_{i=1}^n \phi_{j,k_i},$$

for any $j \in \mathbb{Z}$ and $k = (k_1, \ldots, k_n) \in \mathbb{Z}^n$. Moreover, if h is a filter of $(V_j)_{j\in\mathbb{Z}}$ then Equality (9) implies that a filter of $(V_j^{(n)})_{j\in\mathbb{Z}}$ is given by

$$h^{(n)} = \bigotimes_{i=1}^{n} h.$$

It remains to determine the space $W_j^{(n)}$ which is the orthogonal complement of $V_j^{(n)}$ in $V_{j+1}^{(n)}$. For any $j \in \mathbb{Z}$, we have

$$V_{j+1}^{(n)} = \bigotimes_{i=1}^{n} V_{j+1} = \bigotimes_{i=1}^{n} (V_j \oplus W_j) = \underbrace{\bigotimes_{i=1}^{n} V_j}_{=V_j^{(n)}} \oplus \bigoplus_{i=1}^{2^n-1} A_i^{(j)},$$

where the space $A_i^{(j)}$ is of the form $\bigotimes_{l=1}^{n} B_l^{(j,i)}$, where $B_l^{(j,i)}$ is equal to W_j or V_j and for any i, there is at least one $B_l^{(j,i)}$ which is equal to W_j. One thus obtains

$$W_j^{(n)} = \bigoplus_{i=1}^{2^n-1} A_i^{(j)}.$$

The following theorem defines wavelets of $L^2(\mathbb{R}^n)$ from the multiresolution analysis $(V_j^{(n)})_{j\in\mathbb{Z}}$.

Theorem 1.5.12. *Let $(V_j^{(n)})_{j\in\mathbb{Z}}$ be a multiresolution analysis as defined above. For any $1 \leq i < 2^n$ and $1 \leq l \leq n$, let us set*

$$\psi_l^{(i)} = \begin{cases} \phi & \text{if } B_l^{(0,i)} = V_0 \\ \psi & \text{if } B_l^{(0,i)} = W_0 \end{cases} \qquad \text{and} \quad \psi^{(i)} = \bigotimes_{l=1}^{n} \psi_l^{(i)}.$$

We have that $(\psi^{(i)})_{1\leq i<2^n}$ are wavelets of the $L^2(\mathbb{R}^n)$ space. Moreover, the set $\{2^{jn/2}\psi^{(i)} : k \in \mathbb{Z}^n\}$ form an orthonormal basis of $W_j^{(n)}$.

Consequently, the set

$$\{\phi^{(n)}(\cdot - k) : k \in \mathbb{Z}^n\} \cup \{2^{j/2}\psi_{j,k}^{(i)} : 1 \leq i < 2^n, j \in \mathbb{N}, k \in \mathbb{Z}^n\} \tag{10}$$

form an orthogonal basis of $L^2(\mathbb{R}^n)$. Any function $f \in L^2(\mathbb{R}^n)$ can thus be decomposed as

$$f(x) = \sum_{k\in\mathbb{Z}^n} C_k \phi^{(n)}(x-k) + \sum_{j\in\mathbb{N}} \sum_{k\in\mathbb{Z}^n} \sum_{i=1}^{2^n-1} c_{j,k}^{(i)} \psi_{j,k}^{(i)}(x), \text{ where } C_k = \langle f, \phi^{(n)}(\cdot - k)\rangle. \tag{11}$$

The discrete convolution and the Mallat algorithm are generalised as follows.

Definition 1.5.13. Let $a = (a_k)_{j\in\mathbb{Z}^n}$ and $b = (b_k)_{k\in\mathbb{Z}^n}$ be two sequences of complex numbers. The *discrete convolution* between a and b is the sequence $a * b$ defined as

$$(a * b)_k = \sum_{l\in\mathbb{Z}^n} a_l b_{k-l},$$

for any $k \in \mathbb{Z}^n$.

Theorem 1.5.14 (Mallat algorithm)**.** *Let $(V_j)_{j\in\mathbb{Z}}$ be a multiresolution analysis of $L^2(\mathbb{R})$, $h = (h_k)_{k\in\mathbb{Z}}$ the filter of $(V_j)_{j\in\mathbb{Z}}$ associated to ϕ and $(g_k)_{k\in\mathbb{Z}}$ the sequence defined by $g_k = (-1)^k \overline{h_{1-k}}$. For any $1 \leq i < 2^n$ and $1 \leq l \leq n$, let us set*

$$g_l^{(i)} = \begin{cases} h & \text{if } B_l^{(0,i)} = V_0 \\ g & \text{if } B_l^{(0,i)} = W_0 \end{cases} \quad \text{and} \quad g^{(i)} = \bigotimes_{l=1}^{n} g_l^{(i)}.$$

Let f be a function of $L^2(\mathbb{R}^n)$ and $(c_{j,k}^{(i)})_{1\leq i<2^n,(j,k)\in\mathbb{Z}\times\mathbb{Z}^n}$ its wavelet coefficients associated to the wavelets $(\psi^{(i)})_{1\leq i<2^n}$ given in Theorem 1.5.12. Moreover, let's denote its approximation coefficients at scale j by $a^{(j)} = (a_{j,k})_{k\in\mathbb{Z}^n}$. We have

$$a_{j-1,k} = (a^{(j)} * \tilde{h}^{(n)})_{2k} \quad \text{and} \quad c_{j-1,k}^{(i)} = (a^{(j)} * \tilde{g}^{(i)})_{2k}, \tag{12}$$

where $\tilde{h}_k^{(n)} = \overline{h_{-k}^{(n)}}$ and $\tilde{g}_k^{(i)} = \overline{g_{-k}^{(i)}}$.

If we use the Daubechies wavelets, the filter h is finite and thus Formulas (12) are finite sums. This algorithm is used in Chapter 6 to compute the wavelet coefficients of signals coming from the topography of the planet Mars.

1.5.4 Some Links with the Hölder Exponent

In this section, we present some links between the wavelet coefficients and the Hölder exponent. We assume that we have a compactly supported wavelet basis from a multiresolution analysis. Some results remain valid for other types of wavelets. More details can be found in [39, 67, 69].

To determine the Hölder exponent of a function f from its wavelet coefficients, it is important for the wavelets to have a number of vanishing moments sufficiently large [67]; we said that the wavelets $(\psi^{(i)})_{1\leq i<2^n}$ have their r *first vanishing moments* ($r \in \mathbb{N}\cup\{+\infty\}$), if we have

$$\int_{\mathbb{R}^n} x^\alpha \psi^{(i)}(x)\, dx = 0,$$

for any multi-index α such that $|\alpha| < r$ and for any $1 \leq i < 2^n$.

Theorem 1.5.15. *[60] If $(\psi^{(i)})_{1\leq i<2^n}$ have their r first vanishing moments with $r \geq \lfloor h_f(x) \rfloor + 1$ and if f is uniformly Hölder, then*

$$h_f(x) = \liminf_{j\to+\infty} \inf_{k\in\mathbb{Z}^n,1\leq i<2^n} \frac{\log|c_{j,k}^{(i)}|}{\log(2^{-j} + |k2^{-j} - x|)}.$$

This result shows that the values of $|c_{j,k}^{(i)}|$ are related to the Hölder exponent at the points x close to $k2^{-j}$. This fact motivates the following notations. Let $\lambda_{j,k}^{(i)}$ be the dyadic cube defined as

$$\lambda_{j,k}^{(i)} = \{x \in \mathbb{R}^n : 2^j x - k \in [0,1)^n\},$$

for any $1 \leq i < 2^n$, $j \in \mathbb{Z}$ and $k \in \mathbb{Z}^n$. In the following, we will omit any reference to the indices i, j, k for such cubes by writing $\lambda = \lambda_{j,k}^{(i)}$. Moreover, the notation ϕ_λ refers to the function $\phi_{j,k}^{(i)}$ and c_λ refers to the wavelet coefficient $c_{j,k}^{(i)}$. Let us notice that the index λ gives information on the localisation and the scale of the corresponding wavelet: if $\psi^{(i)}$ are compactly supported then there exists $C > 0$ such that $\text{supp}(\psi^{(i)}) \subset C\lambda$ where $C\lambda$ denotes the cube of same center as λ and C times larger. The function $\psi^{(i)}$ is "essentially" localised around the cube λ.

For any $1 \leq i < 2^n$, $j \in \mathbb{Z}$ and $x \in \mathbb{R}^n$, there exists an unique dyadic cube λ at scale j such that $x \in \lambda$; this dyadic cube is denoted by $\lambda_j(x)$.

Moreover, the previous theorem shows that coefficients c_λ allowing to study the regularity of the function f at x are the coefficients associated to a dyadic cube "close to" x. This motivates the following definition [69].

Definition 1.5.16. The *wavelet leaders* of a function f are defined as

$$d_{\lambda_{j,k}^{(i)}} = \max_{\lambda \in N(\lambda_{j,k}^{(i)})} \sup_{\lambda'^{(i)} \subset \lambda} |c_{\lambda'}|,$$

where $N(\lambda_{j,k}^{(i)})$ is the set of the $3^n - 1$ neighbours of $\lambda_{j,k}^{(i)}$ at the scale j and in the direction i.

If f belongs to the L^∞ space and if the wavelets $(\psi^{(i)})_{1 \leq i < 2^n}$ belong to the L^1 space, then

$$|c_\lambda| \leq ||\psi||_1 \, ||f||_\infty,$$

and therefore, the wavelet leaders are finite[3].

Moreover, the wavelet leader associated to the dyadic cube $\lambda_j(x)$ is denoted $d_j(x)$. The following theorem is the analog of Theorem 1.5.15 for the wavelet leaders.

Theorem 1.5.17. *[67] If $(\psi^{(i)})_{1 \leq i < 2^n}$ have the first r vanishing moments with $r \geq \lfloor h_f(x) \rfloor + 1$ and if f is uniformly Hölder, then*

$$h_f(x) = \liminf_{j \to +\infty} \frac{\log d_j(x)}{\log 2^{-j}}.$$

[3]The hypothesis $f \in L^\infty$ can be replaced by the weaker assumption that f belongs to the Besov space $B_{\infty,\infty}^0$ (see Section 1.6).

1.5.5 Periodised Wavelets

A real-life signal is usually a finite sequence of real numbers. If we study a phenomena that evolves over time, as the temperature for example, we have a finite sequence of real numbers $x_1, \dots, x_m$ which represents the studied signal. This sequence can be interpreted as a function f defined on $[0, 1]$ such that $f(i/m) = x_i$. This function can been seen as a function of period 1 which locally belongs to $L^2(\mathbb{R})$. More generally, we have the following definition.

Definition 1.5.18. Let us denote by $\mathbb{T}^n$ the torus $\mathbb{R}^n / \mathbb{Z}^n$. The space $L^2(\mathbb{T}^n)$ is the set of functions of period 1 which locally belong to $L^2(\mathbb{R}^n)$.

The periodisation operator $[\cdot]$ is defined as

$$[\cdot] : f \mapsto \sum_{k \in \mathbb{Z}^n} f(\cdot - k).$$

The basis defined in (10) allows to obtain a basis of $L^2(\mathbb{T}^n)$. It is proved in [37] that the set

$$\{[\phi]\} \cup \{[\psi_\lambda] : 1 \leq i < 2^n, j \in \mathbb{N}, k \in \{0, \dots, 2^j - 1\}^n\}$$

form an orthonormal basis of $L^2(\mathbb{T}^n)$. The corresponding wavelet coefficients

$$c_\lambda^{\text{per}} = 2^{jn} \int_0^1 f(x)[\psi_\lambda](x)\, dx$$

are naturally called the *periodised wavelet coefficients*. Let us set

$$\Lambda_j = \{\lambda_{j,k}^{(i)} : 1 \leq i < 2^n, k \in \{0, \dots, 2^j - 1\}^n\} \quad \text{and} \quad \Lambda = \bigcup_{j \in \mathbb{N}} \Lambda_j,$$

so the indices λ of the wavelet coefficients c_λ^{per} vary on Λ.

For the sake of simplicity, the notations ψ_λ and c_λ are again used for periodised wavelets and periodised wavelet coefficients.

1.6 Hölder Spaces and a few Generalisations

This section gives some additional information about Hölder spaces and some generalisations of these spaces. In the first part, we discuss about the definition of Hölder spaces (for a given exponent $h \in \mathbb{N}$). In the second part, the Besov spaces are defined. These spaces generalise the uniform Hölder spaces for negative exponents (see [129, 25, 130] for example). The oscillation spaces are also introduced [67]. They allow to approximate the decreasing part of the concave hull of the Hölder spectrum of a function f (see Section 1.7). Finally, a generalisation of the Hölder spaces and the Besov spaces is given with the

help of the admissible sequences (see [49, 4, 82, 83, 84] and references therein). These spaces allow to characterise in a better way the regularity of a function.

In this section, each result about the wavelet coefficients uses a compactly supported wavelet basis from a multiresolution analysis (see Equality (11) and Section 1.5) and the number of vanishing moments of the wavelets is supposed sufficiently great. Some results remains valid for other types of wavelets. More detail can be found in [105, 67, 68, 82, 83, 81, 84].

1.6.1 Additional Information about Hölder Spaces

Let us recall that a function f belongs to the Hölder space $\Lambda^h(x_0)$ ($h \notin \mathbb{N}$) if and only if there exist a constant $C > 0$ and a polynomial P_{x_0} of degree less than h such that

$$|f(x) - P_{x_0}(x)| \leq C|x - x_0|^h,$$

for any x in a neighbourhood of x_0. This condition is equivalent to

$$||f - P_{x_0}||_{L^\infty(B(x_0,2^{-j}))} \leq C2^{-hj}, \tag{13}$$

for any $j \in \mathbb{N}$. This equivalence is also valid if $h \in \mathbb{N}$. Moreover, if $h \notin \mathbb{N}$, Condition (13) is equivalent to the following one[4] [81]:

$$\inf_{P \in \mathbb{P}_{\lfloor h \rfloor}} ||f - P||_{L^\infty(B(x_0,2^{-j}))} \leq C2^{-hj}, \tag{14}$$

for any $j \in \mathbb{N}$, where $\mathbb{P}_m$ is the set of polynomial of degree less than or equal to m. If $h \in \mathbb{N}$, a function verifying Condition (13) also verifies Condition (14), but the converse is not necessarily true. A classical example is the Weierstraß function

$$\sum_{n=0}^{+\infty} b^{-n} \cos(b^n \pi x),$$

which verifies Condition (14) for $h = 1$ but does not verify Condition (13) for $h = 1$ [56, 139, 57].

Let us notice that, if f is m-times continuously differentiable on a neighbourhood of x_0 ($m \geq 1$), then Condition (13) and Condition (14) are equivalent, for any $h \leq m$. Indeed, for a such function f, there exists a constant $C > 0$ such that, $||f - P||_{L^\infty(B(x_0,2^{-j}))} \leq C2^{-mj}$, for any $j \in \mathbb{N}$, where P is the Taylor polynomial of order $m - 1$ of f.

In the literature, there exist several conventions for $h \in \mathbb{N}$ [39, 105, 67, 35, 139, 80]. In this thesis, we use the same as Zygmund [139], i.e. Condition (14). Moreover, Krantz states that this choice is the usual convention in

[4] For any $x \in \mathbb{R}$, the notation $\lfloor x \rfloor$ is defined as

$$\lfloor x \rfloor = \sup\{k \in \mathbb{Z} : k \leq x\}.$$

the harmonic analysis [80]. This convention allows to have the same wavelet characterisation of the Hölder spaces $\Lambda^h(x_0)$ for any $h > 0$ [83, 81, 84].

Definition 1.6.1. Let us fix $x_0 \in \mathbb{R}^n$ and $h > 0$. The *pointwise Hölder space* $\Lambda^h(x_0)$ is the set of locally bounded functions f for which there exists a constant $C > 0$ satisfying

$$\inf_{P \in \mathbb{P}_{\lfloor h \rfloor}} ||f - P||_{L^\infty(B(x_0, 2^{-j}))} \leq C 2^{-hj}, \tag{15}$$

for any $j \in \mathbb{N}$. The *uniform Hölder space* Λ^h is the set of functions f such that Condition (15) holds for any $x_0 \in \mathbb{R}^n$ uniformly in C.

As already mentioned in Section 1.1, a function f does not necessarily belongs to the space $\Lambda^{h_f(x_0)}(x_0)$. The Hölder spaces do not entirely characterise the regularity of a function. For this reason, these spaces have been generalised. The idea is to modify the sequence $(2^{-hj})_{j \in \mathbb{N}}$ in Condition (15) by an admissible sequence. This generalisation is presented in Section 1.6.3.

1.6.2 Besov Spaces and Oscillation Spaces

To define the Besov spaces [25], let us give some definitions and notations.

Definition 1.6.2. A function $f : \mathbb{R}^n \to \mathbb{C}$ is said *rapidly decreasing* if

$$||x \mapsto x^\alpha f(x)||_\infty < +\infty.$$

The *Schwartz space* $\mathcal{S}$ is the set of infinitely differentiable functions f such that, for any multi-index $\alpha \in \mathbb{N}^n$, $\partial^\alpha f$ is rapidly decreasing. The topological dual of the Schwartz space is denoted by $\mathcal{S}'$. This space is the set of *tempered distributions* on $\mathbb{R}^n$.

Let us denote by Φ the set of sequences $(\varphi_j)_{j \in \mathbb{N}}$ such that

- $\varphi_j \in \mathcal{S}$ for any $j \in \mathbb{N}$,
- $\operatorname{supp} \varphi_0 \subset \overline{B(0,2)}$,
- $\operatorname{supp} \varphi_j \subset \overline{B(0, 2^{j+1})} \setminus B(0, 2^{j-1})$ for any $j \geq 1$,
- $||x \mapsto D^\alpha \varphi_j(x)||_\infty \leq c_\alpha 2^{-j|\alpha|}$ for any $j \in \mathbb{N}$ and $\alpha \in \mathbb{N}^n$,
- $\sum_{j=0}^{+\infty} \varphi_j(x) = 1$ for any $x \in \mathbb{R}^n$.

Let us now define the Besov spaces.

Definition 1.6.3. Let $0 < p, q \leq +\infty$, $s \in \mathbb{R}$ and $(\varphi_j)_{j\in\mathbb{N}} \in \Phi$. The *Besov space* $B^s_{p,q}$ is the set of functions $f \in \mathcal{S}'$ such that the sequence

$$(||2^{js}\mathcal{F}^{-1}(\varphi_j \mathcal{F} f)||_p)_{j\in\mathbb{N}}$$

belongs to l^q, i.e.

$$||f||_{B^s_{p,q}} := ||(||2^{js}\mathcal{F}^{-1}(\varphi_j \mathcal{F} f)||_p)_{j\in\mathbb{N}}||_q$$

is finite.

The definition of the $B^s_{p,q}$ space is independent of the chosen sequence $(\varphi_j)_{j\in\mathbb{N}} \in \Phi$. Moreover, the properties of the l_p spaces (see Section 1.4) imply that the space $(B^s_{p,q}, ||\cdot||_{B^s_{p,q}})$ is a Banach space, if $p, q \geq 1$.

The next proposition shows that the Besov spaces are a generalisation of the uniform Hölder space.

Theorem 1.6.4. *[129] If $s > 0$ then we have $B^s_{\infty,\infty} = \Lambda^s$.*

Let us now introduce the discrete counterparts of the Besov spaces which will allow to give their wavelet characterisation.

Definition 1.6.5. Let $0 < p, q \leq +\infty$, $s \in \mathbb{R}$. The space $b^s_{p,q}$ is the set of sequences c such that the sequence

$$(2^{(s-\frac{n}{p})j}||(c_\lambda)_{k\in\mathbb{Z}}||_p)_{i\in\{0,\dots,2^n-1\},j\in\mathbb{N}}$$

belongs to l^q, i.e.

$$||c||_{b^s_{p,q}} := ||(2^{(s-\frac{n}{p})j}||(c_\lambda)_{k\in\mathbb{Z}^n}||_p)_{i\in\{0,\dots,2^n-1\},j\in\mathbb{N}}||_q$$

is finite.

Theorem 1.6.6. *[131] Let $0 < p, q \leq +\infty$, $s \in \mathbb{R}$. A function f belongs to $B^s_{p,q}$ if and only if its wavelet coefficients belongs to $b^s_{p,q}$ and the sequence $(C_k)_{k\in\mathbb{Z}}$ belongs to l^p.*

The idea for defining the oscillation spaces[5] $\mathcal{O}^s_p$ is to replace the wavelet coefficients by the wavelet leaders in the characterisation of the Besov spaces [67].

Definition 1.6.7. Let $s \in \mathbb{R}$. If $p > 0$, the *oscillation space* $\mathcal{O}^s_p$ is the set of functions f belonging to $B^s_{p,\infty}$ such that its wavelet leaders belongs to $b^s_{p,\infty}$. If $p < 0$, the *oscillation space* $\mathcal{O}^s_p$ is the set of function f belonging to $B^0_{\infty,\infty}$ and such that for any $\epsilon > 0$ and for any finite set $K \subset \mathbb{Z}^n$, there exist $C > 0$ and $J \in \mathbb{N}$ satisfying

$$2^{(sp-n)j} \sum_{k\in K} d^p_\lambda \leq C 2^{\epsilon j}$$

for any $j \geq J$ and any $1 \leq i < 2^n$.

[5] The spaces $\mathcal{O}^s_p$ are a particular case of oscillation spaces $\mathcal{O}^{s,s'}_p$ (with $s' = 0$) [62, 68].

The space $\mathcal{O}_p^s$ is not a vector space for $p < 0$. The next proposition shows that the oscillation spaces are a generalisation of the Besov spaces.

Proposition 1.6.8. *[67] Let $p > 0$ and $s \in \mathbb{R}$. One has $\mathcal{O}_p^s \subset B_{p,\infty}^s$ and if $s > n/p$, then $\mathcal{O}_p^s = B_{p,\infty}^s$.*

In the end of Section 1.5, we have defined the periodised wavelets on $L^2(\mathbb{T}^n)$. It is thus natural to define the Besov and oscillation spaces on the torus $\mathbb{T}^n$.

Definition 1.6.9. Let $0 < p, q \leq +\infty$, $s \in \mathbb{R}$. The periodised space $b_{p,q}^s(\mathbb{T}^n)$ is the set of sequences $c = (c_\lambda)_{\lambda \in \Lambda}$ such that

$$(2^{(s-\frac{n}{p})j} ||(c_\lambda)_{\lambda \in \Lambda_j}||_p)_{1 \leq i < 2^n, j \in \mathbb{N}}$$

belongs to l^q, i.e.

$$||c||_{b_{p,q}^s(\mathbb{T}^n)} := ||(2^{(s-\frac{n}{p})j} ||(c_\lambda)_{\lambda \in \Lambda_j}||_p)_{i \in \{0,\dots,2^n-1\}, j \in \mathbb{N}}||_q$$

is finite. The *periodised Besov space* $B_{p,q}^s(\mathbb{T}^n)$ is the set of functions f for which the periodised wavelet coefficients belong to $b_{p,q}^s(\mathbb{T}^n)$.

Definition 1.6.10. Let $s \in \mathbb{R}$. If $p > 0$, the *periodised oscillation space* $\mathcal{O}_p^s(\mathbb{T}^n)$ is the set of the functions f belonging to $B_{p,\infty}^s(\mathbb{T}^n)$ such that their wavelet leaders belong to $b_{p,\infty}^s(\mathbb{T}^n)$.
If $p < 0$, the *periodised oscillation space* $\mathcal{O}_p^s$ is the set of functions f belonging to $B_{\infty,\infty}^0(\mathbb{T}^n)$ and such that for any $\epsilon > 0$, there exist $C > 0$ and $J \in \mathbb{N}$ satisfying

$$2^{(sp-n)j} \sum_{\lambda \in \Lambda_j} d_\lambda^p \leq C 2^{\epsilon j}$$

for any $j \geq J$ and any $1 \leq i < 2^n$.

To simplify the notation, the space $B_{p,q}^s$ will denote either the Besov spaces or the periodised Besov space depending on the context (idem for the oscillation spaces).

1.6.3 Generalisation with the help of the admissible sequences

Besov and Hölder spaces have been generalised in the literature for more than 30 years (see [49, 4, 82, 83, 84] and references therein). In this thesis, we work with a generalisation using admissible sequences. The goal of this generalisation is to characterise in a better way the regularity of functions.

For example, let us take the Brownian motion $B = (B_x)_{x \in \mathbb{R}}$; it is well-known that, almost surely, $B \in \Lambda^h$ for any $h < 1/2$ but $B \notin \Lambda^{1/2}$, i.e. there does not exist a constant $C > 0$ such that

$$||B_\cdot - B_{x_0}||_{L^\infty((x_0 - 2^{-j}, x_0 + 2^{-j}))} \leq C 2^{-j/2}, \tag{16}$$

for any $j \in \mathbb{N}$ and for any $x_0 \in \mathbb{R}$. If we replace the sequence $(2^{-j/2})_{j\in\mathbb{N}}$ in Condition (16) by the sequence $(2^{-j/2}\sqrt{j})_{j\in\mathbb{N}}$, this condition holds for some $C > 0$ (see [73] for example and Theorem 2.3.5). The generalisation of Besov spaces is based on this idea: the sequence $(2^{sj})_{j\in\mathbb{Z}}$ in Definition 1.6.3 of Besov spaces is replaced by an admissible sequence σ.

Definition 1.6.11. Let $0 < p, q \leq +\infty$, σ an admissible sequence and let $(\varphi_j)_{j\in\mathbb{N}} \in \Phi$. The *generalised Besov space* $B^{\sigma}_{p,q}$ is the set of functions $f \in \mathcal{S}'$ such that the sequence

$$(||\sigma_j^{-1}\mathcal{F}^{-1}(\varphi_j \mathcal{F} f)||_p)_{j\in\mathbb{N}}$$

belongs to l^q, i.e.

$$||f||_{B^{\sigma}_{p,q}} := ||(||\sigma_j^{-1}\mathcal{F}^{-1}(\varphi_j \mathcal{F} f)||_p)_{j\in\mathbb{N}}||_q$$

is finite. Moreover, if $\underline{s}(\sigma^{-1}) > 0$, the space $B^{\sigma}_{\infty,\infty}$ is denoted by Λ^{σ} and is called the *generalised uniform Hölder space*[6].

As for the classical Besov spaces, the previous definition is independent of the sequence $(\varphi_j)_{j\in\mathbb{N}} \in \Phi$. The following theorem shows that the spaces Λ^{σ} generalise the uniform Hölder spaces Λ^h.

Theorem 1.6.12. *[82] Let σ be an admissible sequence such that $\underline{s}(\sigma^{-1}) > 0$. A locally bounded function f belongs to Λ^{σ} if and only if there exists $C > 0$ such that*

$$\inf_{P\in\mathbb{P}_{\lfloor \overline{s}(\sigma^{-1})\rfloor}} ||f - P||_{L^{\infty}(B(x_0,2^{-j}))} \leq C\sigma_j,$$

for any $j \in \mathbb{N}$ and for any $x_0 \in \mathbb{R}^n$. In particular, if $\sigma = (2^{-hj})_{j\in\mathbb{N}}$, we have $\Lambda^{\sigma} = \Lambda^h$.

The space $b^s_{p,q}$ is naturally generalised by the following definition.

Definition 1.6.13. Let $0 < p, q \leq +\infty$ and σ an admissible sequence. The space $b^{\sigma}_{p,q}$ is the set of sequences c such that the sequences

$$(\sigma_j^{-1} 2^{-j\frac{n}{p}} ||(c_\lambda)_{k\in\mathbb{Z}}||_p)_{1\leq i<2^n, j\in\mathbb{N}}$$

belong to l^q, i.e.

$$||c||_{b^{\sigma}_{p,q}} := ||(\sigma_j^{-1} 2^{-j\frac{n}{p}} ||(c_\lambda)_{k\in\mathbb{Z}^n}||_p)_{1\leq i<2^n, j\in\mathbb{N}}||_q$$

is finite.

The next proposition gives the wavelet characterisation of the generalised Besov spaces.

[6] The space Λ^{σ} is a particular case of the spaces $\Lambda^{\sigma,\alpha}$ (with $\alpha = \overline{s}(\sigma^{-1})$) defined in [82, 83].

Theorem 1.6.14. *[4] Let $0 < p, q \leq +\infty$ and σ be an admissible sequence. A function f belongs to $B^{\sigma}_{p,q}$ if and only if its wavelet coefficients belong to $b^{\sigma}_{p,q}$ and the sequence $(C_k)_{k\in\mathbb{Z}}$ belongs to l^p.*

We can also define these spaces on $\mathbb{T}^n$ as in the classical case. Again, the notation $B^{\sigma}_{p,q}$ denotes the generalised Besov space or the periodised Besov space, depending on the context.

Finally, the pointwise Hölder space $\Lambda^h(x_0)$ can also be generalised with the help of admissible sequences [84].

Definition 1.6.15. Let $x_0 \in \mathbb{R}^n$, $M \in \mathbb{N}$ and σ an admissible sequence. A locally bounded function f belongs to the *generalised Hölder space* $\Lambda^{\sigma,M}(x_0)$ if there exists a constant $C > 0$ such that

$$\inf_{P\in\mathbb{P}_M} ||f - P||_{L^\infty(B(x_0,2^{-j}))} \leq C\sigma_j,$$

for any $j \in \mathbb{N}$.

Let us notice that $\Lambda^h(x_0) = \Lambda^{\sigma,M}(x_0)$ with $\sigma = 2^{-hj}$ and $M = \lfloor h \rfloor$. The next proposition shows that if $M < \underline{s}(\sigma^{-1})$ then the lower bound of the definition of generalised Hölder spaces is reached.

Proposition 1.6.16. *[84] Let σ be an admissible sequence, $M \in \mathbb{N}$ and $x_0 \in \mathbb{R}^n$. If $M < \underline{s}(\sigma^{-1})$, then $f \in \Lambda^{\sigma,M}(x_0)$ if and only if there exist a constant $C > 0$ and a polynomial P_{x_0} of degree less than M such that*

$$||f - P_{x_0}||_{L^\infty(B(x_0,2^{-j}))} \leq C\sigma_j,$$

for any $j \in \mathbb{N}$.

The next theorem gives a quasi-characterisation of the spaces $\Lambda^{\sigma,M}(x_0)$ via the wavelet leaders. Let us notice that this result is a generalisation of a result of [67] which gives the link between the usual Hölder spaces $\Lambda^h(x_0)$ and the wavelet leaders.

Theorem 1.6.17. *[84] Let σ be an admissible sequence, $M \in \mathbb{N}$ and $x_0 \in \mathbb{R}^n$. If f belongs to $\Lambda^{\sigma,M}(x_0)$, then there exists a constant $C > 0$ such that*

$$d_j(x_0) \leq C\sigma_j,$$

for any $j \in \mathbb{N}$. Conversely, if this inequality holds for an uniformly Hölder function f and if $\sigma_j \to 0$ as $j \to +\infty$, then $f \in \Lambda^{\sigma',M}$, where σ' is defined as $\sigma'_j = \sigma_j |\log \sigma_j|$ and $M + 1 > \overline{s}(\sigma^{-1})$.

This result shows that the behaviour of $\inf_{P\in\mathbb{P}_M} ||f - P||_{L^\infty(B(x_0,2^{-j}))}$ as $j \to +\infty$ is not necessarily the same that the behaviour of $d_j(x_0)$ as $j \to +\infty$; it can have a logarithmic correction between these behaviours. Moreover, this logarithm correction is the best possible [60]. Chapter 2 shows that this correction is not present in the case of the Brownian motion.

1.7 The Wavelet Leaders Method

This section presents the wavelet leaders method (WLM) [67, 68]. This method is an adaptation of the box-counting method in the context of the discrete wavelet transform. It allows to estimate the concave hull of the Hölder spectrum of a function f. This is a classical method to study the multifractal properties of real-life signals (see [88, 135, 2, 42] for example).

Let $f \in L^2(\mathbb{T}^n)$ and let us denote by $(d_\lambda)_{\lambda\in\Lambda}$ its periodised wavelet leaders. The WLM is a method to approximate the Hölder spectrum of f. Let us begin by explaining the algorithm.

The *structure function* S_f is defined as

$$S_f(j,q) = \frac{1}{\#\Lambda_j} \sum_{\lambda\in\Lambda_j}^{*} (d_\lambda)^q, \tag{17}$$

where the symbol $\sum^*$ means that the sum is restricted to the non-vanishing terms d_λ. The *scaling function* η_f is obtained as

$$\eta_f(q) = \liminf_{j\to+\infty} \frac{\log S_f(j,q)}{\log 2^{-j}}. \tag{18}$$

The approximation of the Hölder spectrum is given by

$$d_f^\eta(h) = \inf_q \{hq - \eta_f(q)\} + n,$$

i.e. the Legendre transform of the scaling function.

The heuristic argument that underlies this method is the following. Theorem 1.5.17 states that if λ is a dyadic cube containing a point of Hölder exponent h, then one should have $d_\lambda \sim 2^{-hj}$ as j tends to infinity. Moreover, from the definition of the Hausdorff dimension, the iso-Hölder set of exponent h can be covered by about $2^{d_f(h)j}$ dyadic cubes λ. The most important contribution in the sum $\sum^*_{\lambda\in\Lambda_j}(d_\lambda)^q$ is thus given by

$$2^{\sup_h\{d_f(h)-hq\}j}.$$

Equality (18) shows that

$$\sum_{\lambda\in\Lambda_j}^{*} (d_\lambda)^q \sim 2^{(n-\eta(q))j} \quad \text{as} \quad j\to+\infty.$$

Consequently, we should have

$$\sup_h\{d_f(h) - hq\} = n - \eta(q).$$

Using the inverse Legendre transform, this relation shows that the function d_f^η seems to be a reasonable candidate to approximate the Hölder spectrum d_f. More precisely, one has the following theorem.

Theorem 1.7.1. *[61]*

- *The scaling function is related to the oscillation spaces by the following relation:*
$$\eta_f(p) = \sup\{s \in \mathbb{R} : c \in \mathcal{O}_p^{s/p}\}.$$
Consequently, the scaling function is independent of the chosen wavelet basis.
- *If f is uniformly Hölder, then $d_f \leq d_f^\eta$.*
- *The WLM holds for some classes of functions, as fractional Brownian motions, cascades, etc.*

Let us notice that the genericity of the set $\{f : d_f = d_f^\eta\}$ for a function space is still not proved. If the wavelet leaders in Relation (17) are replaced by the wavelet coefficients, the scaling function is related to the Besov spaces $B_{p,\infty}^{s/p}$ and the genericity is proved in the space $\mathcal{B}^\eta$ defined as

$$\mathcal{B}^\eta = \bigcap_{\epsilon>0} \bigcap_{p>0} B_{p,\infty}^{\frac{\eta(p)-\epsilon}{p}},$$

for a certain function η [65, 51]. However, the Besov spaces $B_{p,\infty}^{s/p}$ are defined only for $p > 0$, which implies that one can only have access to the increasing part of the spectrum.

The WLM allows to approximate the increasing and the decreasing part of the spectrum but a problem remains: a Legendre transform is always a concave function and thus the approximation of the Hölder spectrum is always concave. However, there exist functions with non-concave spectrum (see Figure 1.2). The two following sections define other methods to overcome this problem.

1.8 S^ν SPACES AND THE WAVELET PROFILE METHOD

The previous section presented the WLM which only allows to approximate the concave hull of the Hölder spectrum. This section presents the S^ν spaces [66] which allow to define the Wavelet Profile Method (WPM); this method can approximate non-concave spectra.

The main idea behind the definition of the S^ν spaces is the use of histograms of wavelet coefficients for large scales: Theorem 1.5.15 states that the wavelet coefficients which behaves like 2^{-hj} are the signature of points with Hölder exponent h. It seems therefore natural to try to estimate the spectrum of a function $f \in L^2(\mathbb{T}^n)$ by considering the function

$$\rho_f(h) = \lim_{\epsilon\to 0^+} \limsup_{j\to+\infty} \frac{\log \#\{\lambda \in \Lambda_j : 2^{-(h+\epsilon)j} \leq |c_\lambda| < 2^{-(h-\epsilon)j}\}}{\log 2^j}.$$

Hence, there exist approximately $2^{\rho_f(h)j}$ wavelet coefficients of amplitude 2^{-hj}. From the definition of the Hausdorff dimension and the wavelet characterisation of the Hölder exponent, one can hope to have $\rho_f(h) = d_f(h)$. However, two problems make this formalism useless: the function ρ_f depends on the chosen wavelet basis [66] and a numerical approximation of this function is difficult to obtain. Indeed, in practice, we only have access to a finite number of wavelet coefficients and in order to compute the double limit, one must introduce an arbitrary dependence between ϵ and j to approximate $\rho_f(h)$. To overcome these issues, one modifies the definition of this function to count the number of wavelet coefficients greater in modulus than 2^{-hj} at each scale j. This modification allows to define a function that is independent of the wavelet basis [66] and which can be numerically computable (see Chapter 4).

Definition 1.8.1. The *wavelet profile* of $f \in L^2(\mathbb{T}^n)$ is defined as

$$\nu_f : h \in \mathbb{R} \mapsto \lim_{\epsilon \to 0^+} \limsup_{j \to +\infty} \frac{\log \# E_j(1, h+\epsilon)(f)}{\log 2^j},$$

where

$$E_j(C, h)(f) = \{\lambda \in \Lambda_j : |c_\lambda| \geq C 2^{-hj}\}$$

and $c = (c_\lambda)_{\lambda \in \Lambda}$ are the periodised wavelet coefficients of f.

The function ν_f is obviously non-decreasing, right-continuous and there exists $h_{\min} \in \mathbb{R}$ for which $\nu_f(h) = -\infty$ for any $h < h_{\min}$ and $\nu_f(h) \in [0, n]$ for any $h \geq h_{\min}$. Moreover, $h_{\min} > 0$ if the function f is uniformly Hölder. A function ν satisfying those properties with $h_{\min} > 0$ is called an *admissible profile*.

Definition 1.8.2. Let ν be an admissible profile. The space S^ν is the set of functions $f \in L^2(\mathbb{T}^n)$ such that $\nu_f \leq \nu$.

The definitions of the function ν_f and the S^ν spaces are independent of the chosen wavelet basis [66]. For a fixed wavelet basis, S^ν can be seen as a sequences space matching a function $f \in L^2(\mathbb{T}^n)$ to its sequence of wavelet coefficients. The wavelet profile of a sequence $c = (c_\lambda)_{\lambda \in \Lambda}$ is denoted by ν_c and is defined as

$$\nu_c : h \in \mathbb{R} \mapsto \lim_{\epsilon \to 0^+} \limsup_{j \to +\infty} \frac{\log \# E_j(1, h+\epsilon)(c)}{\log 2^j},$$

where

$$E_j(C, h)(c) = \{\lambda \in \Lambda_j : |c_\lambda| \geq C 2^{-hj}\}.$$

The next proposition gives an equivalent definition of the space S^ν.

Proposition 1.8.3. *[66, 12] A sequence c belongs to S^ν if and only if for any $h \in \mathbb{R}$, $\epsilon > 0$ and $C > 0$, there exists $J \in \mathbb{N}$ such that*

$$E_j(C,h)(c) \leq 2^{(\nu(h)+\epsilon)j},$$

for any $j \geq J$.

In other words, a sequence c belongs to S^ν if at each large scale, the number of dyadic interval $\lambda \in \Lambda_j$ such that $|c_\lambda| \geq 2^{-hj}$, is smaller than $2^{\nu(h)j}$. Let's notice that the S^ν space can be endowed with a metric d such that the space (S^ν, d) is a complete topological vector space (for details, see [12]).

The following proposition shows the upsides of the spaces S^ν compared to the Besov spaces, in the context of the multifractal formalism .

Proposition 1.8.4. *[12] If $(p_n)_{n\in\mathbb{N}}$ is a dense sequence of $(0,+\infty)$ and if $(\epsilon_m)_{m\in\mathbb{N}}$ is a sequence of $(0,+\infty)$ which converges to 0, then*

$$S^\nu \subset \mathcal{B}^\eta = \bigcap_{n\in\mathbb{N}} \bigcap_{m\in\mathbb{N}} b_{p_n,\infty}^{\frac{\eta(p_n)-\epsilon_m}{p_m}},$$

where η is defined by

$$\eta(q) = \inf_{h\geq h_{\min}} \{hq - \nu(h)\} + n.$$

The previous inclusion becomes an equality if and only if ν is concave.

This proposition can be interpreted as follows: since B^η does not contain more information about the Hölder spectrum of a function f than its concave hull (see the end of Section 1.7), if ν is not concave, then S^ν gives additional information. It leads to an estimation of non-concave spectra.

Let us present the multifractal formalism based on the S^ν spaces, called the *Wavelet Profile Method* (WPM).

Let ν be an admissible profile. The WPM is defined as

$$d^\nu(h) = \begin{cases} -\infty & \text{if } h < h_{\min} \\ \min\{h \sup\limits_{h'\in(0,h]} \dfrac{\nu(h')}{h'}, n\} & \text{if } h \geq h_{\min} \end{cases}. \tag{19}$$

The following theorem shows the validity of this formalism.

Theorem 1.8.5. *[13, 14] Let ν be an admissible profile. We have the following properties:*

- *if the function f is uniformly Hölder, then $d_f \leq d^{\nu_f}$,*
- *the WPM holds for some classes of functions, as the Random Wavelet Series,*

- *the sets* $\{f \in S^\nu : \nu = \nu_f\}$ *and*

$$\{f \in S^\nu : d_f(h) = \begin{cases} d^{\nu_f}(h) & \text{if } h \in [h_{\min}, h_{max}] \\ -\infty & \text{otherwise} \end{cases} \},$$

where

$$h_{\max} = \inf_{h \geq h_{\min}} \frac{h}{\nu(h)},$$

are residual and prevalent in S^ν.

The approximation of the Hölder spectrum of a function f is thus given by d^{ν_f} and not directly by ν_f. Chapter 4 shows that for some classes of functions f, the function ν_f can be used directly to approximate the Hölder spectrum.

To understand the transition from ν_f to $d_f^{\nu_f}$, let us introduce the following definition [99].

Definition 1.8.6. Let $0 \leq a < b \leq +\infty$. A function $f : [a, b] \mapsto \mathbb{R}^+$ is with *increasing-visibility* if f is continuous at a and

$$\sup_{y \in (a,x]} \frac{f(y)}{y} \leq \frac{f(x)}{x},$$

for any $x \in (a, b]$.

In other words, a function f is with increasing-visibility if for any $x \in (a, b]$, the segment $((0, 0), (x, f(x))]$ lies above the graph of f on $(a, x]$.

The passage from ν_f to $d_f^{\nu_f}$ transforms the function ν_f into a function with increasing-visibility. This is illustrated in Figure 1.4.

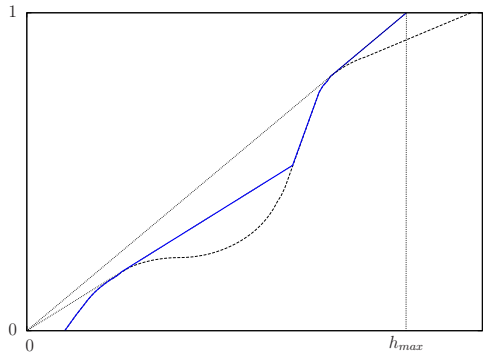

Figure 1.4.: Example of ν_f (---) and $d_f^{\nu_f}$ (—)

Of course, the WPM can only recover spectra with increasing-visibility. Moreover, since one considers wavelet coefficients and not wavelet leaders, this method can only approximate to the increasing part of the spectrum [14]. The next section gives a multifractal formalism to approximate non-concave and non-increasing spectra.

1.9 L^ν SPACES AND THE LEADERS PROFILE METHOD

The previous section presented the WPM which allows to approximate non-concave spectra. A problem still exists: this formalism can only detect increasing spectra. This issue is caused by the use of the wavelet coefficients. As for the WLM (see Section 1.7), a way to circumvent this problem is to use the wavelet leaders [22].

As for the S^ν spaces, the new spaces defined in this section, called the L^ν spaces, can be seen as a sequences space or a functions space by matching a function to its sequence of wavelet coefficients. In this section, we consider the L^ν space as a sequences space and we say that a function f belongs to L^ν if its wavelet coefficients belong to L^ν.

Definition 1.9.1. The *increasing wavelet leaders profile* of a sequence $c \in b^0_{\infty,\infty}$ is defined as[7]

$$\tilde{\nu}_c^+ : h \geq 0 \mapsto \lim_{\epsilon \to 0^+} \limsup_{j \to +\infty} \frac{\log \# \tilde{E}_j^+(1, h+\epsilon)(c)}{\log 2^j},$$

where

$$\tilde{E}_j^+(C,h)(c) = \{\lambda \in \Lambda_j : d_\lambda \geq C 2^{-hj}\},$$

and $d = (d_\lambda)_{\lambda \in \Lambda}$ are the periodised wavelet leaders of the sequence c. Similarly, the *decreasing wavelet leaders profile* of a sequence $c \in b^0_{\infty,\infty}$ is defined as

$$\tilde{\nu}_c^- : h \geq 0 \mapsto \lim_{\epsilon \to 0^+} \limsup_{j \to +\infty} \frac{\log \# \tilde{E}_j^-(1, h-\epsilon)(c)}{\log 2^j},$$

where

$$\tilde{E}_j^-(C,h)(c) = \{\lambda \in \Lambda_j : d_\lambda \leq C 2^{-hj}\}.$$

Let us denote by h_s, the smallest positive number such that $\tilde{\nu}_c^+(h_s) = n$. The *wavelet leaders profile* of a sequence $c \in b^0_{\infty,\infty}$ is defined as

$$\tilde{\nu}_c : h \geq 0 \mapsto \begin{cases} \tilde{\nu}_c^+(h) & \text{if } h \leq h_s \\ \tilde{\nu}_c^-(h) & \text{if } h \geq h_s \end{cases}.$$

These definitions formalise the idea that there are about $2^{\tilde{\nu}_f^+(h)j}$ (resp. $2^{\tilde{\nu}_f^-(h)j}$) wavelet leaders larger (resp. smaller) than 2^{-hj} at each large scale j.

The function $\tilde{\nu}_c$ is obviously increasing and right-continuous (resp. decreasing and left-continuous) on $(-\infty, h_s]$ (resp. on $[h_s, +\infty)$) and there exists

[7] Let us recall that a sequence $c = (c_\lambda)_{\lambda \in \Lambda}$ belongs to $b^0_{\infty,\infty}$, if and only if

$$\sup_{\lambda \in \Lambda} |c_\lambda| < +\infty.$$

For such a sequence, the wavelet leaders are thus finite.

$h_{\min} \leq h_{\max}$ for which $\tilde{\nu}_c(h) \in [0, n]$ for any $h \in [h_{\min}, h_{\max}]$ and $\tilde{\nu}_c(h) = -\infty$ for any $h \notin [h_{\min}, h_{\max}]$. One also has that the function $h \mapsto (\tilde{\nu}_c(h) - n)/h$ is decreasing on $[h_s, h_{\max}]$. Moreover, $h_{\min} > 0$ if $c \in b^{\epsilon}_{\infty,\infty}$ for some $\epsilon > 0$. A function satisfying those properties with $h_{\min} > 0$ is called an *admissible leaders profile*.

Definition 1.9.2. Let ν be an admissible leaders profile. The space L^{ν} is the set of sequences $c \in b^0_{\infty,\infty}$ such that $\tilde{\nu}_c \leq \nu$. Moreover, the space $L^{\nu,+}$ (resp. the space $L^{\nu,-}$) is the set of sequences $c \in b^0_{\infty,\infty}$ such that

$$\tilde{\nu}^+(h) \leq \nu(h) \quad (\text{resp. } \tilde{\nu}^-(h) \leq \nu(h)),$$

for any $h < h_s$ (resp. for any $h > h_s$)

One directly gets

$$L^{\nu} = L^{\nu,+} \cap L^{\nu,-}.$$

The next proposition gives an equivalent definition of these spaces[8].

Proposition 1.9.3. *[23]*

- *A sequence c belongs to $L^{\nu,+}$ if and only if for any $h < h_s$, $\epsilon > 0$ and $C > 0$, there exists $J \in \mathbb{N}$ such that*

$$\#\tilde{E}^+_j(C, h)(c) \leq 2^{(\nu(h)+\epsilon)j},$$

  for any $j \geq J$.

- *A sequence c belongs to $L^{\nu,-}$ if and only if for any $h > h_s$, $\epsilon > 0$ and $C > 0$, there exists $J \in \mathbb{N}$ such that*

$$\#\tilde{E}^-_j(C, h)(c) \leq 2^{(\nu(h)+\epsilon)j},$$

  for any $j \geq J$.

Let us notice that $L^{\nu,+}$ is a vector space while L^{ν} and $L^{\nu,-}$ are not since 0 does not belong to these spaces.

As for S^{ν}, L^{ν} can be endowed with a metric d such that the space $(L^{\nu}, \tilde{d})$ is a complete space. Let us now present the link between S^{ν} and L^{ν}.

Proposition 1.9.4. *[23] Let ν be an admissible leaders profile. One has $L^{\nu,+} = S^{\nu}$ if and only if ν is with increasing-visibility on $[h_{\min}, h_s]$.*

[8] Let us notice that the results presented in this section are also valid if the wavelet leaders are replaced by the restricted wavelet leaders e_λ defined as

$$e_\lambda = \sup_{\lambda' \subset \lambda} |c_{\lambda'}|.$$

This proposition shows that if ν is not with increasing visibility, $L^{\nu,+}$ gives additional information compared to S^ν. Besides, $L^{\nu,-}$ allows to have access to the decreasing part of the spectrum. The next proposition shows that the Hölder spectrum of a function f can be approximated by the function $\tilde{\nu}_c$, where c are the wavelet coefficients of f. This method is called the *Leaders Profile Method* (LPM).

Theorem 1.9.5. *[23] Let ν be an admissible leaders profile. We have the following properties:*

- *if f is a uniformly Hölder function, then $d_f \leq \tilde{\nu}_c$,*
- *the LPM holds for some classes of functions, as fractional Brownian motion, lacunary wavelet series, random wavelet series, sum of deterministic cascades, ...*
- *the set $\{c \in L^\nu : \nu = \tilde{\nu}_c\}$ is residual in L^ν.*

As for the WLM, the genericity of the set $\{f \in L^\nu : d_f = \tilde{\nu}_c\}$ is still not proved.

Let us finish this section by comparing the three methods presented in this chapter: the LPM, the WLM and the WPM. The following propositions show the upsides of the LPM compared to the WLM and of the LPM compared to the WPM, in the context of the multifractal formalism.

Proposition 1.9.6. *[46] If the function*

$$h \mapsto \lim_{\epsilon \to 0^+} \limsup_{j \to +\infty} \frac{\log \#\{\lambda \in \Lambda_j : 2^{-(\alpha+\epsilon)j} \leq d_\lambda < 2^{-(\alpha-\epsilon)j}\}}{\log 2^{-j}}$$

takes the value $-\infty$ outside of a compact set of $[0, +\infty)$, then we have the following properties:

- *we have $\tilde{\nu}_c \leq d_f^\eta$,*
- *the function d_f^η is the concave hull of the function $\tilde{\nu}_c$.*

Proposition 1.9.7. *[46] If f belongs to L^ν, we have the following properties:*

- *we have $\tilde{\nu}_c \leq d_f^\nu$ on $[0, h_s]$,*
- *the previous inequality becomes an equality on $[0, h_s]$ if and only if $\tilde{\nu}_c$ is with increasing-visibility on $[h_{\min}, h_s]$.*

Chapter 2

Hölderian Behaviour through Wavelets

It is well-known that the Brownian motion $B = (B_x)_{x\in\mathbb{R}}$ is a monofractal process with a Hölder exponent equal to $1/2$ but that, almost surely, the behaviour of $|B_x - B_{x_0}|$ is not $|x - x_0|^{1/2}$, for almost every $x_0 \in \mathbb{R}$. The Khintchin law states that, almost surely, the behaviour of $|B_x - B_{x_0}|$ is

$$|x - x_0|^{1/2}\sqrt{\log\log|x - x_0|^{-1}}$$

as $x \to x_0$, for almost every $x_0 \in \mathbb{R}$ (see [76, 73]). In terms of Hölder spaces, this means that $B \notin \Lambda^{1/2}(x_0)$ but $B \in \Lambda^{\sigma,0}(x_0)$ with $\sigma = (2^{-j/2}\sqrt{\log\log 2^j})_{j\in\mathbb{N}}$. Let us recall that Theorem (1.6.17) implies that the asymptotic behaviour of the wavelet leaders of B is not necessarily the same as σ; it can exist a logarithmic correction. A goal of this chapter is to show that this correction is not present for the Brownian motion. This result shows that the coefficients obtained by a wavelet transform can characterise finely the pointwise regularity. This also shows the interest of generalising the space S^ν with the help of admissible sequences (see Chapter 3). Indeed, the classical multifractal formalisms (as the WLM for example) can approximate the Hölder exponent of B but they cannot detect the correction $\sqrt{\log\log 2^j}$ of the Hölderian behaviour on simulations of B. Chapter 5 uses an algorithm based in this generalisation of S^ν to detect some corrections in the Hölderian behaviour.

The first section uses the wavelet decomposition to construct a function with prescribed Hölder exponents whose its wavelet coefficients display a prescribed behaviour. After a few remainder on the probability spaces and the Brownian motion, Section 2.4 shows that the three well-known types of behaviour of points of the Brownian motion B (namely ordinary, slow and rapid points) are also present in the behaviour of wavelet leaders of B. Finally, the last section presents a multifractal process based on the decomposition of the Brownian motion in the Schauder basis which has a local regularity similar to the Brownian motion. This is a variant of the multifractional Brownian motion [116, 24].

The results presented in Section 2.4 are a collaboration with C. Esser and A. Ayache and have been published in [16]. The results presented in Section 2.5

come from the discussions with A. Ayache and are also a collaboration with S. Nicolay.

This chapter is structured as follows:

2.1 Functions with Prescribed Hölder Exponents Displaying a Prescribed Behaviour in its Wavelet Coefficients

This section presents a method relying on the wavelet decomposition to build a function f with a prescribed Hölder exponents whose its wavelet coefficients display a prescribed behaviour. This method is a generalisation of Proposition 4 of [35] which shows that if the wavelet coefficients of a function f are defined as $c_\lambda = 2^{-jH(k2^{-j})}$, with H a well chosen function, then $h_f(x) = H(x)$ for any x. This section shows that the introduction of a certain factor a_j in the definition of the wavelet coefficients of f does not modify $h_f(x)$.

Notation. Let us denote by $\mathcal{H}_K$ the set of the functions from $[0,1]$ to the compact K which are the limit of a sequence of continuous functions. Lemma 2 of [38] implies that for any $H \in \mathcal{H}_K$, there exists a sequence $(Q_j)_{j\in\mathbb{N}}$ of

polynomials such that

$$\begin{cases} H(t) = \lim\limits_{j\to+\infty} Q_j(t) & \forall t \in [0,1] \\ ||Q_j'||_\infty \leq j & \forall j \in \mathbb{N} \end{cases}, \tag{20}$$

where Q_j' is the derivative of Q_j.

The next proposition defines a continuous function f with a prescribed Hölder exponent $h_f(x_0)$ for every point x_0.

Proposition 2.1.1. *Let $K \subset (0,1)$ be a compact set, $H \in \mathcal{H}_K$ and $(Q_j)_{j\in\mathbb{N}}$ be a sequence of polynomials satisfying Relations (20). For any $\lambda_{j,k} \in \Lambda$, set*

$$H_{\lambda_{j,k}} = \max\{\frac{1}{\log j}, Q_j(k2^{-j})\}.$$

If $(a_j)_{j\in\mathbb{N}}$ is a strictly positive real sequence such that

$$\lim_{j\to+\infty} \frac{\log a_j}{\log 2^{-j}} = 0,$$

then the function f defined as

$$f(x) = \sum_{j=0}^{+\infty} \sum_{\lambda\in\Lambda_j} 2^{-H_\lambda} a_j \psi_\lambda(x) \tag{21}$$

satisfies $h_f(x) = H(x)$, for any $x \in [0,1]$.

Proof. Let $x \in [0,1]$; from Proposition (1.5.17) it suffices to prove that

$$\lim_{j\to+\infty} \frac{\log d_j(x)}{\log 2^{-j}} = H(x),$$

where $d_j(x)$ are the wavelet leaders of f associated to the dyadic interval $\lambda_j(x)$. From the definition of f, its wavelet coefficients are $c_\lambda = 2^{-H_\lambda} a_j$. Let $\epsilon > 0$; since the definition of the sequence $(Q_j)_{j\in\mathbb{N}}$, there exists j_0 such that for any $j \geq j_0$ and $\lambda' \subset \lambda$ with $\lambda \in N(\lambda_j(x))$, we have

$$\begin{aligned} |H_{\lambda'} - H(x)| &\leq |Q_{j'}(k'2^{-j'}) - Q_{j'}(x)| + |Q_{j'}(x) - H(x)| \\ &\leq 2j'2^{-j'} + |Q_{j'}(x) - H(x)| \\ &\leq \epsilon. \end{aligned}$$

Consequently, we have

$$\max\{2^{-\frac{j'}{\log j'}} a_{j'}, 2^{-j'\epsilon} 2^{-j'H(x)} a_{j'}\} \leq |c_{\lambda'}| \leq \max\{2^{-\frac{j'}{\log j'}} a_{j'}, 2^{j'\epsilon} 2^{-j'H(x)} a_{j'}\}.$$

We thus obtain

$$\max\{2^{-\frac{j}{\log j}}a_j, 2^{-j\epsilon}2^{-jH(x)}a_j\} \leq d_j(x) \leq \max\{2^{-\frac{j}{\log j}}a_j, 2^{j\epsilon}2^{-jH(x)}a_j\},$$

i.e.

$$H(x)+\epsilon \geq \lim_{j\to+\infty}\frac{\log d_j(x)}{\log 2^{-j}} \geq H(x)-\epsilon,$$

hence the conclusion. ■

Remark 2.1.2.

- The case $a_j = 1$ corresponds to Proposition 4 of [35].
- If H is a continuous function, then the coefficients H_λ can be defined as

$$H_\lambda = \max\{\frac{1}{\log j}, H(k2^{-j})\}.$$

- This result still holds if one replaces the sequence a_j by

$$a'_j(x) = a_j(1+g(x)),$$

  where g is a bounded function such that $\inf g([0,1]) > -1$.
- Although the sequence $(a_j)_{j\in\mathbb{N}}$ in Equality (21) does not modify the Hölder exponent of the function f, this function does not necessarily belong to $\Lambda^{h_f(x_0)}(x_0)$. For example if $H(x) = h \in (0,1)$, then f is a monofractal function with an Hölder exponent equals to h, and $f \in \Lambda^h(x_0)$ if and only if the sequence $(a_j)_{j\in\mathbb{N}}$ is bounded; if $(a_j)_{j\in\mathbb{N}}$ is a unbounded admissible sequence, then $f \in \Lambda^{\sigma,0}(x_0)$ with $\sigma = (2^{-hj}a_j)_{j\in\mathbb{N}}$.

2.2 A Brief Reminder on Probability Spaces

This section briefly presents some notions and fixes some notations about the probability theory. For more details, see [11, 77, 94] for example. In the following of this chapter, we fix a probability space $(\Omega, \mathcal{A}, \mathbb{P})$.

2.2.1 Random Variables and Borel-Cantelli Lemma

Let us recall that a random variable X is a measurable function

$$X : (\Omega, \mathcal{A}) \to (\mathbb{R}, \mathbb{B}),$$

where $\mathbb{B}$ is the Borel σ-algebra. The following definitions give some notions about random variables.

Definition 2.2.1. Let X be a random variable. The *distribution function* of X is the function F_X defined as

$$F_X : x \in \mathbb{R} \mapsto \mathbb{P}(\{\omega \in \Omega : X(\omega) \leq x\}),$$

the *expected value* of X is defined as

$$\mathbb{E}(X) = \int_\Omega X(\omega) d\,\mathbb{P}(\omega)$$

and the *variance* of X is defined as

$$\mathbb{V}(X) = \mathbb{E}((X - \mathbb{E}(X))^2).$$

If X and Y are two random variables such that $F_X = F_Y$, we write $X \simeq Y$.

Definition 2.2.2. Let X, Y be two random variables. The *covariance* between X, Y is defined as

$$\mathrm{Cov}(X, Y) = \mathbb{E}((X - \mathbb{E}(X))(Y - \mathbb{E}(Y))) = \mathbb{E}(XY) - \mathbb{E}(X)\mathbb{E}(Y).$$

The following definition presents the important notion of independent random variables.

Definition 2.2.3. A collection of random variables $(X_\alpha)_{\alpha \in A}$ is said *independent* if for any finite set $I \subset A$ and any $x_i \in \mathbb{R}$, one has

$$\mathbb{P}(\bigcap_{i \in I} \{\omega \in \Omega : X_i(\omega) \leq x_i\}) = \prod_{i \in I} \mathbb{P}(\{\omega \in \Omega : X_i(\omega) \leq x_i\}).$$

Proposition 2.2.4. *[11] Let $(X_\alpha)_{\alpha \in A}$ be a collection of random variables with a finite expected value. If $(X_\alpha)_{\alpha \in A}$ is independent then for any $\alpha, \beta \in A$, $\alpha \neq \beta$, the variables X_α and X_β are uncorrelated, i.e.* $\mathrm{Cov}(X_\alpha, X_\beta) = 0$.

Let us give some notions about a collection of random variables.

Definition 2.2.5. Let $(X_x)_{x \in \mathbb{R}}$ be a collection of random variables. This collection is said

(a) *with stationary increments* if $X_{x+y} - X_x \sim X_y - X_0$ for any $x, y \in \mathbb{R}$,

(b) *with independent increments* if the increments

$$X_{x_2} - X_{x_1}, \ldots, X_{x_n} - X_{x_{n-1}}$$

are independent for any $x_1 < x_2 < \cdots < x_n$, $n \geq 1$.

To conclude this section, let us recall the Borel-Cantelli lemmas about sequences of events[1].

[1] An *event* E is an element of the σ-algebra $\mathcal{A}$.

Definition 2.2.6. A collection of events $(E_\alpha)_{\alpha\in A}$ is said *independent* if for any finite set $I \subset A$, one has

$$\mathbb{P}(\bigcap_{i\in I} E_i) = \prod_{i\in I} \mathbb{P}(E_i).$$

Lemma 2.2.7 (First Borel-Cantelli lemma)**.** *[11] Let $(E_n)_{n\in\mathbb{N}}$ be a sequence of events. If*

$$\sum_{n=1}^{+\infty} \mathbb{P}(E_n) < +\infty,$$

then we have[2]

$$\mathbb{P}(\limsup_{n\to+\infty} E_n) = 0.$$

Lemma 2.2.8 (Second Borel-Cantelli lemma)**.** *[11] Let $(E_n)_{n\in\mathbb{N}}$ be a sequence of events. If this sequence is independent and if*

$$\sum_{n=1}^{+\infty} \mathbb{P}(E_n) = +\infty,$$

then we have

$$\mathbb{P}(\limsup_{n\to+\infty} E_n) = 1.$$

Let us notice that the assumption of independence can be weakened to pairwise independence [11].

2.2.2 Gaussian Process

Let us present an important example of random variables.

Definition 2.2.9. A random variable X is called a *Gaussian random variable* if there exist $\mu \in \mathbb{R}$ and $\sigma > 0$ such that

$$F_X(x) = \frac{1}{\sqrt{2\pi\sigma^2}} \int_{-\infty}^{x} e^{-\frac{1}{2}\left(\frac{y-\mu}{\sigma}\right)^2} dy.$$

In this case, we note $X \sim \mathcal{N}(\mu, \sigma^2)$. If $\mu = 0$, then we say that X is a *centered Gaussian random variable.*

Let us notice that $\mathbb{E}(X) = \mu$, $\mathbb{V}(X) = \sigma^2$ and that X belongs to $L^2(\Omega, \mathcal{A}, \mathbb{P})$. The following proposition shows that any sequence of Gaussian random variables which converge in $L^2(\Omega, \mathcal{A}, \mathbb{P})$, tends to a Gaussian random variable.

[2] Let us recall that

$$\limsup_{n\to+\infty} E_n = \bigcap_{n\in\mathbb{N}} \bigcup_{k\geq n} E_k \quad \text{and} \quad \liminf_{n\to+\infty} E_n = \bigcup_{n\in\mathbb{N}} \bigcap_{k\geq n} E_k$$

Proposition 2.2.10. *For any $n \in \mathbb{N}$, let $X_n \sim \mathcal{N}(\mu_n, \sigma_n^2)$ be a Gaussian random variable. If the sequence $(X_n)_{n\in\mathbb{N}}$ tends to X in $L^2(\Omega, \mathcal{A}, \mathbb{P})$ then $X \sim \mathcal{N}(\mu, \sigma^2)$ with $\mu = \lim_{n\to+\infty} \mu_n$ and $\sigma = \lim_{n\to+\infty} \sigma_n$.*

The following classical lemma provides asymptotic estimates on the tail behaviour of a standard Gaussian distribution.

Lemma 2.2.11. *Let $Z \sim \mathcal{N}(0, 1)$ be a Gaussian random variable. Then, for any $x > 0$, we have*

$$\frac{1}{\sqrt{2\pi}} \frac{x}{x^2+1} e^{-x^2/2} \leq \mathbb{P}(\{\omega \in \Omega : Z(\omega) > x\}) \leq \frac{1}{\sqrt{2\pi}} \frac{1}{x} e^{-x^2/2}.$$

To define a Gaussian process, we need the following definition.

Definition 2.2.12. A vector $(X_1, \ldots, X_n)$ is called a *Gaussian vector* if for any $(t_1, \ldots, t_n) \in \mathbb{R}^n$, the random variable $\sum_{k=1}^n t_k X_k$ is Gaussian.

For such variables, Proposition 2.2.4 becomes an equivalence.

Proposition 2.2.13. *[94] Let $(X_1, \ldots, X_n)$ be a Gaussian vector. The variables $X_1, \ldots, X_n$ are independents if and only if they are uncorrelated.*

Definition 2.2.14. The collection of random variables $(X_x)_{x\in\mathbb{R}}$ is called a *Gaussian process* if for any finite set $I \subset \mathbb{R}$, the vector $(X_i)_{i\in I}$ is a Gaussian vector.

The following proposition is fundamental in the context of the Brownian motion.

Proposition 2.2.15. *[94] Let $(X_x)_{x\in\mathbb{R}}$ be a collection of random variables. The following two statements are equivalent:*

- *$(X_x)_{x\in\mathbb{R}}$ is a Gaussian process with $\mathbb{E}(X_x) = 0$ for any $x \in \mathbb{R}$ and $\mathrm{Cov}(X_y, X_y) = \min(x, y)$ for any $x, y \in \mathbb{R}$,*
- *$(X_x)_{x\in\mathbb{R}}$ has stationary independent increments and $X_x \sim \mathcal{N}(0, |x|)$ for any $x \in \mathbb{R}$.*

2.3 A Brief Remainder on the Brownian Motion

2.3.1 Definition and a few Properties

The Brownian motion is an important Gaussian process that models many phenomena (see e.g. [106, 93, 73, 75, 94] and references therein).

Definition 2.3.1. The *Brownian motion* $B = (B_x)_{x\in\mathbb{R}}$ is the unique Gaussian process such that

- almost surely, $B_0 = 0$ and $x \in \mathbb{R} \mapsto B_x$ is a continuous function,
- it has independent stationary increments such that for any $x_1, x_2 \in \mathbb{R}$, one has
$$B_{x_1} - B_{x_2} \sim \mathcal{N}(0, |x_1 - x_2|).$$

From Proposition 2.2.15, we have that $\mathrm{Cov}(B_x, B_y) = \min(x, y)$, for any $x, y \in \mathbb{R}$. The following proposition gives some classical results about the Brownian motion.

Proposition 2.3.2. *[106] Let $B = (B_x)_{x\in\mathbb{R}}$ be a Brownian motion.*

- *It has the property of* scaling invariance *of parameter* $1/2$*, i.e.*
$$B_{ax} \sim |a|^{1/2} B_x,$$
for any $a, x \in \mathbb{R}$.
- *It has the property of* time inversion*, i.e.*
$$B_x \sim |x| B_{1/x},$$
for any $x \in \mathbb{R}_0$.

To define the local properties of the Brownian motion, let us introduce the notion of *oscillation*.

Definition 2.3.3. Let $f : \mathbb{R} \to \mathbb{R}$ be a continuous function and K a compact interval of $\mathbb{R}$. The *oscillation* of f on K is defined as
$$\mathrm{Osc}_f(K) = \sup_{x,x'\in K} \left|f(x) - f(x')\right|.$$

If K is the interval $[x - \rho, x + \rho]$ ($x \in \mathbb{R}$ and $\rho > 0$), then the oscillation of f on K is denoted by $\mathrm{Osc}_f(x, \rho)$.

Remark 2.3.4. Let us note that we can directly check that if $h \in (0, 1)$ then, a function f belongs to $\Lambda^h(x_0)$ if and only if there exists a constant $C > 0$ such that
$$\mathrm{Osc}_f(x_0, \rho) \leq C\rho^h,$$
for any $\rho > 0$ small enough.

Here is a first result about the oscillation of the Brownian motion.

Theorem 2.3.5. *[73] There exists an event $\Omega^* \subseteq \Omega$ of probability 1 such that for any $\omega \in \Omega^*$, we have*

1. *for any $h \in (0, 1/2)$, there exists a constant $C > 0$ such that for any $x \in \mathbb{R}$, the inequality*
$$\mathrm{Osc}_{B.(\omega)}(x, \rho) \leq C\rho^h$$
holds for $\rho > 0$ small enough; this result is not valid for $h = 1/2$,

2. *there exists a constant $C > 0$ such that for any $x \in \mathbb{R}$, the inequality*
$$\mathrm{Osc}_{B.(\omega)}(x, \rho) \leq C\rho^{1/2}\sqrt{\log \rho^{-1}} \tag{22}$$
holds for $\rho > 0$ small enough,

3. *for almost every $x \in \mathbb{R}$, there exists a constant $C > 0$ such that the inequality*
$$\mathrm{Osc}_{B.(\omega)}(x, \rho) \leq C\rho^{1/2}\sqrt{\log\log \rho^{-1}}$$
holds for $\rho > 0$ small enough.

The first point of this last theorem shows that, almost surely, B is a monofractal process with a Hölder exponent equals to $1/2$ but $B \notin \Lambda^{1/2}$. The second point implies that, almost surely, for any $x_0 \in \mathbb{R}$,
$$B \in \Lambda^{\sigma,0}(x_0), \quad \text{with } \sigma = (2^{-j/2}\sqrt{j})_{j\in\mathbb{N}}$$
and the third point implies that, almost surely, for almost every $x_0 \in \mathbb{R}$,
$$B \in \Lambda^{\sigma,0}(x_0), \quad \text{with } \sigma = (2^{-j/2}\sqrt{\log j})_{j\in\mathbb{N}}.$$
This previous result only gives an upper bound of the behaviour of the oscillation of B. The following theorem gives the exact behaviour: it shows the existence of three different behaviours of the oscillations of B. Note that the last point of this theorem follows from the Khintchin law of the iterated logarithm.

Theorem 2.3.6. *[76, 73] There exists an event $\Omega^* \subseteq \Omega$ of probability 1 such that, for any $\omega \in \Omega^*$ and any non-empty open interval A of $\mathbb{R}$, there are $x_o(\omega), x_r(\omega), x_s(\omega) \in A$ such that*

1. *$x_o(\omega)$ is an* ordinary point *of $B.(\omega)$, i.e.*
$$0 < \limsup_{\rho\to 0^+} \frac{\mathrm{Osc}_{B.(\omega)}(x_o(\omega), \rho)}{\rho^{1/2}\sqrt{\log\log(\rho^{-1})}} < +\infty\,,$$

2. *$x_r(\omega)$ is a* fast or rapid point *of $B.(\omega)$, i.e.*
$$0 < \limsup_{\rho\to 0^+} \frac{\mathrm{Osc}_{B.(\omega)}(x_r(\omega), \rho)}{\rho^{1/2}\sqrt{\log(\rho^{-1})}} < +\infty\,,$$

3. $x_s(\omega)$ *is a* slow point *of* $B.(\omega)$*, i.e.*

$$0 < \limsup_{\rho \to 0^+} \frac{\mathrm{Osc}_{B.(\omega)}(x_s(\omega), \rho)}{\rho^{1/2}} < +\infty \,.$$

Moreover, for any $\omega \in \Omega^*$*, almost every* $x \in \mathbb{R}$ *is an ordinary point of* $B.(\omega)$*.*

The main goal of Section 2.4 is to show that we have a similar result for the behaviours of the wavelet leaders of B. This means that the eventual difference between the behaviour of the oscillation and the wavelet leaders (see Theorem 1.6.17) is not present in the case of the Brownian motion.

2.3.2 The Lévy-Ciesielski Construction

This section presents the Lévy-Ciesielski construction. It allows to decompose the Brownian motion in the Schauder basis (see [28] for example). This construction will be used in Section 2.5 to obtain a multifractal process which shares the same local regularity as the Brownian motion.

Let us begin with the definition of the Schauder functions.

Definition 2.3.7. The Schauder functions evaluated at x are the integrates of the Haar wavelets on $[0, x]$. More precisely, let us set

$$F_0(x) = \begin{cases} 0 & \text{if } x < 0 \\ t & \text{if } x \in [0,1] \\ 1 & \text{else} \end{cases} ,$$

and for any $\lambda_{j,k} \in \Lambda$, define

$$F_{\lambda_{j,k}}(x) = \begin{cases} x - k2^{-j} & \text{if } t \in [k2^{-j}, k2^{-j} + 2^{-(j+1)}] \\ -x + (k+1)2^{-j} & \text{if } t \in [k2^{-j} + 2^{-(j+1)}, (k+1)2^{-j}] \\ 0 & \text{else} \end{cases} .$$

The next proposition recall the well-known properties of the Schauder functions.

Proposition 2.3.8. *We have the following properties:*

1. let $(a_\lambda)_{\lambda \in \Lambda}$ *be a real sequence,* $a_0 \in \mathbb{R}$ *and* $\epsilon \in (0, 1/2)$*. If*

$$\max_{\lambda \in \Lambda_j} |a_\lambda| = O(2^{j\epsilon}) \quad \text{as } j \to +\infty,$$

then the function f *defined by*

$$x \mapsto a_0 F_0(x) + \sum_{j=0}^{+\infty} \sum_{\lambda \in \Lambda_j} a_\lambda 2^{j/2} F_\lambda(x) \tag{23}$$

is uniformly absolutely-convergent on $[0, 1]$*. Besides,* f *is a real continuous function such that* $f(0) = 0$*,*

2. *any continuous function f from $[0,1]$ to $\mathbb{R}$ such that $f(0) = 0$ can be written in the form (23). Besides, if $f \in \Lambda^\alpha(x_0)$ then there exists a constant $C > 0$ such that*

$$|a_\lambda 2^{-j/2}| \leq C(2^{-j} + |k2^{-j} - x_0|)^\alpha,$$

for any $\lambda \in \Lambda$.

The next theorem gives the decomposition of the Brownian motion in the Schauder basis.

Theorem 2.3.9 (The Lévy-Ciesielski Construction)**.** *[28] Let $(Z_\lambda)_{\lambda\in\Lambda}$ be a sequence of independents real-valued $\mathcal{N}(0,1)$ Gaussian random variables. Then, there exists an event $\Omega^* \subset \Omega$ of probability 1 such that, for any $\omega \in \Omega^*$, the function $B_\cdot(\omega)$ defined by*

$$B_\cdot(\omega) : x \mapsto Z_0(\omega)F_0(x) + \sum_{j=0}^{+\infty}\sum_{\lambda\in\Lambda_j} Z_\lambda(\omega)2^{j/2}F_\lambda(x) \tag{24}$$

is uniformly absolutely-convergent on $[0,1]$. Moreover, the process $B = (B_x)_x$ is a Brownian motion.

2.3.3 Wiener Integrate

This section briefly presents the Wiener integrate. It is a stochastic integrate using the Brownian motion and it will be used in the next section to study the wavelet coefficients of the Brownian motion. For more details, see [72, 94] for example. Let $B = (B_x)_{x\in\mathbb{R}}$ be a Brownian motion.

If $f : [a,b] \mapsto \mathbb{R}$ is a simple function given by

$$f = \sum_{i=1}^{p} a_i \chi_{]x_i,x_{i+1}]},$$

where $a \leq x_1 < x_2 < \cdots < x_{p+1} \leq b$, χ_A is the indicator function of the set A and $a_i \in \mathbb{R}$, then the *Wiener integrate* of f is defined as

$$\int_a^b f\, dB = \sum_{i=1}^{p} a_i(B_{x_{i+1}} - B_{x_i}).$$

From properties about the Brownian motion, we directly have that this integrate is a centered Gaussian random variable $\mathcal{N}(0, ||f||_2)$.

If $f \in L^2$ is a compactly supported function, then there exists a sequence of simple functions $(f_n)_{n\in\mathbb{N}}$ which tends to f in L^2. Moreover, the sequence

$$(\int_{a_n}^{b_n} f_n\, dB)_{n\in\mathbb{N}}$$

converges in $L^2(\Omega, \mathcal{A}, \mathbb{P})$. This limit is independent of the sequence $(f_n)_{n\in\mathbb{N}}$ and it is naturally called the *Wiener integrate* of f. It is denoted by $\int_{\mathbb{R}} f\, dB$. From Proposition 2.2.10, we have directly that

$$\int_{\mathbb{R}} f\, dB \sim \mathcal{N}(0, ||f||_2).$$

Let us finish this section by a result showing that this stochastic integrate can be defined using the Lebesgue measure.

Theorem 2.3.10. *[72] Let $f \in L^2$ be a compactly supported function. If f is continuously differentiable then*

$$\int_{\mathbb{R}} f\, dB = -\int_{\mathbb{R}} f'(x) B_x\, dx.$$

2.4 Behaviour of Wavelet Leaders of the Brownian Motion

Theorem 2.3.6 shows the existence of (at least) three types of behaviours of the oscillations of the Brownian motion: $\rho^{1/2}\sqrt{\log\log(\rho^{-1})}$, $\rho^{1/2}\sqrt{\log(\rho^{-1})}$ and $\rho^{1/2}$. The aim of this section is to prove that these behaviours are also present in the context of the wavelet leaders. More precisely, the main goal here is to prove the following result.

Theorem 2.4.1. *There exists an event $\Omega_0^* \subseteq \Omega$ of probability 1 such that for any $\omega \in \Omega_0^*$ and for any non-empty open interval A of $\mathbb{R}$, there are $x_o(\omega), x_r(\omega), x_s(\omega) \in A$ such that*

- *$x_o(\omega)$ is a leader-ordinary point of $B_\cdot(\omega)$, i.e.*

$$0 < \limsup_{j\to+\infty} \frac{d_j(x_o(\omega))}{2^{-j/2}\sqrt{\log j}} < +\infty\,,$$

- *$x_r(\omega)$ is a leader-rapid point of $B_\cdot(\omega)$, i.e.*

$$0 < \limsup_{j\to+\infty} \frac{d_j(x_r(\omega))}{2^{-j/2}\sqrt{j}} < +\infty\,,$$

- *$x_s(\omega)$ is a leader-slow point of $B_\cdot(\omega)$, i.e.*

$$0 < \limsup_{j\to+\infty} \frac{d_j(x_s(\omega))}{2^{-j/2}} < +\infty\,.$$

Moreover, for any $\omega \in \Omega_0^*$, almost every $x \in \mathbb{R}$ is a leader-ordinary point of $B_\cdot(\omega)$.

Let us fix $\psi : \mathbb{R} \to \mathbb{R}$ a compactly supported wavelet whose first moment vanishes, that is:

$$\int_{\mathbb{R}} \psi(x)\, dx = 0\,. \tag{25}$$

Moreover, in the following of this chapter, N is a positive integer such that the support of ψ is included in $[-N, N]$.

The next subsection gives a few comments on the wavelet coefficients and the wavelet leaders of a Brownian motion which will be useful to prove the previous theorem. Subsection 2.4.2 presents this proof and Subsection 2.4.3 gives some links between the behaviour of $\mathrm{Osc}_{B_{\cdot(w)}}(x, \rho)$ as $\rho \to 0$ and the behaviour of $d_j(x)$ as $j \to +\infty$, for $x \in \mathbb{R}$ fixed.

2.4.1 A few Comments on the Wavelet Coefficients and the Wavelet Leaders of a Brownian Motion

The next proposition gives a first link between the wavelet leaders and the oscillations of a function.

Proposition 2.4.2. *Let f be a continuous function, $x \in \mathbb{R}$ and $j \in \mathbb{N}$. One has*

$$d_j(x) \leq c_0 \,\mathrm{Osc}_f(x, (2+N)2^{-j}),$$

where $c_0 = \|\psi\|_1$.

Proof. Let λ be a dyadic interval. The wavelet coefficient c_λ of f is equal to

$$\begin{aligned} c_\lambda &= 2^j \int_{\mathbb{R}} f(x)\psi(2^j x - k)\, dx \\ &= \int_{\mathbb{R}} f((x+k)2^{-j})\psi(x)\, dx \\ &= \int_{\mathbb{R}} (f((x+k)2^{-j}) - f(k2^{-j}))\psi(x)\, dx, \quad \text{since (25)} \\ &= \int_{-N}^{N} (f((x+k)2^{-j}) - f(k2^{-j}))\psi(x)\, dx. \end{aligned}$$

Let x be a real number and $j \in \mathbb{N}$. If $\lambda_{j',k'} \subset \lambda$ with $\lambda \in N(\lambda_j(x))$, one has

$$|x - k'2^{-j'}| \leq 2 \cdot 2^{-j}\,,$$

hence, if $x' \in [-N, N]$,

$$|x - (x' + k')2^{-j'}| \leq (2+N)2^{-j}\,.$$

Therefore, one has

$$\begin{aligned} |c_{\lambda_{j',k'}}| &\leq \int_{-N}^{N} |f((x+k')2^{-j'}) - f(k'2^{-j'})||\psi(x)|\, dx \\ &\leq \|\psi\|_1 \,\mathrm{Osc}_f(x, (2+N)2^{-j}). \end{aligned}$$

As a consequence, one has

$$d_j(x) \leq c_0 \operatorname{Osc}_f(x, (2+N)2^{-j}).$$

■

This last proposition combined with Theorem 2.3.6 directly give the following proposition.

Proposition 2.4.3. *Let Ω^* be an event of probability 1 satisfying Theorem 2.3.6. For any $\omega \in \Omega^*$ and any $x \in \mathbb{R}$,*

1. *if x is an ordinary point of $B_\cdot(\omega)$, then*

$$\limsup_{j\to+\infty} \frac{d_j(x,\omega)}{2^{-j/2}\sqrt{\log j}} < +\infty\,,$$

2. *if x is a rapid point $B_\cdot(\omega)$, then*

$$\limsup_{j\to+\infty} \frac{d_j(x,\omega)}{2^{-j/2}\sqrt{j}} < +\infty\,,$$

3. *if x is a slow point of $B_\cdot(\omega)$, then*

$$\limsup_{j\to+\infty} \frac{d_j(x,\omega)}{2^{-j/2}} < +\infty\,.$$

The next section shows that for well-chosen points x, the previous superior limits can be also strictly positive, which will prove Theorem (2.4.1). Before doing that, let us give some of the properties of the wavelet coefficients of the Brownian motion, arising directly from the properties of this stochastic process. The following result is a particular case of a more general study of stochastic processes presented in [1]. We reproduce a few reasoning in the context of the Brownian motion.

For any $\omega \in \Omega$, the wavelet coefficient associated to the dyadic interval λ is denoted as

$$c_\lambda(\omega) = 2^j \int_{\mathbb{R}} B_x(\omega)\psi(2^j x - k)\, dx.$$

Consequently, the function $c_\lambda : \omega \in \Omega \mapsto c_\lambda(\omega)$ is a random variable.

Proposition 2.4.4. *We have the following properties:*

- *for any $j \in \mathbb{N}$, the sequence $(c_{\lambda_{j,k}})_{k\in\mathbb{Z}}$ is stationary,*
- *for any dyadic interval λ, we have $c_\lambda \sim 2^{-j/2} c_{\lambda_{0,0}}$,*
- *for any dyadic interval λ, c_λ is a centered Gaussian random variable.*

Therefore, for any dyadic interval λ, we have

$$\mathbb{E}(c_\lambda^2) = \mathbb{E}(c_{\lambda_{0,0}}^2)2^{-j} \quad \textit{and so,} \quad c_\lambda \sim \mathcal{N}(0, 2^{-j}\mathbb{E}(c_{\lambda_{0,0}}^2)).$$

Proof. Let $j \in \mathbb{N}$, $k, k_0 \in \mathbb{Z}$. We have

$$\begin{aligned} c_{\lambda_{j,k+k_0}} &= 2^j \int_{\mathbb{R}} B_x \psi(2^j x - k - k_0)\, dx \\ &= 2^j \int_{\mathbb{R}} B_{x+k_0 2^{-j}} \psi(2^j x - k)\, dx \\ &= 2^j \int_{\mathbb{R}} (B_{x+k_0 2^{-j}} - B_{k_0 2^{-j}}) \psi(2^j x - k)\, dx \\ &\simeq 2^j \int_{\mathbb{R}} (B_x - B_0) \psi(2^j x - k)\, dx, \end{aligned}$$

where the last relation is obtained from the fact that B has stationary increments. Consequently, the sequence $\{c_{\lambda_{j,k}} : k \in \mathbb{Z}\}$ is stationary in k. Moreover, we have

$$\begin{aligned} c_{\lambda_{j,k}} &= 2^j \int_{\mathbb{R}} B_x \psi(2^j x - k)\, dx \\ &= \int_{\mathbb{R}} B_{x 2^{-j}} \psi(x - k)\, dx \\ &\simeq 2^{-j/2} \int_{\mathbb{R}} B_x \psi(x - k)\, dx, \end{aligned}$$

where the last relation is obtained from the fact that B has the property of scaling invariance (see Proposition (2.3.2)). We thus obtained that $c_{\lambda_{j,k}} \sim 2^{-j/2} c_{\lambda_{0,k}}$. This implies the second point of the proposition.

Finally, Theorem 2.3.10 shows that

$$c_\lambda = -\int_{\mathbb{R}} \psi^{(-1)}(2^j x - k)\, dB(x) \quad \text{where} \quad \psi^{(-1)}(x) = \int_{-\infty}^{x} \psi(y)\, dy.$$

The last point of the proposition is thus proved.

■

The following proposition gives a sufficient condition for the wavelet coefficients to be independent.

Proposition 2.4.5. *The wavelet coefficients $c_{\lambda_1}, \ldots, c_{\lambda_n}$ are independent if*

$$\left(\frac{k_i - N}{2^{j_i}}, \frac{k_i + N}{2^{j_i}}\right) \cap \left(\frac{k_l - N}{2^{j_l}}, \frac{k_l + N}{2^{j_l}}\right) = \emptyset, \tag{26}$$

for any $i, l \in \{1, \ldots, n\}$, $i \neq l$. In particular, the coefficients $c_{\lambda_{j,k}}$ and $c_{\lambda_{j,l}}$ are independent if $|l - k| \geq 2N$.

Proof. This proposition follows directly from the fact that the increments of B are independent and that the wavelet coefficient c_λ is equal to

$$c_\lambda = \int_{-N}^{N} (B_{(x+k)2^{-j}} - B_{k2^{-j}})\psi(x)\, dx.$$

■

This proposition leads us to define the following condition.

Definition 2.4.6. Let $n \geq 2$ and $N \in \mathbb{N}$. We say that the dyadic intervals $\lambda_{J_1,K_1}, \ldots, \lambda_{J_n,K_n}$ satisfy Condition $(\mathcal{C}_N)$, if (26) is satisfied for any $i, l \in \{1, \ldots, n\}$, $i \neq l$.

2.4.2 Proof of Theorem (2.4.1)

The proof is based on several successive lemmas and propositions. In this section, Λ denotes the set of dyadic intervals and Λ_j denote the set of dyadic intervals of size 2^{-j}. From Proposition 2.4.4 and Proposition 2.4.5, the sequence $\{\varepsilon_\lambda : \lambda \in \Lambda\}$ defined by

$$\varepsilon_\lambda = \frac{1}{2^{-j/2}\sqrt{\mathbb{E}(c^2_{\lambda_{0,0}})}} c_\lambda \tag{27}$$

is a sequence of real-valued $\mathcal{N}(0,1)$ random variable such that for any $n \geq 2$, and for any dyadic intervals $\lambda_1, \ldots, \lambda_n$ satisfying Condition $(\mathcal{C}_N)$, the random variables $\varepsilon_{\lambda_1}, \ldots, \varepsilon_{\lambda_n}$ are independent.

In the sequel, we fix an arbitrary sequence $\{\varepsilon_\lambda : \lambda \in \Lambda\}$ of real-valued $\mathcal{N}(0,1)$ random variable verifying the property above. Moreover, for any dyadic interval λ and for any $m \in \mathbb{N}$, we define the set $\mathcal{S}_{\lambda,m}$ as

$$\mathcal{S}_{\lambda_{j,k},m} = \{\lambda_{j+m,l} : \lambda_{j+m,l} \subset \lambda_{j,k}\};$$

roughly speaking, "$\mathcal{S}_{\lambda,m}$ is the set of the 2^m descendants of λ at the m-th generation".

The following lemma allows to obtain a general lower bound for the amplitude of the wavelet leaders of the Brownian motion.

Lemma 2.4.7. *There exists an event $\Omega_1^* \subseteq \Omega$ of probability 1 such that, for any $\omega \in \Omega_1^*$ and for any $x \in \mathbb{R}$, one has*

$$\limsup_{j \to +\infty} \max_{\substack{\lambda' \in \mathcal{S}_{\lambda, \lfloor \log_2(N) \rfloor + 2} \\ \lambda \in N(\lambda_j(x))}} \left|\varepsilon_{\lambda'}(\omega)\right| > 0\,. \tag{28}$$

Proof. Let us fix $\lambda \in \Lambda$. For any $m \in \mathbb{N}$ and any $S \in \mathcal{S}_{\lambda,m}$, there is a unique finite sequence $(I_n)_{0\leq n\leq m}$ of dyadic intervals which is decreasing in the sense of the inclusion and satisfies $I_0 = \lambda$, $I_m = S$ and $I_n \in \mathcal{S}_{\lambda,n}$ for any $n \in \{1,\dots,m\}$. Next, we consider the sequence $(T_n)_{1\leq n\leq m}$ of dyadic intervals constructed as follows: for every $n \in \{1,\dots,m\}$, T_n is the unique dyadic interval of $\mathcal{S}_{\lambda,n}$ such that $I_{n-1} = T_n \cup I_n$. Note that, since the sequence $(I_n)_{0\leq n\leq m}$ is decreasing, this construction ensures that the intervals $(T_n)_{1\leq n\leq m}$ are pairwise disjoints. Moreover, let us also note that, for any $n \in \{1,\dots,m\}$, one has $T_n \in N(I_n)$. For any $n \in \{1,\dots,m\}$, there is a dyadic interval $T'_n \in \mathcal{S}_{T_n,\lfloor \log_2(N)\rfloor+2}$ such that

$$\left(\frac{k_n - N}{2^{j_n}}, \frac{k_n + N}{2^{j_n}}\right) \subseteq T_n,$$

where $T'_n = \lambda_{j_n,k_n}$. Consequently, by assumption, the corresponding Gaussian random variables $(\varepsilon_{T'_n})_{1\leq n\leq m}$ are independent. In the following, the set $\{T'_n : 1 \leq n \leq m\}$ is denoted by $\mathcal{T}'_{\lambda,m}(S)$.

Let $c_0 = 2^{-3/2}\sqrt{\pi}$ and denote by p_0 the probability that an arbitrary real-valued $\mathcal{N}(0,1)$ Gaussian random variable belongs to the interval $(-c_0, c_0)$. Elementary calculations allows to obtain that

$$0 < p_0 < \frac{1}{2}\,. \tag{29}$$

For any $S \in \mathcal{S}_{\lambda,m}$, we denote by $B_{\lambda,m}(S)$ the Bernoulli random variable defined as

$$B_{\lambda,m}(S) = \prod_{T'\in\mathcal{T}'_{\lambda,m}(S)} \chi_{\{\omega\in\Omega:|\varepsilon_{T'}(w)|<c_0\}}\,. \tag{30}$$

Notice that, using the definition of p_0 and the independence property of the random variables $\varepsilon_{T'}$ for $T' \in \mathcal{T}'_{\lambda,m}(S)$, one has

$$\mathbb{E}\big(B_{\lambda,m}(S)\big) = p_0^m\,. \tag{31}$$

Next, let $G_{\lambda,m}$ be the random variable with values in $\{0,\dots,2^m\}$ defined as

$$G_{\lambda,m} = \sum_{S\in\mathcal{S}_{\lambda,m}} B_{\lambda,m}(S)\,.$$

Since the cardinality of $\mathcal{S}_{\lambda,m}$ equals 2^m, using Equality (31), one gets that $\mathbb{E}(G_{\lambda,m}) = (2p_0)^m$. It follows from the Fatou Lemma[3] and (29) that

$$0 \leq \mathbb{E}\left(\liminf_{m\to+\infty} G_{\lambda,m}\right) \leq \lim_{m\to+\infty} \mathbb{E}(G_{\lambda,m}) = 0.$$

[3]Let us recall that the Fatou lemma asserts that if $(f_n)_{n\in\mathbb{N}}$ is a sequence of real measured functions on a measured space $(\Omega,\mathcal{A},\mu)$ then

$$\int \liminf_{n\to+\infty} f_n d\mu \leq \liminf_{n\to+\infty} \int f_n d\mu.$$

See [11] for example.

Hence, the event

$$\Omega^*_{1,\lambda} = \left\{ \omega \in \Omega : \liminf_{m \to +\infty} G_{\lambda,m}(\omega) = 0 \right\} \tag{32}$$

has a probability equal to 1. Since Λ is a countable set, the probability of the event

$$\Omega^*_1 = \bigcap_{\lambda \in \Lambda} \Omega^*_{1,\lambda} \tag{33}$$

is also equal to 1.

Let us now consider $\omega \in \Omega^*_1$ and $x \in \mathbb{R}$, and let us prove that Inequality (28) is satisfied. We fix $j \in \mathbb{N}$. Since for any $m \in \mathbb{N}$, $G_{\lambda_j(x),m}$ takes values in $\{0, \dots, 2^m\}$, (32) and (33) imply that there are infinitely many m such that

$$B_{\lambda_j(x),m}(S) = 0,$$

for any $S \in \mathcal{S}_{\lambda_j(x),m}$, i.e. using (30), there exists $T' \in \mathcal{T}'_{\lambda_j(x),m}(S)$ such that

$$|\varepsilon_{T'}| \geq c_0 \, .$$

In particular, this result is validated for $S = \lambda_{j+m}(x)$. Consequently, T' belongs to $\mathcal{S}_{\lambda,\lfloor \log_2(N) \rfloor + 2}$n with $\lambda \in N(\lambda_{j+m}(x))$. The conclusion follows. ■

Proposition 2.4.8. *There exists an event $\Omega^*_1 \subset \Omega$ of probability 1 such that for any $\omega \in \Omega^*_1$ and for any $x \in \mathbb{R}$, one has*

$$\limsup_{j \to +\infty} \frac{d_j(x,\omega)}{2^{-j/2}} > 0 \, .$$

Proof. From the fact that the support of the wavelet is included in $[-N, N]$, Proposition 2.4.4 and Proposition 2.4.5 imply that the assumptions of Lemma 2.4.7 are fulfilled for the Gaussian variable ϵ_λ defined in Relation (27). Therefore, there exists an event $\Omega^*_1 \subseteq \Omega$ of probability 1 such that, for any $\omega \in \Omega^*_1$ and for any $x \in \mathbb{R}$, one has

$$\limsup_{j \to +\infty} \max_{\substack{\lambda' \in \mathcal{S}_{\lambda,\lfloor \log_2(N) \rfloor + 2} \\ \lambda \in N(\lambda_j(x))}} \left| \varepsilon_{\lambda'}(\omega) \right| > 0 \, . \tag{34}$$

For any $j \in \mathbb{N}$, from the definition of wavelet leaders and Relation (27), one has

$$\begin{aligned} d_j(x,\omega) &\geq \max_{\substack{\lambda' \in \mathcal{S}_{\lambda,\lfloor \log_2(N) \rfloor + 2} \\ \lambda \in N(\lambda_j(x))}} \left| c_{\lambda'}(\omega) \right| \\ &\geq 2^{-(j + \lfloor \log_2(N) \rfloor + 2)/2} \sqrt{\mathbb{E}\left(c^2_{0,0}\right)} \max_{\substack{\lambda' \in \mathcal{S}_{\lambda,\lfloor \log_2(N) \rfloor + 2} \\ \lambda \in N(\lambda_j(x))}} \left| \varepsilon_{\lambda'}(\omega) \right| , \end{aligned}$$

and together with (34), this implies that

$$\limsup_{j\to+\infty} \frac{d_j(x,\omega)}{2^{-j/2}} > 0\,.$$

This gives the conclusion. ■

As we will see in the proof of Theorem 2.4.1, this result allow to get the existence of leader-slow points. Let us now focus on leader-ordinary points.

Lemma 2.4.9. *There exists an event $\Omega_2^* \subseteq \Omega$ of probability 1 such that, for any $\omega \in \Omega_2^*$ and almost every $t \in \mathbb{R}$, one has*

$$\limsup_{j\to+\infty} \frac{1}{\sqrt{\log j}} \max_{\substack{\lambda'\in\mathcal{S}_{\lambda,\lfloor\log_2(N)\rfloor+2}\\ \lambda\in N(\lambda_j(t))}} |\varepsilon_{\lambda'}| > 0\,.$$

Proof. Within this proof, we will use the same notations as in the proof of Lemma 2.4.7. Let us fix $x \in \mathbb{R}$. Let $j \in \mathbb{N}$. For every $m \in \mathbb{N}$, we consider the dyadic interval $S = \lambda_{j+m}(x) \in \mathcal{S}_{\lambda(x),m}$ and the associated sequence $(T'_n)_{1\le n\le m}$ of dyadic intervals. Next, we set

$$\mathcal{E}_{j,m}(x) := \left\{\omega\in\Omega : \max_{1\le n\le m} |\varepsilon_{T'_n}(\omega)| \ge \sqrt{\log(2m)}\right\}.$$

By construction, the Gaussian random variables $(\varepsilon_{T'_n})_{1\le n\le m}$ are independent. Therefore, one has

$$\begin{aligned}\mathbb{P}\left(\mathcal{E}_{j,m}(x)\right) &= 1 - \prod_{1\le n\le m} \mathbb{P}\left\{\omega\in\Omega : |\varepsilon_{T'_n}(\omega)| < \sqrt{\log(2m)}\right\}\\ &= 1 - \left(1 - \mathbb{P}\left\{\omega\in\Omega : |\varepsilon(\omega)| > \sqrt{\log(2m)}\,\right\}\right)^m,\end{aligned}$$

where $\varepsilon \sim \mathcal{N}(0,1)$. Let us set $C = 1/2\ (2\pi^{-1})^{1/2} > 0$. Using Lemma 2.2.11 and the fact that $\log(1-x) \le -x$ if $x \in (0,1)$, there exists $M \in \mathbb{N}$ such that for any $m > M$, we have

$$\begin{aligned}\mathbb{P}\left(\mathcal{E}_{j,m}(x)\right) &\ge 1 - \left(1 - C\frac{e^{-\frac{1}{2}\log(2m)}}{\sqrt{\log(2m)}}\right)^m\\ &\ge 1 - \exp\left(-Cm\frac{e^{-\frac{1}{2}\log(2m)}}{\sqrt{\log(2m)}}\right)\\ &\ge 1 - \exp\left(-C\sqrt{\frac{m}{2\log(2m)}}\right)\\ &\ge 1 - \exp(-m^\gamma),\end{aligned}$$

for $\gamma \in (0, 1/2)$. Consequently, one has in particular

$$\sum_{M\in\mathbb{N}} \mathbb{P}\left(\mathcal{E}_{2^M,2^M}(t)\right) = +\infty\,.$$

In view of the fact that the events $\mathcal{E}_{2^M,2^M}(t)$ $(M \in \mathbb{N})$ are independents, it follows from the second Borel-Cantelli lemma (Lemma 2.2.8) that

$$\mathbb{P}\left(\limsup_{M\to+\infty} \mathcal{E}_{2^M,2^M}(t)\right) = 1\,.$$

Therefore, for a fixed $x \in \mathbb{R}$, almost surely, there are infinitely many scales $j \in \mathbb{N}$ such that

$$\max_{\substack{\lambda'\in\mathcal{S}_{\lambda,\lfloor\log_2(N)\rfloor+2}\\ \lambda\in N(\lambda_j(x))}} |\varepsilon_{\lambda'}| \geq \sqrt{\log j}\,.$$

Fubini's theorem applied to the function $(x,\omega) \in \mathbb{R}\times\Omega \mapsto \chi_{S(x)}(\omega)$, where

$$S(x) = \{\omega \in \Omega : \limsup_{j\to+\infty} \frac{1}{\sqrt{\log j}} \max_{\substack{\lambda'\in\mathcal{S}_{\lambda,\lfloor\log_2(N)\rfloor+2}\\ \lambda\in N(\lambda_j(x))}} |\varepsilon_{\lambda'}| < 1\}\,,$$

implies then that there is an event $\Omega_2^* \subseteq \Omega$ of probability 1 on which for almost every $x \in \mathbb{R}$,

$$\limsup_{j\to+\infty} \frac{1}{\sqrt{\log j}} \max_{\substack{\lambda'\in\mathcal{S}_{\lambda,\lfloor\log_2(N)\rfloor+2}\\ \lambda\in N(\lambda_j(x))}} |\varepsilon_{\lambda'}| > 0\,.$$

■

Proposition 2.4.10. *There exists an event Ω_2^* of probability 1 such that for every $\omega \in \Omega_2^*$ and almost every $x \in \mathbb{R}$, one has*

$$\limsup_{j\to+\infty} \frac{d_j(x,\omega)}{2^{-j/2}\sqrt{\log j}} > 0\,.$$

Proof. We proceed as in the proof of Proposition 2.4.8. Using Lemma 2.4.9, Proposition 2.4.4, Proposition 2.4.5 and the fact that the support of the wavelet is included in $[-N, N]$, we know that there exists an event $\Omega_2^* \subseteq \Omega$ of probability 1 such that, for every $\omega \in \Omega_2^*$ and almost every $x \in \mathbb{R}$, one has

$$\limsup_{j\to+\infty} \frac{1}{\sqrt{\log j}} \max_{\substack{\lambda'\in\mathcal{S}_{\lambda,\lfloor\log_2(N)\rfloor+2}\\ \lambda\in N(\lambda_j(x))}} |\varepsilon_{\lambda'}(\omega)| > 0\,,$$

where

$$\varepsilon_\lambda = \frac{1}{\sqrt{2^{-j}\mathbb{E}(c_{\lambda_{0,0}}^2)}} c_\lambda\,.$$

In particular,

$$\max_{\substack{\lambda'\in\mathcal{S}_{\lambda,\lfloor\log_2(N)\rfloor+2}\\ \lambda\in N(\lambda_j(x))}}\left|c_{\lambda'}(\omega)\right| = 2^{-(j+\lfloor\log_2(N)\rfloor+2)/2}\sqrt{\mathbb{E}(c^2_{\lambda_{0,0}})}\max_{\substack{\lambda'\in\mathcal{S}_{\lambda,\lfloor\log_2(N)\rfloor+2}\\ \lambda\in N(\lambda_j(t))}}\left|\varepsilon_{\lambda'}(\omega)\right|.$$

Consequently, if $\omega\in\Omega_2^*$, for almost every $x\in\mathbb{R}$, one has

$$\limsup_{j\to+\infty}\frac{d_j(x,\omega)}{2^{-j/2}\sqrt{\log j}}\geq\limsup_{j\to+\infty}\frac{1}{2^{-j/2}\sqrt{\log j}}\max_{\substack{\lambda'\in\mathcal{S}_{\lambda,\lfloor\log_2(N)\rfloor+2}\\ \lambda\in N(\lambda_j(x))}}\left|c_{\lambda'}(\omega)\right|>0$$

and the conclusion follows. ■

Let us end with a result which will be useful for rapid points.

Lemma 2.4.11. *There exists an event $\Omega_3^*\subseteq\Omega$ of probability 1 such that, for any $\omega\in\Omega_3^*$ and for any non-empty open interval A of $\mathbb{R}$, there is $x\in A$ such that*

$$\limsup_{j\to+\infty}\frac{|\varepsilon_{\lambda_j(t)}|}{\sqrt{j}}>0\,.$$

Proof. To avoid making the notations heavier, we suppose that $A=(0,1)$. The proof can be adapted in the general case. The conclusion then follows by covering $\mathbb{R}$ with open intervals with rational endpoints.

Let us fix $a\in(0,1)$ and $C>0$ such that $C^2<2a\log 2$. Let us also consider for every $j\in\mathbb{N}$ and $l\in\{0,\dots,\lfloor 2^{j(1-a)}\rfloor-1\}$, the event

$$\mathcal{F}_{j,l}:=\left\{\omega\in\Omega:\max_{k\in\{l\lfloor 2^{aj}/(2N)\rfloor,\dots,(l+1)\lfloor 2^{aj}/(2N)\rfloor-1\}}|\varepsilon_{\lambda_{j,2kN}}(\omega)|\geq C\sqrt{j}\right\}.$$

Besides, let j_0 be the smallest $j\in\mathbb{N}$ such that $\lfloor 2^{aj}/(2N)\rfloor\geq 1$.

Assume for a while that

$$\mathbb{P}\left(\complement\left(\bigcap_{l\in\{0,\dots,\lfloor 2^{j(1-a)}\rfloor-1\}}\mathcal{F}_{j,l}\right)\right)\tag{35}$$

is the general term of a convergent series; then the first Borel-Cantelli lemma (Lemma 2.2.7) implies that

$$\mathbb{P}\left(\bigcup_{J\geq j_0}\bigcap_{j\geq J}\bigcap_{l\in\{0,\dots,\lfloor 2^{j(1-a)}\rfloor-1\}}\mathcal{F}_{j,l}\right)=1.$$

Now, let us set

$$\Omega_3^*:=\bigcup_{J\geq j_0}\bigcap_{j\geq J}\bigcap_{l\in\{0,\dots,\lfloor 2^{j(1-a)}\rfloor-1\}}\mathcal{F}_{j,l}\tag{36}$$

and let us consider $\omega \in \Omega_3^*$. For any $j \geq j_0$, let us set

$$G_j(\omega) := \left\{k \in \{0, \ldots, 2^j - 1\} : |\varepsilon_{\lambda_{j,k}}(\omega)| \geq C\sqrt{j}\right\} \tag{37}$$

and

$$U_j(\omega) := \bigcup_{k \in G_j(\omega)} \left(\frac{k}{2^j}, \frac{k+1}{2^j}\right). \tag{38}$$

Finally, for any $n \geq j_0$, one considers

$$O_n(\omega) := \bigcup_{j \geq n} U_j(\omega).$$

This last open set is dense in $(0,1)$. Indeed, let us consider $x \in (0,1)$, $j \geq j_0$ and k such that $\lambda_j(t) = \lambda_{j,k}$. Then, either there exists $l \in \{0, \ldots, \lfloor 2^{j(1-a)} \rfloor - 1\}$ such that

$$k \in \{l\lfloor 2^{ja} \rfloor, \ldots, (l+1)\lfloor 2^{ja} \rfloor - 1\} \quad \text{or} \quad k \in \{\lfloor 2^{j(1-a)} \rfloor \lfloor 2^{ja} \rfloor, \ldots, 2^j - 1\}.$$

In the first case, using (36) and (37), there exists

$$k' \in \{l\lfloor 2^{aj}/(2N) \rfloor, \ldots, (l+1)\lfloor 2^{aj}/(2N) \rfloor - 1\}$$

such that $2k'N \in G_j(\omega)$. From (38), we get that x is at a distance at most $2 \cdot 2^{j(a-1)}$ of $U_j(\omega)$. In the second case, there is

$$k' \in \{(\lfloor 2^{j(1-a)} \rfloor - 1)\lfloor 2^{aj}/(2N) \rfloor, \ldots, \lfloor 2^{j(1-a)} \rfloor \lfloor 2^{aj}/(2N) \rfloor - 1\}$$

such that $2k'N \in G_j(\omega)$, and similarly, we get that x is at a distance at most $c \cdot 2^{j(a-1)}$ of $U_j(\omega)$, for some constant $c > 0$ depending only on N and a. The density follows. Hence, Baire's theorem gives that the set

$$\bigcap_{n \geq j_0} O_n(\omega)$$

is not empty. If $x \in \bigcap_{n \geq j_0} O_n(\omega)$, for any $n \geq j_0$, there is $j \geq n$ such that $|\varepsilon_{\lambda_j(t)}(\omega)| \geq C\sqrt{j}$, and the conclusion follows.

It remains to show that (35) is the general term of a convergent series. Let us note that the variables $\varepsilon_{\lambda_{j,2kN}}$ for $k \in \{l\lfloor 2^{aj}/(2N) \rfloor, \ldots, (l+1)\lfloor 2^{aj}/2N \rfloor - 1\}$ and $l \in \{0, \ldots, \lfloor 2^{j(1-a)} \rfloor - 1\}$ are independent. Consequently, one has

$$\begin{aligned}
& \mathbb{P}\left(\complement\left(\bigcap_{l \in \{0, \ldots, \lfloor 2^{j(1-a)} \rfloor - 1\}} \mathcal{F}_{j,l}\right)\right) \\
= \; & 1 - \left(1 - \mathbb{P}\left\{\omega \in \Omega : |\varepsilon(\omega)| < C\sqrt{j}\right\}^{\lfloor 2^{aj}/(2N) \rfloor}\right)^{\lfloor 2^{j(1-a)} \rfloor} \\
= \; & 1 - \left(1 - \left(1 - \mathbb{P}\left\{\omega \in \Omega : |\varepsilon(\omega)| \geq C\sqrt{j}\right\}\right)^{\lfloor 2^{aj}/(2N) \rfloor}\right)^{\lfloor 2^{j(1-a)} \rfloor} \\
\leq \; & 1 - \exp\left(2^{j(1-a)} \log(1 - x_j)\right)
\end{aligned} \tag{39}$$

where $\varepsilon \sim \mathcal{N}(0,1)$ and

$$x_j = \left(1 - \mathbb{P}\left\{\omega \in \Omega : |\varepsilon(\omega)| \geq C\sqrt{j}\right)\right)^{\lfloor 2^{aj}/(2N)\rfloor}.$$

Let us note that x_j is always positive and tends to 0 as $j \to +\infty$. Indeed, let us set $C' = (1/2)(2\pi^{-1})^{1/2}$. Using Lemma 2.2.11 and the fact that $\log(1-x) \leq -x$ if $x \in (0,1)$, there exists $J \in \mathbb{N}$ such that for any $j \geq J$, one has

$$\begin{aligned} 0 \leq x_j &\leq (1 - C'\sqrt{j}\exp(-C^2 j/2))^{\lfloor 2^{aj}/(2N)\rfloor} \\ &\leq \exp\left(-\left\lfloor \frac{2^{aj}}{2N}\right\rfloor C'\sqrt{j}\exp(-C^2 j/2)\right) \\ &\leq \exp\left(-C''\sqrt{j}\exp(j(a\log 2 - C^2/2)\right), \end{aligned} \tag{40}$$

where C'' is a strictly positive constant depending only on a, N and C. The expression (40) tends to 0 as $j \to +\infty$, since $C^2 < 2a\log 2$. Moreover, the same argument shows that $2^{j(1-a)}x_j$ tends to 0 as $j \to +\infty$. Using the fact that $\log(1-x) = -x + o(x)$ and $\exp(x) = 1 + x + o(x)$ as $x \to 0$, we obtain that, for any $\epsilon > 0$, Expression (47) is upper bounded by

$$2^{j(1-a)}(\epsilon(x_j + \epsilon x_j) + x_j + \epsilon x_j) \tag{41}$$

for j large enough. Therefore Expression (47) is the general term of a convergent series using Inequality (41) and Inequality (40). ■

Proposition 2.4.12. *There exists an event $\Omega_3^* \subset \Omega$ of probability 1 such that for every $\omega \in \Omega_3^*$ and every non-empty open interval A of $\mathbb{R}$, there is $x(\omega) \in A$ such that*

$$\limsup_{j\to+\infty} \frac{d_j(x(\omega),\omega)}{2^{-j/2}\sqrt{j}} > 0\,.$$

Proof. We proceed as in the proof of Propositions 2.4.8 and 2.4.10, using Lemma 2.4.11, the assumption that the support of the wavelet is included in $[-N,N]$, Remark 2.4.4 and Remark 2.4.5. ■

We are now able to prove Theorem 2.4.1.

Proof of Theorem 2.4.1. From Inequality (22) and Proposition 2.4.2, there exists an event $\Omega_4^* \subseteq \Omega$ of probability 1 such that for any $\omega \in \Omega_4^*$ and for any $x \in \mathbb{R}$, one has

$$\limsup_{j\to+\infty} \frac{d_j(t,\omega)}{2^{-j/2}\sqrt{j}} < +\infty. \tag{42}$$

Let us consider the event

$$\Omega_0^* := \Omega^* \cap \Omega_1^* \cap \Omega_2^* \cap \Omega_3^* \cap \Omega_4^*$$

of probability 1, where the event Ω^* (resp. Ω_1^*, Ω_2^* and Ω_3^*) is the event of Theorem 2.3.6 (resp. Proposition 2.4.8, Proposition 2.4.10 and Proposition 2.4.12). Let us fix $\omega \in \Omega_0^*$ and let us consider a non-empty open interval A of $\mathbb{R}$.

Let us first show that almost every $x \in \mathbb{R}$ is a leader-ordinary point of $B_\cdot(\omega)$. Using Theorem 2.3.6, we know that almost every $x \in \mathbb{R}$ is an ordinary point of $B_\cdot(\omega)$. Together with Proposition 2.4.3 and Proposition 2.4.10, this implies that for almost every $x \in \mathbb{R}$,

$$0 < \limsup_{j \to +\infty} \frac{d_j(t,\omega)}{2^{-j/2}\sqrt{\log j}} < +\infty\,.$$

In particular, there exist leader-ordinary points of $B_\cdot(\omega)$ in A.

Secondly, Proposition 2.4.12 shows that there exists $x_r(\omega) \in A$ such that

$$\limsup_{j \to +\infty} \frac{d_j\big(x_r(\omega),\omega\big)}{2^{-j/2}\sqrt{j}} > 0.$$

This result combined with Equation (42) implies that the point $x_r(\omega)$ is a leader-rapid point of $B_\cdot(\omega)$.

Finally, Theorem 2.3.6 and Proposition 2.4.3 show that there exists $x_s(\omega) \in A$ such that

$$\limsup_{j \to +\infty} \frac{d_j\big(x_s(\omega),\omega\big)}{2^{-j/2}} < +\infty\,.$$

Using Proposition 2.4.8, we see that the point $x_s(\omega)$ is a leader-slow point of $B_\cdot(\omega)$.

■

2.4.3 Some Links between the Behaviours of the Oscillation and the Wavelet Leaders

Theorem 2.4.1 shows that there are (at least) three different behaviours for the amplitude of the wavelet leaders of the Brownian motion and that they correspond to the behaviours of the oscillations. A natural question is to determine, for $x \in \mathbb{R}$ fixed, if the behaviour of $\mathrm{Osc}_{B_\cdot(\omega)}(x,\rho)$ as $\rho \to 0$ is the same as $d_j(x)$ as $j \to +\infty$, and conversely. This section gives a partial answer to this question.

First, let us note that Inequality (2.4.2) directly leads to the following proposition, which is an equivalent of Proposition 2.4.3.

Proposition 2.4.13. *Let Ω_0^* be the event of probability 1 given in Theorem 2.4.1. For any $\omega \in \Omega_0^*$ and for any $x \in \mathbb{R}$, we have*

1. *if x is a leader-ordinary point of $B_\cdot(\omega)$, then*

$$\limsup_{\rho \to 0^+} \frac{\mathrm{Osc}_{B_\cdot(\omega)}(x_o(\omega),\rho)}{\rho^{1/2}\sqrt{\log\log(\rho^{-1})}} > 0\,,$$

2. *if x is a leader-rapid point of $B_\cdot(\omega)$, then*

$$\limsup_{\rho\to 0^+} \frac{\mathrm{Osc}_{B_\cdot(\omega)}(x_o(\omega),\rho)}{\rho^{1/2}\sqrt{\log(\rho^{-1})}} > 0\,,$$

3. *if x is a leader-slow point of $B_\cdot(\omega)$, then*

$$\limsup_{\rho\to 0^+} \frac{\mathrm{Osc}_{B_\cdot(\omega)}(x_o(\omega),\rho)}{\rho^{1/2}} > 0\,.$$

We can now give some links between the behaviours of the oscillations and the amplitude of the wavelet leaders.

Theorem 2.4.14. *Let Ω_0^* be the event of probability 1 given in Theorem 2.4.1 and let us fix $\omega \in \Omega_0^*$.*

1. *For any $x \in \mathbb{R}$,*
   - *if x is a leader-rapid point of $B_\cdot(\omega)$, then x is a rapid point of $B_\cdot(\omega)$,*
   - *if x is a slow point of $B_\cdot(\omega)$, then x is a leader-slow point of $B_\cdot(\omega)$.*
2. *For almost every $x \in \mathbb{R}$, x is an ordinary point and a leader-ordinary point of $B_\cdot(\omega)$.*

Proof. If x is a leader-rapid point, Proposition 2.4.13 and Inequality (22) directly imply that x is a rapid point. If x is a slow point, Proposition 2.4.3 and Proposition 2.4.8 give that x is a leader-slow point. Finally, the result for the ordinary points can be deduced from the last parts of Theorems 2.3.6 and 2.4.1. ■

2.5 From the Brownian Motion in the Schauder Basis to a Multifractal Process

This last section presents a process based on the Lévy-Ciesielski construction (see Section 2.3.2). We modify the decomposition of the Brownian motion in the Schauder basis in order to obtain a multifractal process which shares the same local regularity as the Brownian motion. This is a variant of the multifractional Brownian motion [116, 24]. As for the example of Section 2.1, we use a factor $2^{-H_\lambda j}$, for a well-chosen sequence $(H_\lambda)_{\lambda\in\Lambda}$. This idea comes from a discussion with A. Ayache and is inspired of [38]. Similar approaches using random wavelet-type series can be found in [18, 17] for example.

Notation. Let us denote by $\underline{\mathcal{H}}_K$ the set of the functions from $[0,1]$ to the compact K which are the lower limit of a sequence of continuous functions.

Lemma 2 of [38] implies that for any $H \in \underline{\mathcal{H}}_K$, there exists a sequence $(Q_j)_{j\in\mathbb{N}}$ of polynomials such that

$$\begin{cases} H(t) = \liminf_{j\to+\infty} Q_j(t) & \forall t \in [0,1] \\ ||Q_j'||_\infty \leq j & \forall j \in \mathbb{N} \end{cases}, \tag{43}$$

where Q_j' is the derivative of Q_j.

This leads to the main result of this section.

Theorem 2.5.1. *Let K be a compact of $(-1/2, 1/2)$, $H \in \underline{\mathcal{H}}_K$ and $(Q_j)_{j\in\mathbb{N}}$ be a sequence of polynomials satisfying Relation (43). For any $\lambda_{j,k} \in \Lambda$, set*

$$H_{\lambda_{j,k}} = Q_j(k2^{-j}).$$

Let $(Z_\lambda)_{\lambda\in\Lambda}$ be a sequence of independents real-valued $\mathcal{N}(0,1)$ Gaussian random variables and let us define

$$B_x^H(\omega) = Z_0(\omega)F_0(x) + \sum_{j=0}^{+\infty}\sum_{\lambda\in\Lambda_j} 2^{-jH_\lambda} Z_\lambda(\omega) 2^{j/2} F_\lambda(x), \tag{44}$$

for any $x \in [0,1]$ and any $w \in \Omega$. Then, there exists an event $\Omega^* \subset \Omega$ of probability 1 such that, for any $\omega \in \Omega^*$, we have the following properties:

1. *the function*
$$x \mapsto B_x^H(\omega)$$
is a continuous function defined on $[0,1]$,

2. *we have the following relation:*
$$h_{B_\cdot^H(\omega)}(x) = 1/2 + H(x),$$
for any $x \in [0,1]$,

3. *let $x \in [0,1]$; if there exists $C > 0$ such that*
$$H(x) - Q_j(x) \leq Cj^{-1}, \tag{45}$$
for any $j \in \mathbb{N}$ then there exist a constant $C' > 0$ independent of x such that
$$|B_{x+h}^H(\omega) - B_x^H(\omega)| \leq C' 2^C |h|^{1/2+H(x)} \sqrt{\log |h|^{-1}},$$
for any h in a neighbourhood of 0.

Proof. First, Relation (20) implies that, for any $\epsilon' > 0$, there exists $J \in \mathbb{N}$ such that for any $j \geq J$, $\lambda \in \Lambda_j$ and for any $x \in \lambda$, one has

$$H(x) - H_\lambda = H(x) - Q_j(x) + Q_j(x) - Q_j(k2^{-j}) \leq \epsilon'/2 + j2^{-j} \leq \epsilon'. \quad (46)$$

One gets $\inf K - \epsilon' \leq H_\lambda$, and thus

$$2^{-jH_\lambda} \leq 2^{-j \inf K} 2^{j\epsilon'}. \quad (47)$$

Let us prove the first point of the theorem. Let $\epsilon \in (0, 1/2)$ and choose a constant $C > 0$. Let us define

$$A_j = \{w \in \Omega : \max_{\lambda \in \Lambda_j} |Z_\lambda(\omega)| > C2^{j(\epsilon - \epsilon' + \inf K)}\}.$$

One has

$$\begin{aligned}\mathbb{P}(A_j) &\leq \sum_{\lambda \in \Lambda_j} \mathcal{P}(\{w \in \Omega : |Z_\lambda(\omega)| > C2^{j(\epsilon - \epsilon' + \inf K)}\}) \\ &\leq 2^j \mathbb{P}(\{|Z| > C2^{j(\epsilon - \epsilon' + \inf K)}\},\end{aligned}$$

where $Z \sim \mathcal{N}(0, 1)$. Using Lemma 2.2.11, one has

$$\mathbb{P}(A_j) \leq \sqrt{\frac{2}{\pi C^2}} 2^{j(1 - (\epsilon - \epsilon' + \inf K))} e^{-(C^2 2^{2j(\epsilon - \epsilon' + \inf K)})/2}.$$

Since $\inf K \in (-1/2, 1/2)$, there exists $\epsilon \in (0, 1/2)$ such that $\epsilon - \epsilon' + \inf K > 0$ for ϵ' small enough. In this case,

$$\sum_{j=0}^{+\infty} \mathbb{P}(A_j) < +\infty.$$

It follows from the Borel-Cantelli lemma that

$$\mathbb{P}\left(\limsup_{j \to +\infty} A_j\right) = 0.$$

Hence, the event

$$\Omega^* = \liminf_{j \to +\infty} \{\omega : \max_{\lambda \in \Lambda_j} 2^{-jH_\lambda} |Z_\lambda(\omega)| \leq C2^{j\epsilon}\}$$

has a probability equal to 1. The first point of the theorem is thus proved, thanks to Proposition 2.3.8.

Now, let us prove that $h_f(x) \geq 1/2 + H(x)$. The third point is a particular case of this reasoning. From the Borel-Cantelli lemma, for a constant $C > 0$ large enough, the event

$$\liminf_{j \to +\infty} \{\omega : \max_{\lambda \in \Lambda_j} |Z_\lambda(\omega)| \leq C\sqrt{j}\}$$

has probability 1. Let ω be a element of this event. There thus exists $J \in \mathbb{N}$ such that for any $j \geq J$,

$$\max_{\lambda \in \Lambda_j} |Z_\lambda(\omega)| \leq C\sqrt{j}.$$

Let $x \in [0,1]$, $\epsilon' > 0$ and suppose that J is large enough in order for Inequality (46) to be satisfied. Let h be a real number such that $x, x+h \in \lambda$, for some $\lambda \in \Lambda_J$, and let $l > J$ be such that $2^{-l} < |h| \leq 2^{-l+1}$. By construction, for any $j \leq l$, there exists a unique dyadic interval $\lambda_j(x) \in \Lambda_j$ such that $x, x+h \in \lambda_j(x)$. One has

$$\begin{aligned}
&|B^H_{x+h}(\omega) - B^H_x(\omega)| \leq \\
&Z_0(\omega)|h| + C_J|h| && (48)\\
&+ \sum_{j=J+1}^{l-1} 2^{-jH_{\lambda_j(x)}} |Z_{\lambda_j(x)}(\omega)| 2^{j/2} |F_{\lambda_j(x)}(x+h) - F_{\lambda_j(x)}(x)| && (49)\\
&+ \sum_{j=l}^{+\infty} \sum_{\lambda \in \Lambda_j} 2^{-jH_\lambda} |Z_\lambda(\omega)| 2^{j/2} |F_\lambda(x+h) - F_\lambda(x)|, && (50)
\end{aligned}$$

for some constant C_J depending only on J.

By eventually reducing h, we can suppose that the terms in (48) are smaller than

$$C|h|^{1/2+\sup K}\sqrt{\log|h|^{-1}} \leq C|h|^{1/2+H(t)}\sqrt{\log|h|^{-1}},$$

for some constant $C > 0$ independent of t and h.

Using Inequality (46) and since the supports of the functions $F_{\lambda_j(x)}$ are included in $\lambda_j(x)$, each term in (49) is smaller than

$$\begin{aligned}
|h| \sum_{j=J+1}^{l-1} 2^{j(1/2-H_{\lambda_j(x)})} \max_{\lambda \in \Lambda_j} |Z_\lambda(w)| &\leq C|h| \sum_{j=J+1}^{l} 2^{j(1/2-H(t)+\epsilon')}\sqrt{j} \\
&\leq C'|h| 2^{l(1/2-H(t)+\epsilon')}\sqrt{l} \qquad (51)\\
&\leq C'|h|^{1/2+H(t)-\epsilon'}\sqrt{\log|h|^{-1}},
\end{aligned}$$

where $C' > 0$ is a constant that does not depend on t or l. The last inequality is valid by definition of l.

For any $j \geq l$, there exist unique dyadic intervals $\lambda_j(x), \lambda_j(x+h) \in \Lambda_j$ such that $x \in \lambda_j(x)$ and $x+h \in \lambda_j(x+h)$. Since $|F_\lambda| \leq 2^{-j-1}$, the terms in (50) are smaller than

$$\begin{aligned}
&\sum_{j=l}^{+\infty} 2^{-j/2} \max_{\lambda \in \Lambda_j} |Z_\lambda(\omega)| (2^{-jH_{\lambda_j(x)}} + 2^{-jH_{\lambda_j(x+h)}}) \\
&\leq C'' 2^{-l/2} (2^{-lH_{\lambda_l(x)}} + 2^{-jH_{\lambda_l(x+h)}})\sqrt{l} \\
&\leq C'' 2^{-l(1/2+H(t)-\epsilon')}\sqrt{l}, && (52)
\end{aligned}$$

where $C'' > 0$ is a constant independent of t and l. The last inequality is obtained by remarking that $\lambda_l(x+h) \in N(\lambda_l(x))$. Since the terms in (50) are smaller than

$$C''|h|^{1/2+H(t)-\epsilon'}\sqrt{\log|h|^{-1}},$$

there exists a constant C''' independent of x such that for any $\epsilon' > 0$, one has

$$|B^H_{x+h}(\omega) - B^H_x(\omega)| \leq C'''|h|^{1/2+H(x)-\epsilon'}\sqrt{\log|h|^{-1}}.$$

We deduce that $h_f(x) \geq 1/2 + H(x)$. Now, using hypothesis (45), we obtain

$$H(x) - H_{\lambda_l(x)} \leq (C+1)l^{-1}.$$

We can directly take $\epsilon' = (C+1)l^{-1}$ in Inequalities (51) and (52) to obtain the third point of the theorem.

To conclude, it remains to prove that $h_f(x) \leq 1/2 + H(x)$. Using Relations (20), for any $J \in \mathbb{N}$ and for any $\epsilon > 0$, there exists $j_J \geq J$ such that

$$Q_{j_J}(x) \leq H(x) + \epsilon \qquad \text{and} \qquad |H_{\lambda_{j_J}(x)} - Q_{j_J}(x)| \leq j_J 2^{-j_J} \leq \epsilon.$$

Moreover, the Borel-Cantelli lemma applied to the independent events

$$A_{j_J} = \{\omega : |Z_{\lambda_{j_J}(x)}(\omega)| > 2^{-\epsilon j_J}\}$$

implies that, almost surely, for any $J \in \mathbb{N}$, there exists $J' > J$ such that $|Z_{\lambda_{j_{J'}}(x)}(\omega)| > 2^{-\epsilon j_{J'}}$. We thus have

$$\begin{aligned} 2^{-j_{J'}H_{\lambda_{j_{J'}}(x)}}|Z_{\lambda_{j_{J'}}(x)}(\omega)|2^{-j_{J'}/2} &\geq 2^{-j_{J'}(j_{J'}2^{-j_{J'}}+\epsilon+H(t)+1/2)}|Z_{j_{J'},k}(\omega)| \\ &> 2^{-j_{J'}(1/2+H(t)+3\epsilon)}. \end{aligned}$$

We can conclude using point (2) of Proposition 2.3.8. ■

The next proposition studies the local regularity of the process B^H.

Proposition 2.5.2. *Under Hypothesis (45), there exists an event $\Omega^* \subset \Omega$ of probability 1 such that, for any $\omega \in \Omega^*$ and for almost every $x \in [0,1]$, there exists a constant $C > 0$ such that*

$$|B^H_{x+h}(\omega) - B^H_x(\omega)| \leq C|h|^{1/2+H(x)}\sqrt{\log\log|h|^{-1}},$$

for any h in a neighbourhood of 0.

Proof. We will use the same notations as in the proof of the previous theorem. Let us fix $x \in [0,1]$ and recall that, for any $j \in J$, there exists a unique dyadic interval $\lambda_j(x) \in \Lambda_j$ such that $x \in \lambda_j(x)$. From the Borel-Cantelli lemma, for a constant $C > 0$ large enough, the event

$$\liminf_{j\to+\infty}\{\omega : |Z_{\lambda_j(x)}(\omega)| \leq C\sqrt{\log j}\}$$

has probability 1. Using the same argument as in the previous proof, we obtain that, for any $x \in [0,1]$, there exists almost surely a constant $C > 0$ such that

$$|B^H_{x+h}(\omega) - B^H_x(\omega)| \leq C|h|^{1/2+H(x)}\sqrt{\log\log|h|^{-1}},$$

for any h small enough. Fubini's theorem allows to conclude. ■

Remark 2.5.3. If H is the zero function, then B^H is the classical Brownian motion. In this case, Section 2.4 shows that almost surely, $d_j(x_0)$ behaves like $2^{-j/2}\sqrt{\log j}$ as $j \to +\infty$, for almost every x_0. In the general case, the result is not still established because some problems of dependence between the wavelet coefficients appear. Chapter 5 shows that on several numerical simulations, the general case seems to behave like the Brownian motion through its wavelet coefficients.

Chapter 3

A Generalisation of the S^ν spaces with the Help of the Admissible Sequences

As already mentioned, $||f - P_{x_0}||_{L^\infty(B(x_0,2^{-j}))}$ behaves not necessarily like $2^{-h_f(x_0)j}$ as $j \to +\infty$; some (logarithmic) corrections can appear. In order to characterise the Hölder behaviour in a better way, the Besov and Hölder spaces have been generalised with the help of admissible sequences (see Section 1.6.3).

Let us recall that the wavelet coefficients $c = (c_\lambda)_{\lambda\in\Lambda}$ belong to S^ν if and only if, for any $h \in \mathbb{R}$, $\epsilon > 0$, $C > 0$, there exists $J \in \mathbb{N}$ such that, for any $j \geq J$, the number of $\lambda \in \Lambda_j$ for which

$$|c_\lambda| \geq 2^{-hj} \tag{53}$$

is smaller than $2^{(\nu(h)+\epsilon)j}$. The previous chapter shows that the wavelets allow an efficient study of the Hölderian behaviour of some classes of functions. Consequently, it is natural to generalise the spaces S^ν using the same idea as for the Besov and Hölder spaces: to replace the sequence $(2^{-hj})_{j\in\mathbb{N}}$ of Inequality (53) by a more general sequence σ. This chapter studies these new spaces from a theoretical point of view and Chapter 4 states a new numerical method based on these new spaces to analyse the regularity of signals.

The first section consists in checking that the topological properties holding for the usual S^ν spaces are preserved. Moreover, it is crucial to show that different wavelet bases give rise to identical spaces. Therefore, the second section shows the robustness of these new spaces. Finally, because S^ν is relying on Besov spaces, it is also natural to study the link between these new spaces and the generalised Besov spaces, which is the subject of the third section.

The results presented in this chapter are a collaboration with S. Nicolay.

This chapter is structured as follows:

3.1 Definition and First Properties

Throughout this chapter, ν refers to a right-continuous increasing function for which there exists $h_{\min} \in \mathbb{R}$ such that $\nu(h) = -\infty$ if $h < h_{\min}$ and $\nu(h) \in [0, n]$ if $h \geq h_{\min}$. Let us recall that Λ is the set of dyadic cubes included in $[0,1]^n$ and Λ_j is the set of those of size 2^{-j}.

This section defines the spaces $S^{\nu,\sigma^{(\cdot)}}$ as a generalisation of the spaces S^ν and shows that the basic topological properties of S^ν are preserved, if we put a few natural hypothesis on the sequences $\sigma^{(\cdot)}$. The strategy to define a topology on $S^{\nu,\sigma^{(\cdot)}}$ is the same as for S^ν [12]. At the end of this section, an equivalent definition of $S^{\nu,\sigma^{(\cdot)}}$ using a generalised profile is given.

Let us recall that the space S^ν is the set of complex sequences $c = (c_\lambda)_{\lambda\in\Lambda}$ such that for any $h \in \mathbb{R}$, $\epsilon > 0$ and $C > 0$, there exists $J > 0$ for which for any $j \geq J$, we have

$$\#E_j(C,h)(c) \leq 2^{(\nu(h)+\epsilon)j},$$

where

$$E_j(C,h)(c) = \{\lambda \in \Lambda_j : |c_\lambda| \geq C2^{-hj}\}. \tag{54}$$

As mentioned in the introduction of this chapter, the generalisation of these spaces is based on the same idea as for the Besov and Hölder spaces: to replace the sequence $(2^{-hj})_{j\in\mathbb{N}}$ in Relation (54) by a more general sequence σ.

Definition 3.1.1. For any $h \in \mathbb{R}$, let $\sigma^{(h)} = (\sigma_j^{(h)})_{j\in\mathbb{N}}$ be a sequence of positive real numbers. The space $S^{\nu,\sigma^{(\cdot)}}$ is the set of complex sequences $c = (c_\lambda)_{\lambda\in\Lambda}$ such that for any $h \in \mathbb{R}$, $\epsilon > 0$ and $C > 0$, there exists $J > 0$ for which for any $j \geq J$, we have

$$\#E_j(C,\sigma^{(h)})(c) \leq 2^{(\nu(h)+\epsilon)j},$$

where

$$E_j(C,\sigma^{(h)})(c) = \{\lambda \in \Lambda_j : |c_\lambda| \geq C\sigma_j^{(h)}\}.$$

To define a topology on these vector spaces, let us introduce some auxiliary spaces.

Definition 3.1.2. Let us set $h \in \mathbb{R}$ and $\beta \in \mathbb{R}\cup\{-\infty\}$. The space $E(\sigma^{(h)},\beta)$ is the set of complex sequences $c = (c_\lambda)_{\lambda\in\Lambda}$ such that there exist $C, C' > 0$ for which we have

$$\#E_j(C,\sigma^{(h)}) \leq C'2^{\beta j},$$

for any $j \in \mathbb{N}$. A metric $d_{\sigma^{(h)},\beta}$ is defined on this space as

$$d_{\sigma^{(h)},\beta}(c,d) = \inf\{C+C' : C, C' \geq 0\ \#E_j(C,\sigma^{(h)})(c-d) \leq C'2^{\beta j} \text{ for any } j \in \mathbb{N}\}.$$

Let us give the basic properties of these spaces.

Proposition 3.1.3. *We have the following properties:*

1. *the space $E(\sigma^{(h)}, \beta)$ is a vector space,*
2. *the sum is a continuous operation in $(E(\sigma^{(h)}, \beta), d_{\sigma^{(h)},\beta})$, while the product is not necessarily continuous,*
3. *the metric $d_{\sigma^{(h)},\beta}$ is invariant by translation and satisfies the inequality*
$$d_{\sigma^{(h)},\beta}(\kappa c, 0) \leq \sup\{1, |\lambda|\} d_{\sigma^{(h)},\beta}(c, 0),$$
for any $\kappa \in \mathbb{C}$,
4. *if $\beta' \leq \beta$ and if there exists $J \in \mathbb{N}$ such that $\sigma_j^{(h')} \leq \sigma_j^{(h)}$ for any $j \geq J$, then $E(\sigma^{(h')}, \beta')$ is included in $E(\sigma^{(h)}, \beta)$,*
5. *suppose that*
$$\sigma_j^{(h')}/\sigma_j^{(h)} \to 0 \quad as \quad j \to +\infty$$
and $\beta' < \beta$. If the sequence $(\kappa_m)_{m\in\mathbb{N}}$ converges to κ in $\mathbb{C}$ and if $(c^{(m)})_{m\in\mathbb{N}}$ is a sequence of $E(\sigma^{(h)}, \beta)$ which converges to $c \in E(\sigma^{(h')}, \beta')$ for $d_{\sigma^{(h)},\beta}$, then the sequences $(\kappa_m c^{(m)})_{m\in\mathbb{N}}$ converges to κc for $d_{\sigma^{(h)},\beta}$.

Proof. The first four points are straightforward; let us note that the product is not necessarily continuous because it was already the case for the S^ν spaces [12]. It remains to prove the last point. From the properties of the metric $d_{\sigma^{(h)},\beta}$, we obtain

$$d_{\sigma^{(h)},\beta}(\kappa_m c^{(m)}, \kappa c^{(m)}) \leq \sup\{1, |\kappa_m|\} d_{\sigma^{(h)},\beta}(c^{(m)} - c, 0) + d_{\sigma^{(h)},\beta}((\kappa_m - \kappa)c, 0).$$

So, it suffices to show that $d_{\sigma^{(h)},\beta}((\kappa_m - \kappa)c, 0)$ converges to 0 as $m \to +\infty$. There exist $C, C' \geq 0$ such that

$$\#\{\lambda \in \Lambda_j : |c_\lambda| \geq C\sigma_j^{(h')}\} \leq C' 2^{\beta' j},$$

for any $j \in \mathbb{N}$. Let us set $\epsilon > 0$ and $M \in \mathbb{N}$ such that $|\kappa_m - \kappa| < 1$, for any $m \geq M$. There exists $J \geq 0$ such that $C' 2^{\beta' j} \leq \epsilon 2^{\beta j}$ and $C\sigma_j^{(h')} \leq \epsilon \sigma_j^{(h)}$, for any $j \geq J$. In this case, we have

$$\begin{aligned}\#\{\lambda \in \Lambda_j : |(\kappa_m - \kappa)c_\lambda| \geq \epsilon\sigma_j^{(h)}\} &\leq \#\{\lambda \in \Lambda_j : |c_\lambda| \geq C\sigma_j^{(h')}\} \\ &\leq \epsilon 2^{\beta j},\end{aligned}$$

for any $j \geq J$. Besides, we can suppose that $|(\kappa_m - \kappa)c_\lambda| < \epsilon\sigma_j^{(h)}$ for any $\lambda \in \Lambda_j$, $j < J$ and $m \geq M$. With this hypothesis, we get

$$d_{\sigma^{(h)},\beta}((\kappa_m - \kappa)c, 0) \leq 2\epsilon,$$

for any $m \geq M$. ∎

Proposition 3.1.4. *The space $(E(\sigma^{(h)},\beta), d_{\sigma^{(h)},\beta})$ is complete.*

Proof. Let $(c^{(m)})_{m\in\mathbb{N}}$ be a Cauchy sequence of $E(\sigma^{(h)},\beta)$. Let us first show that the sequence $(c_\lambda^{(m)})_{m\in\mathbb{N}}$ is a pointwise Cauchy sequence for any fixed $\lambda\in\Lambda$. Let us set $\epsilon>0$, $j\in\mathbb{N}$ and $\epsilon' = \inf\{\epsilon(\sigma_j^{(h)})^{-1}, 1/2\ 2^{\beta j}\}$. Since $(c^{(m)})_{m\in\mathbb{N}}$ is a Cauchy sequence, there exists $J>0$ such that, for any $p,q\geq J$,

$$\#\{\lambda\in\Lambda_j : |c_\lambda^{(p)} - c_\lambda^{(q)}| \geq \epsilon'\sigma_j^{(h)}\} \leq \epsilon' 2^{\beta j},$$

i.e. $|c_\lambda^{(p)} - c_\lambda^{(q)}| \leq \epsilon$ for any $\lambda\in\Lambda_j$.

Therefore, for any $\lambda\in\Lambda$, there exists c_λ such that $c_\lambda^{(m)}\to c_\lambda$ as $m\to+\infty$. It remains to prove that $c^{(m)}\to c$ in $E(\sigma^{(h)},\beta)$ as $m\to+\infty$. If $\epsilon>0$, there exists M such that

$$\forall j\geq 0,\ \forall p,q\geq M,\ \#\{\lambda\in\Lambda_j : |c_\lambda^{(p)} - c_\lambda^{(q)}| \geq \epsilon\sigma_j^{(h)}\} \leq \epsilon 2^{\beta j},$$

which implies

$$\forall p,q\geq M,\ c^{(q)} \in \{d : \#\{\lambda\in\Lambda_j : |c_\lambda^{(p)} - d_\lambda| \geq \epsilon'\sigma_j^{(h)}\} \leq \epsilon 2^{\beta j}\ \forall j\geq 0\}.$$

As these sets are closed for the pointwise convergence, we get that

$$\forall p\geq M,\ c \in \{d : \#\{\lambda\in\Lambda_j : |c_\lambda^{(p)} - d_\lambda| \geq \epsilon'\sigma_j^{(h)}\} \leq \epsilon 2^{\beta j}\ \forall j\geq 0\}.$$

We thus have $c\in E(\sigma^{(h)},\beta)$ (and $c^{(m)}$ converges to c in $E(\sigma^{(h)},\beta)$). ■

The next theorem gives a link between the space $S^{\nu,\sigma^{(\cdot)}}$ and the spaces $E(\sigma^{(h)},\beta)$. This will allow us to define a topology on $S^{\nu,\sigma^{(\cdot)}}$.

Theorem 3.1.5. *Suppose that $h<h'$ implies*

$$\sigma_j^{(h')}/\sigma_j^{(h)} \to 0 \quad as \quad j\to+\infty.$$

For any sequence $(h_n)_{n\in\mathbb{N}}$ dense in $\mathbb{R}$ and any sequence $(\epsilon_m)_{m\in\mathbb{N}}$ of strictly positive real numbers which converges to 0, we have

$$S^{\nu,\sigma^{(\cdot)}} = \bigcap_{m\in\mathbb{N}}\bigcap_{n\in\mathbb{N}} E(\sigma^{(h_n)}, \nu(h_n)+\epsilon_m).$$

Proof. We directly have that $S^{\nu,\sigma^{(\cdot)}}$ is included in $E(\sigma^{(h_n)},\nu(h_n)+\epsilon_m)$, for any $m,n\in\mathbb{N}$. Let us show that

$$\bigcap_{m\in\mathbb{N}}\bigcap_{n\in\mathbb{N}} E(\sigma^{(h_n)}, \nu(h_n)+\epsilon_m)$$

is a subset of $S^{\nu,\sigma^{(\cdot)}}$. Let c be an element of the intersection and let $h \in \mathbb{R}$, $\epsilon > 0$, $C > 0$. For any $m, n \in \mathbb{N}$, there exist $C_{n,m}, C'_{n,m} \geq 0$ such that

$$\#\{\lambda \in \Lambda_j : |c_\lambda| \geq C_{n,m}\sigma_j^{(h_n)}\} \leq C'_{n,m} 2^{(\nu(h_n)+\epsilon_m)j},$$

for any $j \in \mathbb{N}$. Let $m \in \mathbb{N}$ be such that $2\epsilon_m < \epsilon$.

If $\nu(h) = -\infty$ let us take $n \in \mathbb{N}$ such that $h_n \in (h, h_{\min})$. If $\nu(h) \in \mathbb{R}$, let us take $n \in \mathbb{N}$ such that $h_n > h$ and $\nu(h) < \nu(h_n) < \nu(h) + \epsilon_m$. In any case, there exists $J_{n,m} \in \mathbb{N}$ such that $C_{n,m}\sigma_j^{(h_n)} \leq C\sigma_j^{(h)}$ and $C'_{n,m} 2^{(\nu(h_n)+\epsilon_m)j} \leq 2^{(\nu(h)+\epsilon)j}$, for any $m \geq M$ and $j \geq J_{n,m}$. We thus have

$$\begin{aligned}\#\{\lambda \in \Lambda_j : |c_\lambda| \geq C\sigma_j^{(h)}\} &\leq \#\{\lambda \in \Lambda_j : |c_\lambda| \geq C_{n,m}\sigma_j^{(h_n)}\} \\ &\leq 2^{(\nu(h)+\epsilon)j},\end{aligned}$$

for any $j \geq J_{n,m}$, which implies $c \in S^{\nu,\sigma^{(\cdot)}}$. ■

Let us recall a classical topological property which be useful to define a metric on $S^{\nu,\sigma^{(\cdot)}}$.

Proposition 3.1.6. *[86] If (E_m, d_m) is a metric space for any $m \in \mathbb{N}$, then*

$$d : (e, f) \mapsto \sum_{m=1}^{+\infty} 2^{-m} \frac{d_m(e, f)}{1 + d_m(e, f)}$$

is a metric on $E = \cap_{m\in\mathbb{N}} E_m$. Moreover, for any $m \in \mathbb{N}$, the projection

$$i_m : (E, d) \to (E_m, d_m)$$

is continuous and the topology induced by d is the weakest topology on E which satisfies this property. Finally, a sequence is a Cauchy sequence (resp. converges to e) in (E, d) if and only if for any $m \in \mathbb{N}$, it is also a Cauchy sequence (resp. it also converges to e) in (E_m, d_m).

Theorem 3.1.7. *Under the hypothesis of Theorem 3.1.5, if we set*

$$d_{m,n} = d_{\sigma^{(h_n)},\nu(h_n)+\epsilon_m},$$

then the application

$$d : (c, d) \in S^{\nu,\sigma^{(\cdot)}} \times S^{\nu,\sigma^{(\cdot)}} \mapsto \sum_{m=1}^{+\infty} \sum_{n=1}^{+\infty} \frac{1}{2^{m+n}} \frac{d_{m,n}(c, d)}{1 + d_{m,n}(c, d)}$$

is a metric on $S^{\nu,\sigma^{(\cdot)}}$. This application is invariant by translation and the space $(S^{\nu,\sigma^{(\cdot)}}, d)$ is a complete topological vector space. The induced topology is independent of the sequences $(h_n)_{n\in\mathbb{N}}$ and $(\epsilon_m)_{m\in\mathbb{N}}$.

Proof. We will prove that the product is continuous and that the topology is complete and independent of the sequences $(h_n)_{n\in\mathbb{N}}$ and $(\epsilon_m)_{m\in\mathbb{N}}$, the other properties being straightforward.

First, let us show that if $\lambda_l \to \lambda$ in $\mathbb{C}$ and if $c^{(l)} \to c$ in $S^{\nu,\sigma^{(\cdot)}}$, then $\lambda_l c^{(l)} \to \lambda c$ in $E(\sigma^{(h_n)}, \nu(h_n)+\epsilon_m)$, for any $n, m \in \mathbb{N}$. Let us set $n, m \in \mathbb{N}$; if $\nu(h_n) = -\infty$, then there exists $p \in \mathbb{N}$ such that $h_p \in (h_n, h_{\min})$. If $\nu(h_n) \in \mathbb{R}$, there exist $p, q \in \mathbb{N}$ such that $h_p > h_n$ and $\nu(h_p) + \epsilon_q < \nu(h_n) + \epsilon_m$. In any case, we have $c^{(l)} \to c$ in $E(\sigma^{(h_n)}, \nu(h_n)+\epsilon_m)$ and $c \in E(\sigma^{(h_p)}, \nu(h_p)+\epsilon_q)$. Using Proposition 3.1.3, we have $\lambda_l c^{(l)} \to \lambda c$ in $E(\sigma^{(h_n)}, \nu(h_n)+\epsilon_m)$, which implies that the product is continuous.

Now, let us prove that the topology is independent of the sequences $(h_n)_{n\in\mathbb{N}}$ and $(\epsilon_m)_{m\in\mathbb{N}}$. We have to show that if $c^{(l)} \to c$ in $S^{\nu,\sigma^{(\cdot)}}$, then $c^{(l)} \to c$ in $E(\sigma^{(h)}, \nu(h)+\epsilon)$, for any $h \in \mathbb{R}$ and $\epsilon > 0$. Let h be a real number and $\epsilon > 0$. Since $c^{(l)} \to c$ in $S^{\nu,\sigma^{(\cdot)}}$, there exist $C_{n,m}, C'_{n,m} \geq 0$ such that

$$\#\{\lambda \in \Lambda_j : |c_\lambda^{(l)} - c_\lambda| \geq C_{n,m}\sigma_j^{(h_n)}\} \leq C'_{n,m} 2^{(\nu(h_n)+\epsilon_m)j},$$

for any $j \in \mathbb{N}$. Let δ be a strictly positive number and take $m \in \mathbb{N}$ such that $2\epsilon_m < \epsilon$. Using the same arguments as in the proof of Theorem 3.1.5, there exist $n \in \mathbb{N}$ and $J_{n,m} \in \mathbb{N}$ such that $C_{n,m}\sigma_j^{(h_n)} \leq \delta\sigma_j^{(h)}$ and

$$C'_{n,m} 2^{(\nu(h_n)+\epsilon_m)j} \leq \delta 2^{(\nu(h)+\epsilon)j},$$

for any $j \geq J_{n,m}$. We get

$$\begin{aligned}\#\{\lambda \in \Lambda_j : |c_\lambda^{(l)} - c_\lambda| \geq \delta\sigma_j^{(h)}\} &\leq \#\{\lambda \in \Lambda_j : |c_\lambda^{(l)} - c_\lambda| \geq C_{n,m}\sigma_j^{(h_n)}\} \\ &\leq \delta 2^{(\nu(h)+\epsilon)j},\end{aligned}$$

for any $j \geq J_{n,m}$. We thus obtain $d_{\sigma^{(h)},\nu(h)+\epsilon}(c_\lambda^{(l)}, c_\lambda) \leq 2\delta$.

Finally, let us show that the topology is complete. Let $(c^{(l)})_{l\in\mathbb{N}}$ be a Cauchy sequence of $S^{\nu,\sigma^{(\cdot)}}$. This sequence is a Cauchy sequence of $E(\sigma^{(h_n)}, \nu(h_n)+\epsilon_m)$, for any $n, m \in \mathbb{N}$. By Proposition 3.1.4, there exists a sequence $c^{(m,n)}$ such that $(c^{(l)})_{l\in\mathbb{N}}$ converges to $c^{(m,n)}$ in $E(\sigma^{(h_n)}, \nu(h_n)+\epsilon_m)$, for any n, m. Similar arguments as in the first part of the proof of Proposition 3.1.4 show that, if a sequence $(c^l)_{l\in\mathbb{N}}$ converges to c in $E(\sigma^{(h)}, \beta)$, then $(c_\lambda^{(l)})_{l\in\mathbb{N}}$ converges to c_λ in $\mathbb{C}$ for any $\lambda \in \Lambda$. This implies the equality $c^{(m,n)} = c^{(m',n')}$ is valided, for any $m, m', n, n' \in \mathbb{N}$. ∎

To finish this section, let us now give another definition of $S^{\nu,\sigma^{(\cdot)}}$ by introducing a new notion.

Definition 3.1.8. The *generalised wavelet profile* of a sequence c is defined as

$$\nu_{c,\sigma^{(\cdot)}} : h \in \mathbb{R} \mapsto \lim_{\epsilon\to 0^+} \limsup_{j\to+\infty} \frac{\log \#E_j(1, \sigma^{(h+\epsilon)})(c)}{\log 2^j}.$$

This definition is well-founded if we suppose that for any $h < h'$ there exists $J \in \mathbb{N}$ such that $\sigma_j^{(h')} \leq \sigma_j^{(h)}$ for any $j \geq J$.

The following proposition gives a few properties of the function $\nu_{c,\sigma^{(\cdot)}}$ and leads to an alternative definition of $S^{\nu,\sigma^{(\cdot)}}$.

Proposition 3.1.9. *Suppose that $h < h'$ implies $\sigma_j^{(h')}/\sigma_j^{(h)} \to 0$ as $j \to +\infty$. We have the following properties:*

1. *the function $\nu_{c,\sigma^{(\cdot)}}$ is right-continuous and increasing; moreover, we have $\nu_{c,\sigma^{(\cdot)}}(h) \in [0, n] \cup \{-\infty\}$,*
2. *a sequence c belongs to $S^{\nu,\sigma^{(\cdot)}}$ if and only if $\nu_{c,\sigma^{(\cdot)}}(h) \leq \nu(h)$ for any $h \in \mathbb{R}$,*
3. *if for any $h_1 < h_2$, we have $\sigma_j^{(h_2)} < \sigma_j^{(h_1)}$ for any $j \in \mathbb{N}$, then there exists $c \in S^{\nu,\sigma^{(\cdot)}}$ such that $\nu_{c,\sigma^{(\cdot)}} = \nu$.*

Proof. The first property is immediate. Let c be a sequence of $S^{\nu,\sigma^{(\cdot)}}$ and $h \in \mathbb{R}$. For any $\epsilon > 0$, there exists $J \in \mathbb{N}$ such that

$$\#E_j(1, \sigma^{(h+\epsilon)})(c) \leq 2^{(\nu(h+\epsilon)+\epsilon)j},$$

for any $j \geq J$; we thus have $\nu_{c,\sigma^{(\cdot)}}(h) \leq \nu(h)$.

Let c be a sequence such that $\nu_{c,\sigma^{(\cdot)}} \leq \nu$ and let $h \in \mathbb{R}$, $\epsilon > 0$ and $C > 0$. There exist $\epsilon' > 0$, $J \in \mathbb{N}$ such that for any $\epsilon'' < \epsilon'$ and $j \geq J$, we have

$$\frac{\log \#E_j(1, \sigma^{(h+\epsilon'')}(c)}{\log 2^j} \leq \nu(h) + \epsilon,$$

which gives $\#E_j(1, \sigma^{(h+\epsilon'')}) \leq 2^{(\nu(h)+\epsilon)j}$. We can suppose that $\sigma_j^{(h+\epsilon'')} \leq C\sigma_j^{(h)}$ for any $j \geq J$, so that $\#E_j(C, \sigma^{(h)})(c) \leq 2^{(\nu(h)+\epsilon)j}$.

Now, let us construct a sequence $c \in S^{\nu,\sigma^{(\cdot)}}$ such that $\nu_{c,\sigma^{(\cdot)}} = \nu$. Let $(h_m)_{m\in\mathbb{N}}$ be a dense sequence of $[h_{\min}, +\infty)$ and let $(c^{(m)})_{m\in\mathbb{N}}$ be a sequence defined as

$$c^{(m)}_{\lambda_{j,k}} = \begin{cases} \sigma_{j+m}^{(h_m)} & \text{for } \lfloor 2^{\nu(h_m)j} \rfloor \text{ values of } k \\ 0 & \text{else} \end{cases}.$$

Next, we define c by

$$c_{\lambda_{j,k}} = \begin{cases} 0 & \text{if } k = 0 \\ c^{(j-l)}_{\lambda_{l,k-2^l}} & \text{if } k \in \{2^l, \ldots, 2^{l+1} - 1\} \text{ with } l \in \{0, \ldots, j\} \end{cases}.$$

Let us set $h < h_{\min}$. We have

$$\nu_{c,\sigma^{(\cdot)}}(h) = \lim_{\epsilon\to 0^+} \limsup_{j\to+\infty} \frac{\log \#\{\lambda \in \Lambda_j : |c_\lambda| \geq \sigma_j^{(h)}\}}{\log 2^j}$$

and for any $\lambda_{j,k} \in \Lambda$, there exists $m \in \{0, \dots, j\}$ such that

$$c_{\lambda_{j,k}} = c^{(m)}_{\lambda_{j-m,k-2^{j-m}}} = (\sigma_j^{(h_m)} \text{ or } 0).$$

So, using the last hypothesis, we get $\nu_{c,\sigma^{(\cdot)}}(h) = -\infty$. To conclude, it remains to prove that $\nu_{c,\sigma^{(\cdot)}}(h_m) = \nu(h_m)$ for any $m \in \mathbb{N}$.

Let m be a natural number and let $\epsilon > 0$. For any $j \geq m$, we have $\sigma_j^{(h_m)} \geq \sigma_j^{(h_m+\epsilon)}$ and $c_{\lambda_{j,k}}$ is equal to $\sigma_j^{(h_m)}$ for $\lfloor 2^{\nu(h_m)(j-m)} \rfloor$ values of k. So, we obtain

$$\limsup_{j\to+\infty} \frac{\log \lfloor 2^{\nu(h_m)(j-m)} \rfloor}{\log 2^j} \leq \limsup_{j\to+\infty} \frac{\log \#\{\lambda \in \Lambda_j : |c_\lambda| \geq \sigma_j^{(h_m+\epsilon)}\}}{\log 2^j},$$

which gives $\nu(h_m) \leq \nu_{c,\sigma^{(\cdot)}}(h_m)$. Besides, we have, for any $j \geq m$,

$$\begin{aligned}
\#\{\lambda \in \Lambda_j : |c_\lambda| \geq \sigma_j^{(h_m+\epsilon)}\} &\leq \sum_{\substack{l=1 \\ h_l \leq h_m+\epsilon}}^{j} 2^{\nu(h_l)(j-l)} \\
&\leq 2^{\nu(h_m+\epsilon)j} \sum_{\substack{l=1 \\ h_l \leq h_m+\epsilon}}^{j} 2^{-l\nu(h_l)} \\
&\leq 2^{\nu(h_m+\epsilon)j} j,
\end{aligned}$$

which allows us to write $\nu_{c,\sigma^{(\cdot)}}(h_m) \leq \nu(h_m)$. ■

3.2 Robustness

Until now, we have considered the spaces $S^{\nu,\sigma^{(\cdot)}}$ as sequence spaces, but we should keep in mind that such a sequence represents wavelet coefficients and thus a function. To associate these spaces to functions, we have to check that the definition does not depend on the chosen wavelet basis. This section shows this independence for the wavelets belonging to the Schwartz class, i.e. the wavelets infinitely differentiable whose derivatives are rapidly decreasing. In order to achieve this, the sequences $\sigma^{(h)}$ are supposed admissible. This assumption is natural because all generalisations of function spaces that characterise the regularity of functions (see Section 1.6.3) also use this hypothesis.

Let us now state definitions and properties related to important classes of linear operators in the context of wavelet bases [66, 105].

Definition 3.2.1. For $\gamma > 0$, we set

$$w_\gamma(\lambda, \lambda') = \frac{2^{-(\gamma+d+1)|j-j'|}}{(1 + 2^{\inf\{j,j'\}}|2^{-j}k - 2^{-j'}k'|)^{\gamma+d+1}},$$

for any $\lambda, \lambda' \in \Lambda$. The space $\mathscr{A}_\gamma$ is the set of matrix $A = (A_{\lambda,\lambda'})_{\lambda,\lambda'\in\Lambda}$ for which there exists $C \geq 0$ such that

$$|A_{\lambda,\lambda'}| \leq C w_\gamma(\lambda, \lambda'),$$

for any $\lambda, \lambda' \in \Lambda$. The infimum of these constants is denoted by $\|A\|_\gamma$.
The matrix A is *almost diagonal* (resp. *quasidiagonal*) if $A \in \mathscr{A}_\gamma$ for any $\gamma > 0$ (resp. A is invertible and $A, A^{-1} \in \mathscr{A}_\gamma$ for any $\gamma > 0$).

Let us recall the important following theorem.

Theorem 3.2.2 ([105])**.** *The matrix of the operator which maps a orthonormal wavelet basis in the Schwartz class into another C^∞ orthonormal wavelet basis in the Schwartz class is quasidiagonal.*

Consequently, in order to check that a condition defined on wavelet coefficients does not depend of the chosen wavelet basis (in the Schwartz class), we can check the stronger property that it is invariant under the action of quasidiagonal matrices.

Definition 3.2.3. A property $\mathscr{P}$ is *linear robust* if the following properties hold:

- the set of c such that $\mathscr{P}(c)$ holds is a vector space;
- if $\mathscr{P}(c)$ holds then, for any almost diagonal operator A, $\mathscr{P}(Ac)$ holds.

Definition 3.2.4. A property $\mathscr{P}$ is *robust* if the following property holds: if $\mathscr{P}(c)$ holds then, for any quasidiagonal operator A, $\mathscr{P}(Ac)$ holds.

Let us first generalise the following classical result of [105]: if $\gamma > |h|$ and $A \in \mathscr{A}_\gamma$ then there exists a constant $\tilde{C}$ (which only depends on the dimension n) such that

$$|c_\lambda| \leq C 2^{-hj} \ \forall \lambda \in \Lambda \Rightarrow |(Ac)_\lambda| \leq C\tilde{C}\|A\|_\gamma 2^{-hj} \ \forall \lambda. \tag{55}$$

Lemma 3.2.5. *Let σ be an admissible sequence and γ be a strictly positive number such that $\gamma > \max\{-\underline{s}(\sigma) - 1, \overline{s}(\sigma)\}$. If there exists a constant $C > 0$ such that*

$$|c_\lambda| \leq C\sigma_j,$$

for any $\lambda \in \Lambda$, then there exists a constant $\tilde{C}$ which depends on γ, σ and the dimension n such that for any matrix $A \in \mathscr{A}_\gamma$, we have

$$|(Ac)_\lambda| \leq C\tilde{C}\|A\|_\gamma \sigma_j,$$

for any $\lambda \in \Lambda$.

Proof. Let us set $\epsilon = \gamma - \max\{-\underline{s}(\sigma) - 1, \overline{s}(\sigma)\} > 0$. Since the sequence σ is admissible, there exists a constant $C_{\gamma,\sigma} > 0$ such that

$$\sigma_j \leq C_{\gamma,\sigma} 2^{-(j'-j)(\underline{s}(\sigma)-\epsilon)} \sigma_{j'},$$

for any $j \leq j'$ and

$$\sigma_j \leq C_{\gamma,\sigma} 2^{(j-j')(\overline{s}(\sigma)+\epsilon)} \sigma_{j'},$$

for any $j' \leq j$. Let A be a matrix of $\mathscr{A}_\gamma$ and choose a constant D such that $D > \|A\|_\gamma$. Let us note that

$$|(Ac)_{\lambda'}| \leq DC \left(\sum_{j=0}^{j'} \sum_{\lambda \in \Lambda_j} w_\gamma(\lambda, \lambda') \sigma_j + \sum_{j=j'+1}^{+\infty} \sum_{\lambda \in \Lambda_j} w_\gamma(\lambda, \lambda') \sigma_j \right).$$

If $j \leq j'$, we have

$$\begin{aligned}
\sum_{\lambda \in \Lambda_j} w_\gamma(\lambda, \lambda') &= \sum_{k=0}^{2^j-1} \left(\frac{1}{1 + |k - 2^{-(j'-j)} k'|} \right)^{\gamma+n+1} 2^{-(j'-j)(\gamma+n+1)} \\
&\leq \sum_{k=0}^{+\infty} \left(\frac{1}{1 + |k - 2^{-(j'-j)} k'|} \right)^{n+1} 2^{-(j'-j)(\gamma+n+1)} \\
&\leq C_n 2^{-(j'-j)(\gamma+n+1)},
\end{aligned}$$

where C_n is a positive constant that only depends on the dimension n.

If $j > j'$, we have

$$\begin{aligned}
\sum_{\lambda \in \Lambda_j} w_\gamma(\lambda, \lambda') &= \sum_{k=0}^{2^j-1} \left(\frac{1}{1 + |2^{-(j-j')} k - k'|} \right)^{\gamma+n+1} 2^{-(j-j')(\gamma+n+1)} \\
&\leq \sum_{k=0}^{2^j-1} \frac{1}{2^{j-j'}} \left(\frac{1}{1 + |2^{-(j-j')} k - k'|} \right)^{n+1} 2^{-(j-j')(\gamma+n)} \\
&\leq C'_n 2^{-(j-j')(\gamma+n)},
\end{aligned}$$

where C'_n is a positive constant only depending on the dimension n.
Therefore, there exists a constant $C''_n > 0$ only depending on the dimension n such that

$$|(Ac)_{\lambda'}| \leq CC''_n C_{\gamma,\sigma} D \sigma_{j'},$$

for any $\lambda' \in \Lambda$. ■

Let us note that the constant $C_{\gamma,\sigma}$ is equal to 1 if $\sigma_j = 2^{-hj}$, which implies that the previous result is a generalisation of (55).

The next theorem shows the robustness of the $S^{\nu,\sigma^{(\cdot)}}$ spaces.

Theorem 3.2.6. *Suppose that $h < h'$ implies*

$$\sigma_j^{(h')}/\sigma_j^{(h)} \to 0 \quad as \quad j \to +\infty.$$

If for any $h \in \mathbb{R}$, the sequence $\sigma^{(h)}$ is admissible, then $S^{\nu,\sigma^{(\cdot)}}$ is a linear robust space. Moreover, for any $c \in S^{\nu,\sigma^{(\cdot)}}$, the function $\nu_{c,\sigma^{(\cdot)}}$ is robust, i.e. $\nu_{c,\sigma^{(\cdot)}} = \nu_{Ac,\sigma^{(\cdot)}}$ for any quasidiagonal matrix A.

Proof. Let A be an almost diagonal matrix and take $c \in S^{\nu,\sigma^{(\cdot)}}$. Let us prove that Ac belongs to $S^{\nu,\sigma^{(\cdot)}}$. Let $h \in \mathbb{R}$, $\epsilon > 0$ and $C > 0$.

If $h < h_{\min}$, then let h' be an element of $(h, h_{\min})$. Since $c \in S^{\nu,\sigma^{(\cdot)}}$, there exists $C' > 0$ such that $|c_\lambda| \leq C'\sigma_j^{(h')}$, for any $\lambda \in \Lambda$. By Lemma 3.2.5, there exists a constant $\tilde{C} > 0$ depending on A, h' and the dimension n such that $|(Ac)_\lambda| \leq C'\tilde{C}\sigma_j^{(h')}$, for any λ. By hypothesis, there exists $J \in \mathbb{N}$ such that $|(Ac)_\lambda| < C\sigma_j^{(h)}$ for any $j \geq J$.

It remains to examine the case $h \geq h_{\min}$. Let γ be a strictly positive number such that

$$\gamma > \max\{-\underline{s}(\sigma^{(h)}) - 1, \overline{s}(\sigma^{(h)})\}$$

and let C' be the constant $\tilde{C}\|A\|_\gamma$ from Lemma 3.2.5. For any $j \in \mathbb{N}$, let us define the set

$$Q_j = \{\lambda \in \Lambda_j : |c_\lambda| \geq \frac{C}{2C'}\sigma_j^{(h)}\}.$$

Let us note that we have $Ac = Ac^{(1)} + Ac^{(2)}$, where

$$c^{(1)}_{\lambda_{j,k}} = \begin{cases} c_{\lambda_{j,k}} & \text{if } k \in Q_j \\ 0 & \text{else} \end{cases} \quad \text{and} \quad c^{(2)}_{\lambda_{j,k}} = \begin{cases} c_{\lambda_{j,k}} & \text{if } k \notin Q_j \\ 0 & \text{else.} \end{cases},$$

and that $|c_\lambda^{(2)}| < C/(2C')\ \sigma_j^{(h)}$, for any $\lambda \in \Lambda$. Therefore, using Lemma 3.2.5, we get $|(Ac^{(2)})_\lambda| \leq C/2\ \sigma_j^{(h)}$ for any $\lambda \in \Lambda$, which implies

$$\#\{\lambda \in \Lambda_j : |(Ac)_\lambda| \geq C\sigma_j^{(h)}\} \leq \#\{\lambda \in \Lambda_j : |(Ac^{(1)})_\lambda| \geq \frac{C}{2}\sigma_j^{(h)}\}.$$

As in [66], let us define the δ-neighbourhood $N^\delta(\lambda)$ ($\delta > 0$) of $[k/2^j, (k+1)/2^j)$ as the set of $\lambda' \in \Lambda$ such that

$$\begin{cases} |j - j'| \leq \delta j \\ \left|\frac{k}{2^j} - \frac{k'}{2^{j'}}\right| \leq 2^{2\delta j}2^{-j} \end{cases}.$$

Let us recall that if $\lambda' \notin N^\delta(\lambda)$ then

$$w_{2\delta^{-2}}(\lambda, \lambda') \leq w_{\delta^{-2}}(\lambda, \lambda')2^{-j\delta^{-1}}.$$

Let us take λ such that for any $k' \in Q_{j'}$, we have $\lambda' \notin N^\delta(\lambda)$. If $h' < h_{\min}$, for any constant C'' large enough and any constant δ small enough, we get

$$\begin{aligned}
|(Ac^{(1)})_\lambda| &\leq \sum_{j'\in\mathbb{N}} \sum_{k'\in Q_{j'}} \|A\|_{2\delta^{-2}} w_{2\delta^{-2}}(\lambda,\lambda')|c_{\lambda'}| \\
&\leq \|A\|_{2\delta^{-2}} 2^{-j\delta^{-1}} \sum_{j'\in\mathbb{N}} \sum_{k'\in Q_{j'}} w_{\delta^{-2}}(\lambda,\lambda')|c_{\lambda'}| \\
&\leq \|A\|_{2\delta^{-2}} 2^{-j\delta^{-1}} \sum_{j'\in\mathbb{N}} \sum_{k'\in Q_{j'}} w_{\delta^{-2}}(\lambda,\lambda') C'' \sigma_{j'}^{(h')} \\
&\leq \|A\|_{2\delta^{-2}} 2^{-j\delta^{-1}} C'' \sum_{\lambda'\in\Lambda} w_{\delta^{-2}}(\lambda,\lambda')\sigma_{j'}^{(h')}.
\end{aligned}$$

Using the proof of the previous lemma, there exists a constant C''' depending on δ, h' and the dimension n such that

$$\sum_{\lambda'\in\Lambda} w_{\delta^{-2}}(\lambda,\lambda')\sigma_{j'}^{(h')} \leq C'''\sigma_j^{(h')}.$$

Since the sequences $\sigma^{(h)}$ and $\sigma^{(h')}$ are admissible, there exists $s>0$ such that $\sigma^{(h')}/\sigma^{(h)} \leq 2^{sj}$. So, there exists $J \in \mathbb{N}$ such that

$$\begin{aligned}
|(Ac^{(1)})_\lambda| &\leq \|A\|_{2\delta^{-2}} C'' C''' 2^{-j(\delta^{-1}-s)} \sigma_j^{(h)} \\
&\leq \frac{C}{4}\sigma_j^{(h)},
\end{aligned}$$

for any $j \geq J$. We thus have

$$\begin{aligned}
\#\{\lambda\in\Lambda_j : |(Ac^{(1)})_\lambda| \geq \frac{C}{2}\sigma_j^{(h)}\} &\leq \#\{\lambda\in\Lambda_j : \exists\lambda'\in N^\delta(\lambda),\ k'\in Q_{j'}\} \\
&\leq \sum_{j':|j-j'|\leq\delta j} \sum_{k'\in Q_{j'}} \#\{\lambda\in\Lambda_j : \left|\frac{k}{2^j}-\frac{k'}{2^{j'}}\right| \leq 2^{2\delta j}2^{-j}\} \\
&\leq \sum_{j':|j-j'|\leq\delta j} \sum_{k'\in Q_{j'}} (2^{2\delta j+1}+1)^n \\
&\leq \sum_{j':|j-j'|\leq\delta j} \#Q_{j'}\ (2^{2\delta j+1}+1)^n,
\end{aligned}$$

for any $j \geq J$. Since c belongs to $S^{\nu,\sigma^{(\cdot)}}$, we have $\#Q_{j'} \leq 2^{(\nu(h)+\epsilon/2)j'}$, for j' large enough. We get

$$\begin{aligned}
\#\{k : |(Ac^{(1)})_\lambda| \geq \frac{C}{2}\sigma_j^{(h)}\} &\leq 2\delta j 2^{(\nu(h)+\epsilon/2)j(1+\delta)} 2^{3\delta j n} \\
&\leq 2^{(\nu(h)+\epsilon/2)j} 2^{(1+\nu(h)+\epsilon/2+3n)\delta j} \\
&\leq 2^{(\nu(h)+\epsilon)j},
\end{aligned}$$

for any $j \geq J$ (for large enough J). We thus have shown that the space $S^{\nu,\sigma^{(\cdot)}}$ is linear robust. The second part of the theorem is obtained by using Proposition 3.1.9 and the fact that c belongs to $S^{\nu_{c,\sigma^{(\cdot)}},\sigma^{(\cdot)}}$. ■

Consequently, $S^{\nu,\sigma^{(\cdot)}}$ can be seen as a function space matching a function $f \in L^2(\mathbb{T}^n)$ to its sequence of wavelet coefficients:

$$S^{\nu,\sigma^{(\cdot)}} = \{f \in L^2(\mathbb{T}^n) : \forall h \in \mathbb{R}\ \ \forall \epsilon > 0\ \forall C > 0 \\ \exists J > 0\ \forall j \geq J,\ \#E_j(C, \sigma^{(h)})(f) \leq 2^{(\nu(h)+\epsilon)j}\},$$

where

$$E_j(C, \sigma^{(h)})(f) = \{\lambda \in \Lambda_j : |c_\lambda| \geq C\sigma_j^{(h)}\},$$

and $c = (c_\lambda)_{\lambda\in\Lambda}$ is the wavelet coefficients of f in a given wavelet basis.

3.3 Some Connections with Generalised Besov Spaces

Let us recall that Proposition 1.8.4 gives a connection between the Besov spaces and the S^ν spaces by the following relation:

$$S^\nu \subseteq \bigcap_{p>0} \bigcap_{\epsilon>0} b_{p,\infty}^{\frac{\eta(p)-\epsilon}{p}},$$

where $\eta(q) = \inf_{h\geq h_{\min}}\{hq - \nu(h)\} + n$, and the inclusion becomes an equality if and only if ν is concave.

The Besov spaces have been generalised with the help of the admissible sequences (see Section 1.6.3). It is thus natural to study the connections between these spaces and the spaces $S^{\nu,\sigma^{(\cdot)}}$ defined in Section 3.1.

The next theorem gives a condition under which the $S^{\nu,\sigma^{(\cdot)}}$ spaces are included in an intersection of generalised Besov spaces.

Theorem 3.3.1. *For any $h \in \mathbb{R}$, let $\sigma^{(h)}$ be an admissible sequence and let us suppose that*

- *$h < h'$ implies $\sigma_j^{(h')}/\sigma_j^{(h)} \to 0$ as $j \to +\infty$,*
- *$\overline{s}(\sigma^{(h)}) \to -\infty$ as $h \to +\infty$.*

For any $p > 0$, let $\theta^{(p)}$ be an admissible sequence. We have

$$S^{\nu,\sigma^{(\cdot)}} \subseteq \bigcap_{p>0} \bigcap_{\epsilon>0} b_{p,\infty}^{(\theta_j^{(p)} 2^{-j\epsilon/p})_j}$$

if and only if for any $p, \epsilon > 0$ and for any $h \geq h_{\min}$, there exists $C > 0$ such that

$$\theta_j^{(p)} 2^{-j\epsilon/p} \leq C 2^{jn/p} 2^{-j\nu(h)/p} (\sigma_j^{(h)})^{-1}, \tag{56}$$

for any $j \in \mathbb{N}$.

Proof. First, let us suppose that the inclusion is satisfied. For any $h \geq h_{\min}$, let $c^{(h)}$ be a sequence defined as

$$c^{(h)}_{\lambda_{j,k}} = \begin{cases} \sigma_j^{(h)} & \text{for } \lfloor 2^{\nu(h)j} \rfloor \text{ values of } k \\ 0 & \text{else} \end{cases}.$$

We directly have that $c^{(h)}$ belongs to $S^{\nu,\sigma^{(\cdot)}}$ and thus, for any $p, \epsilon > 0$, there exists $C > 0$ such that

$$\theta_j^{(p)} 2^{-j\epsilon/p} 2^{-jn/p} \left(\sum_{\lambda \in \Lambda_j} |c_\lambda^{(h)}|^p \right)^{1/p} < C,$$

for any $j \in \mathbb{N}$. From the definition of the sequence $c^{(h)}$, we obtain

$$\theta_j^{(p)} 2^{-j\epsilon/p} \leq C 2^{jn/p} 2^{-j\nu(h)/p} (\sigma_j^{(h)})^{-1},$$

for any j.

Now, let us suppose that (56) is satisfied and let us show the required inclusion. Let c be a sequence belonging to $S^{\nu,\sigma^{(\cdot)}}$ and let $p, \epsilon > 0$. Since $\overline{s}(\sigma^{(h)}) \to -\infty$ as $h \to +\infty$, there exists $h' \geq h_{\min}$ such that the sequence $(\theta_j^{(p)} 2^{-j\epsilon/p} \sigma_j^{(h')})_j$ is bounded. We have

$$\begin{aligned}
&(\theta_j^{(p)})^p 2^{-j\epsilon} 2^{-jn} \sum_{\lambda \in \Lambda_j} |c_\lambda|^p \\
&\leq (\theta_j^{(p)})^p 2^{-j\epsilon} 2^{-jn} \left(\sum_{\lambda \in \Lambda_j : |c_\lambda| < \sigma_j^{(h')}} |c_\lambda|^p + \sum_{\lambda \in \Lambda_j : |c_\lambda| \geq \sigma_j^{(h')}} |c_\lambda|^p \right) \\
&\leq (\theta_j^{(p)} 2^{-j\epsilon/p} \sigma_j^{(h')})^p + (\theta_j^{(p)})^p 2^{-j\epsilon} 2^{-jn} \sum_{\lambda \in \Lambda_j : |c_\lambda| \geq \sigma_j^{(h')}} |c_\lambda|^p,
\end{aligned}$$

for any $j \in \mathbb{N}$. It remains to prove that the second term of the previous inequality is bounded.

Let β be a real number smaller than $h_{\min}$ and let J be such that $|c_\lambda| < \sigma_j^{(\beta)}$ for any $\lambda \in \Lambda_j$ with $j \geq J$. We have

$$\{\lambda \in \Lambda_j : |c_\lambda| \geq \sigma_j^{(h')}\} = \{\lambda \in \Lambda_j : \sigma_j^{(\beta)} > |c_\lambda| \geq \sigma_j^{(h')}\},$$

for any $j \geq J$. Moreover, for any $\eta > 0$, there exist $\gamma_1, \dots, \gamma_N \in (\beta - \eta, h')$ such that

$$[\beta, h'] \subset \bigcup_{i=1}^{N} [\gamma_i, \gamma_i + \eta], \ [\sigma_j^{(h')}, \sigma_j^{(\beta)}] \subset \bigcup_{j=1}^{N} [\sigma_j^{(\gamma_i+\eta)}, \sigma_j^{(\gamma_i)}]$$

and

$$\#\{\lambda \in \Lambda_j : |c_\lambda^{(i)}| \geq \sigma_j^{(\gamma_i+\eta)}\} \leq 2^{(\nu(\gamma_i+\eta)+\eta)j},$$

for any $j \geq J$ (with J large enough). Since ν is a right-continuous function, there exists $\eta > 0$ such that $\nu(\gamma_i + \eta) + \eta < \nu(\gamma_i) + \epsilon/2$ for any $i \in \{1, \dots, N\}$. As a consequence, there exists a constant $C' > 0$ such that

$$\begin{aligned}(\theta_j^{(p)})^p 2^{-j\epsilon} 2^{-jn} \sum_{\lambda \in \Lambda_j : |c_\lambda| \geq \sigma_j^{(h')}} |c_\lambda|^p &\leq \sum_{i=1}^{N} (\theta_j^{(p)})^p 2^{-j\epsilon} 2^{-jn} (\sigma_j^{(\gamma_i)})^p 2^{(\nu(\gamma_i)+\epsilon/2)j} \\ &\leq C' N,\end{aligned}$$

for any $j \geq J$. The conclusion follows.

■

Let us recall that $b_{p,\infty}^{\sigma'} \subset b_{p,\infty}^{\sigma}$ if $\sigma_j \leq \sigma_j'$ for any j large enough. Therefore, to get the equality in the previous theorem, we must choose the "largest" sequences $\theta^{(p)}$ satisfying the condition. To do so, we will introduce a new function $\hat{\nu}$. Let us first rewrite the condition on the sequences $\theta^{(p)}$. We have

$$\begin{aligned}&\theta_j^{(p)} 2^{-j\epsilon/p} \leq C 2^{jn/p} 2^{-j\nu(h+\eta/2)/p} (\sigma_j^{(h+\eta/2)})^{-1} \\ &\Leftrightarrow \theta_j^{(p)} 2^{-j\epsilon/p} \leq 2^{jn/p} 2^{-j\nu(h+\eta/2)/p} (\sigma_j^{(h+\eta)})^{-1} \\ &\Leftrightarrow 2^{j\nu(h+\eta/2)/p} 2^{-j\epsilon/p} \leq 2^{jn/p} (\theta_j^{(p)} \sigma_j^{(h+\eta)})^{-1} \\ &\Leftrightarrow \nu(h) \leq \lim_{\eta \to 0^+} \inf_{p>0} \limsup_{j \to +\infty} n - p \frac{\log(\theta_j^{(p)} \sigma_j^{(h+\eta)})}{\log 2^j}.\end{aligned}$$

Definition 3.3.2. The function $\hat{\nu}$ is defined as

$$\hat{\nu}(h) = \begin{cases} \lim_{\eta \to 0^+} \inf_{p>0} \limsup_{j \to +\infty} n - p \frac{\log(\theta_j^{(p)} \sigma_j^{(h+\eta)})}{\log 2^j} & \text{if } h \geq h_{\min} \\ -\infty & \text{else} \end{cases}.$$

The function $\hat{\nu}$ is a right-continuous increasing function such that $\hat{\nu}(h) \geq 0$ for any $h \geq h_{\min}$. Besides, if $\hat{\nu}$ is an admissible profile (i.e. if $\hat{\nu} \leq n$) then we directly have

$$S^{\nu,\sigma^{(\cdot)}} \subset S^{\hat{\nu},\sigma^{(\cdot)}}.$$

Theorem 3.3.3. *Under the hypothesis of Theorem 3.3.1, if $\hat{\nu} \leq n$ and if for any $h < h_{\min}$, there exist $p, \epsilon > 0$ such that $2^{-jn/p}\sigma_j^{(h)}\theta_j^{(p)}2^{-j\epsilon/p} \to +\infty$ as $j \to +\infty$, then we have*

$$\bigcap_{p>0}\bigcap_{\epsilon>0} b_{p,\infty}^{(\theta_j^{(p)}2^{-j\epsilon/p})_j} \subset S^{\hat{\nu},\sigma^{(\cdot)}}.$$

Remark 3.3.4. Hypothesis $2^{-jn/p}\sigma_j^{(h)}\theta_j^{(p)}2^{-j\epsilon/p} \to +\infty$ means that the sequence $\theta_j^{(p)}$ must be "sufficiently large". Moreover,

- if we suppose that

$$\bigcap_{p>0}\bigcap_{\epsilon>0} b_{p,\infty}^{(\theta_j^{(p)}2^{-j\epsilon/p})_j} \subset S^{\hat{\nu},\sigma^{(\cdot)}},$$

  then, for any $h < h_{\min}$, there exist $p, \epsilon > 0$ such that

$$\limsup_{j\to+\infty} 2^{-jn/p}\sigma_j^{(h)}\theta_j^{(p)}2^{-j\epsilon/p} = +\infty, \tag{57}$$

- let us define the sequence c such that, for any $j \in \mathbb{N}$, $c_{\lambda_{j,k}} = \sigma_j^{(h)}$ for one and only one k, and $c_{\lambda_{j,k}} = 0$ otherwise; if we assume that there exists $h < h_{\min}$ such that, for any $p, \epsilon > 0$, Limit superior (57) is bounded, then we directly have that the sequence c belongs to $\bigcap_{p>0}\bigcap_{\epsilon>0} b_{p,\infty}^{(\theta_j^{(p)}2^{-j\epsilon/p})_j}$, but c does not belong to $S^{\hat{\nu},\sigma^{(\cdot)}}$.

Proof. Let c be a sequence belonging to $\bigcap_{p>0}\bigcap_{\epsilon>0} b_{p,\infty}^{(\theta^{(p)}2^{-j\epsilon/p})_j}$. For any $p, \epsilon > 0$, there exists $C_{p,\epsilon} > 0$ such that

$$(\theta_j^{(p)})^p 2^{-j\epsilon}2^{-jn}\sum_{\lambda\in\Lambda_j}|c_\lambda|^p \leq C_{p,\epsilon},$$

for any $j \in \mathbb{N}$.

If $h < h_{\min}$, we have

$$\#\{\lambda \in \Lambda_j : |c_\lambda| \geq \sigma_j^{(h)}\} \leq C_{p,\epsilon}(2^{-jn/p}\theta_j^{(p)}2^{-j\epsilon/p}\sigma_j^{(h)})^{-p}.$$

Let us take p, ϵ as in the hypothesis; there thus exists $J > 0$ such that $|c_\lambda| < \sigma_j^{(h)}$ for any $\lambda \in \Lambda_j$ with $j \geq J$, i.e. $\nu_{c,\sigma^{(\cdot)}}(h) = -\infty$.

If $h \geq h_{\min}$, we have

$$\begin{aligned}\#\{\lambda \in \Lambda_j : |c_\lambda| \geq \sigma_j^{(h+\epsilon/2)}\} &\leq C_{p,\epsilon}2^{jn}(\theta_j^{(p)})^{-p}2^{\epsilon j}(\sigma_j^{(h+\epsilon/2)})^{-p} \\ &\leq 2^{jn}(\theta_j^{(p)})^{-p}2^{\epsilon j}(\sigma_j^{(h+\epsilon)})^{-p},\end{aligned}$$

for j large enough; we thus have $\nu_{c,\sigma^{(\cdot)}}(h) \leq \hat{\nu}(h)$. This implies that c belongs to $S^{\hat{\nu},\sigma^{(\cdot)}}$.

■

The previous theorem allows to assert that if $\nu = \hat{\nu}$ then

$$S^{\nu,\sigma^{(\cdot)}} = \bigcap_{p>0} \bigcap_{\epsilon>0} b_{p,\infty}^{(\theta_j^{(p)} 2^{-j\epsilon/p})_j}.$$

The next corollary shows that when Inequalities (56) are satisfied for $\hat{\nu}$, the previous implication becomes an equivalence.

Corollary 3.3.5. *Under the hypothesis of the previous theorem, if for any $p, \epsilon > 0$ and for any $h \geq h_{\min}$, there exists $C > 0$ such that*

$$\theta_j^{(p)} 2^{-j\epsilon/p} \leq C 2^{jn/p} 2^{-j\hat{\nu}(h)/p} (\sigma_j^{(h)})^{-1},$$

for any $j \in \mathbb{N}$ and if for any $h < \beta$, we have $\sigma_j^{(\beta)} \leq \sigma_j^{(h)}$ for any $j \in \mathbb{N}$, then we have

$$S^{\nu,\sigma^{(\cdot)}} = \bigcap_{p>0} \bigcap_{\epsilon>0} b_{p,\infty}^{(\theta_j^{(p)} 2^{-j\epsilon/p})_j}$$

if and only if $\nu = \hat{\nu}$.

Proof. We directly have

$$\bigcap_{p>0} \bigcap_{\epsilon>0} b_{p,\infty}^{(\theta_j^{(p)} 2^{-j\epsilon/p})_j} = S^{\hat{\nu},\sigma^{(\cdot)}},$$

and we can conclude using Proposition 3.1.9. ■

If $\nu = \hat{\nu}$, a natural question concerns the link between the topology of the space $(S^{\nu,\sigma^{(\cdot)}}, d)$ defined in Theorem 3.1.7, and the topology induced on the intersection in the previous theorem. The canonical topology on the generalised Besov space is metrizable, complete and stronger than the pointwise convergence, and so is the topology on $(S^{\nu,\sigma^{(\cdot)}}, d)$. If the intersection of the generalised Besov spaces can be written as a countable intersection of $b_{p,\infty}^{\sigma^{(i)}}$ spaces ($i \in \mathbb{N}$) then, from the closed graph theorem, the topology τ defined on $S^{\nu,\sigma^{(\cdot)}}$ as the weakest topology such that each identity map $(S^{\nu,\sigma^{(\cdot)}}, \tau) \mapsto b_{p,\infty}^{\sigma^{(i)}}$ is continuous, is equivalent to the topology on $(S^{\nu,\sigma^{(\cdot)}}, d)$. The next proposition gives some conditions on the sequences $\theta_j^{(p)}$ to have a countable intersection.

Proposition 3.3.6. *If the function $p > 0 \mapsto \log_{2^j} \theta_j^{(p)}$ is left continuous uniformly with respect to j then, if p_m ($m \in \mathbb{N}$) is a dense sequence of $(0, +\infty)$*

and if ϵ_l ($l \in \mathbb{N}$) is a sequence of strictly positive numbers converging to 0, we have

$$\bigcap_{p>0}\bigcap_{\epsilon>0} b_{p,\infty}^{(\theta_j^{(p)}2^{-j\epsilon/p})_j} = \bigcap_{m\in\mathbb{N}}\bigcap_{l\in\mathbb{N}} b_{p_m,\infty}^{(\theta_j^{(p_m)}2^{-j\epsilon_l/p_m})_j}.$$

Proof. The inclusion of the second space in the first space is straightforward. Let us prove the other inclusion.

Let us take $p > 0$ and $\epsilon > 0$. It suffices to find p_m and ϵ_l such that

$$p_m \leq p \text{ and } \theta_j^{(p_m)}2^{-j(\epsilon_l+n)/p_m} \geq \theta_j^{(p)}2^{-j(\epsilon+n)/p},$$

for j large enough. This is equivalent to ask

$$p_m \leq p \text{ and } \frac{\epsilon}{p} - \frac{\epsilon_l}{p_m} \geq \frac{n}{p_m} - \frac{n}{p} - \left(\log_{2^j}\theta_j^{(p_m)} - \log_{2^j}\theta_j^{(p)}\right),$$

for j large enough. Since we can choose $p_m \leq p$ such that

$$|\log_{2^j}\theta_j^{(p_m)} - \log_{2^j}\theta_j^{(p)}| < \frac{\epsilon}{3p} \text{ and } \frac{n}{p_m} - \frac{n}{p} < \frac{\epsilon}{3p},$$

for any $j \in \mathbb{N}$, we can conclude by taking ϵ_l sufficiently small. ■

To end this section, let us show that the preceding results are generalisations of Proposition 1.8.4. For $\sigma_j^{(h)} = 2^{-hj}$, let us find an admissible sequence $\theta_j^{(p)}$ such that for any $p, \epsilon > 0$ and for any $h \geq h_{\min}$, there exists $C > 0$ such that

$$\theta_j^{(p)}2^{-j\epsilon/p} \leq C2^{jn/p}2^{-j\nu(h)/p}(\sigma_j^{(h)})^{-1},$$

i.e.

$$\theta_j^{(p)}2^{-j\epsilon/p} \leq C2^{j(n-\nu(h)+hp)/p}.$$

If we take $\theta_j^{(p)} = 2^{j\eta(p)/p}$ with

$$\eta(p) = \inf_{h\geq h_{\min}}\{hp - \nu(h)\} + n,$$

we get $\hat{\nu}(h) = \inf_{p>0}\{hp - \eta(p)\} + n$ for any $h \geq h_{\min}$ and the hypothesis of Corollary 3.3.5 and Proposition 3.3.6 are satisfied. We thus obtain

$$S^\nu = \bigcap_{p>0}\bigcap_{\epsilon>0} b_{p,\infty}^{(\theta_j^{(p)}2^{-j\epsilon/p})_j} = \bigcap_{p>0}\bigcap_{\epsilon>0} b_{p,\infty}^{\frac{\eta(p)-\epsilon}{p}} = \bigcap_{m\in\mathbb{N}}\bigcap_{l\in\mathbb{N}} b_{p_m,\infty}^{\frac{\eta(p_m)-\epsilon_l}{p_m}}$$

if and only if $\nu = \hat{\nu}$, i.e. if ν is concave.

Part II.

Numerical Applications

Chapter 4

From Theory to Practice: Implementation of Multifractal Formalisms based on Profiles

Now that the theoretical setting has been formulated and the theoretical interest has been shown, we can describe an algorithm to effectively approximate the spectrum d_f associated with a numerical signal f, with the help of the profiles ν_f, $\tilde{\nu}_f^+$, $\tilde{\nu}_f^-$ and $\nu_{f,\sigma^{(\cdot)}}$. Each profile is defined in the same way and consequently, we introduce the following notations:

$$\breve{\nu}_f(h) = \limsup_{j\to+\infty} \frac{\log \#\breve{E}_j(1,\sigma^{(h+\epsilon)})(f)}{\log 2^j}, \tag{58}$$

where for any $h \in \mathbb{R}$, $\sigma^{(h)}$ is an admissible sequence and the set $\breve{E}_j(C,\sigma^{(h)})(f)$ corresponds either to

- the set $E_j(C,\sigma^{(h)})(f)$, which means that $\breve{\nu}_f$ is the generalised wavelet profile $\nu_{f,\sigma^{(\cdot)}}$,
- or, if $\sigma^{(h)} = (2^{-hj})_{j\in\mathbb{N}}$, then it corresponds either to
  - the set $E_j(C,h)(f)$, which means that $\breve{\nu}_f$ is the wavelet profile ν_f,
  - or to the set $\tilde{E}_j^+(C,h)(f)$, which means that $\breve{\nu}_f$ is the increasing wavelet leaders profile $\tilde{\nu}_f^+$,
  - or to the set $\tilde{E}_j^-(C,h)(f)$, which means that $\breve{\nu}_f$ is the decreasing wavelet leaders profile $\tilde{\nu}_f^-$.

Section 4.1 first gives a complement to the WPM in order to show that, under some hypothesis on f, the wavelet profile ν_f can directly be used to approximate the spectrum d_f. Secondly, we show that the constant 1 appearing in the definition of $\breve{\nu}_f$ is arbitrary. It is important to notice that this fact is not valid for a real-life signal f because, in this case, we only have access to a finite number of scales j; consequently, the constant is not arbitrary and its choice becomes a crucial point to compute $\breve{\nu}_f$. An algorithm to approximate $\breve{\nu}_f$ is presented in Second 4.2. Let us mention that this one is a stand-alone

method: no operation but fine tuning is required by the user. Section 4.3 compares the approximation of the spectrum d_f by applying the WPM, the LPM and the WLM on numerical signals f, as the fractional Brownian motion, the Mandelbrot cascades and the Lévy processes. We show that the WPM and the LPM are usually as good as the WLM with monofractal functions and multifractal functions with a concave spectrum. We also show that the WPM and the LPM can approximate non-concave spectra, while the WLM can only approximate the concave hull of spectra. Section 4.4 presents an improvement of the algorithm which improves the approximation of the spectrum in some cases. Section 4.5 shows the robustness of the algorithm and Section 4.6 gives some remarks on several parameters of the algorithm presented in this chapter. The last section summaries the effectiveness of the WPM and of the LPM. The numerical contributions obtained with the generalised wavelet profile $\nu_{f,\sigma^{(\cdot)}}$ is presented in Chapter 5.

As already mentioned in Section 1.5, for each numerical simulation of a function f, we use the Mallat algorithm and the Daubechies wavelets of order 3 to compute a finite number of wavelet coefficients corresponding to f.

The main ideas developed in this chapter were published in [46, 78]. It is important to notice that the algorithm to approximate $\breve{\nu}_f$ has evolved between the two articles: the first one presents the first version of the algorithm in the context of the L^ν spaces and the second one presents a first improvement in the context of the S^ν spaces. This improvement (presented in Section 4.2.2) had not yet been tested with L^ν. This chapter presents the algorithm having obtained the best results and illustrates it in the context of S^ν and L^ν spaces. Moreover, the new improvement presented in Section 4.4 is for the first time presented; it has not yet been the subject of an article. These works are a collaboration with C. Esser and S. Nicolay.

This chapter is structured as follows:

4.1 Preliminary Results

This section first shows that, for the WPM, the wavelet profile ν_f can directly be used to approximate the spectrum d_f, if f verifies some hypothesis. Secondly, we establish the key result on which the algorithm presented in the following section is based; this result states that the constant 1 appearing in the definition of the profiles (see Equality 58) is arbitrary.

As already mentioned in Section 1.8, the approximation of the spectrum of f with the WPM is given by the function

$$d_f^{\nu_f} = \sup_{h' \in (0,h]} \frac{\nu_f(h')}{h'},$$

which transform the function ν_f into a function with increasing-visibility (see Definition 1.8.6). Let us show that, under some hypothesis on f, we can avoid this transformation. Before establishing this result, let us recall a few notions about measures (for more details, see [21]).

Definition 4.1.1. Let μ be a positive Borel measure on $[0,1]^n$. The *Hölder exponent* of $x_0 \in [0,1]^n$ and the *Hölder spectrum* of μ are respectively defined as

$$h_\mu(x_0) = \liminf_{r \to 0^+} \frac{\log \mu\big(B(x_0,r)\big)}{\log r}$$

and

$$d_\mu : [0,+\infty] \to \{-\infty\} \cup [0,n],\ h \mapsto \dim_{\mathcal{H}}(\{x \in [0,1]^n : h_\mu(x) = h\}).$$

The following proposition constructs a function f from a measure μ, whose the spectrum is the same as the spectrum of μ.

Proposition 4.1.2. *[122]) If μ is an uniformly regular measure[1], then there exists a function f, called the* associated wavelet series*, whose wavelet coefficients are defined as*

$$c_\lambda = \mu(\lambda),$$

[1] A measure μ is called an *uniformly regular measure* if there exist a constant $C > 0$ and an exponent $h_{\min} > 0$ such that $\mu(B(x,r)) \leq C r^{h_{\min}}$, for any ball $B(x,r) \subset [0,1]^n$.

for any $\lambda \in \Lambda$. Moreover, we have $d_f = d_\mu$.

In this setting, the following result shows that the estimation of the spectrum with the WPM can be directly given by ν_f.

Proposition 4.1.3. *Let μ be an uniformly regular measure and let f be the associated wavelet series. If*

$$\inf \left\{ \frac{\nu_f(x) - \nu_f(y)}{x - y} : x, y \in [h_{\min}, h_{\max}],\ x < y \right\} > 0, \tag{59}$$

then the wavelet profile ν_f is an approximation of the increasing part of d_f, i.e. it gives an upper bound of the Hölder spectrum.

Proof. Let us notice that, if f_β denotes the function whose wavelet coefficients are given by $2^{-\beta j} c_\lambda$, then we have

$$d_{f_\beta}(h) = d_f(h - \beta) \quad \text{and} \quad \nu_{f_\beta}(h) = \nu_f(h - \beta), \tag{60}$$

for any $h \in [0, +\infty]$. The hypothesis on the wavelet profile ν_f implies that there exists $\beta > 0$ such that the function ν_{f_β} is with increasing-visibility. In this case, ν_{f_β} approximates d_{f_β}. Using property (60), we can conclude that the increasing part of d_f can be approximated by ν_f. ■

Remark 4.1.4. Obviously, if the infimum in (59) equals 0 and if the infimum taken on $x, y \in [h_{\min}, h]$ is strictly positive for any $h < h_{\max}$, then the result is still valid.

To close this section, let us establish a key result for an effective implementation of $\breve{\nu}_f$. This result shows that the constant 1 appearing in the definition of profiles (see Equality (58)) is arbitrary.

Proposition 4.1.5. *Let $\boldsymbol{C} = (C_j)_{j \in \mathbb{N}}$ be a sequence of positive numbers for which there exists $D > 0$ such that $D^{-1} \leq C_j \leq D$ for any $j \in \mathbb{N}$. Moreover, for any $h \in \mathbb{R}$, let $\sigma^{(h)}$ be an admissible profile and let us suppose that, $h < h'$ implies $\sigma_j^{(h')} / \sigma_j^{(h)} \to 0$ as $j \to +\infty$. If we denote*

$$\breve{\nu}_f^{\boldsymbol{C}} : h \in \mathbb{R} \mapsto \lim_{\epsilon \to 0^+} \limsup_{j \to +\infty} \frac{\log \# \breve{E}_j(C_j, \sigma^{(h+\epsilon)})(f)}{\log 2^j},$$

we have $\breve{\nu}_f^{\boldsymbol{C}}(h) = \breve{\nu}_f(h)$ for any $h \in \mathbb{R}$.

If $\boldsymbol{C}$ is the constant sequence $C_j = C$, for any $j \in \mathbb{N}$, we naturally write $\breve{\nu}_f^C$ instead of $\breve{\nu}_f^{\boldsymbol{C}}$.

Proof. The proof is given in the case where the set $\breve{E}_j(C, \sigma^{(h+\epsilon)})(f)$ corresponds to the set $E_j(C, \sigma^{(h+\epsilon)})(f)$ (i.e. $\breve{\nu}_f = \nu_{f,\sigma^{(\cdot)}}$); the other cases are similar.

First, notice that

$$\#E_j(D^{-1}, \sigma^{(h+\epsilon)})(f) \leq \#E_j(C_j, \sigma^{(h+\epsilon)})(f) \leq \#E_j(D, \sigma^{(h+\epsilon)})(f),$$

for any $j \in \mathbb{N}$, $h \in \mathbb{R}$ and $\epsilon > 0$. We thus have $\nu^{D^{-1}}_{f,\sigma^{(\cdot)}} \leq \nu^{\boldsymbol{C}}_{f,\sigma^{(\cdot)}} \leq \nu^{D}_{f,\sigma^{(\cdot)}}$; therefore it is enough to prove that $\nu^{C}_{f,\sigma^{(\cdot)}} = \nu_{f,\sigma^{(\cdot)}}$ for any $C > 0$.

Fix $h \in \mathbb{R}$, $C > 0$. For any $\epsilon > 0$, the hypothesis on the sequences $\sigma^{(\cdot)}$ implies that there exists $J > 0$ such that for any $j > J$, $\sigma_j^{(h+\epsilon/2)} \geq C\sigma_j^{(h+\epsilon)}$; in other words, we have

$$\#E_j(C, \sigma_j^{(h+\epsilon)})(f) \geq \#E_j(1, \sigma_j^{(h+\epsilon/2)})(f).$$

It thus leads $\nu^{C}_{f,\sigma^{(\cdot)}}(h) \geq \nu_{f,\sigma^{(\cdot)}}(h)$.

A similar reasoning allows to obtain the other inequality. ∎

4.2 An Algorithm to Compute $\breve{\nu}_f$

In this section, the different steps of an algorithm to approximate $\breve{\nu}_f$, where f is a real-life signal, are presented. First, for a fixed $h \in \mathbb{R}$ and $C > 0$, we explain how to approximate $\breve{\nu}^C_f(h)$. A discussion is done about the influence of the value of C on the approximation of $\breve{\nu}^C_f(h)$, since we only have access to a finite number of coefficients of f. We then explain, for a fixed $h \in \mathbb{R}$, how to choose this constant to correctly approximate $\breve{\nu}_f(h)$. Finally, we give the pseudocode of the algorithm approximating the function $\breve{\nu}_f$.

4.2.1 For Fixed $h \in \mathbb{R}$ and $C > 0$, Computation of $\breve{\nu}^C_f(h)$

For a real-life signal f, we only have access to a finite number of scales j. Consequently, an approximation of the theoretical value of $\breve{\nu}_f(h)$ should be the slope of

$$j \mapsto \frac{\log \#\breve{E}_j(C, \sigma^{(h)})(f)}{\log 2}, \tag{61}$$

for large values of j. In practice, it is important to carefully chose the scales, because they can influence the computed value approximating $\breve{\nu}_f(h)$. Moreover, it can to be interesting to compute this slope on several different sets of scales to have some additional information about the signal (see Section 5.1.3 for a example). The slope is computed as the one of the linear regression on the points corresponding to the chosen scales, using the least squares method, if these points are correlated. We fix a threshold for the correlation of the points used to compute the slope: we only keep the slope if this correlation is

higher than the chosen threshold (typically 0.95 or 0.99). From now on, the notation $\breve{\nu}_f^C(h)$ will refer to this slope.

This notation can be surprising because it does refer to the constant C, while Proposition 4.1.5 implies that the value of $\breve{\nu}(h)$ is independent of C. It is important to notice that this independence it is not valid in practice, since we only have access to a finite number of coefficients, and thus the slope is computed on a finite number of points. Indeed, let us recall that the notation $\#\breve{E}_j(C, \sigma^{(h)})(f)$ represents the number of (wavelet or leaders) coefficients larger or smaller than $C\sigma_j^{(h)}$. If the typical value of coefficients is too large or too small with respect to C, the slope $\breve{\nu}_f^C(h)$ will be very different from the theoretical value $\breve{\nu}_f(h)$. For example, in the case of the LPM,

- if C is close to 0, then almost all the coefficients are larger than $C2^{-hj}$. This implies that the slope of $j \mapsto \log_2 \#\tilde{E}_j^+(C,h)(f)$ is close to n; the larger C is, the smaller this slope is,
- if C is large, then almost all the coefficients are smaller than $C2^{-hj}$. This implies that the slope of $j \mapsto \log_2 \#\tilde{E}_j^-(C,h)(f)$ is close to n; the larger C is, the larger this slope is.

The next section explains how to define a "good" constant C for the approximation of $\breve{\nu}_f(h)$.

4.2.2 For a Fixed $h \in \mathbb{R}$, Choice of the Constant $C > 0$ to Approximate $\breve{\nu}_f(h)$

In order to determine a good approximation of $\breve{\nu}_f(h)$, we must use a constant C which is adapted to the amplitude of the coefficients. Our approach is not based on the choice of a specific constant, but on the choice of an interval of "good" constants. For a fixed $h \in \mathbb{R}$, let us construct the function

$$C > 0 \mapsto \breve{\nu}_f^C(h).$$

If $h \in [h_{\min}, h_{\max}]$, it should exist an interval I for which the values $\breve{\nu}_f^C(h)$, with $C \in I$, are close from each other. In the other cases (i.e. if $h < h_{\min}$ or $h > h_{\max}$), such an interval should not exist, i.e. the function should be decreasing or increasing without stabilisation. During my thesis's years, several strategies have been studied about the determination of I. Two points are important to have a relevant interval: choosing a "good" length, and having an effective method to detect a stabilisation of the chosen length.

Two Strategies to choose the length of the interval I. First, the greatest value among the moduli of the coefficients has been used for the length of the stabilisation. It gives some good results (see [46]) but it is less efficient for

signals with small size and it may be influenced by aberrant values in the signal. Moreover, the length of the stabilisation to approximate $\breve{\nu}_f(h)$ is thus the same for any $h > 0$. However, the number of coefficients used to approximate $\breve{\nu}_f(h)$ strongly depends on h, which implies that the approximation of $\breve{\nu}_f(h)$ for small h is not possible. Consequently, the length of the stabilisation must depend on h. A more robust approach is proposed in [78] where the length of the stabilisation depends on h. Let us recall that $\#\breve{E}_j(C, \sigma^{(h)})(f)$ corresponds to the number of coefficients that are larger (or smaller) than $C\sigma_j^{(h)}$. The idea is thus to consider a length of stabilisation equal to the median of the computed values

$$((\sigma_j^{(h)})^{-1}|c_\lambda|)_\lambda \quad \text{or} \quad ((\sigma_j^{(h)})^{-1}d_\lambda)_\lambda, \tag{62}$$

depending on whether the wavelet coefficients or the wavelet leaders are used. This length is denoted l_h. This approach gives good results in the context of ν_f [78].

Two Strategies to Detect a Stabilisation. First, a non-parametric gradient descent, where the gradient is calculated as the slope of the regression line over several consecutive points (typically 3 or 5 points) is proposed in [46, 78]: if this gradient is close to 0 for several consecutive points corresponding to the chosen length for the interval I, then we claim that a stabilisation has been detected and the mean (or the median) of these points is used to approximate $\breve{\nu}_f(h)$. This approach gives good results but it proved less effective on small real-life signals. To overcome this problem, we propose a new strategy: to use a sliding window of the length equal to the length of I on the function $C \mapsto \breve{\nu}_f^C(h)$. If the difference between the ninth decile and the first decile in this window[2] is small (typically, smaller than 0.03), then we say that a stabilisation is detected.

Strategy Chosen in this thesis. After many tests, the most efficient method is the following: we choose l_h for the length of I, and we use a sliding window on the function $C \mapsto \breve{\nu}_f^C(h)$ to determine the existence of a stabilisation. Consequently, the approximation of $\breve{\nu}_f(h)$ is

- $-\infty$ if no stabilisation is detected;
- the median of the values $\breve{\nu}_f^C(h)$ belonging to the first window of length l_h for which a stabilisation has been detected.

As we will show in the following sections, this method is not influenced by aberrant values in the signal and allows to have a better approximation of the spectrum than other wavelet-based methods.

[2]These deciles have been chosen to avoid rejecting a stabilisation if only a few extreme values are too apart. Let us notice that choosing the percentiles 5 and 95 give similar results.

Remark 4.2.1. For a small h, l_h can be very small and in this case the stabilisation will not be relevant, because it is computed with values of C too close from each other. Concerning the signals studied in this thesis, we have noticed that a value of l_h smaller than $0.1c_{\max}$ does not allow to have an acceptable length for the stabilisation. Consequently, we replace l_h with $\max\{l_h, 0.1c_{\max}\}$. In the same way, for the approximation of the decreasing part of the spectrum with $\tilde{\nu}_f^-(h)$, l_h can be very large if h is large, and it becomes impossible to have a stabilisation of this length. In this case, we replace l_h with the median of the values

$$(2^{(h-h_{dom})j} d_\lambda)_\lambda, \tag{63}$$

where h_{dom} is defined as the smallest h such that $\tilde{\nu}_f^+(h)$ equals n.

4.2.3 Computation of the Function $\breve{\nu}_f$

The first step consists in the detection of the smallest h for which $\breve{\nu}_f(h) \neq -\infty$, i.e. for which the function $C > 0 \mapsto \breve{\nu}_f^C(h)$ has a stabilisation of length l_h, as explained in the previous section. From the fact that, if $\breve{\nu}_f(h) \neq -\infty$, then $\breve{\nu}_f(h') \neq -\infty$ for any $h' > h$, we use a bisection method to detect this smallest h. We begin this procedure between 0 and 1; if no value is found, we restart this procedure between 1 and 2, and so on. Algorithm 1 gives the pseudocode of this method. Let us recall that the choice of the scales j where the regression is done is important and influences the approximation of $\breve{\nu}_f(h)$; for this reason, they are part of the parameters of the method. Once this h is detected, we can compute the function $\breve{\nu}_f$, by step of length 0.01 for example. Algorithm 2 gives the pseudocode of the approximation of $\breve{\nu}_f(h)$ for a given h, described in the previous section.

4.3 WPM and LPM in Action: Standard Setting

The next step is to test the algorithm described in the previous section on several classical examples, in the context of the WPM and the LPM. We show that this algorithm gives results at least as good as the ones obtained using other wavelet-methods (mainly, the WLM), when the function is monofractal or multifractal with a concave spectrum. Moreover, we show that this algorithm can detect non-concave spectra. For each signal, the chosen scales j for the regressions are the same for each method, and corresponds to the first scales computed with the Mallat algorithm, since we want approximate the theoretical spectrum of the signals.

Algorithm 1 Bisection method to detect the smallest h for which $\breve{\nu}_f(h) \neq -\infty$

procedure SMALLESTH(c,$\sigma^{(\cdot)}$,*chosen scales* j) ▷ c are the wavelet coefficients or the wavelet leaders of f
  $h_0 \leftarrow 0$
  $h_1 \leftarrow 1$
  $prec \leftarrow 0.01$ ▷ depends on the wished precision
  repeat
    $h_{\min} \leftarrow h_0$
    $h_{\max} \leftarrow h_1$
    $h \leftarrow (h_{\max} + h_{\min})/2$
    repeat
      if Approx$\breve{\nu}_f(h, c, \sigma^{(h)}$, *chosen scales* $j) \neq -\infty$ **then** ▷ see Algorithm 2
        $h_{\max} \leftarrow h$
      else
        $h_{\min} \leftarrow h$
      end if
      $h \leftarrow (h_{\max} + h_{\min})/2$
    until $|h_{\min} - h_{\max}| < prec$
    $h_0 \leftarrow h_0 + 1$
    $h_1 \leftarrow h_1 + 1$
  until a h such that $\breve{\nu}_f(h) \neq -\infty$ is detected
  return h
end procedure

Algorithm 2 Algorithm to approximate $\breve{\nu}_f(h)$

procedure Approx$\breve{\nu}_f(h, c, \sigma^{(h)}$, *chosen scales* j) ▷ c are the wavelet coefficients or the wavelet leaders of f
  thresholdCor $\leftarrow 0.95$
  thresholdStab $\leftarrow 0.03$
  $ł_h \leftarrow$ the median of $((\sigma_j^{(h)})^{-1}|c_\lambda|)_\lambda$ (and see Remark 4.2.1)
  maxValueForC $\leftarrow 10 l_h$ ▷ greater is not relevant to the signals of thesis
  stepOfC $\leftarrow l_h/100$ ▷ allows to have 100 points by window
  for $C \leftarrow 0$ **to** *maxValueForC* **by step of** *stepOfC* **do**
    Compute the *slope* and the *correlation* of the function $j \mapsto \log_2 \#\breve{E}_j(C, \sigma^{(h)})(c)$, on the *chosen scales* j
    if *correlation* $<$ *thresholdCor* **then**
      $\breve{\nu}_f^C(h) \leftarrow -\infty$
    else
      $\breve{\nu}_f^C(h) \leftarrow$ *slope*
    end if
  end for
  $\breve{\nu}_f(h) \leftarrow -\infty$
  $W \leftarrow$ the first window of length l_h of the function $C \mapsto \breve{\nu}_f^C(h)$
  repeat
    if |9th decile of W − 1st decile of W| $<$ *thresholdStab* **then**
      $\breve{\nu}_f(h) \leftarrow$ the median of W
      Break
    else
      $W \leftarrow$ the next window
    end if
  until there does not exist a window
  return $\breve{\nu}_f(h)$
end procedure

4.3.1 A Monofractal Example: The Fractional Brownian Motion

The first example is the classical monofractal process: the fractional Brownian motion [101]. It is a generalisation of the Brownian motion, studied in Chapter 2.

Definition 4.3.1. The *fractional Brownian motion* of parameter $H \in (0,1)$, noted $B^H = (B_x^H)_{x\in\mathbb{R}}$, is the unique Gaussian process such that

- almost surely, $B_0^H = 0$ and $x \in \mathbb{R} \mapsto B_x^H$ is a continuous function,
- it has stationary increments such that, for any $x_1, x_2 \in \mathbb{R}$, one has

$$B_{x_1}^H - B_{x_2}^H \sim \mathcal{N}(0, |x_1 - x_2|^{2H}).$$

The parameter H is called the *Hurst index*.

The following proposition gives some properties of the fractional Brownian motion.

Proposition 4.3.2. *[73] Let $B^H = (B_x^H)_{x\in\mathbb{R}}$ be a fractional Brownian motion of parameter H.*

- *It has the property of* scaling invariance *of parameter H, i.e.*

$$B_{ax}^H \sim |a|^H B_x^H,$$

  for any $a, x \in \mathbb{R}$.

- *If γ is the autocovariance function of the Gaussian process $(B_{j+1}^H - B_j^H)_{j\in\mathbb{Z}}$, i.e. $\gamma(j) = \mathrm{Cov}(B_{j+1}^H - B_j^H, B_1^H - B_0^H)$, then*

$$\gamma(j) = \frac{1}{2}(|j-1|^{2H} - 2|j|^{2H} + |j+1|^{2H}),$$

  for any $j \in \mathbb{Z}$.

The second point of this proposition shows that, if $H = 1/2$, then $\gamma(j) = 0$, for any $j \in \mathbb{Z}\setminus\{0\}$; consequently, the increments are independent. This implies that the fractional Brownian motion of parameter $1/2$ is the Brownian motion presented in Section 2.3. If $H \neq 1/2$, then the increments are not independent and we have

$$\gamma(j) \sim H(2H-1)j^{2H-2},$$

as $j \to +\infty$. This relation shows that, if $H \in (1/2, 1)$, then $\gamma(j) \sim cj^k$ ($c > 0$ and $k \in (-1, 0)$) as $j \to +\infty$; in other words, B^H presents *long-range dependencies*. If $H \in (0, 1/2)$, then $\gamma(j)$ is strictly negative and we thus say

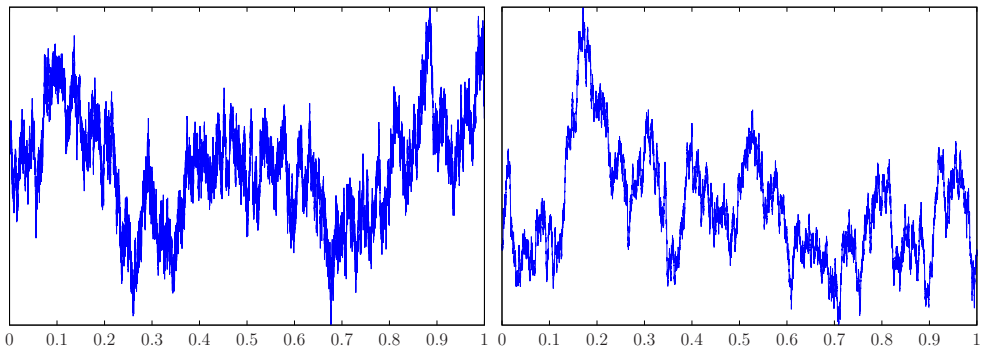

(a) $H = 0.3$ (b) $H = 0.5$

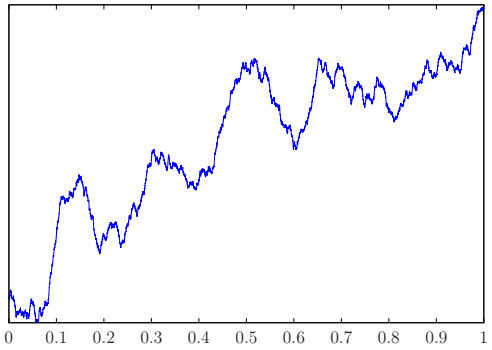

(c) $H = 0.7$

Figure 4.1.: Simulation of fractional Brownian motions of parameter H.

that B^H has *negative dependence*. This is illustrated on numerical simulations in Figure 4.1 (to simulate fractional Brownian motions, we use the algorithm described in [138]). Such dependencies are detected in many experimental observations and that is why the fractional Brownian motion models many monofractal phenomena [101, 36, 15, 111].

The following proposition shows that the *Hurst index* H characterises the Hölderian regularity of B^H.

Proposition 4.3.3. *[73] There exists an event $\Omega^* \subseteq \Omega$ of probability 1 such that, for any $\omega \in \Omega^*$, the walk $x \mapsto B_x^H(\omega)$ is a monofractal function with a Hölder exponent equal to H.*

Now that the fractional Brownian motion has been recalled, let us show the efficiency of the WPM and LPM to approximate the Hurst index H on numerical simulations of B^H.

Approximation of H. Let us recall that to approximate $d_f(h)$, we look for a stabilisation of the function $C \mapsto \breve{\nu}_f^C(h)$. If there is no stabilisation, we set $d_f(h) = -\infty$. Let us begin with the WPM.

The WPM only approximates the increasing part of the spectrum with the help of the function ν_f. Consequently, no stabilisation should be detected for $h < H$ and a stabilisation equal to 1 should appear for $h \geq H$. Consequently, the Hurst index H is approximated as the smallest h for which a stabilisation equal to 1 is found. Figure 4.2 shows some stabilisations for a simulation of the Brownian motion (i.e. $H = 1/2$).

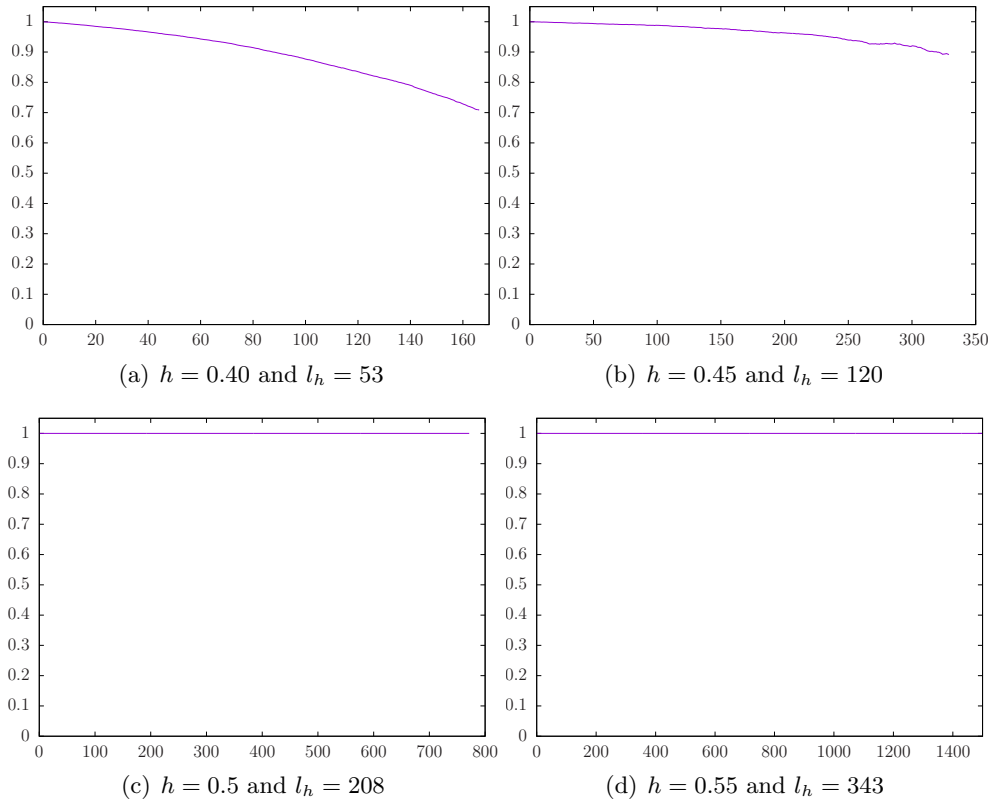

(a) $h = 0.40$ and $l_h = 53$ (b) $h = 0.45$ and $l_h = 120$

(c) $h = 0.5$ and $l_h = 208$ (d) $h = 0.55$ and $l_h = 343$

Figure 4.2.: Function $C \mapsto \nu_f^C(h)$ for a simulation of a Brownian motion. We search for a stabilisation on an interval I, whose the length l_h depends on h (see Section 4.2.2).

The LPM allows to approximate the increasing and the decreasing part of the spectrum with the help of the function $\tilde{\nu}_f^+$ and the function $\tilde{\nu}_f^-$ respectively. Consequently, no stabilisation should be detected for the function $C \mapsto \tilde{\nu}_{B^H}^{+,C}(h)$ if $h < H$, and a stabilisation equal to 1 should appear if $h \geq H$. While no stabilisation should be detected for the function $C \mapsto \tilde{\nu}_{B^H}^{-,C}(h)$ if

$h > H$, and a stabilisation equal to 1 should appear if $h \leq H$. Consequently, the Hurst index H can be approximated in three different ways:

- as the smallest h for which the function $C \mapsto \tilde{\nu}_{B^H}^{+,C}(h)$ has a stabilisation equal to 1,
- as the largest h for which $C \mapsto \tilde{\nu}_{B^H}^{-,C}(h)$ has a stabilisation equals 1,
- as the intersection between the functions $\tilde{\nu}_{B^H}^{+}$ and $\tilde{\nu}_{B^H}^{-}$.

This three methods give similar results and this is the third method that was chosen in the further sections. Figures 4.3 and 4.4 shows some stabilisations for a simulation of the Brownian motion (i.e. $H = 1/2$).

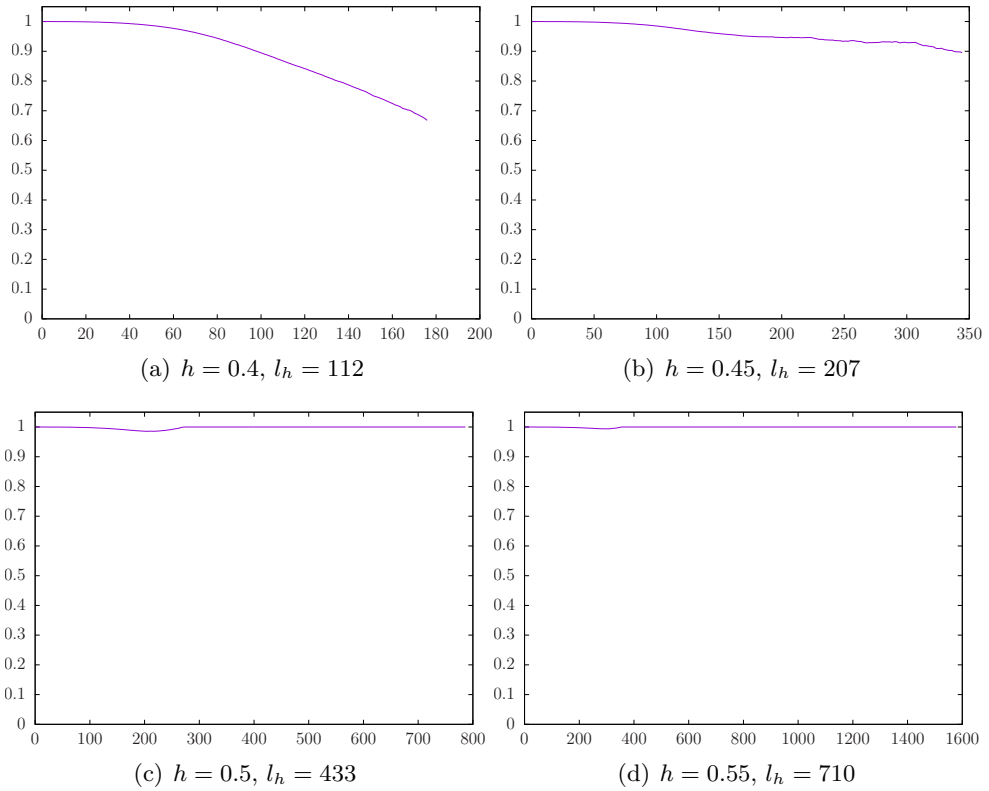

(a) $h = 0.4$, $l_h = 112$ (b) $h = 0.45$, $l_h = 207$

(c) $h = 0.5$, $l_h = 433$ (d) $h = 0.55$, $l_h = 710$

Figure 4.3.: Function $C \mapsto \tilde{\nu}_f^{+,C}(h)$ for a simulation of a Brownian motion. We search for a stabilisation on an interval I whose length l_h depends on h (see Section 4.2.2).

Remark 4.3.4. The value $\tilde{\nu}_f^{-,C}(h)$ will always be equal to 1 if C is sufficiently large, because we count the number of wavelet leaders that are smaller than $C2^{-hj}$. Consequently, we say that $\nu_f^{-}(h)$ is approximated by 1 if $\nu_f^{-,C}(h)$ equals 1 for most of the constants $C > 0$.

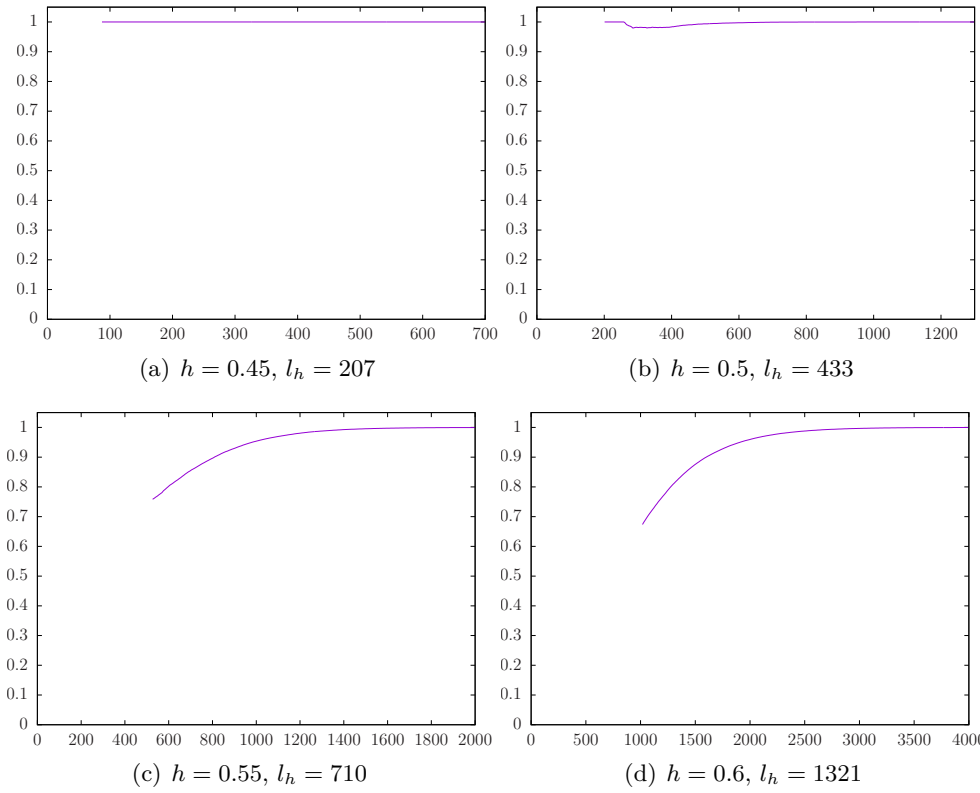

(a) $h = 0.45$, $l_h = 207$ (b) $h = 0.5$, $l_h = 433$

(c) $h = 0.55$, $l_h = 710$ (d) $h = 0.6$, $l_h = 1321$

Figure 4.4.: Function $C \mapsto \tilde{\nu}_f^{-,C}(h)$ for a simulation of a Brownian motion. We search for a stabilisation on an interval I whose length l_h depends on h (see Section 4.2.2).

Data and Results. For a fixed size 2^j ($11 \leq j \leq 20$), we have simulated one hundred walks of fractional Brownian motion with a parameter H varying between 0.2 and 0.8 by steps of 0.05. In Figure 4.5, the methods WPM, LPM and WLM are compared. The mean and the boxplot of the distances between the detected Hölder exponent and H, for simulations of size 2^j, are represented. The three methods give similar results. For the signals of size larger than 2^{16}, the average value of this distance is 0.02 with the WPM and the WLM, and is 0.03 with the LPM. For the signals of smaller size, this average value is close to $0.04 - 0.05$ for the three methods. Let us notice that some signals have a distance between the detected Hölder exponent and H larger than 0.08, for the three methods.

Approximation of the Spectrum of B. Let us finish this section by noticing that some stabilisations smaller than 1 can be found for h close to H. This implies that the approximation of the spectrum is not reduced to one point.

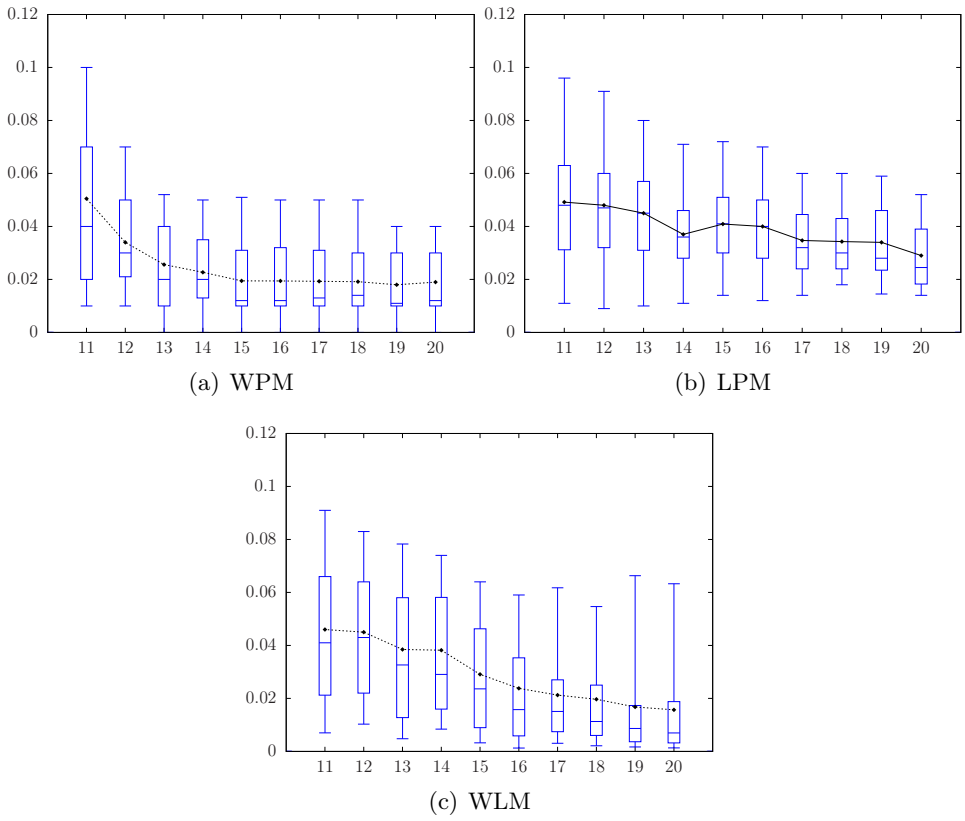

(a) WPM (b) LPM

(c) WLM

Figure 4.5.: For every j, the boxplot of the distances between the Hölder exponent detected and H (for H varying between 0.2 and 0.8 by steps of 0.05) of walks of fractional Brownian motion of size 2^j with a parameter H. The mean of these distances is also represented (in black).

Figure 4.6 shows a typical example of spectrum obtained with the WPM and the LPM for a Brownian motion. These examples show that the length of the support of these spectra is relatively small. In fact, this length can be a criterion to decide if a signal is monofractal or multifractal. This criterion will be detailed in Chapter 6.

Data and Results. Let us compute the length of the support of the spectrum on the simulations of fractional Brownian motions with the LPM. Figure 4.7 shows the mean and the boxplot of this length, as well as the smallest value obtained for a stabilisation of the functions $\tilde{\nu}_f^+$ and $\tilde{\nu}_f^-$, for simulations of fractional Brownian motions of size 2^j, for $j \in \{11, \ldots, 20\}$, with a parameter H varying between 0.2 and 0.8 by steps of 0.05.

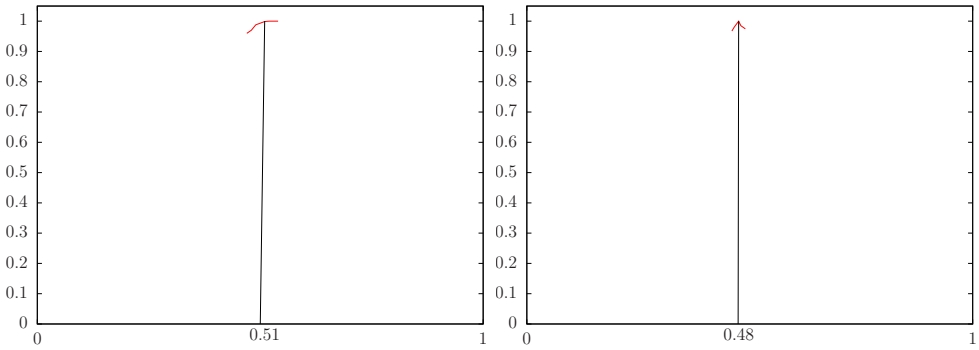

(a) WPM (b) LPM

Figure 4.6.: Typical approximation of the spectrum of a Brownian motion

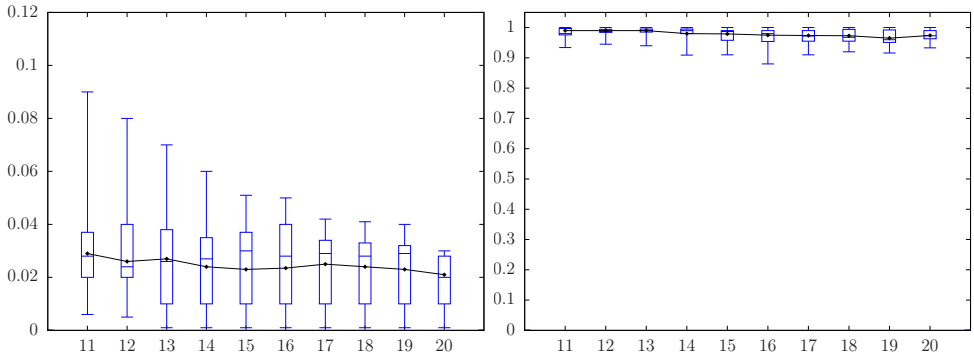

(a) Length of the support of the spectrum obtained (b) the smallest value obtained for a stabilisation of the increasing part of the spectrum

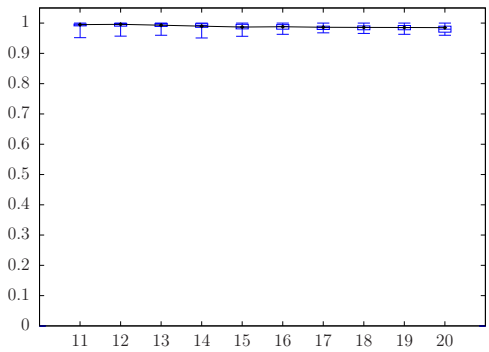

(c) the smallest value obtained for a stabilisation of the decreasing part of the spectrum

Figure 4.7.: For every j, the boxplot of some parameters of the LPM applied on fractional Brownian motions of size 2^j, with a parameter H varying between 0.2 and 0.8 by steps of 0.05. The mean of these parameters is also represented (in black).

We see that the average of the lengths of the support of the spectrum is close to 0.03, no matter the size of the signal. Nevertheless, some signals of smaller size are associated to a spectrum with support of size larger than 0.06. Moreover, the smallest value obtained for a stabilisation is on average close to 0.97.

4.3.2 A Multifractal Example with Concave Spectrum: The Mandelbrot Cascades

The most classical function with a concave spectrum is based on the notion of Mandelbrot cascades [100]. It models many phenomena, a lot of them occurring in turbulence [103, 108, 8, 127].

Definition 4.3.5. Let W be a given positive random variable such that $E[W] = 1$ and let $(W_\epsilon)_{\epsilon\in\Sigma}$ be an independent collection of copies of W indexed with the infinite binary tree $\Sigma = \bigcup_{n\geq 1}\{0,1\}^n$. For any $n \in \mathbb{N}$, the random measure μ_n on $[0,1]$ is defined as

$$\mu_n([\sum_{k=1}^{n}\frac{\epsilon_k}{2^k}, \sum_{k=1}^{n}\frac{\epsilon_k}{2^k} + \frac{1}{2^n})) = W_{\epsilon_1}W_{\epsilon_1\epsilon_2}\dots W_{\epsilon_1\epsilon_2\dots\epsilon_n}.$$

In [21], it is proved that the sequence μ_n converges almost surely to a Borel measure μ_W on the interval $[0,1]$.

In the sequel, we only consider the case where the random variable W is log-normal[3]. The following theorem gives the spectrum of μ_W in this case.

Theorem 4.3.6. *[8, 21] If the law of W is log-normal with parameters $\mu < 0$ and σ^2 such that $|\mu|/\sigma > \sqrt{2\log 2}$, then the spectrum of μ_W is given almost surely by*

$$d_{\mu_W}(h) = -\frac{(h + \mu/\log 2)^2 \log 2}{2\sigma^2} + 1$$

if $h \in [-\sqrt{\frac{2}{\log 2}}\sigma - \frac{\mu}{\log 2}, \sqrt{\frac{2}{\log 2}}\sigma - \frac{\mu}{\log 2}]$.

Approximation of the Spectrum d_{μ_W}. Let us recall that, for the two methods WPM and LPM, a stabilisation of the function $C \mapsto \breve{\nu}^C(h)$ is searched. Figure 4.8 represents this function, for some values of h.

The theoretical spectrum is compared with the spectrum obtained with the WPM, the LPM and the WLM in Figure 4.9: one can see that the three methods give a good approximation of the spectrum; let us recall that the WPM can only approximate the increasing part of the spectrum. The WPM and the LPM hardly detect the spectrum for small h; this problem depends on

[3] A random variable W is called a *log-normal variable* with parameters $\mu \in \mathbb{R}$ and $\sigma > 0$, if $\log(X) \sim \mathcal{N}(\mu, \sigma^2)$.

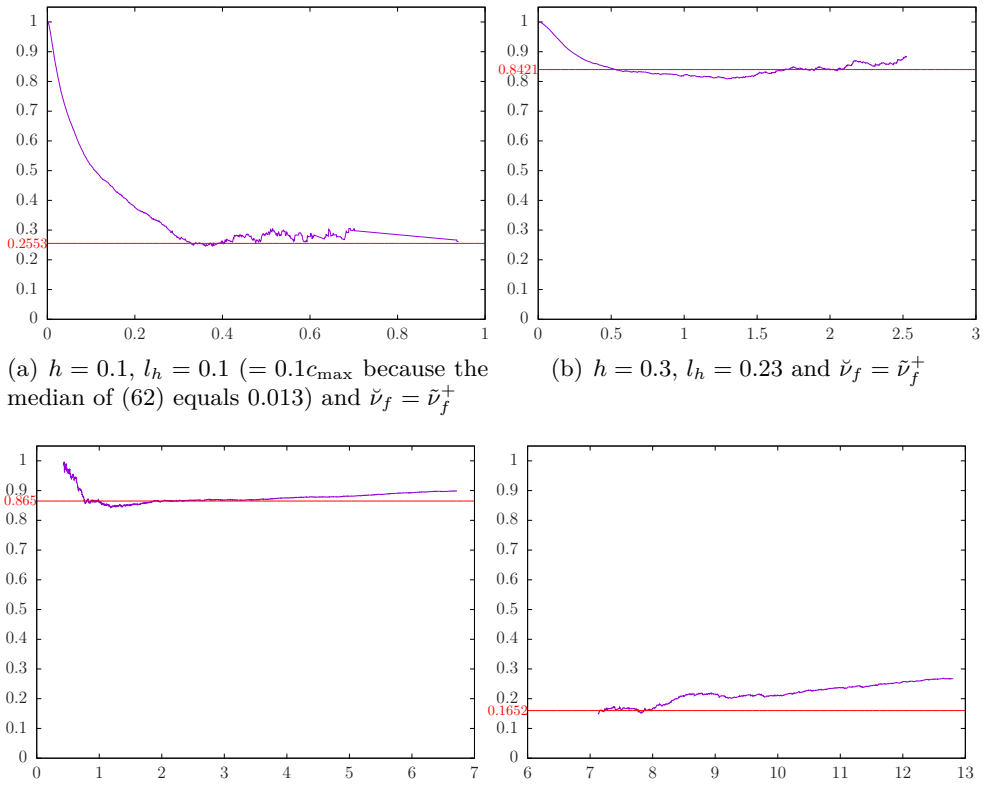

(a) $h = 0.1$, $l_h = 0.1$ ($= 0.1 c_{\max}$ because the median of (62) equals 0.013) and $\breve{\nu}_f = \tilde{\nu}_f^+$

(b) $h = 0.3$, $l_h = 0.23$ and $\breve{\nu}_f = \tilde{\nu}_f^+$

(c) $h = 0.6$, $l_h = 0.1$ ($= 0.1 c_{\max}$ because the median of (63) equals 0.03 and the median of (62) equals 9) and $\breve{\nu}_f = \tilde{\nu}_f^-$

(d) $h = 0.85$, $l_h = 0.81$ (this is the median of (63) because the median of (62) equals 259) and $\breve{\nu}_f = \tilde{\nu}_f^-$

Figure 4.8.: Function $C \mapsto \breve{\nu}_f^C(h)$ for a simulation of a log-normal cascade of size 2^{20} ($\mu = -0.45 \log 2$ and $\sigma^2 = 0.1 \log 2$). We search for a stabilisation on an interval I whose length l_h depends on h (see Section 4.2.2).

the size of the signal (on average, the first h is equal to 0.03 for size 2^{20} and 0.08 for size 2^{15}). Let us recall that these methods are based on the investigation of the behaviour of the number of coefficients that are larger than 2^{-hj} across scales j. For very small h, there are not enough remaining coefficients to have a stabilisation.

Data and Results. For a fixed size 2^j ($11 \leq j \leq 20$), we have simulated fifty log-normal cascades and computed the root-mean-square deviation (RMSE) of each simulation. The boxplot and the mean of these RMSE are represented in Figure 4.10. The three methods give similar results. For signals of size larger than 2^{17}, the average value of the RMSE is close to 0.05, with the three

methods. For the signals of smaller size, this average value is close to 0.07, for the increasing part of the spectrum with the WPM and LPM. The WLM keeps an average value for the RMSE close to 0.05 for the signals of size larger than 2^{14}, and this average value becomes 0.07 for the signals of size smaller than 2^{13}. Let us notice that, with the LPM, the decreasing part of the spectrum is less well approximated than the increasing part.

4.3.3 A Multifractal Example with a linear Spectrum: The Lévy Processes without Brownian Component

The second multifractal example considered here is the Lévy process. It is mostly used in the field of financial modelling, in particular for the purpose of modelling the evolution of risky assets [119, 20, 31, 126, 121].

Definition 4.3.7. A *Lévy process* $L = (L_x)_{x\in\mathbb{R}}$ is a stochastic process such that

- almost surely, $L_0 = 0$ and $x \mapsto L_x$ is right-continuous and admits a left limit at any point,
- it has independent stationary increments.

Let us notice that the Brownian motion is thus a Lévy processes. The next theorem shows that L is characterised with the help of three parameters.

Theorem 4.3.8. *[92, 59] If L is a Lévy process, then there exists a triple (a, σ, π), with $a \in \mathbb{R}$, $\sigma > 0$ and π a Radon measure satisfying*[4]

$$\int_{\mathbb{R}} (1 \wedge x^2)\, d\pi(x) < \infty,$$

such that the characteristic function $\mathbb{E}(e^{itL})$ is equal to $e^{-t\phi(t)}$, where

$$\phi(t) = iat + \frac{1}{2}\sigma^2 t^2 + \int_{\mathbb{R}} (1 - e^{itx} + itx\chi_{(-1,1)}(x))\, d\pi(x),$$

for any $t \in \mathbb{R}$. Reciprocally, if the triple (a, σ, π) is defined as above, then there exists a Lévy process L whose characteristic function is equal to $e^{-t\phi(t)}$.

[4]The notation $1 \wedge x^2$ means

$$1 \wedge x^2 = \begin{cases} 1 & \text{if } |x| > 1 \\ x^2 & \text{if } |x| \leq 1 \end{cases}.$$

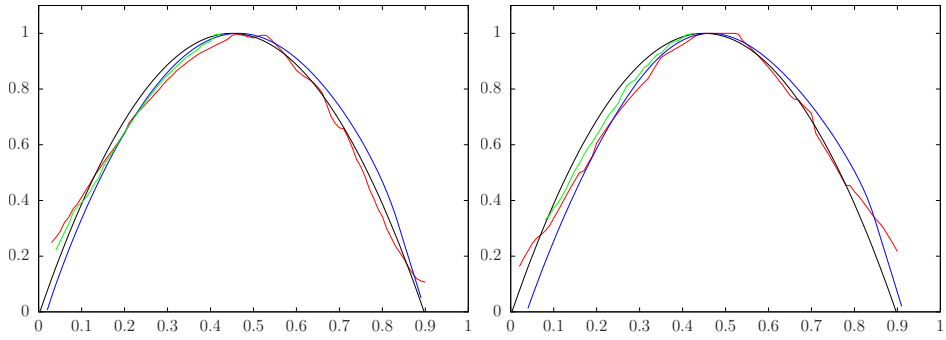

(a) $j = 20$ (b) $j = 15$

Figure 4.9.: Spectrum of the log-normal cascade ($\mu = -0.45 \log 2$ and $\sigma^2 = 0.1 \log 2$). Theoretical spectrum (—), WPM spectrum (—), LPM spectrum (—) and WLM spectrum (—). The results are obtained with a realisation of length 2^j.

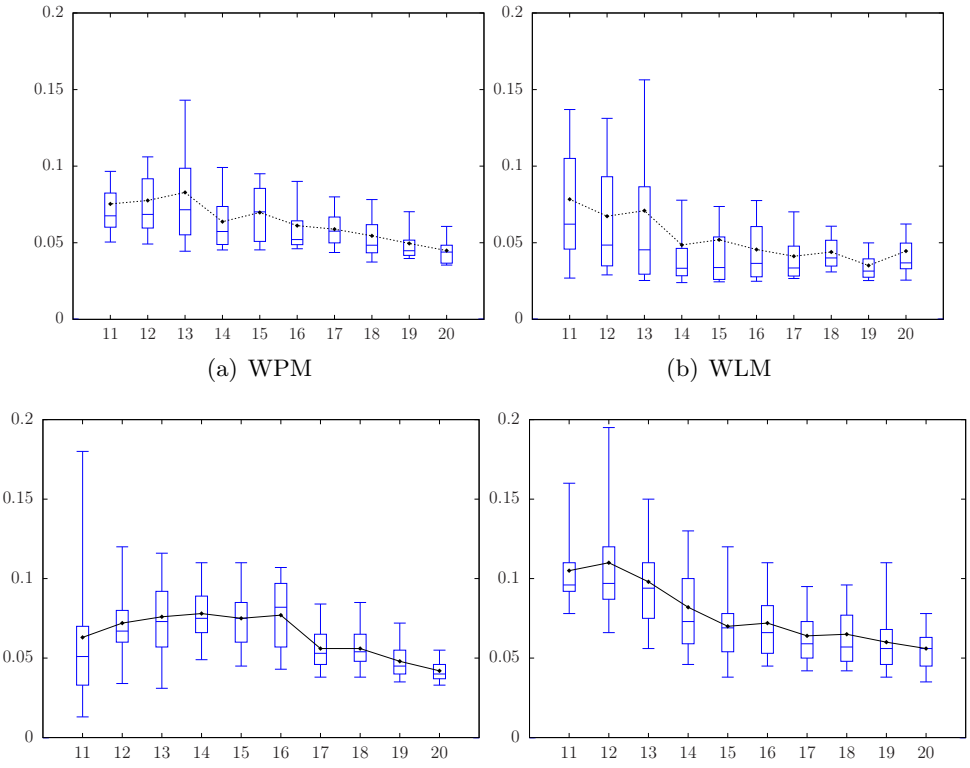

(a) WPM (b) WLM

(c) LPM (increasing part of the spectrum) (d) LPM (decreasing part of the spectrum)

Figure 4.10.: For every j, the boxplot of the RMSE of fifty log-normal cascades of size 2^j. The mean of these RMSE is also represented (in black).

The multifractal properties of the sample paths of a Lévy process are governed by an index $\beta \in [0, 2]$, called the *Blumenthal and Getoor lower index* [29]: if π is the measure of the previous theorem, then the index β is defined as

$$\beta = \inf\{\gamma \geq 0 : \int_{|x|\leq 1} |x|^\gamma \, d\pi(x) < \infty\} = \sup\{0, \limsup_{j\to+\infty} \frac{\log C_j}{\log 2^j}\},$$

where

$$C_j = \int_{2^{-j-1}\leq|x|\leq 2^{-j}} d\pi(x).$$

The following theorem gives the Hölder spectrum of a path of a Lévy process.

Theorem 4.3.9. *[64] Let L be a Lévy process satisfying $\beta > 0$ and*

$$\sum_{j\in\mathbb{N}} 2^{-j}\sqrt{C_j \log(1 + C_j)} < +\infty.$$

- *If L has no Brownian component (i.e. $\sigma = 0$), the spectrum of L is given, almost surely, by*

  $$d(h) = \beta h,$$

  for any $h \in [0, 1/\beta]$.

- *If L has a Brownian component (i.e. $\sigma \neq 0$), the spectrum of L is given, almost surely, by*

  $$d_L(h) = \begin{cases} \beta h & \text{if } h \in [0, 1/2) \\ 1 & \text{if } h = 1/2 \end{cases}.$$

Consequently, if L has no Brownian component, the spectrum is linear and thus is concave; if L has a Brownian component, the spectrum is not concave. In this section, we treat the case of a Lévy process without Brownian component. The case with a Brownian component will be treated in the next section.

To simulate Lévy processes without Brownian component, the algorithm described in [102] is used.

Approximation of the Spectrum d_L. Figure 4.11 compares the theoretical spectrum with the approximation of the increasing part of the spectrum obtained with the WPM, the LPM and the WLM. The spectrum detected with the WPM and LPM fits better the spectrum than the spectrum obtained via the WLM. This last method tends to make a strictly concave spectrum. Moreover, the LPM seems to detect the spectrum for smaller h than the WPM.

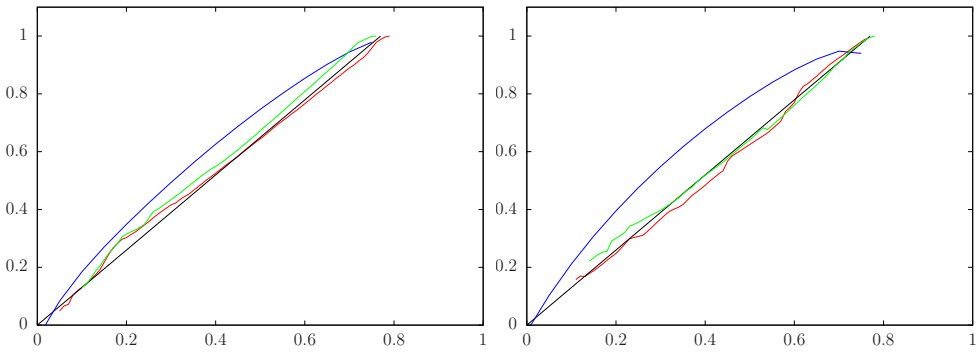

(a) $j = 19$ (b) $j = 14$

Figure 4.11.: Spectrum of the Lévy process without Brownian component ($\beta = 1.3$). Theoretical spectrum (—), WPM spectrum (—), LPM spectrum (—) and WLM spectrum (—). The results are obtained with a realisation of length 2^j.

Data and Results for the RMSE. For a fixed size 2^j ($11 \leq j \leq 20$), we have simulated fifty Lévy processes without Brownian component ($\beta = 1.3$) and the RMSE of each simulation has been computed. The boxplot and the mean of these RMSE are represented in Figure 4.12. For larger j, the LPM gives clearly better results than the two others methods. For signals of size larger than 2^{15}, the average value of the RMSE is close to 0.02 for the LPM, while this average value is close to 0.05 (resp. 0.07) for the WPM (resp. the WLM). For the signals of smaller size, the three methods are similar, with a slight advantage for the LPM.

Results for the Smallest Detected Value of the Spectrum d_L. It is important to determine the smallest h for which $d_f(h)$ can be approximate with the WPM and the LPM. The boxplot and the mean of this h are represented in Figure 4.13. We see that, for the large values of j, the LPM is clearly better than the WPM. For the signals of size larger than 2^{15}, the first method detects the spectrum, in average, from 0.05 , while the WPM detects from 0.09. For the signals of smaller size, the two methods are similar, with a slight advantage for the LPM.

Results for the (non-) Detection of the Decreasing Part of the Spectrum d_L, with the LPM. Let us finish this section by a complement on the LPM. Since the Lévy process has a spectrum with an increasing part only, we have only used the function $\tilde{\nu}_f^+$. However, for a real-life signal f, we do not know a priori if the spectrum of f has a decreasing part. It is thus interesting to see how the LPM behaves in the approximation of the decreasing part on a signal,

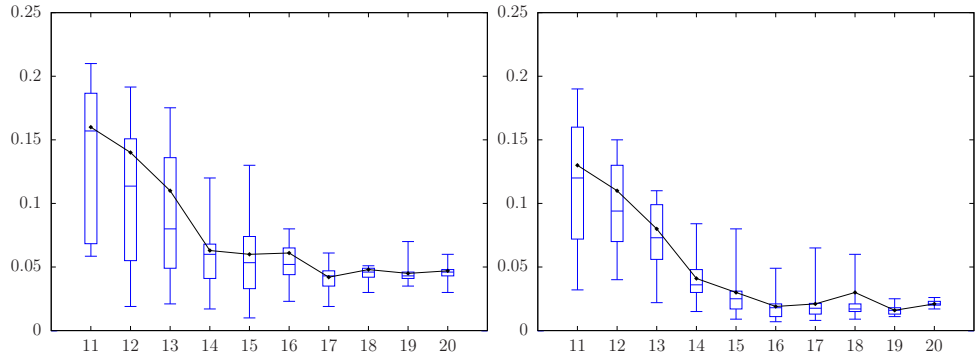

(a) WPM (b) LPM

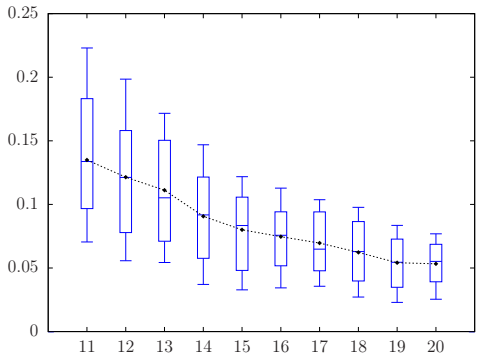

(c) WLM

Figure 4.12.: For every j, the boxplot of the RMSE of fifty Lévy processes without Brownian component ($\beta = 1.3$) of size 2^j. The mean of these RMSE is also represented (in black).

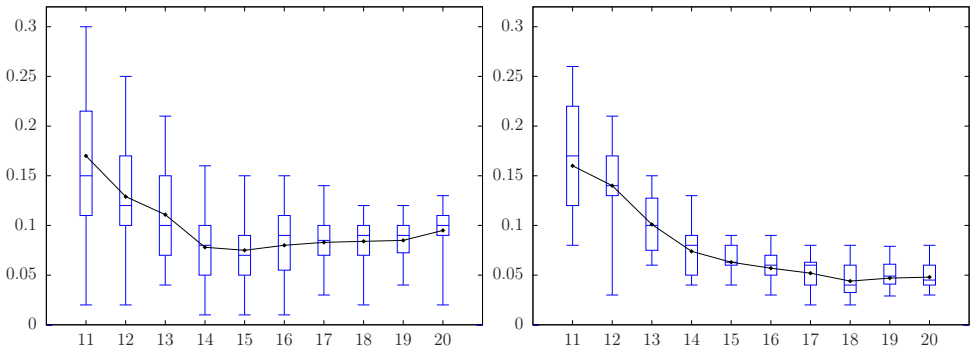

(a) WPM (b) LPM

Figure 4.13.: For every j, the boxplot of the smaller h where the spectrum is detected. The mean is also represented (in black).

which does not have one. For the Lévy process without a Brownian part, no stabilisation should be detected in the function $C \mapsto \tilde{\nu}_f^-(h)$ for $h > 1/\beta$. In practice, we detect some stabilisation for h close to $1/\beta$. Figure 4.14 shows the boxplot and the mean of the distance between $1/\beta$ and the larger h for which a stabilisation is detected, and the boxplot and the mean of the values of this stabilisation.

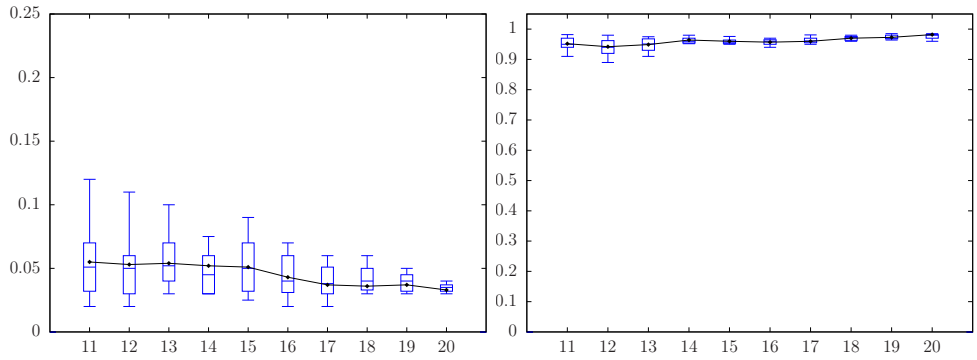

Figure 4.14.: For every j, the boxplot of the distance between $1/\beta$ and the larger h for which a stabilisation is detected with the LPM (left), and the boxplot and the mean of the value of this stabilisation (right). The mean is also represented (in black).

We see that the distance between $1/\beta$ and the largest h for which a stabilisation is detected, is on average $0.03 - 0.05$. This stabilisation is on average greater than 0.95.

4.3.4 A Multifractal Example with a Non-Concave Spectrum: The Lévy Processes with a Brownian Component

Let us now complete the study of the Lévy process by considering the case where the Brownian component of the Lévy process is non-vanishing. Let us recall that in this case, the Hölder spectrum is non-concave and, almost surely, is equal to

$$d_L(h) = \begin{cases} \beta h & \text{if } h \in [0, 1/2) \\ 1 & \text{if } h = 1/2 \end{cases} .$$

To simulate this process, we add a Brownian motion to Lévy processes generated in the previous section. Figure 4.15 shows a simulation of this process.

Approximation of the spectrum d_L. In Figure 4.16, we have represented the function $C \mapsto \tilde{\nu}_f^{+,C}(h)$ ($h = 0.4$ and $h = 0.52$) for a simulation of a Lévy

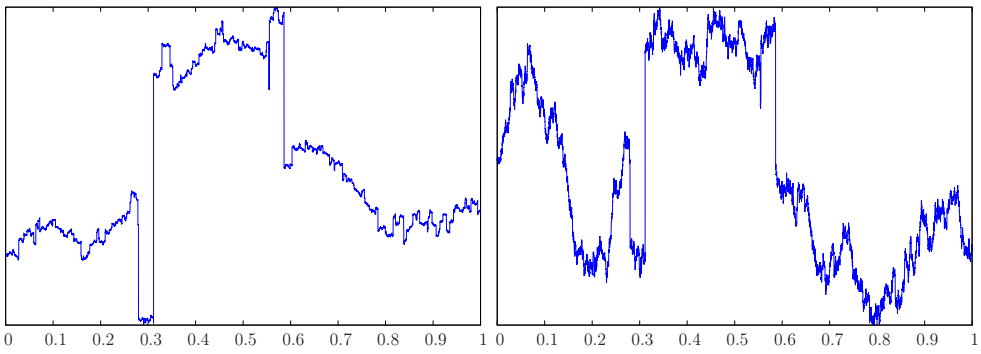

(a) without Brownian component (b) with Brownian component

Figure 4.15.: Simulations of a Lévy process

process with a Brownian part. It is interesting to note that for $h < 0.5$, one stabilisation is detected and corresponds to the approximation of the spectrum at h (see Figure 4.16(a)); for $h > 0.5$, two stabilisations are sometimes detected (see Figure 4.16(b)). The first one is the approximation of the spectrum at h, and the second one seems to correspond to the Lévy process without Brownian part used to simulate the signal. The profile methods can thus detect the presence of several processes in a single signal. We will confirm this observation at the end of this section.

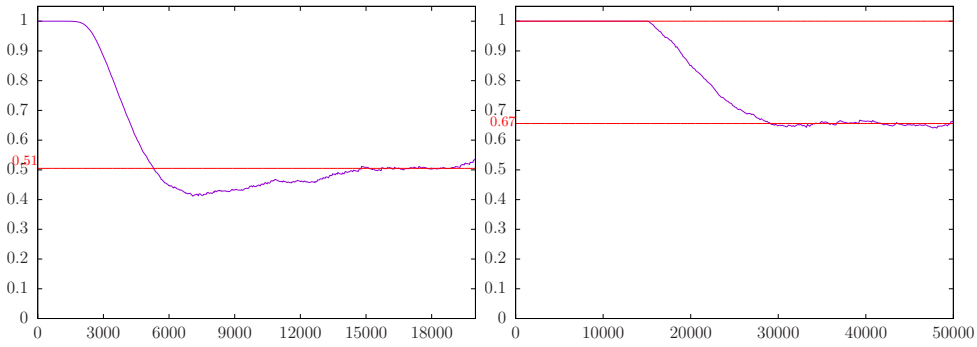

(a) $h = 0.4$ and $l_h = 628.746$ (b) $h = 0.52$ and $l_h = 3605.66$

Figure 4.16.: Function $C \mapsto \nu_f^{+,C}(h)$ for a simulation of a Lévy process ($\beta = 1.3$) with a Brownian motion. We search for a stabilisation on an interval I whose length l_h depends on h (see Section 4.2.2).

In Figure 4.17, we compare the spectra obtained with the WPM, the LPM and the WLM. With the WPM and the LPM, the non-concave part is detected. Let us notice that for a size of 2^{16}, the approximation of the spectrum obtained with the WPM and the LPM oscillates. In Section 4.4, we give a method to

improve the approximation of the spectrum and get rid of this oscillation. The WLM can only detected the concave hull of the spectrum. The superiority of the WPM and the LPM is clear.

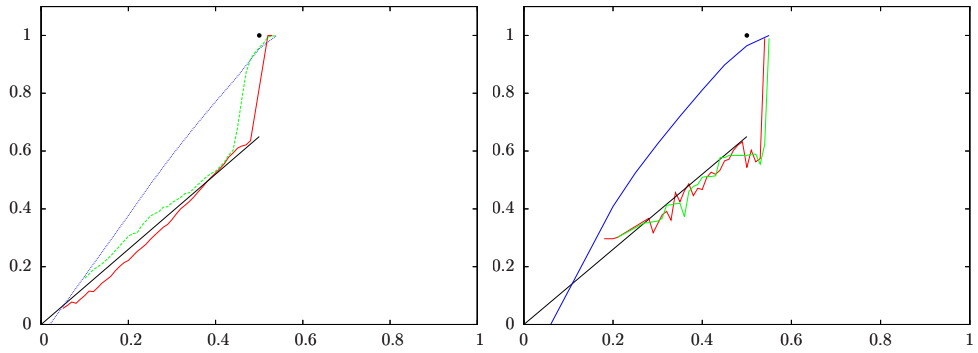

(a) $j = 20$ (b) $j = 16$

Figure 4.17.: Spectrum of the Lévy process with a Brownian component ($\beta = 1.3$). Theoretical spectrum (—), WPM spectrum (—), LPM spectrum (—) and WLM spectrum (—). The results are obtained with a realisation of length 2^j.

Data and Results. For a fixed size 2^j ($11 \leq j \leq 20$), we have simulated fifty Lévy processes with a Brownian part ($\beta = 1.3$). For each fixed j, we have computed the RMSE of each simulation. The boxplot and the mean of these RMSE are represented in Figure 4.18. The WPM and the LPM are obviously better than the WLM, due to the fact that this last one gives the concave hull of the spectrum. Let us notice that, for signals of size 2^{11}, it is very difficult to have acceptable stabilisations for the function $C \mapsto \nu_f^C(h)$. We have less than 15% of the signals with an acceptable stabilisation; it is thus impossible to represent the boxplot of these signals for the WPM.

Results for the (non-) Detection of the Decreasing Part of the Spectrum d_L, with the LPM. As for the case without Brownian component, we can look at the approximation of the decreasing part with the LPM. The results are similar to Figure 4.14.

Detection of two Stabilisations with the LPM. Let us finish this section by returning to Figure 4.16(b). For $h > 0.5$, the function $C \mapsto \breve{\nu}_f^C(h)$ has two stabilisations. The second one corresponds to the approximation of the spectrum evaluated at h of the Lévy process without Brownian component used to simulate the process. Figure 4.19 shows the values obtained with the second stabilisation with the LPM.

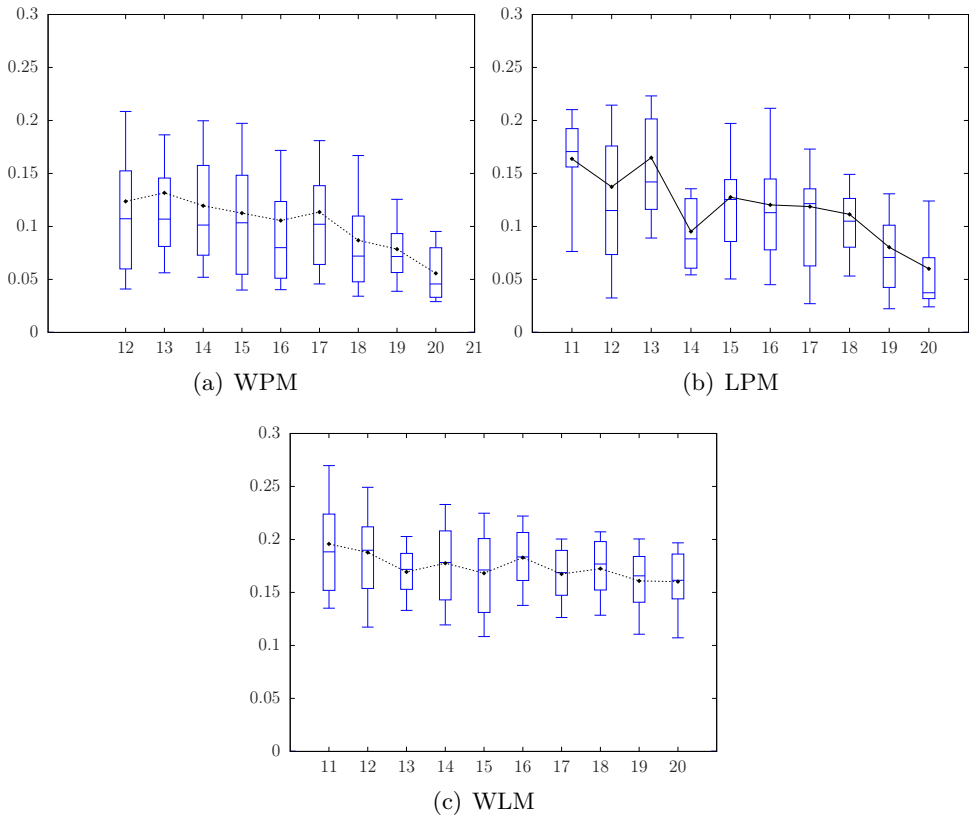

(a) WPM (b) LPM

(c) WLM

Figure 4.18.: For every j the boxplot of the RMSE of fifty Lévy processes which are the sum of a pure jump process ($\beta = 1.3$) and a Brownian motion ($H = 0.5$) of size 2^j. The mean of these RMSE is also represented (in black).

For a fixed size 2^j ($11 \leq j \leq 20$), we have simulated fifty Lévy processes with a Brownian part ($\beta = 1.3$). For each fixed j, we have computed the RMSE of the distance between the value of the second stabilisation and the spectrum of the Lévy process without Brownian part used in the simulation. The boxplot and the mean of these RMSE are represented in Figure 4.20. Obviously, this approximation is less good than the approximation obtained directly on the Lévy process without Brownian component, but they remain good. The most important is to notice than the LPM (and more generally profile methods) can show the existence of several phenomena in a single signal.

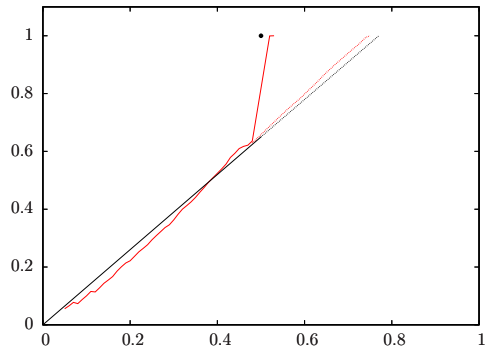

Figure 4.19.: Spectrum of the Lévy process with a Brownian component ($\beta = 1.3$). Theoretical spectrum (—), LPM spectrum (—) and the dotted points correspond to the spectrum of the Lévy process without Brownian component. The results are obtained with a realisation of length 2^{20}.

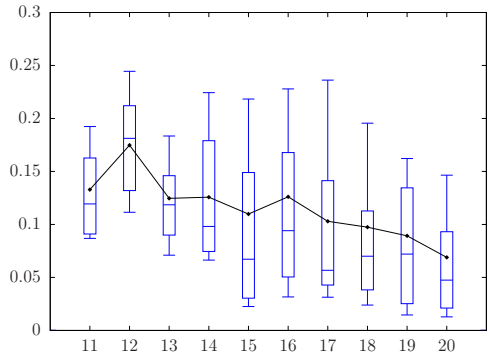

Figure 4.20.: For every j, the boxplot of the RMSE between the second stabilisation and the spectrum of the Lévy process without Brownian component ($\beta = 1.3$) used to simulate the Lévy process with a Brownian component. The mean of these RMSE is also represented (in black).

4.4 Improvement of the Stability of the Function $C \mapsto \breve{\nu}_f^{(C)}(h)$: Better Approximation of the Spectrum

As seen in the previous section, the approximation of the spectrum d_f of a real-life signal f, is based on the research of a stabilisation of the function

$$C \mapsto \breve{\nu}_f^{(C)}(h).$$

It can be sometimes difficult to find such a stabilisation. The main causes are the following: the presence of noise in the coefficients, the values of the coefficients are not enough variable or the size of the signals is too small. In this section, we propose a method to improve the stability, and consequently the approximation of the spectrum.

To understand one of the problems in which the stability is difficult to get, let us recall the simplest example of cascade: the binomial cascade.

Definition 4.4.1. The *binomial cascade of parameter* $p \in (0,1)$ is the only Borel measure μ defined on $[0,1]$ such that

$$\mu([\sum_{k=1}^{n} \frac{\epsilon_k}{2^k}, \sum_{k=1}^{n} \frac{\epsilon_k}{2^k} + \frac{1}{2^n})) = p^{\sum_{k=1}^{n} \epsilon_k}(1-p)^{n-\sum_{k=1}^{n} \epsilon_k},$$

for all $n \in \mathbb{N}$ and $\epsilon_k \in \{0,1\}$ $(k \in \{1,...,n\})$.

Proposition 4.1.2 ensures the existence of a function f such that $c_\lambda = \mu(\lambda)$, for any $\lambda \in \Lambda$, and that shares the same multifractal properties than μ. We will say that f is a binomial cascade of parameter p. The following theorem gives the spectrum of f.

Theorem 4.4.2 ([127])**.** *The spectrum of a binomial cascade f of parameter $p \in (0,1/2)$ is given by*

$$d_f(h) = -(\alpha \log_2 \alpha + (1-\alpha)\log_2(1-\alpha)),$$

where

$$\alpha = \frac{h + \log_2(1-p)}{\log_2(1-p) - \log_2 p},$$

for any $h \in [-\log_2(1-p), -\log_2 p]$.

Approximation of the Spectrum of a Binomial Cascade: Highlighting of the Problem. Let us use the LPM to approximate the spectrum of a simulation of a binomial cascade f. We fix $h \in [-\log_2(1-p), -\log_2 p]$ and we must thus construct the function

$$C \mapsto \tilde{\nu}_f^{+,(C)}(h). \tag{64}$$

Let us recall that $\tilde{\nu}_f^{+,(C)}(h)$ is the slope of the function

$$j \mapsto \frac{\log \#\tilde{E}_j^+(C,h)(f)}{\log 2},$$

where $\#\tilde{E}_j^{(+)}(C,h)(f)$ represents the number of wavelet leaders that are larger than $C2^{-hj}$. In the case of the binomial cascade, the wavelet coefficients c_λ take only j different values within a scale j. This implies that there are "jumps" in the function (64). These jumps affect the existence of a (clear) stabilisation of this function. This is illustrated in Figure 4.21.

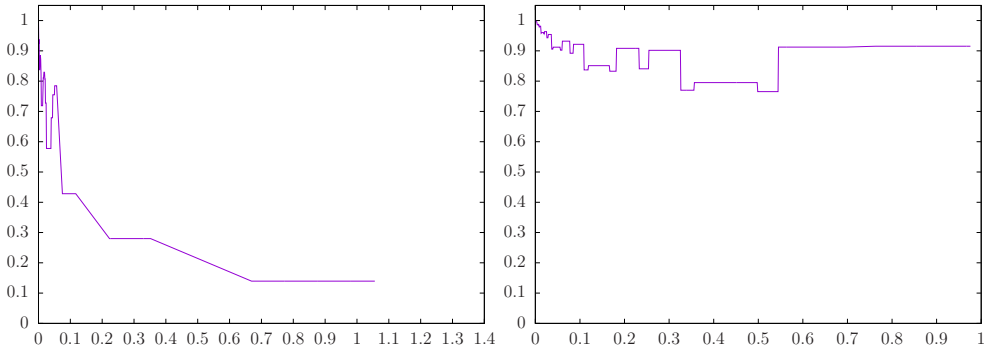

(a) $h = 0.6$ ($d_f(0.6) = 0.519$) (b) $h = 0.9$ ($d_f(0.9) = 0.888$)

Figure 4.21.: Function $C \mapsto \tilde{\nu}_f^{+,(C)}(h)$ for a binomial cascade f of parameter $p = 0.25$ of size 2^{15}.

A New Method to Overcome this Problem: adding Variability. The problem comes from the fact that the values of the coefficients do not vary enough within a fixed scale j. To overcome this problem, we propose a method that will add variability to the values taken by the wavelet coefficients. Before applying the algorithm explained in Section 4.2, we modify the wavelet coefficients of the function f as follows: the coefficients c_λ is replaced by

$$c_\lambda U_\lambda, \tag{65}$$

where $(U_\lambda)_{\lambda\in\Lambda}$ is an arbitrary sequence of independent random variables with respect to the uniform probability measure on $[C_1, C_2]$ with $0 < C_1 < C_2$.

Remark 4.4.3. If f is uniformly Hölder, then the function $\tilde{f}$, whose the wavelet coefficients are defined by (65), has the same Hölder spectrum than f. Indeed, for any $x \in [0,1]$, we have

$$C_1 d_j^{(f)}(x) \leq d_j^{(\tilde{f})}(x) \leq C_2 d_j^{(f)}(x),$$

where $d_j^{(f)}(x)$ (resp. $d_j^{(\tilde{f})}(x)$) is the wavelet leader of f (resp. of $\tilde{f}$) associated to the dyadic cube $\lambda_j(x)$. Consequently, we have

$$\liminf_{j\to+\infty} \frac{\log C_1 + \log d_j^{(f)}(x)}{\log 2^{-j}} \leq \liminf_{j\to+\infty} \frac{\log d_j^{(\tilde{f})}(x)}{\log 2^{-j}} \leq \liminf_{j\to+\infty} \frac{\log C_2 + \log d_j^{(f)}(x)}{\log 2^{-j}}.$$

From Theorem 1.5.17, we conclude that $h_f(x) = h_{\tilde{f}}(x)$, and thus the spectrum of f is the same as $\tilde{f}$.

We must now choose constants C_1, C_2 in order to help us to improve the stability of the function (64). After several tests, $C_1 = 0.5$ and $C_2 = 1.5$ seems to be a good choice. This is motivated by the three following reasons:

- on average, we multiply the coefficients by 1,
- the standard deviation is not too small, which insure a sufficient variability in the values of the coefficients,
- the standard deviation is not too large, in order to not have some values of the coefficients "totally arbitrary", from the fact that we only have a finite number of wavelet coefficients.

The advantage of this transformation is that we can repeat this method as much as wanted, which allows to compute an average spectrum; this technique improve the approximation of the spectrum.

Application of this New Method to the Binomial Cascades. Let us apply this method to the binomial cascade. Figure 4.22 shows the function (64) obtained when one modifies the wavelet coefficients by (65) with $C_1 = 0.5$ and $C_2 = 1.5$: now, we can clearly see the stabilisation.

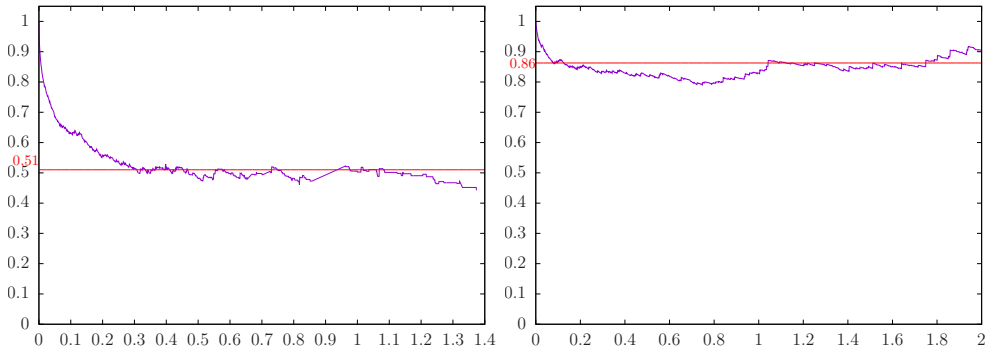

(a) $h = 0.6$ ($d_f(0.6) = 0.519$) (b) $h = 0.9$ ($d_f(0.9) = 0.888$)

Figure 4.22.: Function $C \mapsto \tilde{\nu}_f^{+,(C)}(h)$ for a binomial cascade f of parameter $p = 0.25$ of size 2^{15}.

Figure 4.23 shows the average spectrum of a binomial cascade of size 2^{16}; the above procedure has been repeated 50 times. We clearly see that the spectrum is concave, but the obtained spectrum is slightly shifted to the left. For strictly concave spectra, the WLM is a good method, but our method allows to ensure that the spectrum is concave.

Application of this New Method to the Lévy Process with a Brownian Component. The second example showing the effectiveness of this method is the Lévy process with a Brownian component. Let us recall that, for a simulation of this process with a size 2^{16}, the approximation of the spectrum

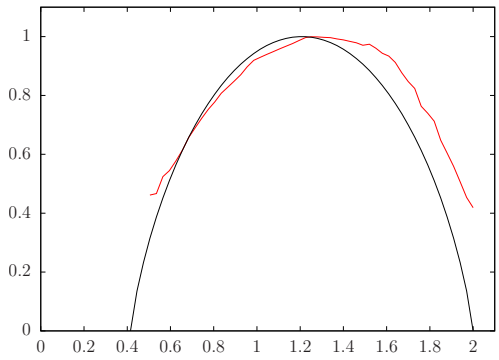

Figure 4.23.: Average spectrum obtained with LPM (—) on the binomial cascade of parameter $p = 0.25$ of size 2^{16}, where the wavelet coefficients have been replaced by (65).

tends to oscillate around the theoretical spectrum, as illustrated in Figure 4.17. This is because the stabilisations obtained with a signal of this size are not as good as those with a signal of a larger size. Now, let us take the signal which is associated to the spectrum of this figure and compute the average spectrum obtained with the method explained in this section. Figure 4.24 shows the new approximation of the spectrum. We clearly see that an improvement in the approximation of the spectrum. The oscillations showed in Figure 4.17, for a size of 2^{16}, are vanishing, while we always see the non-concave part.

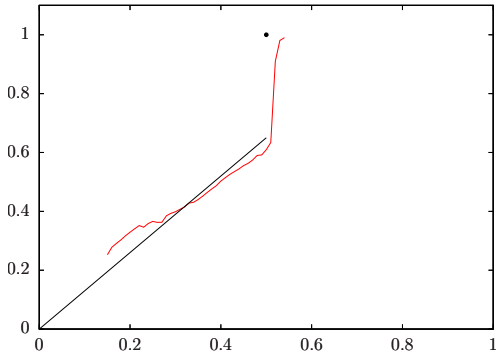

Figure 4.24.: Average spectrum obtained with LPM (—) on a Lévy process with a Brownian component ($\beta = 1.3$) of size 2^{16}, where the wavelet coefficients have been replaced by (65).

4.5 Profile Methods vs WLM: Robustness of the Method

In practice, aberrant values can appear in a signal (for example, see [41]). These values can influence the analysis of the signal. It is important to check the influence of such values in the algorithm presented in this chapter. This is illustrated in this section with a disturbance of the fractional Brownian motion. More precisely, one point of the signal is replaced by four times the largest value of the signal (such a modification is inspired by real-life signals [41]). We will compare here the results obtained between the WPM and the WLM. Let us notice that the results obtained with the LPM are similar to the WPM.

Let us recall that, the WLM approximates the Hölder exponent of a monofractal signal by the slope of the function $q \mapsto \eta_f(q)$, where

$$\eta_f(q) = \liminf_{j \to +\infty} \frac{2^{-j} \sum_{\lambda \in \Lambda_j} |d_\lambda|^q}{\log 2^{-j}}.$$

For the fractional Brownian motion, this method gives good results (see Section 4.1), but the function η_f is strongly modified with the disturbed signal, as illustrated in Figure 4.25. Indeed, if one point of the signal is much larger than the others, at each scale j, at least one wavelet coefficient is strongly modified. As a result, the function η_f has a flat part for the largest values of q and the slope of the increasing part does not give a correct approximation of the Hölder exponent. For example, the WPM (resp. WLM) approximates the Hölder exponent by 0.81 and 0.82 (resp. 0.81 and 0.87) for the fractional Brownian motion of parameter $H = 0.8$ and its disruption respectively.

Figure 4.26 shows for every j, the mean and the boxplot of the distance between the Hölder exponent detected for the fractional Brownian motion and the exponent detected for the corresponding disturbed signal using the WPM and the WLM. The robustness of the WPM is clear. For sizes 2^j with $15 \leq j \leq 20$, this distance is smaller than 0.01. For smaller sizes, this distance is also very small, excepted for a few signals of size 2^{11}. By contrast, the WLM is very disturbed. For sizes 2^j with $16 \leq j \leq 20$, the distance has the same order of magnitude as the approximation of the exponent of the original signal (see Figure 4.5). For smaller sizes, the exponent detected for the disturbed fractional Brownian motion is significantly different from the true exponent.

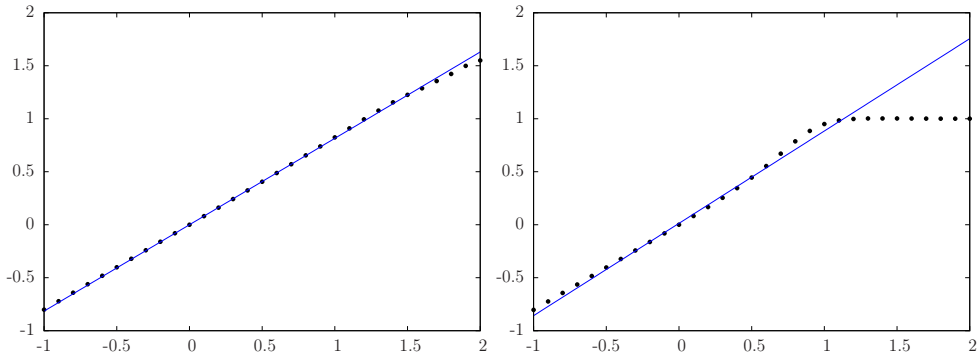

(a) the slope equals 0.815168 (b) the slope equals 0.871209

Figure 4.25.: Function $q \mapsto \eta_f(q)$. Left (resp. right) for the fractional Brownian motion (resp. the fractional Brownian motion where one point is replaced by four times the largest value of the signal) of size 2^{15} with $H = 0.8$.

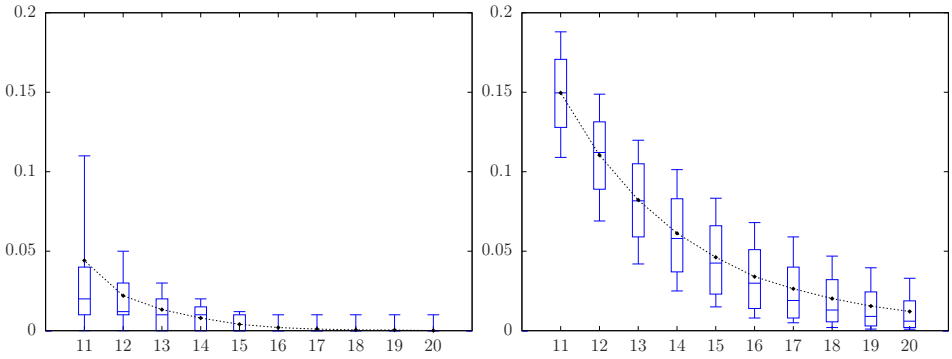

(a) WPM (b) WLM

Figure 4.26.: For every j, the boxplot of the distances between the Hölder exponent detected for the fractional Brownian motion and the exponent detected for the corresponding disturbed signal of size 2^j. The mean of these distances is also represented (in black).

4.6 Remarks about the Length of the Stabilisation

In practice, the choice of the constant C used to compute an approximation of the value $\breve{\nu}_f(h)$ is very important; the computed value $\breve{\nu}_f^C(h)$ is dependent of C and can be very different from the theoretical value $\breve{\nu}(h)$. As already explained, the approach used in this thesis is not to find a constant C, but rather an interval where the values $\breve{\nu}_f^C(h)$ are close.

As already mentioned in Section 4.2, the first approach developed during my thesis's years consisted in taking the greatest value among the moduli of the wavelet coefficients (or wavelet leaders) for the length of the interval (see [46]). This approach gives some good results but a few problems are presents:

- it is less efficient for the signals of small size,
- it is very difficult to have an approximation of $\breve{\nu}_f(h)$ for small h,
- the method is strongly influenced by aberrant values in the signal.

The idea to use h as parameter for the length of this interval has been developed for the first time in [78], in the context of S^ν, with a non-parametric gradient descent to detect the stabilisation. This last section shows that the approach used in this chapter solves a large part of the problems encountered with the method presented in [78]. In what follows, the approach consisting in using the greatest value among the moduli of the wavelet coefficients for the length of the interval is called method 1, and the approach developed in this chapter using the median of the values $(2^{hj}|c_\lambda|)_\lambda$ is called method 2.

Approximation of the Hurst Index H. First, we compare the two approaches to detect the Hölder exponent of the fractional Brownian motion in Figure 4.27. We clearly see that method 1 is less efficient for the smallest sizes of the signal than method 2. For this last method, i.e. the one proposed in this thesis, the average value of the distance between the Hölder exponent detected and H is always smaller than 0.05, while for the first method, the average value is close to 0.08. Moreover, with method 1, some signals are associated to a distance larger than 0.1, while method 2 none is.

Detection of the Smallest Detected Value of the Spectrum d_L. Secondly, method 2 allows to approximate the spectrum for smaller values of h than method 1. Table 4.1 gives the median value for the smallest detected h for a Lévy process of size 2^j. We clearly see the advantages of the suggested method in this chapter. The value of the smallest h detected for method 1 is often three times larger than the one for method 2.

Approximation of the Hurst Index H for a Disturbed Signal. Finally, it is easy to convince oneself that method 1 is strongly influenced by aberrant values in the signal, since the size of the interval is given by the largest wavelet coefficient. To illustrate this fact, we use the same modification of the fractional Brownian motion as in Section 4.5: one point of the walks of a fractional Brownian motion is replaced by four times the largest value of the signal. In Figure 4.28, we compare the two methods for such a signal: we clearly see the influence of an aberrant value in the signal in method 1. This last one gives

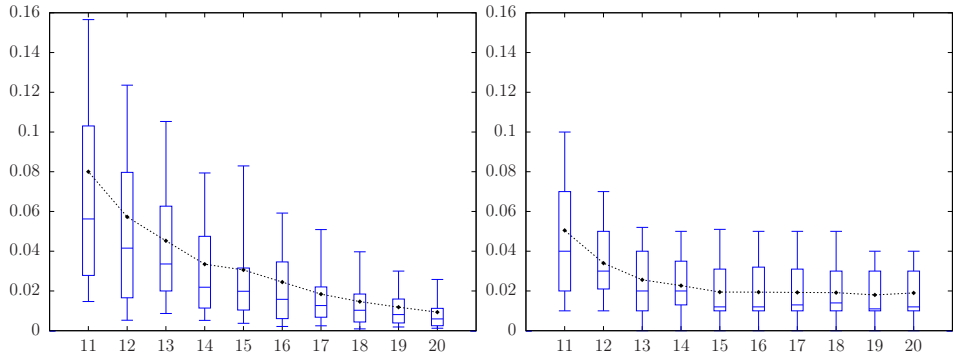

(a) method 1 (b) method 2

Figure 4.27.: For every j, the boxplot of the distances between the Hölder exponent detected and H (for H varying between 0.2 and 0.8 by steps of 0.05) for walks of fractional Brownian motion of size 2^j with parameter H. The mean of these distances is also represented (in black).

an average value of the distance between the Hölder exponent detected and H always larger than 0.1, and even an average value larger than 0.3 for the signals of size smaller than 2^{15}.

Table 4.1.: The median value of the smallest h detected in a Lévy process of size 2^j ($\beta = 1.3$).

	method 1	method 2	difference between the two methods
$j = 20$	0.26	0.09	0.17
$j = 19$	0.27	0.08	0.19
$j = 18$	0.27	0.08	0.19
$j = 17$	0.28	0.08	0.2
$j = 16$	0.3	0.09	0.21
$j = 15$	0.33	0.09	0.24
$j = 14$	0.34	0.09	0.25
$j = 13$	0.37	0.11	0.26
$j = 12$	0.43	0.13	0.3
$j = 11$	0.56	0.17	0.39

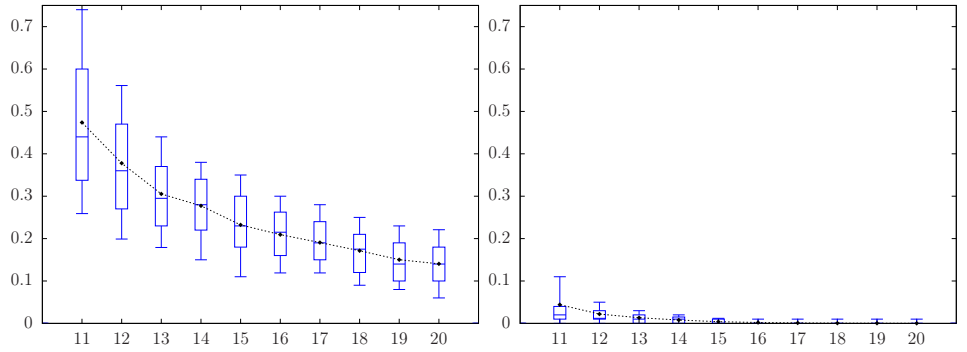

(a) method 1 (b) method 2

Figure 4.28.: For every j, the boxplot of the distances between the Hölder exponent detected and H (for H varying between 0.2 and 0.8 by steps of 0.05) of walks of fractional Brownian motion with a parameter H of size 2^j where one point of the walks is replaced by four times the largest value of the signal. The mean of these distances is also represented (in black).

4.7 Effectiveness of Profile-based Methods: Summary

In this chapter, profile-based methods allowing to approximate the Hölder spectrum have been presented. The main idea to approximate the spectrum d_f of a real-life signal f is to look at the behaviour of the function

$$C \mapsto \breve{\nu}_f^C(h), \tag{66}$$

for a fixed $h > 0$. If this function has a large enough stabilisation, then this one corresponds to the approximation of $d_f(h)$. If no stabilisation is detected, then $d_f(h) = -\infty$. The two profile-based methods studied in this chapter are the WPM and the LPM. We compare their results with the classical wavelet-based method WLM.

The monofractal case is illustrated with the fractional Brownian motion. The three methods give good and similar approximations of the Hölder exponent. Moreover, the LPM can approximate the length of the support of the spectrum, which allows to check more effectively if the signal is monofractal.

The multifractal case is considered on three examples. The first one is a signal with a strictly concave spectrum: a Mandelbrot cascade. The three methods give a good approximation of the spectrum, with an advantage for the WLM for the signals with a smaller size. Let us recall that this last method uses a Legendre transform, which explains this advantage. Let us notice that the decreasing part of the spectrum is less well approximated than

the increasing part when using the LPM. The second example of multifractal signal is a signal with a linear spectrum: the Lévy process without Brownian part. The WPM and the LPM correctly approximate the spectrum, while the WLM only tends to give a strictly concave spectrum. Moreover, the LPM allows to check if the spectrum has no decreasing part. The last example is a signal with a non-concave spectrum: the Lévy process with a Brownian part. The WPM and the LPM correctly approximate the spectrum, and thus allow to detect the non-concave part. The WLM only approximates the concave hull of the spectrum. The benefits to use a profile-based method are clear on these two last examples.

Moreover, the profile based-methods can also detect the presence of two different processes within the same signal f. The presence of two stabilisations in Function (66) indicates the existence of two processes within f. This is illustrated on the Lévy process with a Brownian component. For $h > 0.5$, Function (66) has two stabilisations: a first one corresponding to the Brownian motion, and the second one corresponding to the Lévy process without Brownian part used to simulate the process. However, this last one is less accurate than the first.

Let us notice that the approximation of the spectrum obtained with the profile-based methods sometimes strongly oscillates around the theoretical spectrum. To overcome this problem, a method adding variability within wavelet coefficients is proposed. This method allows to compute an average spectrum, which approximates the theoretical spectrum without oscillation. This result is validated on Binomial cascades and Lévy processes.

Finally, the robustness of the profile-based methods is showed with a disturbance of the fractional Brownian motion, where one point of the signal is replaced by four times the largest value of the signal. Using the LPM, the disturbance does not impact the approximation of the Hölder exponent, while the WLM is no more able to correctly approximate this exponent.

Chapter 5

Multifractal Formalisms based on Profiles in Action: Contributions on Numerical Signals

This chapter contains numerical applications of the profile-based multifractal formalisms. More precisely, we focus on two methods: the LPM and the method associated to the profile $\nu_{f,\sigma^{(\cdot)}}$, where $(\sigma^{(h)})_{h\in\mathbb{R}}$ is a sequence of admissible sequences.

The two first sections are related to the LPM. The first one studies signals with a finite number of Hölder exponents. The first signal is the most natural case: the concatenation of two fractional Brownian motions. While the WLM is unable to detect the Hurst index of each fractional Brownian motion, we show that the LPM can approximate these indexes. This allows us to study the specificity of this method in more detail, through the histograms of wavelet coefficients, and to understand some drawbacks of the LPM. The second signal is a numerical signal with multi-Hölder exponents based on Cantor set. We show how the LPM behaves on this kind of signals and we show the benefits of this method compared to the WLM. Finally, the third signal considered is a signal having Hölder exponents according to the scales j chosen to make the regression in the algorithm used. This kind of signals is often met in practice (see [7, 10, 110, 40, 87, 113, 3, 42] and references therein), it is thus natural to apply the LPM on these signals. On this first study, the LPM gives similar results as the WLM.

The second section presents a classical method used in the literature to create non-concave spectra: the concatenation of two multifractal processes (see [91, 90, 19, 33] for example). More precisely, the LPM is applied on the concatenation of two log-normal cascades. We confirm that the LPM can detect the non-concave part of a spectrum.

Section 5.3 presents the numerical contributions of the method using the profile $\nu_{f,\sigma^{(\cdot)}}$. The purpose of this section is to answer the following question: is it possible to detect the admissible sequence σ appearing in the Hölderian behaviour? The goal is to define a method detecting the law of the iterated logarithm on numerical simulations of the Brownian motion. For a real-life signal, it is obviously difficult to distinguish a noise and a structured irregular

signal. Nevertheless, with a simulation of a theoretical function, it is easier to control the numerical instability and to have a signal with a sufficiently large size. Consequently, it is interesting to apply the method on simulations of these kind of signals. Moreover, this method could be helpful to study theoretical signals, for which the Hölderian behaviour is not know. A second application could be found in the study of processes for which one can obtain many realisations.

The last section summaries contributions of the LPM and of the generalised profile $\nu_{f,\sigma^{(\cdot)}}$.

Aside from the Section 5.3 that comes from [79], the other sections using the LPM contains some new studies that have not been published yet. This is the first time that such a study is done with the LPM and the first results are presented. In this chapter, the considered signals are always of size 2^{20}. A further study will be the subject of a forthcoming article. This work is a collaboration with S. Nicolay.

This chapter is structured as follows:

5.1 Signals with a Finite Number of Hölder Exponents

In this section, the effectiveness of the LPM is tested on signals having a finite number of Hölder exponents. The first example is the simplest case of the bifractality[52, 111]: the concatenation of two fractional Brownian motions. On this tool example, the LPM is very effective to approximate the two Hölder

exponents if there are not too close, while the WLM is unable to distinguish them.

The second example is based on the process defined in the Schauder Basis presented in Section 2.5. Thanks to this process with the help of the Cantor set, it is easily to simulate signals behave like signals with one Hölder exponent located in the Cantor set and another outside. On this example, the contribution of the LPM is clear: it shows the existence of two Hölder exponents and it approximates the Hausdorff dimension of the Cantor set; moreover, the Hölder exponent located outside of the Cantor set is well approximated. The only negative issue is the approximation of the value of the exponent in the Cantor set which is not enough precised. The WLM can only approximate the Hölder exponent which lies outside the Cantor set but does not allow to see the existence of an exponent in the Cantor set and even to see that the Cantor set is related to the signal. After that, a generalisation of the Cantor set is used to generate signals with more than two Hölder exponents.

Finally, the case of signals having Hölder exponents according to the scales is presented. This kind of signal is often met in practice (see [7, 10, 110, 40, 87, 113, 3, 42] and references therein) and we show that the LPM gives results similar to the WLM.

5.1.1 Concatenation of Two Fractional Brownian Motions

The first example of signals with two Hölder exponents is the concatenation of two independent fractional Brownian motions. This is the tool example of the bifractality. This notion is presented in [52] and can be found in real-life signals (see [111] for example). Let us define this concatenation and then applied the LPM.

Definition 5.1.1. Let B^{H_1} and B^{H_2} be two independent fractional Brownian motions of parameters H_1 and H_2 respectively; the concatenation f_{H_1,H_2} of these two processes is defined as

$$f_{H_1,H_2}(x) = \begin{cases} B_x^{H_1} & \text{if } x \in [0, 1/2] \\ B_x^{H_2} + (B_{1/2}^{H_1} - B_0^{H_2}) & \text{if } x \in (1/2, 1] \end{cases}.$$

The Hölder spectrum of f_{H_1,H_2} is directly given by

$$d_{f_{H_1,H_2}}(h) = \begin{cases} 1 & \text{if } h \in \{h_1, h_2\} \\ -\infty & \text{otherwise} \end{cases}.$$

Approximation of H_1 and H_2. As mentioned in Section 4.3.4, when we look at the function $C \mapsto \tilde{\nu}_f^C(h)$, we can see the presence of several processes within the same signal f. In the case of f_{H_1,H_2}, the function $C \mapsto \tilde{\nu}_{f_{H_1,H_2}}^{+,C}(h)$ should be

- decreasing, if $h < H_1$,
- have a stabilisation equal to 1 followed by a decreasing part, if $h \in [H_1, H_2)$,
- have all its values equal to 1, if $h \geq H_2$.

Likewise, the function $C \mapsto \tilde{\nu}^{-,C}_{f_{H_1,H_2}}(h)$ should be

- increasing, if $h > H_2$,
- have an increasing part followed by a stabilisation equal to 1, if $h \in [H_1, H_2)$,
- have all its values equal to 1, if $h \leq H_1$.

Figure 5.1 shows that these different cases are effectively encountered.

Let us notice that the detection of H_2 with the function $\tilde{\nu}^{-}_{f_{H_1,H_2}}$ is difficult: the function $C \mapsto \tilde{\nu}^{-,C}_{f_{H_1,H_2}}(h)$ is always equal to 1 for C sufficiently large; consequently, it is difficult to distinguish the two first cases. It is easier to detect the third case: it suffices to get values of $\nu^{-,C}_{f_{H_1,H_2}}(h)$ (if it exists[1]) equal to 1, for any $C > 0$.

The strategy is thus the following: H_1 is approximated as the greatest h such that the function $C \mapsto \tilde{\nu}^{-,C}_{f_{H_1,H_2}}(h)$ has all its values equal to 1 and H_2 is approximated as the smallest h such that $C \mapsto \tilde{\nu}^{+,C}_{f_{H_1,H_2}}(h)$ has all its values equal to [2] 1.

Data and Results. This method is illustrated with $H_1 = 0.5-l$ and $H_2 = 0.5+l$, where $l \in \{0.01, 0.02, \ldots, 0.1\}$. Figure 5.2(a) and 5.2(b) show the boxplot of the distance between the smallest (resp. greatest) Hölder exponent detected and H_1 (resp. H_2). We clearly see that H_1 is well approximated, while H_2 is less well approximated. For the most signals, the LPM approximates H_1 with an error less than 0.01, while H_2 is approximated with an error greater than 0.02. These approximations are very good. However, let us notice that, when l is small (that is H_1 and H_2 are close), the function $\tilde{\nu}^{+}_{f_{H_1,H_2}}$ detects the average exponent between H_1 and H_2 (i.e. 0.5 in our case). This is illustrated in Figure 5.2(c).

[1] Let us recall that the value of $\nu^{-,C}_{f}(h)$ exists only if the correlation of the points of the function

$$j \mapsto \frac{\log \#\tilde{E}^{-}_{j}(C,h)(f)}{\log 2}$$

is sufficiently large (see Section 4.2.1)

[2] In the case of a signal f with exactly one exponent H such that $d_f(H) = 1$, the use of the function $\nu^{+}_{f_{H_1,H_2}}$ or $\nu^{-}_{f_{H_1,H_2}}$ to approximate H gives similar results, as already mentioned for the fractional Brownian motion (see Section 4.1).

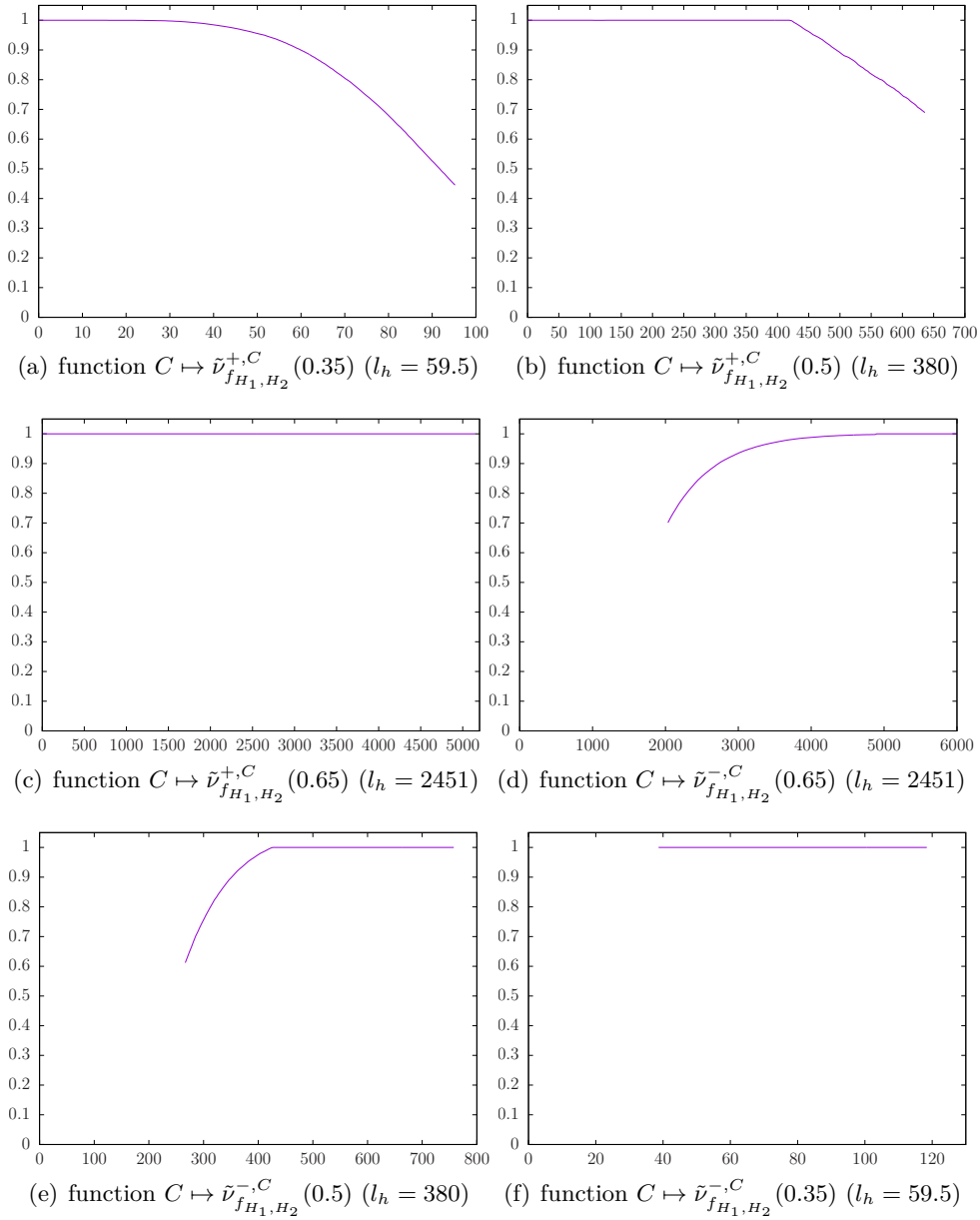

(a) function $C \mapsto \tilde{\nu}^{+,C}_{f_{H_1,H_2}}(0.35)$ ($l_h = 59.5$)
(b) function $C \mapsto \tilde{\nu}^{+,C}_{f_{H_1,H_2}}(0.5)$ ($l_h = 380$)
(c) function $C \mapsto \tilde{\nu}^{+,C}_{f_{H_1,H_2}}(0.65)$ ($l_h = 2451$)
(d) function $C \mapsto \tilde{\nu}^{-,C}_{f_{H_1,H_2}}(0.65)$ ($l_h = 2451$)
(e) function $C \mapsto \tilde{\nu}^{-,C}_{f_{H_1,H_2}}(0.5)$ ($l_h = 380$)
(f) function $C \mapsto \tilde{\nu}^{-,C}_{f_{H_1,H_2}}(0.35)$ ($l_h = 59.5$)

Figure 5.1.: The different cases of stabilisations for the function f_{H_1,H_2} with $H_1 = 0.4$ and $H_2 = 0.6$.

Statistic Study of the Histograms of Wavelet Coefficients. To understand why the method gives the average exponent when H_1 and H_2 are close, let us recall the idea of the algorithm: for any scale j, we count the number

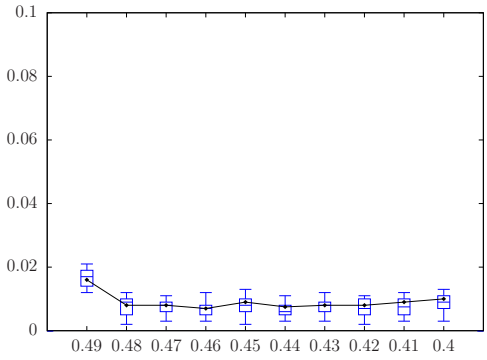

(a) Distance between the smallest Hölder exponent detected and H_1. The axis of the abscissa gives the value of H_1.

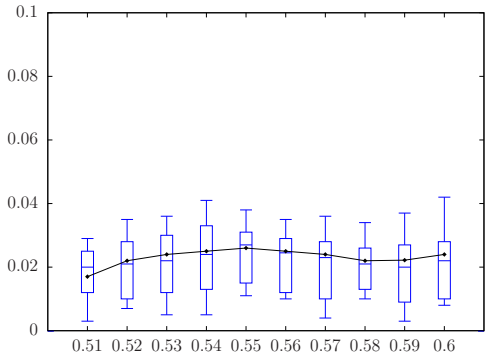

(b) Distance between the greatest Hölder exponent detected and H_2. The axis of the abscissa gives the value of H_2.

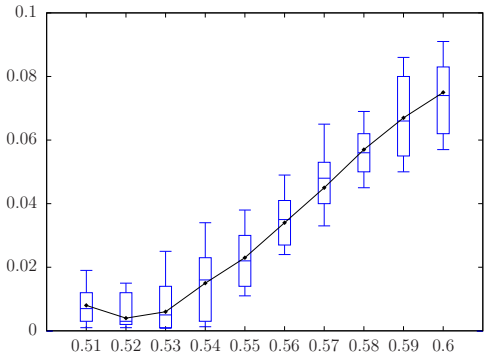

(c) Distance between the greatest Hölder exponent detected and 0.5. The axis of the abscissa gives the value of H_2.

Figure 5.2.: Above: Boxplot of the distances between the Hölder exponent detected with $\tilde{\nu}^-_{f_{H_1,H_2}}$ (resp. with $\tilde{\nu}^+_{f_{H_1,H_2}}$) and H_1 (resp. H_2). Below: Boxplot of the distances between the Hölder exponent detected with $\tilde{\nu}^+_{f_{H_1,H_2}}$ and 0.5.

of coefficients that are greater than $C2^{-hj}$; in other words, we study the behaviour of the histogram of coefficients at each scale j.

Figure 5.3 and Figure 5.4 show, for a fixed scale j, a few histograms of wavelet coefficients of the fractional Brownian motions, and Figure 5.5 shows a few of those of f_{H_1,H_2}. For these last ones, if the distance between H_1 and H_2 is sufficiently large, we can infer two behaviours within the histograms: for example, for $H_1 = 0.2$ and $H_2 = 0.9$, the central peak is reminiscent of the one of the histogram of the fractional Brownian motion of parameter $H_1 = 0.2$, while the expanse of the basis is reminiscent of the one of parameter $H_2 = 0.9$. This fact is less visible with the histogram associated to $H_1 = 0.4$

and $H_2 = 0.6$, and seems totally nonexistent with the one associated with $H_1 = 0.48$ and $H_2 = 0.52$. Moreover, the latter seems very similar to the one associated with $H = 0.5$.

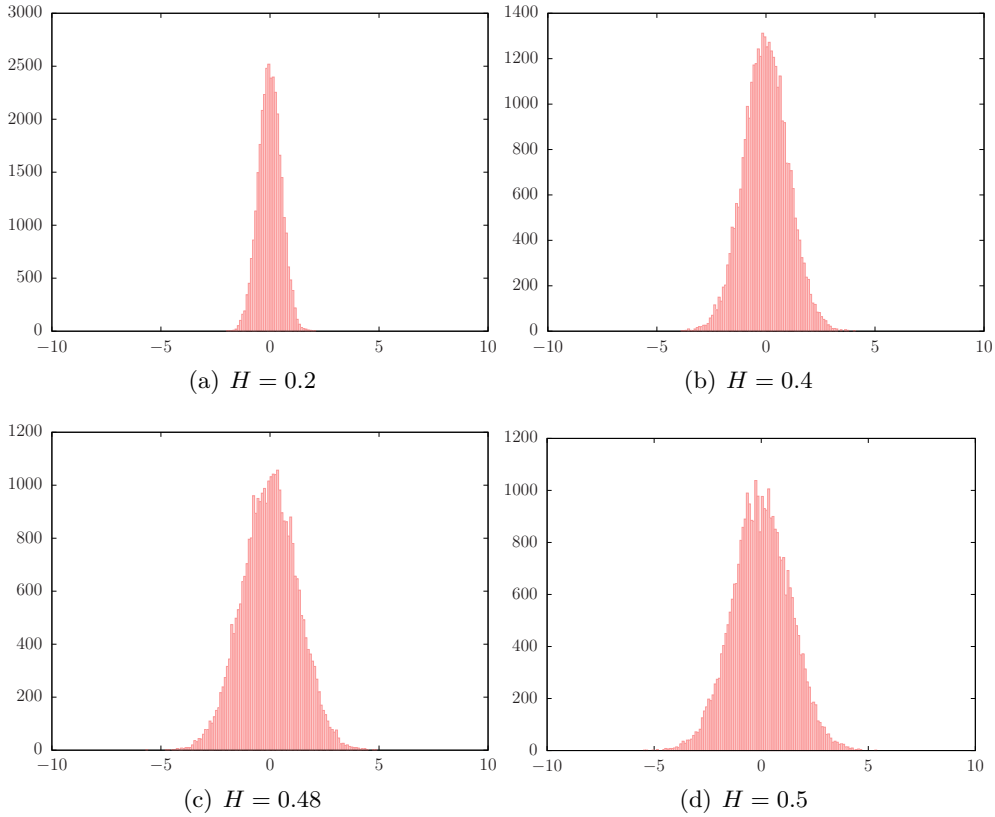

(a) $H = 0.2$ (b) $H = 0.4$

(c) $H = 0.48$ (d) $H = 0.5$

Figure 5.3.: Histogram of wavelet coefficients $(c_{\lambda_{15,k}})_{k\in\{0,\dots,2^{15}-1\}}$ of a realisation of a fractional Brownian motion of parameter H of size 2^{20}.

To confirm these hypotheses, we perform the (two-sample) Kolmogorov-Smirnov test. The null-hypothesis states that the two data samples come from the "same distribution"[3]. When we perform this test with a level $\alpha = 0.05$, the test rejects the null-hypothesis when the histogram of the wavelet coefficients

[3]The statistic of the Kolmogorov-Smirnov test is defined as

$$D_{n,m} = \sup_x |F_{1,n(x)-F_{2,m}(x)}|,$$

where $F_{1,n}$ and $F_{2,m}$ are the two empirical distribution functions of size n and m respectively. The null-hypothesis is rejected at level α if

$$D_{n,m} > c(\alpha)\sqrt{\frac{n+m}{nm}}.$$

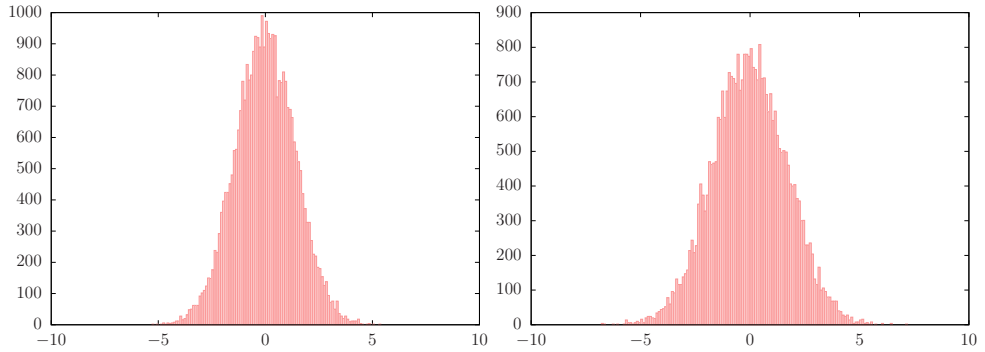

(a) $H = 0.52$

(b) $H = 0.6$

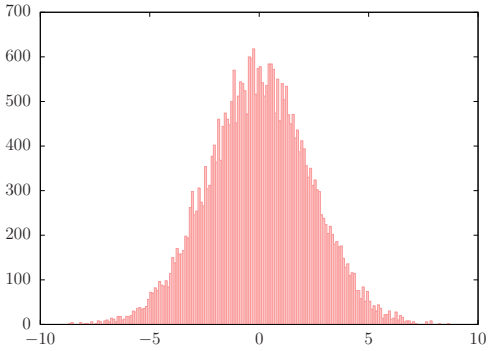

(c) $H = 0.9$

Figure 5.4.: Histogram of wavelet coefficients $(c_{\lambda_{15,k}})_{k\in\{0,\dots,2^{15}-1\}}$ of a realisation of a fractional Brownian motion of parameter H of size 2^{20}.

of a fractional Brownian motion of parameter $H = 0.48$ is compared with those of parameter $H = 0.52$; the null-hypothesis is not reject when the histogram of wavelet coefficients of $f_{0.48,0.52}$ is compared with those of a Brownian motion, for more than 90 percent of the tests. More precisely, Figure 5.6 shows the number of Kolmogorov-Smirnov test that cannot reject the null-hypothesis, when the histogram of wavelet coefficients of f_{H_1,H_2} is compared with those of a Brownian motion. We clearly see that, when H_1 and H_2 are close, the distribution of the wavelet coefficients of f_{H_1,H_2} is statistically the same as the distribution of those of a Brownian motion.

Statistic Study of $c_\lambda(w)$, for a fixed $\lambda \in \Lambda$. Let us recall that, in the case of the Brownian motion, for any scale j, the sequence $(c_{\lambda_{j,k}})_k$ follows a centred Gaussian law. Contrariwise, for a fractional Brownian motion of parameter $H \neq 1/2$, this fact is not valid because of the dependence between the coefficients. Nevertheless, for any fixed λ, the wavelet coefficient c_λ from a fractional Brownian motion follows a centred Gaussian law and, for each scale

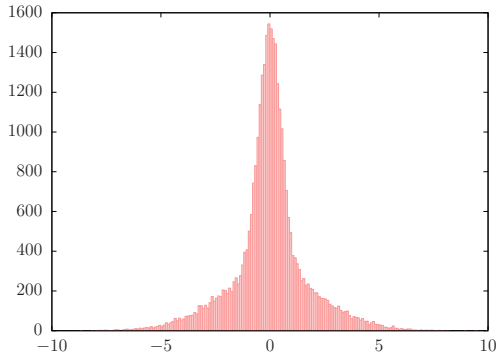

(a) $H_1 = 0.2$ and $H_2 = 0.9$

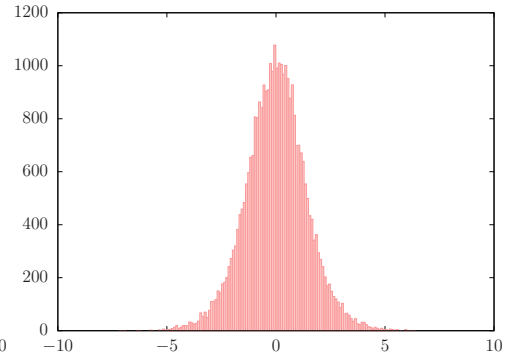

(b) $H_1 = 0.4$ and $H_2 = 0.6$

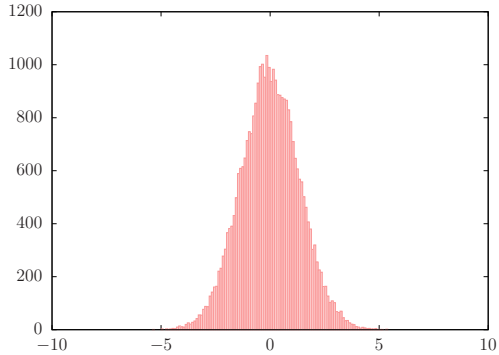

(c) $H_1 = 0.48$ and $H_2 = 0.52$

Figure 5.5.: Histogram of wavelet coefficients of a realisation of f_{H_1,H_2}.

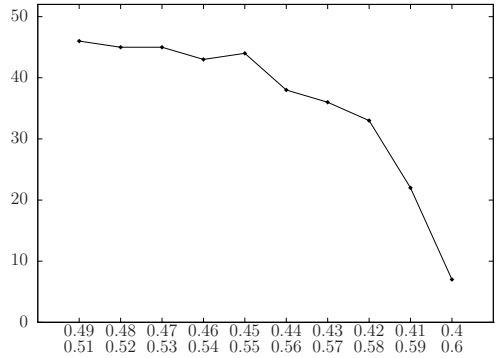

Figure 5.6.: Number of Kolmogorov-Smirnov tests that cannot reject the fact that the distribution of the wavelet coefficients of a Brownian motion and the distribution of those of f_{H_1,H_2} are the same. We have do 50 Kolmogorov-Smirnov tests. The axis of the abscissa gives the value of H_1 (above) and H_2 (below).

j, the variance of $c_{\lambda_{j,k}}$ is independent of k. We can thus perform a Fisher test, whose null-hypothesis is "two Gaussian law have the same variance" [4]. Again, a level $\alpha = 0.05$ is chosen.

From the fact that this test supposes that the distributions are Gaussian, we use the (one-sample) Kolmogorov-Smirnov test to determine the number of signals generated for each Fisher test, to ensure the Gaussian hypothesis. After several try, we have noticed that, if we use 30 fractional Brownian motion of size 2^{20} to do a Kolmogorov-Smirnov test on the 30 coefficients $c_{15,k}$ (k fixed), there are less than five percents of the tests rejecting the null-hypothesis. We have thus decided to perform the Fisher test on realisations of 30 fractional Brownian motions, to compare the variance between the 30 wavelet coefficients $c_{\lambda_{15,0.25*2^{15}}}$ and $c_{\lambda_{15,0.75*2^{15}}}$. Theoretically, the null-hypothesis is valid and in practice, we have noticed that more than 90 percents of the tests do not reject the null-hypothesis.

Based on these findings, we do the same on f_{H_1,H_2}. Figure 5.7 shows the number of Fisher tests that can not reject the null-hypothesis. When H_1 and H_2 are close, the null-hypothesis is not rejecting for 90 percents of the tests. It is thus statistically difficult to differentiate the wavelet coefficients of fractional Brownian motions of parameter H_1 and H_2 in this case.

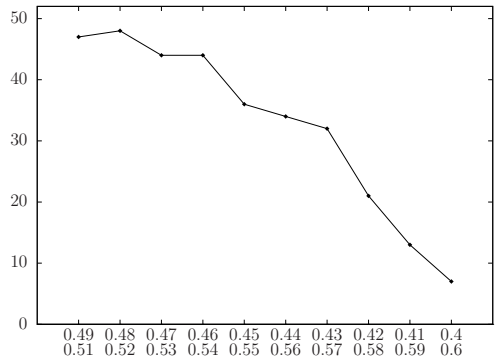

Figure 5.7.: Number of Fisher tests that can not reject the fact that the standard deviation is the same between the wavelet coefficients $c_{\lambda_{15,0.25*2^{15}}}$ and $c_{\lambda_{15,0.75*2^{15}}}$, using 30 signals. We have perform 50 Fisher tests. The axis of the abscissa gives the value of H_1 (above) and H_2 (below).

[4] The statistic of the Fisher test is defined as

$$Z = \frac{\sigma_1^2}{\sigma_2^2},$$

where σ_1^2 and σ_2^2 are the two variances; if $\sigma_1^2 \geq \sigma_2^2$, Z follows the Fisher-Snedecor distribution of parameter $(n_1 - 1, n_2 - 1)$, where n_1 and n_2 are the sizes of the two samples.

In conclusion, due to the statistical difficulty of differentiating the histograms of the wavelet coefficients of fractional Brownian motion whose parameters are close, the LPM does not well approximate the greater exponent H_2. However, the detection of H_1 is not affected by these statistical problems and the first exponent is well approximated, even when H_1 and H_2 are close.

A Problem with the WLM. To close this section, let us show that the WLM does not allow to detect neither H_1 nor H_2: this method behaves like if the signal is monofractal with an exponent equals to $(H_1 + H_2)/2$. Let us take as example $H_1 = 0.4$ and $H = 0.6$. Figure 5.8 shows a typical example of the approximation of the function $\eta_{f_{H_1,H_2}}$ (see Section 1.7 for more details).

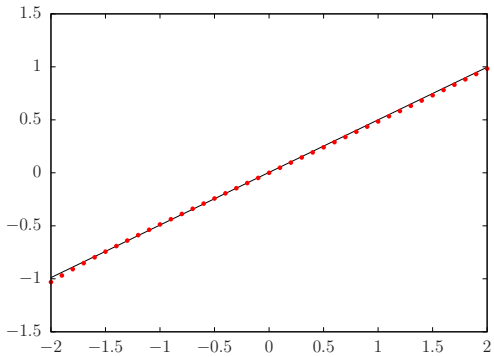

Figure 5.8.: Function $q \mapsto \eta_{f_{H_1,H_2}}(q)$, with $H_1 = 0.4$ and $H_2 = 0.6$.

Visually, this function is clearly linear and its slope is close too 0.5. In practice, there exists several methods to verify the linearity of this function. The first one is to look at the correlation of the points computed and the second one consists in performing the Taylor expansion of $\eta_{f_{H_1,H_2}}$ at $q = 0$:

$$\eta_{f_{H_1,H_2}}(q) = \sum_{p \geq 1} c_p \frac{q^p}{p!}.$$

The coefficients c_2 is often used to test the linearity of this function (see [43, 136]). On 100 simulations, the correlation is always greater than 0.99 and the coefficient $|c_2|$ is always smaller than 0.005. Consequently, the WLM does not allow to approximate H_1 and H_2. A possible reason is that the method computes the quantities

$$2^{-j} \sum_{\lambda \in \Lambda_j} (d_\lambda)^q.$$

This sum gives an average value between the coefficients corresponding to the fractional Brownian motion of parameters H_1 and those of parameters H_2, because there is the same number of coefficients for each signal in this example.

5.1.2 Multi-Hölder Numerical Signals based on the Cantor Set

In this section, we use the process B^H defined in Section 2.5 to create signals with multi-Hölder exponents based on the Cantor set and its generalisations. Let us notice that the construction of the numerical signal use a finite number of scales j; no attempt is made to give a meaning to the process as $j \to +\infty$. Consequently, we will talk about *numerical Hölder spectrum* d_f^n because the (theoretical) Hölder spectrum d_f does not make sense in this context.

Let us recall that the process B^H is defined as

$$B_x^H = Z_0 F_0(x) + \sum_{j=0}^{+\infty} \sum_{\lambda \in \Lambda_j} 2^{-jH_\lambda} Z_\lambda 2^{j/2} F_\lambda(x), \tag{67}$$

where the random variables Z_0 and Z_λ, with $\lambda \in \Lambda$, are independent real-valued $\mathcal{N}(0,1)$ Gaussian random variables, the set $\{F_0\} \cup \{F_\lambda : \lambda \in \Lambda\}$ forms the Schauder basis and the real numbers H_λ are defined as[5] $H_\lambda = H(k2^{-j})$, where the function $H : [0,1] \to K \subset (-1/2, 1/2)$ belongs to $\underline{\mathcal{H}}_K$. Moreover, we have seen in Theorem 2.5.1 that $h_{B^H}(x) = H(x)/1/2$, for any $x \in [0,1]$.

As indicated in the beginning of this section, a generalisation of the Cantor set is used. Let us first recall the definition of the Cantor set (for more details, see [50] and references therein)

Definition 5.1.2. The *Cantor set* $\mathcal{C}$ is the set of all real numbers on the unit interval that can to be written, in base 3, using only the digits 0 and 2.

The Cantor set $\mathcal{C}$ can also be defined by the following construction: Let us set $\mathcal{C}_0 = [0,1]$ and define $\mathcal{C}_{n+1}$ as the set of closed intervals obtained by removing the open middle third of each interval of $\mathcal{C}_n$; the Cantor set is then equal to

$$\mathcal{C} = \bigcap_{n \in \mathbb{N}} \mathcal{C}_n.$$

We directly see that $\mathcal{C}$ has a vanishing Lebesgue measure. The following theorem gives its Hausdorff dimension.

Theorem 5.1.3. *[48] The Hausdorff dimension of the Cantor set $\mathcal{C}$ is given by*

$$\dim_{\mathcal{H}}(\mathcal{C}) = \frac{\log 2}{\log 3}.$$

[5] More precisely, $H_\lambda = Q_j(k2^{-j})$ (see Section 2.5), but in practice, when the process B^H is simulated, the series of Expression (67) is replaced by a finite sum and in this case, the values H_λ are directly replaced by $H(k2^{-j})$.

Simulation of a multi-Hölder Numerical Signal with the help of $\mathcal{C}$. Let us now create a numerical signal that behaves like a signal having two Hölder exponents associated to different Hausdorff dimensions. Let us replace the series in Expression (67) with a sum with index varying from 0 to 20. Moreover, the Cantor set $\mathcal{C}$ is approximated by the set[6]

$$\bigcap_{n=0}^{12} \mathcal{C}_n = \mathcal{C}_{12}.$$

The function H must thus be defined only on the dyadic numbers $x_k = k2^{-20}$, $k \in \{0, \ldots, 2^{20} - 1\}$. Let us set $-1/2 < h_0 < h_1 < 1/2$ and

$$H(x_k) = \begin{cases} h_0 & \text{if } x_k \in \mathcal{C}_{12} \\ h_1 & \text{otherwise} \end{cases} . \tag{68}$$

Consequently, the numerical Hölder spectrum of B^H is given by

$$d^n_{B^H}(h) = \begin{cases} \frac{\log 2}{\log 3} & \text{if } h = h_0 + 1/2 \\ 1 & \text{if } h = h_1 + 1/2 \\ -\infty & \text{otherwise} \end{cases} .$$

Figure 5.9 shows a simulation of B^H, with $h_0 = 0.3$ and $h_1 = 0.6$.

Approximation of the Numerical Spectrum $d^n_{B^H}$. Figure 5.10 shows the typical numerical spectrum obtained with the LPM and the WLM on such a simulation.

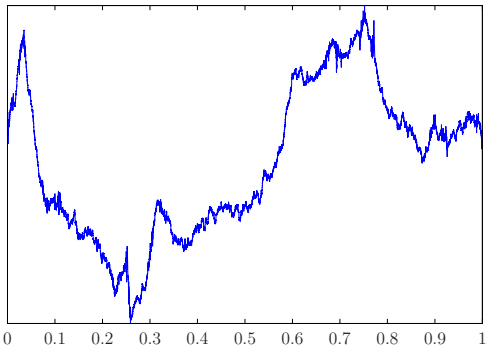

Figure 5.9.: Simulation of B^H (with H defined as (68) with $h_0 = 0.3$ and $h_1 = 0.6$)

We see that the LPM does not allow to approximate h_0 (the approximation of the spectrum starts clearly before h_0) but we have a level close to

[6] We have chosen $\mathcal{C}_{12}$ because we must have intervals of length larger than 2^{-20}.

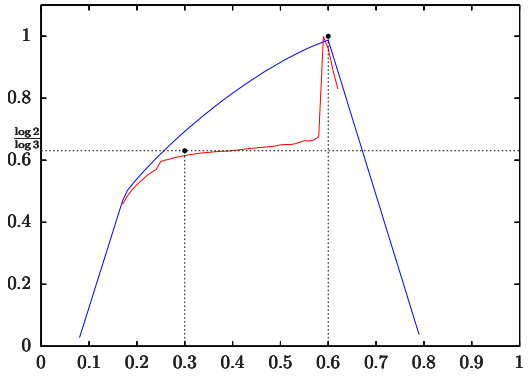

Figure 5.10.: Spectrum of B^H (with H defined as (68) with $h_0 = 0.3$ and $h_1 = 0.6$). Theoretical spectrum (•), LPM spectrum (—) and WLM spectrum (—). The results are obtained with a realisation of length 2^{20}.

$\log 2/\log 3$ and the exponent h_1 is well approximated. The WLM only allows to approximate h_1, and looking only at the spectrum, it is impossible to see the presence of the exponent h_0, whose Hausdorff dimension is equal to $\log 2/\log 3$. However, the function $q \mapsto \eta_{B^H}(q)$ (see Figure 5.11) shows two linear behaviours, which correspond to the two Hölder exponents, but only h_1 is correctly approximated.

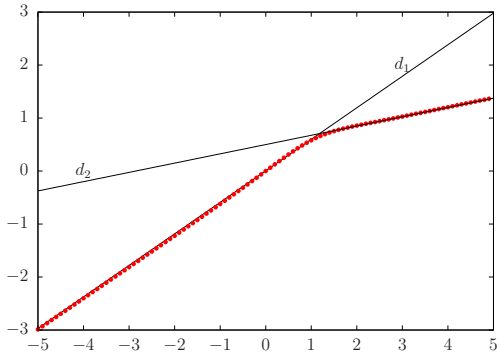

Figure 5.11.: Function $q \mapsto \eta_{B^H}(q)$ (with H defined as (68) with $h_0 = 0.3$ and $h_1 = 0.6$). The slope of d_1 (resp. d_2) is equal to 0.595 (resp. 0.175).

Consequently, the superiority of the LPM is clear: from the fact that it can detect non-concave spectra, it clearly shows the presence of two exponents. Moreover, it correctly approximates the value of the spectrum at these exponents. The exponent located in the Cantor set is not well approximated

(but the WLM does not approximate this exponent either), whereas the other exponent is.

Remark 5.1.4. In the case $h_0 > h_1$, meaning that the point $(h_0, \log 2/\log 3)$ is located in the decreasing part of the spectrum, none of the methods allows to detect this point; only the exponent h_1 located outside the Cantor set is detected.

Let us now use a generalisation of the Cantor set [50].

Definition 5.1.5. Let $b \geq 3$ be a natural number. The *b-Cantor set* $\mathcal{C}^{(b)}$ is the set of all real numbers on the unit interval that can be written, in base b, using only the digits 0 and $b-1$.

The b-Cantor set $\mathcal{C}^{(b)}$ can also be defined by the following construction: Let us set $\mathcal{C}_0^{(b)} = [0,1]$ and define $\mathcal{C}_{n+1}^{(b)}$ as the set of closed intervals obtained by removing the open middle interval of length $(1-\frac{2}{b})^{n+1}$ of each interval of $\mathcal{C}_n$; the b-Cantor set is thus equal to

$$\mathcal{C}^{(b)} = \bigcap_{n\in\mathbb{N}} \mathcal{C}_n^{(b)}.$$

The following theorem gives its Hausdorff dimension.

Theorem 5.1.6. *[48] The Hausdorff dimension of the b-Cantor set $\mathcal{C}^{(b)}$ is given by*

$$\dim_{\mathcal{H}}(\mathcal{C}^{(b)}) = \frac{\log 2}{\log b}.$$

Simulation of a multi-Hölder Numerical Signal with the help of $\mathcal{C}^{(b)}$. We will combine the sets $\mathcal{C}^{(3)}$ and $\mathcal{C}^{(10)}$ to construct a signal that behaves like a signal having four Hölder exponents. The set $\mathcal{C}^{(10)}$ is approximated by

$$\bigcap_{n=0}^{5} \mathcal{C}_n^{(10)} = \mathcal{C}_5^{(10)}.$$

The function H is defined as

$$H(x_k) = \begin{cases} -0.4 & \text{if } x_k \in \mathcal{C}_{12}^{(3)} \cap [0,1/2) \\ 0.2 & \text{if } x_k \notin \mathcal{C}_{12}^{(3)} \cap [0,1/2) \\ -0.1 & \text{if } x_k \in \mathcal{C}_5^{(10)} \cap [1/2,1] \\ 0.4 & \text{if } x_k \notin \mathcal{C}_5^{(10)} \cap [1/2,1] \end{cases}. \tag{69}$$

Consequently, the numerical Hölder spectrum of B^H is given by

$$d_{B^H}^n(h) = \begin{cases} \frac{\log 2}{\log 10} & \text{if } h = 0.1 \\ \frac{\log 2}{\log 3} & \text{if } h = 0.4 \\ 1 & \text{if } h \in \{0.7, 0.9\} \\ -\infty & \text{otherwise} \end{cases}.$$

Figure 5.12 shows a simulation of B^H.

Approximation of the numerical spectrum $d^n_{B^H}$. Figure 5.13 shows the typical numerical spectrum obtained with the LPM and the WLM on such a simulation.

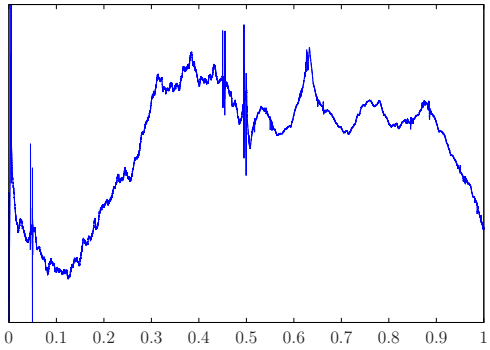

Figure 5.12.: Simulation of B^H (with H defined as (69))

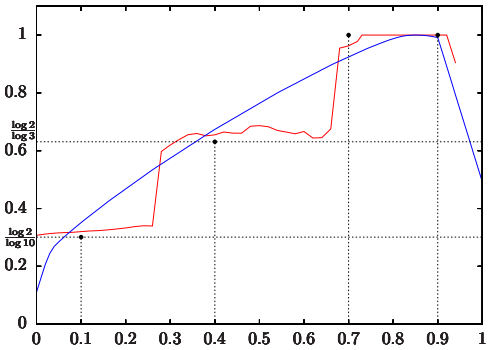

Figure 5.13.: Spectrum of B^H (with H defined as (69)). Theoretical spectrum (•), LPM spectrum (—) and WLM spectrum (—). The results are obtained with a realisation of length 2^{20}.

We see again that the LPM does not allow to approximate the exponents located in a b-Cantor set but we have two levels, each one corresponding to the Hausdorff dimension of a b-Cantor set. Moreover, the LPM detects the two exponents located outside of b-Cantor sets. As we look at the spectrum obtained with the WLM, only the larger exponent is well approximated. Even worse, when we look at the function $q \mapsto \eta_{B^H}(q)$ (see Figure 5.14), we only see two linear behaviours, exactly as in the previous case (with only the Cantor set); it is thus impossible to see the presence of the four exponents within the signal. Again, the largest exponent is well approximated. In conclusion, the LPM is clearly better for this kind of signals.

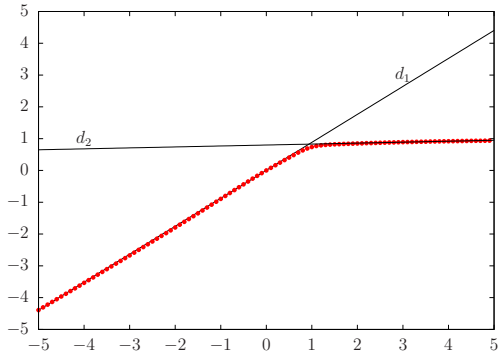

Figure 5.14.: Function $q \mapsto \eta_{B^H}(q)$ (with H defined as (69)). The slope of d_1 (resp. d_2) is equal to 0.885 (resp. 0.03).

5.1.3 Hölder Exponents According to Scales

In practice, it is well-known that the scales j chosen to perform the regressions are very important and influence the spectrum obtained. This fact is not specific to the wavelet based-methods: many methods in signal analysis have such a same specificity (see [7, 10, 110, 40, 87, 113, 3, 42] and reference therein). For the LPM (resp. the WLM), this choice is done when we compute the slope of the function

$$j \mapsto \frac{\log \#\tilde{E}_j(C,h)(f)}{\log 2} \quad (\text{resp. } j \mapsto \frac{\log S_f(j,q)}{\log 2}).$$

Usually, this regression is done on the "small scales" and the "large scales", that is the first scales and the last scales obtained when we apply the Mallat algorithm (see Theorem 1.5.7 and 1.5.14). The functions $C \mapsto \tilde{\nu}_f^C(h)$ and $q \mapsto \eta(q)$ can be different according to the chosen regressions. Despite the fact that theoretically, the regressions on large scales are not connected to the Hölder spectrum, they can help to study and to classify real-life signals. For the WLM, it is well-known that this technique gives good results (see [40, 42] and references therein). This section contains a first study to this approach with the LPM.

Simulation of B^H. Let us take again the process B^H defined in Section 2.5. In the previous section, we have approximated this process by replacing the series by a finite sum ($j = 0, \ldots, 20$) and we have constructed a function H on the dyadic numbers. Now, let us consider the following signal:

$$\sum_{j=0}^{10} \sum_{\lambda \in \Lambda_j} 2^{-jH_0} Z_\lambda 2^{j/2} F_\lambda(x) + \sum_{j=11}^{20} \sum_{\lambda \in \Lambda_j} 2^{-jH_1} Z_\lambda 2^{j/2} F_\lambda(x), \tag{70}$$

with $H_0, H_1 \in (-1/2, 1/2)$. Figure 5.15 shows a simulation of this signal with $H_0 = 0.1$ and $H_1 = 0.3$. This signal can be interpreted as follows: an exponent equals to $H_0+1/2$ is present at large scales and an exponent equals to $H_1+1/2$ is present at small scales.

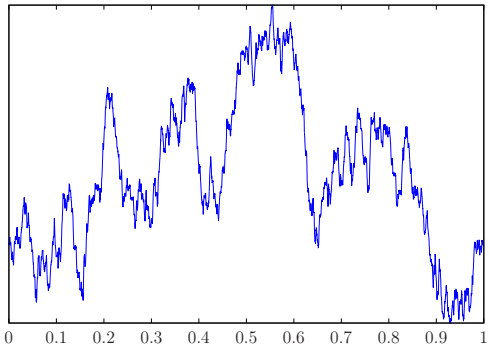

Figure 5.15.: Simulation of the signal defined as (70) with $H_0 = 0.1$ and $H_1 = 0.3$.

Approximation of Hölder Exponents According to Scales. Let us now compare the results obtained with the LPM and the WLM on simulations of size 2^{20}. For the LPM, we have already seen that there exists three ways to approximate the Hölder exponent of a monofractal signal (see Section 4.1). In the case of the Brownian motion, these three methods give similar results but we have seen in Section 5.1.1 that the method which consists in taking the largest h for which $\nu_f^{-,C}(h)$ is equal to 1 for any $C > 0$, gives better results in some cases. Again, we take this approach to approximate the Hölder exponent with the LPM in this section.

Results. For each method, the boxplot 1 and 2 of Figure 5.16 represent the distance between the exponent approximated and H_0 (resp. H_1) when the regression is done at the largest scales (resp. the smallest scales). We see that the two methods give similar results, with a slight advantage for the WLM at the small scales. Moreover, we notice a large difference between the approximation of the two exponents: the exponent associated to the large scales is less well approximated than the other one. The exponent associated with the small scales is approximated with an error less than 0.01 for both methods, while the one associated with the large scale is approximate with an average error of 0.07 with the LPM, and of 0.05 with the WLM. This difference between the small and large scales comes from the regression. Indeed, if we take $H_0 = H_1$ (that is a signal with the same exponent at small and large scales) and we apply the methods by regressing only on the large scales, the distance between the exponent approximated and H_0 is given in the boxplot

3 of Figure 5.16. We see that this boxplot is similar to the boxplot 2. The average error is 0.05 with the LPM and is 0.03 with the WLM, which is greater than the error at small scales.

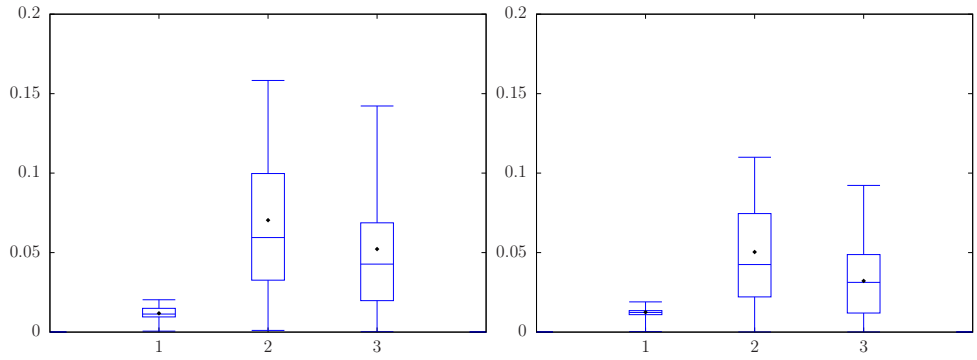

(a) LPM (b) WLM

Figure 5.16.: Boxplot 1: distance between the exponent approximated and H_1 when the regression is done at small scales on the signal defined as (70) with $H_0 = 0.1$ and $H_1 = 0.3$. Boxplot 2: distance between the exponent approximated and H_0 when the regression is done at large scales on the signal defined as (70) with $H_0 = 0.1$ and $H_1 = 0.3$. Boxplot 3: distance between the exponent approximated and H_0 when the regression is done at large scales on the signal defined as (70) with $H_0 = H_1 = 0.1$.

In conclusion, although it is necessary to investigate further the efficiency of the LPM to approximate exponents located at different scales, this section shows that it can be achieved, but that the exponents detected at largest scales is less well approximated than those at smallest scales, exactly as with the WLM.

5.2 Concatenation of Two Log-Normal Cascades

This section shows that the LPM is a suitable method to study signals obtained by a concatenation of two log-normal cascades. The concatenation is an usual method in the literature to create processes with a non-concave spectrum (see [91, 90, 19, 33] for example). We are interested in two aspects of these signals: first, we study the effectiveness of the LPM to detect the two exponents associated to the Hausdorff dimension equals 1, and secondly, the ability of the LPM to detect the non-concave part of the spectrum.

Definition 5.2.1. Let μ_{W_1} and μ_{W_2} be two independent measures associated with a log-normal cascade, and f_{W_1} and f_{W_2} their associated wavelet series (see Proposition 4.1.2). The concatenation f_{W_1,W_2} of these processes is defined as

$$f_{W_1,W_2}(x) = \begin{cases} f_{W_1}(2x) & \text{if } x \in [0,1/2] \\ f_{W_2}(2x) & \text{if } x \in (1/2,1] \end{cases}.$$

Using the properties of the Hausdorff dimension (see Proposition 1.2.5), we directly obtain the following proposition, which gives the spectrum of f_{W_1,W_2}.

Proposition 5.2.2. *Let μ_{W_1} and μ_{W_2} be two independent measures associated to two log-normal cascades. The spectrum of f_{W_1,W_2} is given, almost surely, by*

$$d_{f_{W_1,W_2}}(h) = \sup\{d_{\mu_{W_1}}(h), d_{\mu_{W_2}}(h)\},$$

for any $h \geq 0$.

Approximation of Hölder Exponents associated to the Hausdorff Dimension equals 1. Before applying the LPM to approximate this spectrum, we use this method to approximate the two Hölder exponents associated to the Hausdorff dimension equals 1. To do this, we use the same approach as in Section 5.1.1: if we denote by H_1 and H_2 these two exponents and if we suppose that $H_1 < H_2$, then H_1 is approximated as the greatest h such that the function $C \mapsto \tilde{\nu}^{-,C}_{f_{W_1,W_2}}(h)$ has all its values equal to 1, and H_2 is approximated as the smallest h such that $C \mapsto \tilde{\nu}^{+,C}_{f_{W_1,W_2}}(h)$ has all these values equal to 1.

Results. As in the case of the concatenation of two fractional Brownian motions, it is not always possible to detect these two exponents. This problem comes from histograms of wavelet coefficients that are a concatenation of two "similar" histograms. For a few concatenations of cascades, Figure 5.17 shows the detected exponents with the methods described above.

About the method using $\nu^{-,C}_{f_{W_1,W_2}}$, we see that, when the parameters of the two log-normal W_1 and W_2 are close (see the two boxplots on the right in Figure 5.17(a)), the median of the results slightly overestimates H_1. Let us notice that the average is close to 0.5, which corresponding to $(H_1+H_2)/2$. When the parameters of two log-normal cascades are sufficiently different, the method approximates H_2 and no H_1 (see the boxplot on the left in Figure 5.17(a)). Let us explain these results.

Let us recall that the function

$$C \mapsto \nu^{-,C}_{f_{W_1,W_2}}(h) \tag{71}$$

contains information about the functions $\nu^{-,C}_{f_{W_1}}(h)$ and $\nu^{-,C}_{f_{W_2}}(h)$. When H_1 and H_2 are close, if h is close to these exponents, the values of $\nu^{-,C}_{f_{W_1}}(h)$ and $\nu^{-,C}_{f_{W_2}}(h)$

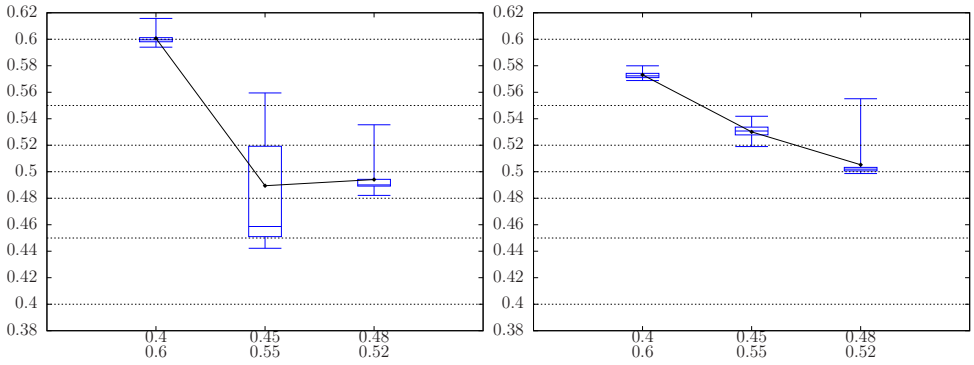

(a) Use of $\nu^{-}_{f_{W_1,W_2}}$ (b) method $\nu^{-}_{f_{W_1,W_2}}$

Figure 5.17.: Boxplots of the approximation of the greatest h such that the function $C \mapsto \tilde{\nu}^{-,C}_{f_{W_1,W_2}}(h)$ has all these values equal to 1 (left) and the smallest h such that $C \mapsto \tilde{\nu}^{+,C}_{f_{W_1,W_2}}(h)$ has all these values equal to 1 (right), for simulations of f_{W_1,W_2}, where W_1 is a log-normal cascade of parameters $\mu_1 = H_1 \log 2$ and $\sigma_1^2 = 0.005 \log 2$ and W_2 is a log-normal cascade of parameters $\mu_1 = H_2 \log 2$ and $\sigma_1^2 = 0.005 \log 2$. The axis of the abscissa gives the value of H_1 (above) and H_2 (below). The results are obtained with a realisation of length 2^{20}.

exist (see Section 4.2.1 to see the criterion of existence of these values) and thus Function (71) has information about the two processes. Consequently, the method detects the smallest exponents h such that $d_f(h) = 1$, that is H_1. Contrariwise, in the case of the log-normal cascade μ_{W_1} of parameters $\mu_1 = 0.4 \log 2$ and $\sigma_1^2 = 0.005$, the detected value of $\nu^{-,C}_{f_{W_1}}(h)$ is $-\infty$ if h is close to 0.6. Consequently, when we superpose this cascade with the log-normal cascade μ_{W_2} of parameters $\mu_2 = 0.6 \log 2$ and $\sigma_2^2 = 0.005$, Function (71) contains only the information about the cascade μ_{W_2}, if h is close to 0.6. Consequently, the method approximates H_2 and no H_1.

Concerning the method using $\nu^{+,C}_{f_{W_1,W_2}}$, when the parameters are "very close" (see the boxplot of the right in Figure 5.17(b)), we obtain on average an exponent equals 0.5, which corresponds to $(H_1 + H_2)/2$. The more the parameters are apart, the more the method gives an exponent close to H_2 (see the two boxplots on the left in Figure 5.17(b)). This exactly what happened in Section 5.1.1.

When we look at the approximation of the distance between H_1 and H_2 with $H_1 = 0.45$ and $H_2 = 0.55$, the average is 0.056 with a standard deviation of 0.024, and the median is 0.07.

Approximation of the spectrum $d_{f_{W_1,W_2}}$. To finish this section, let us look at how the LPM approximated the spectrum of f_{W_1,W_2}. Let us recall that this method has been introduced to approximate non-increasing and non-concave spectra. We thus choose μ_{W_1} and μ_{W_2} for which the spectrum of f_{W_1,W_2} has a non-concave decreasing part. Figure 5.18 shows the spectra obtained with the LPM and the WLM. For the LPM, we use the method adding variability of Section 4.4 to approximate the spectrum.

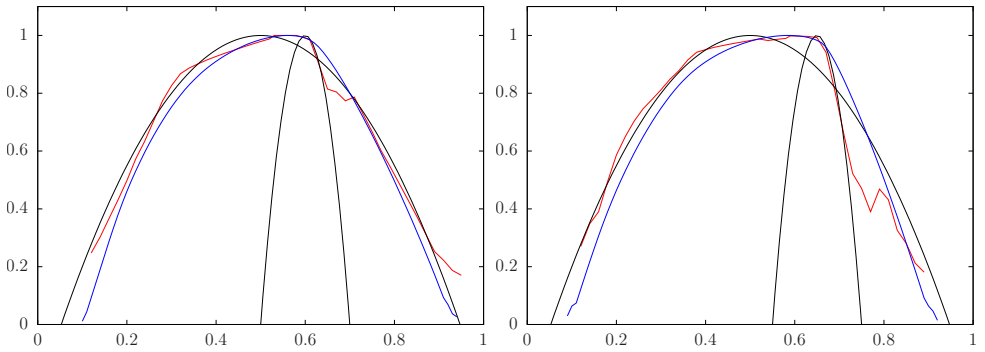

(a) $\mu_1 = 0.5 \log 2$, $\sigma_1^2 = 0.1 \log 2$, $\mu_2 = 0.6 \log 2$ and $\sigma_2^2 = 0.005 \log 2$

(b) $\mu_1 = 0.5 \log 2$, $\sigma_1^2 = 0.1 \log 2$, $\mu_2 = 0.65 \log 2$ and $\sigma_2^2 = 0.005 \log 2$

Figure 5.18.: Spectrum of f_{W_1,W_2} where W_1 is a log-normal cascade of parameters μ_1 and σ_1^2 and W_2 is a log-normal cascade of parameters μ_2 and σ_2^2. Theoretical spectrum (—), LPM spectrum (—) and WLM spectrum (—).

We clearly see the superiority of the LPM over the WLM. The second method can only compute the concave hull of the theoretical spectrum; it is thus impossible to detect the presence of two log-normal cascades. With this method, one could conclude that there is only one cascade in the signal. On the other hand, the LPM shows the existence of a non-concave part and thus the presence of a second phenomenon in the signal. Let us notice that when the parameters of the two log-normal cascades are apart, the non-concave part is not detected at the right place. This is explained by the interaction between the histograms of wavelet coefficients of two log-normal cascades, as for the detection of the exponents presented in the beginning of this section.

5.3 Numerical Contribution of Admissible Sequences

In Chapter 2, three classes of signals were studied: functions with prescribed behaviour in their wavelet coefficients, Brownian motions and multifractal processes defined in the Schauder basis. Each of these signals has a Hölderian

behaviour of the form of

$$2^{-h_f(x)j}\tau_j,$$

where $\tau = (\tau_j)_{j\in\mathbb{N}}$ is an admissible sequence. This section tries to answer to the next question: is it possible to detect numerically the admissible sequence τ? Let us recall that Chapter 3 has presented a generalisation of the spaces S^ν with the help of admissible sequences: the $S^{\nu,\sigma^{(\cdot)}}$ spaces. We have also defined a generalised profile $\nu_{f,\sigma^{(\cdot)}}$ that is independent of the chosen wavelet basis. The algorithm presented in the previous chapter make sense for this profile.

Let us notice that the sequence τ is negligible compared with a power of 2, in the sense that it verifies

$$\lim_{j\to+\infty}\frac{\log\tau_j}{\log 2^{-j}} = 0.$$

Consequently, implementing an algorithm to detect τ is a real challenge that cannot always be achieved for the two following main reasons: signal with too small size and numerical instability. For a real-life signal, it is very difficult to distinguish a noise from the sequence τ. From another point of view, it is easier to control the numerical instability and to have a signal with a sufficiently large size when we simulate a theoretical function. In this section, we work with simulations of size 2^{20} for the three theoretical signals presented in Chapter 2. In particular, we show that we can detect the Khintchin Law in simulations of a Brownian motion. This method should help to determine an unknown Hölderian behaviour of theoretical signals.

5.3.1 Detection of the Hölderian Behaviour for Functions with Prescribed Hölder Exponent Defined by their Wavelet Decomposition

To evaluate the efficiency of the method, let us begin with the simplest case: functions with prescribed Hölder exponents defined by their wavelet decomposition. This example allows to put an arbitrary admissible sequence directly in the value of the wavelet coefficients. Let us recall that, if $H : [0,1] \to K \subset (0,1)$ is a continuous function (K is a compact set), then we can define a function f with the help of its wavelet coefficients as

$$c_\lambda = 2^{-H_\lambda j}a_j \quad \text{with} \quad H_\lambda = \max\{\frac{1}{\log j}, H(k2^{-j})\}, \tag{72}$$

and $a = (a_j)_{j\in\mathbb{N}}$ a strictly positive real sequence such that

$$\lim_{j\to+\infty}\frac{\log a_j}{\log 2^{-j}} = 0.$$

In this case, we have $h_f(x) = H(x)$, for any $x \in [0,1]$ (see Section 2.1 for more details). The presence of the sequence a does not modify the Hölder exponent but modifies the Hölderian behaviour: f does not necessarily belong to $\Lambda^{H(x_0)}(x_0)$, but rather to $\Lambda^{\sigma,M}(x_0)$, for an admissible sequence σ depending on a. The goal of this section is to show that the correction a can be detected using numerical simulations, with the help of the algorithm presented in the previous chapter applied on $\nu_{f,\sigma^{(\cdot)}}$.

Simulation. In order to perform a statistical study of the results and to improve of the stability required by the algorithm, we replace the wavelet coefficients $2^{-H_\lambda j}a_j$ appearing in Equality (72) by

$$c_\lambda = 2^{-H_\lambda j}a_j U_\lambda, \tag{73}$$

where each U_λ ($\lambda \in \Lambda$) is chosen independently with respect to the uniform probability measure on $[0.5, 1.5]$, as explained in Section 4.4. In the sequel, the coefficients a_j will be defined by $a_j = w(2^{-j})$, where w is a function belonging to the set

$$\mathcal{W} := \{h \mapsto 1, h \mapsto \sqrt{|\log|\log h^{-1}||}, h \mapsto |\log|\log h^{-1}||, h \mapsto \sqrt{|\log h^{-1}|}\}.$$

This choice is not arbitrary and comes from of the Khintchin law of the iterated logarithm; indeed, in the following section, we want to show that we can detect the Khintchin law on simulations of the Brownian motion, we thus choose analogous corrections w involving a logarithm to test the method. Finally, let us define the set

$$\Sigma := \{h \mapsto (2^{-hj}w(2^{-j}))_{j\in\mathbb{N}} : w \in \mathcal{W}\}.$$

Let us begin with a toy example to check the method associated to $\nu_{f,\sigma^{(\cdot)}}$.

A Toy Example. Let us begin with the simplest case.

Proposition 5.3.1. *Let $n \geq 1$ and $\tau = (\tau_j)_j$ an admissible sequence. Let us set*

$$0 = x_0 < x_1 < \cdots < x_n = 1, \quad 0 < b_0 < \cdots < b_{n-1} < 1,$$

and let us define the function H by

$$H(x) = b_i, \quad \text{if} \quad x \in [x_i, x_{i+1}).$$

If there exists $\epsilon' > 0$ such that for any $0 < \epsilon < \epsilon'$, there exists $J \in \mathbb{N}$ such that

$$2^{-\epsilon j}\tau_j \leq a_j, \tag{74}$$

for any $j \geq J$, then we have

$$\nu_{f,\sigma^{(\cdot)}}(h) = \begin{cases} 1 & \text{if } h \geq b_0 \\ -\infty & \text{else} \end{cases},$$

where $\sigma_j^{(\cdot)} = 2^{-\cdot j}\tau_j$. If Condition (74) is not satisfied, we have

$$\nu_{f,\sigma} = -\infty.$$

Proof. Indeed, if τ_j satisfies Condition (74) then, for any dyadic interval $\lambda \in \Lambda$ such that $\lambda \subset [x_0, x_1[$, we have

$$|2^{-H_\lambda j} a_j| \geq 2^{-j(a+\epsilon/2)} a_j = 2^{-j(a+\epsilon)} 2^{j\epsilon/2} a_j \geq 2^{-j(a+\epsilon)} \tau_j,$$

for j large enough. The conclusion follows. ■

Let us notice that the Hölder spectrum of f is given by

$$d_f(h) = \begin{cases} 1 & \text{if } h = b_i \text{ for some } i \in \{0, \ldots, n-1\} \\ -\infty & \text{else} \end{cases},$$

and the wavelet profile of f is given by

$$\nu_f(h) = \begin{cases} 1 & \text{if } h \geq b_0 \\ -\infty & \text{else} \end{cases}.$$

Consequently, the smallest h such that $\nu_f(h) = 1$ is the same as the smallest h such that $\nu_{f,\sigma}(h) = 1$, if $\sigma_j^{(\cdot)} = 2^{-\cdot j}\tau_j$ with an admissible sequence τ satisfying Condition (74). In this case, it is not possible to differentiate the corrections $\tau_1 = (\sqrt{\log 2^j})_j$ and $\tau_2 = (\sqrt{\log|\log 2^j|})_j$ for example. This result is only valid in theory, because it is based on the fact that the number of available scales j is infinite. However, when dealing with real-life signals, we only have access to a finite number of scales j. Therefore, the value of the threshold J appearing in Condition (74) is primordial, since the scales j smaller than J can be influenced by the presence of the sequence τ. Let us illustrate on two examples.

Data and Results of Signals of Proposition 5.3.1 with $n = 1$. The simplest case is the monofractal case, where $H(x) = H \in (0, 1)$. We have computed 20 simulations of the wavelet coefficients $(c_\lambda)_{\lambda \in \Lambda_j, j \in \{0,\ldots,20\}}$ defined as in (73), for each $H \in \{0.3, 0.35, \ldots, 0.7\}$ and for each function $w \in \mathcal{W}$. Given a simulation and $\sigma^{(\cdot)} \in \Sigma$, the smallest h for which $\nu_{f,\sigma^{(\cdot)}}(h) = 1$ has been computed. Figure 5.19 shows, for each function w and each $\sigma^{(\cdot)}$, the boxplot of the distance between H and the detected h (i.e. the absolute value of their difference).

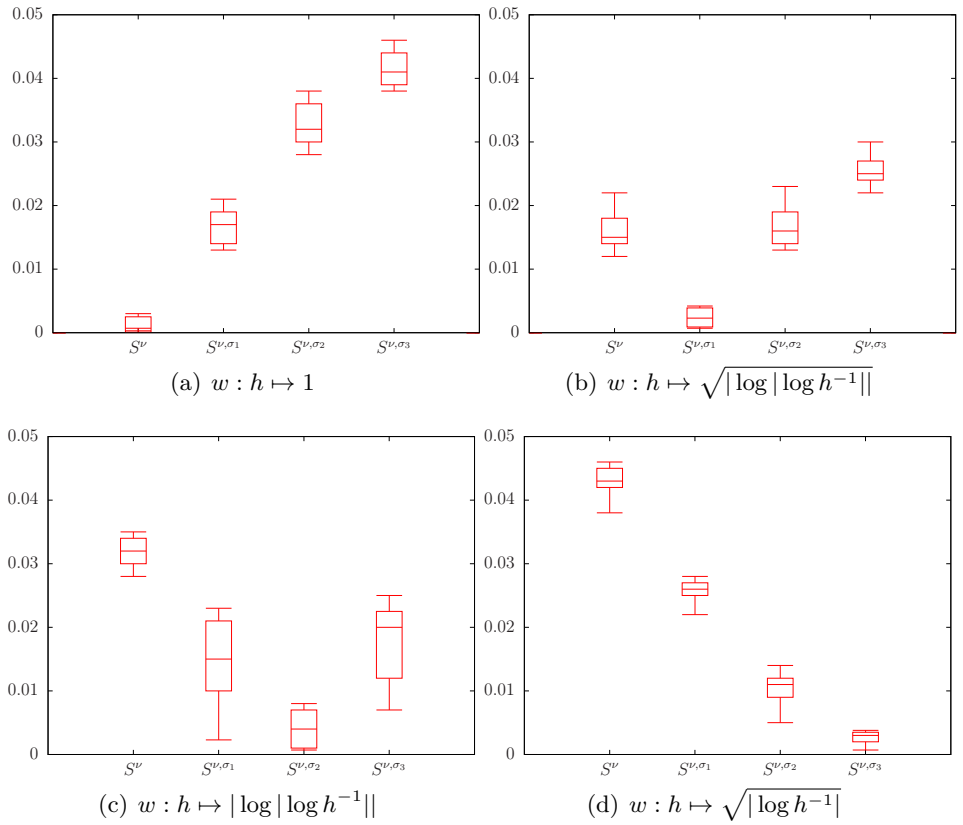

(a) $w : h \mapsto 1$ (b) $w : h \mapsto \sqrt{|\log|\log h^{-1}||}$

(c) $w : h \mapsto |\log|\log h^{-1}||$ (d) $w : h \mapsto \sqrt{|\log h^{-1}|}$

Figure 5.19.: Boxplot of the distance between H and the smallest h such that the profile evaluated in h equals 1. The left boxplot corresponds to the profile ν_f, and the three others correspond to the generalised profile $\nu_{f,\sigma^{(\cdot)}}$, with $\sigma_1^{(\alpha)} = (2^{-\alpha j}\sqrt{\log\log 2^j})_{j\in\mathbb{N}}$, $\sigma_2^{(\alpha)} = (2^{-\alpha j}\log\log 2^j)_{j\in\mathbb{N}}$ and $\sigma_3^{(\alpha)} = (2^{-\alpha j}\sqrt{\log 2^j})_{j\in\mathbb{N}}$.

Clearly, the best approximation of the Hölder exponent is obtained with the method associated to the logarithmic correction used for building the signal. As a consequence, such a method allows to detect the right logarithmic correction in the signal, since other approximations lead to less precise estimations of the Hölder exponent.

Data and Results of Signals of Proposition 5.3.1 with $n = 2$. Let $x_1 = 0.5$; for each $b_0 \in \{0.2, 0.25, 0.3, 0.35\}$, $b_1 \in \{0.65, 0.7, 0.75, 0.8\}$ and each function $w \in \mathcal{W}$, we have computed 20 simulations of the wavelet coefficients $(c_{\lambda_{j,k}})_{j\in\{0,\dots,20\},k\in\{0,\dots,2^j-1\}}$ defined as in (73). As in the previous case, for each simulation and each $\sigma^{(\cdot)} \in \Sigma$, the smallest h for which $\nu_{f,\sigma^{(\cdot)}}(h) = 1$

has been computed. Figure 5.20 shows, for each function w and each $\sigma^{(.)}$, the boxplot of the distance between b_0 and the detected h (i.e. the absolute value of their difference). Once again, the method involving the appropriate logarithmic correction clearly displays the best results.

Let us notice that in the case $w : h \mapsto \sqrt{|\log h^{-1}|}$, the lengths of the boxplots corresponding to the methods associated to the profiles ν_f (i.e. the WPM) and ν_{f,σ_1} are very large. A deeper analysis of the results shows a problem with the simulated signals if b_0 and b_1 are too close from each other. This case has already been encountered with the LPM in Section 5.1.1 and 5.2. The interesting fact is that there is no problem with the method using the proper correction.

Another Multifractal Example. Let us end this section with a last multifractal example. Let a, b, c be real numbers belonging to $(0, 1)$, with $a < c$, and consider the function H explicitly defined by

$$H(x) = \begin{cases} \frac{c-a}{b}x + a & \text{if } x < b \\ c & \text{if } x \geq b \end{cases} . \tag{75}$$

Data and Results. For each $a \in \{0, 0.1, \ldots, 0.5\}$, $b \in \{0.1, 0.2, \ldots, 0.5\}$, $c \in \{0.2, 0.3, \ldots, 0.8\}$ $(a < c)$ and for each function $w \in \mathcal{W}$, we have computed 20 simulations of the wavelet coefficients $(c_{\lambda_{j,k}})_{j\in\{0,\ldots,20\},k\in\{0,\ldots,2^j-1\}}$ defined as in (73) and for each simulation and each $\sigma^{(.)} \in \Sigma$, the smallest h for which $\nu_{f,\sigma^{(.)}}(h) = 1$ has been computed. Figure 5.21 shows, for each function w and each $\sigma^{(.)}$, the boxplot of the distances between c and the detected h (i.e. the absolute value of their difference).

As expected, the method using the proper correction displays the best estimation.

5.3.2 Detection of the Khintchin Law: Brownian Motion vs Uniform Weierstrass Function

We show here that the generalised S^ν spaces allow to detect a statistical difference between the Hölderian behaviours of the Brownian motion and the uniform Weierstraß function. Moreover, the Khintchin law can be detected.

Let us recall that the sample path $B = (B_x)_{x\in\mathbb{R}}$ of a Brownian motion belongs to the Hölder space $\Lambda^{1/2-\epsilon}(\mathbb{R})$ almost surely for any $\epsilon > 0$, but not to $\Lambda^{1/2}(\mathbb{R})$. On the other hand, the Weierstraß function

$$W(x) = \sum_{n=0}^{\infty} \frac{1}{2^n} \cos(2^{2n} x\pi)$$

belongs to $\Lambda^{1/2}(\mathbb{R})$ (but not to $\Lambda^{1/2+\epsilon}(\mathbb{R})$ as soon as $\epsilon > 0$). As a consequence, the Hölder exponents of both B and W are equal to $1/2$. However, we have

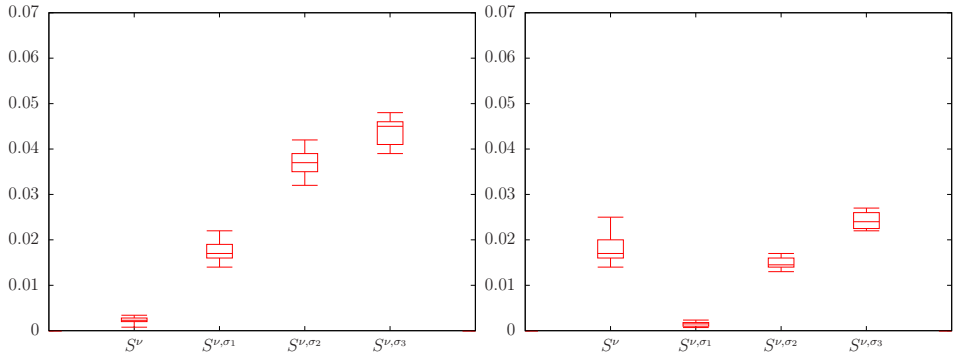

(a) $w : h \mapsto 1$ (b) $w : h \mapsto \sqrt{|\log|\log h^{-1}||}$

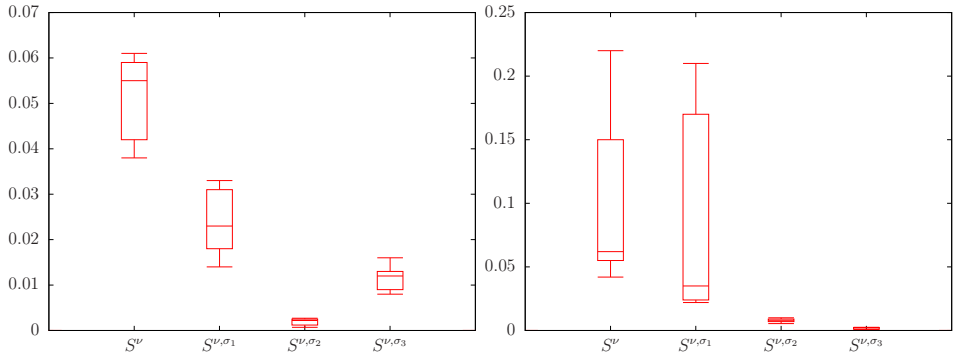

(c) $w : h \mapsto |\log|\log h^{-1}||$ (d) $w : h \mapsto \sqrt{|\log h^{-1}|}$

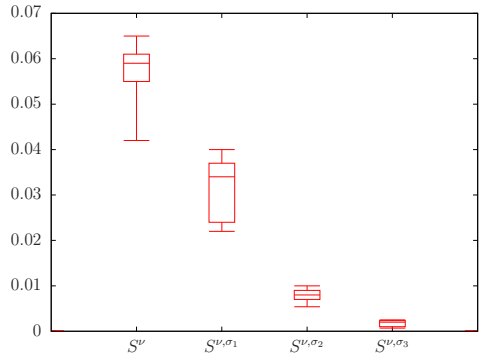

(e) $w : h \mapsto \sqrt{|\log h^{-1}|}$ with $|b_0 - b_1| \geq 0.3$

Figure 5.20.: Boxplot of the distance between H and the smallest h such that the profile evaluated in h equals 1. The left boxplot corresponds to the profile ν_f, and the three others correspond to the generalised profile $\nu_{f,\sigma^{(\cdot)}}$, with $\sigma_1^{(\alpha)} = (2^{-\alpha j}\sqrt{\log\log 2^j})_{j\in\mathbb{N}}$, $\sigma_2^{(\alpha)} = (2^{-\alpha j}\log\log 2^j)_{j\in\mathbb{N}}$ and $\sigma_3^{(\alpha)} = (2^{-\alpha j}\sqrt{\log 2^j})_{j\in\mathbb{N}}$.

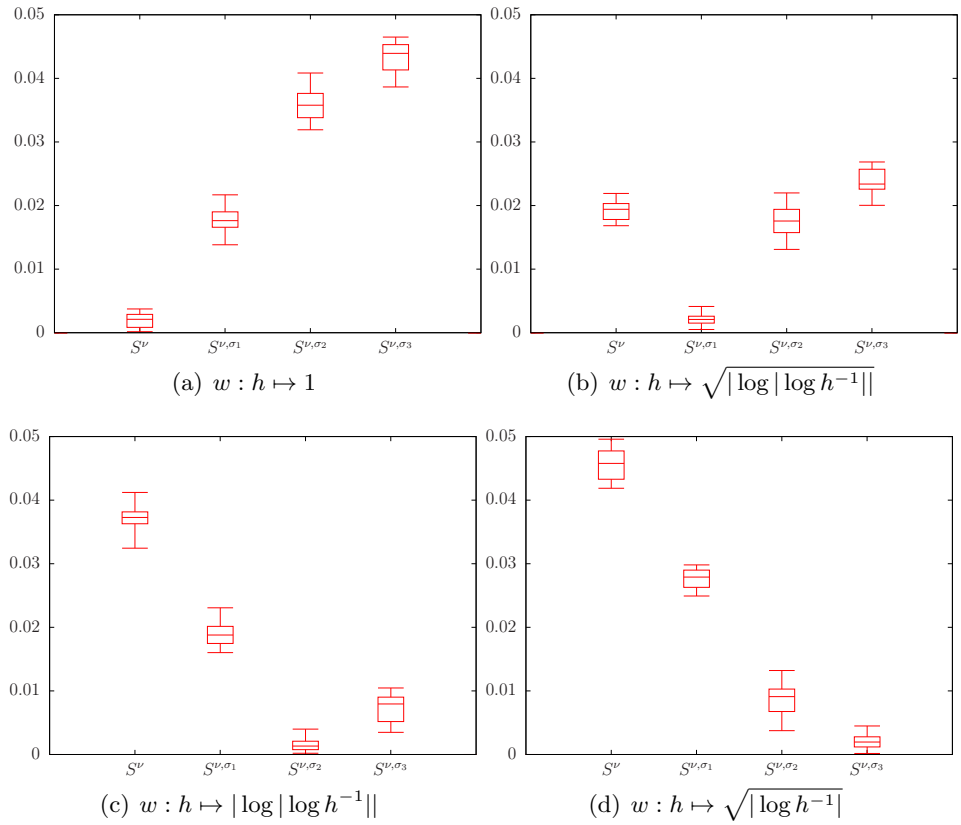

(a) $w : h \mapsto 1$

(b) $w : h \mapsto \sqrt{|\log|\log h^{-1}||}$

(c) $w : h \mapsto |\log|\log h^{-1}||$

(d) $w : h \mapsto \sqrt{|\log h^{-1}|}$

Figure 5.21.: Boxplot of the distance between c and the smallest h such that the profile evaluated in h equals 1. The left boxplot corresponds to the profile ν_f, and the three others correspond to the generalised profile $\nu_{f,\sigma^{(\cdot)}}$, with $\sigma_1^{(\alpha)} = (2^{-\alpha j}\sqrt{\log\log 2^j})_{j\in\mathbb{N}}$, $\sigma_2^{(\alpha)} = (2^{-\alpha j}\log\log 2^j)_{j\in\mathbb{N}}$ and $\sigma_3^{(\alpha)} = (2^{-\alpha j}\sqrt{\log 2^j})_{j\in\mathbb{N}}$.

seen that the generalised Hölder spaces give additional information: B belongs to $\Lambda^{\tau}(\mathbb{R})$, with $\tau = (2^{-j/2}\sqrt{\log 2^j})_{j\in\mathbb{N}}$ (see Chapter 1 for more details). The Khintchin law of the iterated logarithm (see Theorem 2.3.6) implies that B belongs, almost surely, to the generalised pointwise Hölder space $\Lambda^{\sigma,0}(x)$, with $\sigma = (2^{-j/2}\sqrt{\log\log 2^j})_{j\in\mathbb{N}}$. Moreover, Chapter 2 has studied more in details the wavelet leaders of a Brownian motion. We have seen in Theorem 2.4.1 that, almost surely, for almost every $x \in \mathbb{R}$, x is a leader-ordinary point, that is

$$0 < \limsup_{j\to+\infty} \frac{d_j(x)}{2^{-j/2}\sqrt{\log j}} < +\infty.$$

In other words, the wavelet leaders $d_j(x)$ behave like $2^{-j/2}\sqrt{\log j}$, as $j \to +\infty$; there is thus a logarithmic correction in the behaviour of the wavelet leaders.

The generalised wavelet profile $\nu_{f,\sigma^{(\cdot)}}$ is defined with the wavelet coefficients, and no the wavelet leaders. Nothing guarantees that it is possible to detect the logarithmic correction with this profile. However, by analysing the results of Chapter 2, we notice that the scale j' of the wavelet coefficient $c_{\lambda'}$ inducing the logarithmic correction in the behaviour of the wavelet leader $d_{\lambda_{j,k}}$ is such that, the smaller the size of the support of the wavelet is, the closer j' from j is. It is thus reasonable to test the method with $\nu_{f,\sigma^{(\cdot)}}$.

In the future, we should be defining a generalisation of the profiles $\tilde{\nu}_f^+$ and $\tilde{\nu}_f^-$ in the same way as ν_f (namely replacing the sequence $(2^{-hj})_{j\in\mathbb{N}}$ by an admissible sequence with good properties). The independence of the chosen wavelet basis of this generalisation is still not proven, but considering the work done on $S^{\nu,\sigma^{(\cdot)}}$, it is reasonable to think that this property is still valid. When all the theoretical results will be established, it will be interesting to test this new method on the simulations of this section, to confirm the detection of the Khintchin Law.

Let us now define the function with which the Brownian motion is compared: the uniform Weierstraß function [58].

Definition 5.3.2. Let a, b be two real numbers such that $0 < a < 1 < b$, with $ab \geq 1$, and let $(U_n)_{n\in\mathbb{N}}$ be an arbitrary sequence on independents random variables with respect to the uniform probability measure on $[0, 1]$. The *uniform Weierstraß function* of parameters (a, b) is defined as

$$W(x) = \sum_{n=0}^{+\infty} a^n \cos((b^n x + U_n)\pi),$$

for any $x \in \mathbb{R}$. In other words, this process is the classical Weierstraß function coupled with an uniform random phase.

It is straightforward to check that the Hölder exponent of this process is almost surely the same as the Hölder exponent of the classical deterministic Weierstraß function, i.e. it is equal to $-\log(a)/\log(b)$. Moreover it belongs almost surely to $\Lambda^{-\log(a)/\log(b)}(\mathbb{R})$; as a matter of consequence, there is no logarithmic correction in such a process. Figure 5.22 represents a simulation of a Brownian motion and a uniform Weierstraß function. Visually, there is little to no perceptible difference between these two representations. Since the Hölder regularity of these processes is the same, the usual multifractal formalisms cannot differentiate them. Let us now show that the method presented above allows to catch the logarithmic correction which distinguishes these two processes.

Data and Results. We have computed 20 simulations of size 2^{20} of a uniform Weierstraß function of parameters (a, b), for each $a \in \{0.65, 0.7, \ldots, 0.85\}$ and $b = \exp(-\log(a)/0.5)$. For each Brownian motion, each uniform Weierstraß

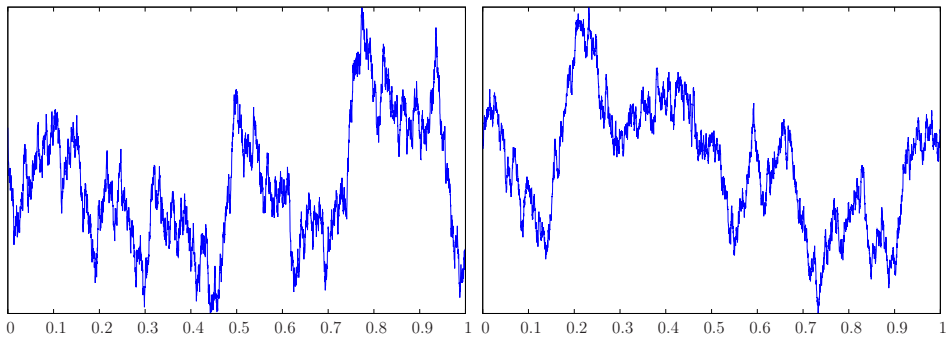

Figure 5.22.: Simulation of a Brownian motion (left) and a uniform Weierstraß function (right) of parameters $(0.8, 1.5625)$; the Hölder exponents are equal to $1/2$.

function and each $\sigma^{(\cdot)} \in \Sigma$, the smallest h for which $\nu_{c,\sigma^{(\cdot)}}(h) = 1$ has been computed. Figure 5.23 shows, for each function w and each $\sigma^{(\cdot)}$, the boxplot of the distances between $1/2$ and the detected h (i.e. the absolute value of their difference).

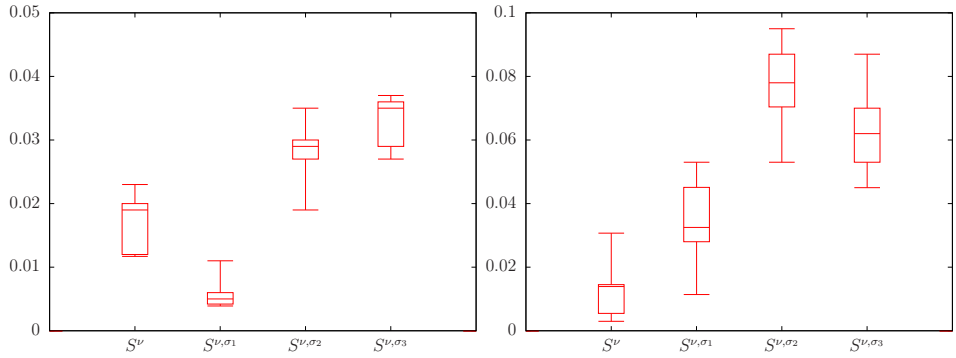

(a) Brownian motion

(b) Uniform Weierstraß function of parameters $(a, \exp(-\log(a)/0.5))$ with $a \in \{0.65, 0.7, \ldots, 0.85\}$

Figure 5.23.: Boxplot of the distance between $1/2$ and the smallest h such that the profile evaluated in h equals 1. The left boxplot corresponds to the profile ν_f, and the three others correspond to the generalised profile $\nu_{f,\sigma^{(\cdot)}}$, with $\sigma_1^{(\alpha)} = (2^{-\alpha j}\sqrt{\log\log 2^j})_{j\in\mathbb{N}}$, $\sigma_2^{(\alpha)} = (2^{-\alpha j}\log\log 2^j)_{j\in\mathbb{N}}$ and $\sigma_3^{(\alpha)} = (2^{-\alpha j}\sqrt{\log 2^j})_{j\in\mathbb{N}}$.

In the case of the Brownian motion, the method using the correction

$$\sigma_1^{(\alpha)} = (2^{-\alpha j}\sqrt{\log\log 2^j})_{j\in\mathbb{N}}$$

displays a significant difference from the other ones. This is in agreement with the Khintchin law of the iterated logarithm. In the case of the uniform Weierstraß functions, the Wavelet Profile Method is better than the other ones. One can conclude that there is no logarithmic correction in this process.

5.3.3 Detection of the Hölderian Behaviour for the Processes defined in the Schauder Basis

This last section uses again the process $B_\cdot^H$ defined in Section 2.5. Proposition 2.5.2 shows that there is surely a logarithmic correction, as for the Brownian motion.

Simulation of a First Class of Multifractal Signals. The first example consists in defining the function H as follows: let us set $-1/2 < b_0 < b_1 < 1/2$ and

$$H(x_k) = \begin{cases} b_0 & \text{if } x_k \in (-1/2, 0] \\ b_1 & \text{if } x_k \in (0, 1/2) \end{cases} ;$$

before going further, we define a second sequence $(H'(x_k))_{k\in\{0,\dots,2^{20}\}}$ by shuffling by blocks of length 10 the original sequence $(H(x_k))_{k\in\{0,\dots,2^{20}\}}$. The shuffle by blocks is important to numerically maintain the multifractal properties of the original signal. This allows to have a signal with two Hölder exponents distributed on $[0, 1]$ which cannot be divided into two monofractal signals. Figure 5.24 simulations with unshuffled and shuffled H.

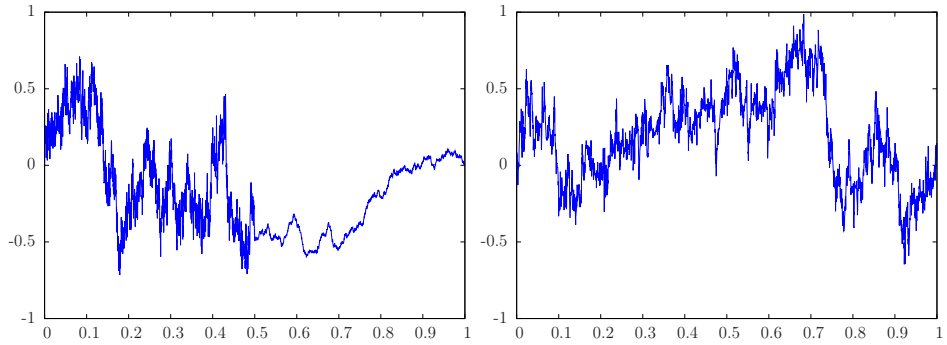

(a) Unshuffled H. (b) Shuffled H.

Figure 5.24.: Simulation of the signal $B_\cdot^H$ with $b_0 = -0.2$ and $b_1 = 0.2$.

Data and Results. We have computed 20 simulations of the function $B_\cdot^H$ (with shuffled H), for each b_0 belongs to $\{0.2, 0.25, 0.3, 0.35, 0.4\}$ and for each b_1 belongs to $\{0.6, 0.65, 0.7, 0.75, 0.8\}$. For each simulation and each $\sigma^{(\cdot)} \in \Sigma$, the smallest h for which $\nu_{c,\sigma^{(\cdot)}}(h) = 1$ has also been computed. Figure 5.25

shows, for each $\sigma^{(.)}$, the boxplot of the distance between b_0 and the detected h (i.e. the absolute value of their difference).

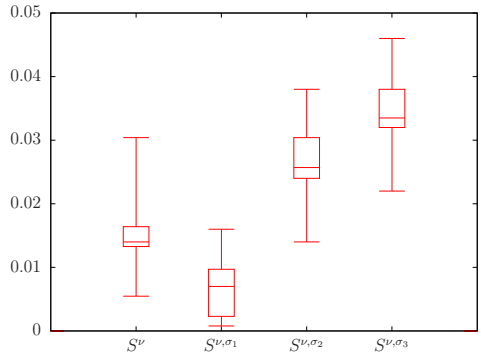

Figure 5.25.: Boxplot of the distance between b_0 and the smallest h such that the profile evaluated in h equals 1. The left boxplot corresponds to the profile ν_f, and the three others correspond to the generalised profile $\nu_{f,\sigma^{(.)}}$, with $\sigma_1^{(\alpha)} = (2^{-\alpha j}\sqrt{\log\log 2^j})_{j\in\mathbb{N}}$, $\sigma_2^{(\alpha)} = (2^{-\alpha j}\log\log 2^j)_{j\in\mathbb{N}}$ and $\sigma_3^{(\alpha)} = (2^{-\alpha j}\sqrt{\log 2^j})_{j\in\mathbb{N}}$.

The method using the correction $\sigma_1^{(\alpha)} = (2^{-\alpha j}\sqrt{\log\log 2^j})_{j\in\mathbb{N}}$ displays results clearly more accurate than the other ones.

Simulation of a Second Class of Multifractal Signals. To end this section, let us introduce a last multifractal example. We use again the function H defined as in (75) with a translation of $1/2$ down; again, we shuffle by blocks of length 10 the function as explained above. Let us recall that the shuffle by blocks is important to numerically maintain the multifractal properties of the original signal. Figure 5.26 shows simulations with unshuffled and shuffled H.

Data and Results. For $a = 0$, $b = 0.1$ and for each $c \in \{0.2, 0.3, 0.4\}$, we have computed 20 simulations of the function $B_{\cdot}^{H}$ with H both shuffled by blocks and unshuffled. For each simulation and each $\sigma^{(.)} \in \Sigma$, the smallest h for which $\nu_{c,\sigma^{(.)}}(h) = 1$ has been computed. Figure 5.27 shows, for each $\sigma^{(.)}$, the boxplot of the distance between c and the detected h (i.e. the absolute value of their difference).

In the case where H is not shuffled, the method using the correction

$$\sigma_1^{(\alpha)} = (2^{-\alpha j}\sqrt{\log\log 2^j})_{j\in\mathbb{N}}$$

displays again the best estimation. In the case where H is shuffled by blocks, the distinction between the method associated with $\sigma_1^{(\alpha)} = (2^{-\alpha j}\sqrt{\log\log 2^j})_{j\in\mathbb{N}}$

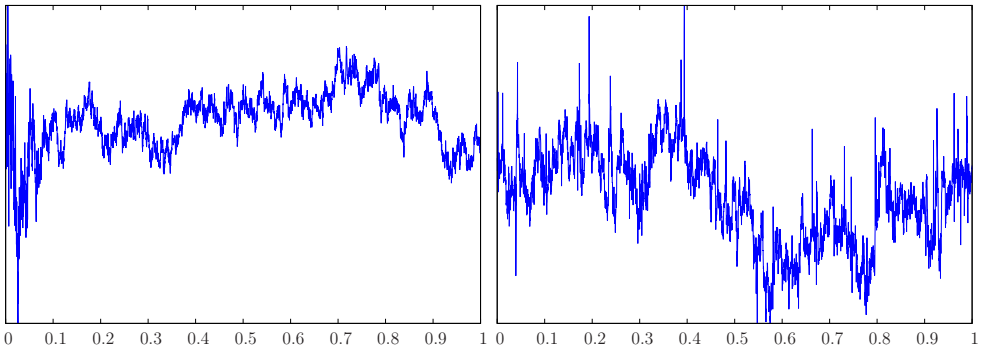

(a) Unshuffled H. (b) Shuffled H.

Figure 5.26.: Simulation of the signal $B_\cdot^H$ with $a = 0$, $b = 0.1$ and $c = 0.3$.

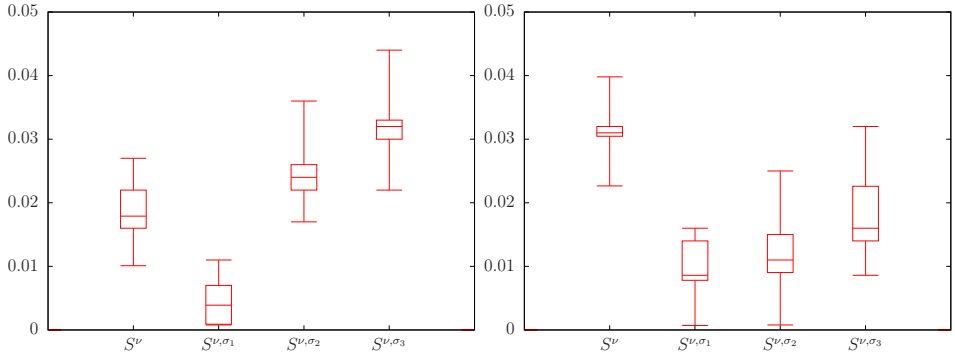

(a) Unshuffled H (b) Shuffled H

Figure 5.27.: Boxplot of the distance between c and the smallest h such that the profile evaluated in h equals 1 ($a = 0$ and $b = 0.1$). The left boxplot corresponds to the profile ν_f, and the three others correspond to the generalised profile $\nu_{f,\sigma^{(\cdot)}}$, with $\sigma_1^{(\alpha)} = (2^{-\alpha j}\sqrt{\log\log 2^j})_{j\in\mathbb{N}}$, $\sigma_2^{(\alpha)} = (2^{-\alpha j}\log\log 2^j)_{j\in\mathbb{N}}$ and $\sigma_3^{(\alpha)} = (2^{-\alpha j}\sqrt{\log 2^j})_{j\in\mathbb{N}}$.

and the one associated with $\sigma_2^{(\alpha)} = (2^{-\alpha j}\log\log 2^j)_{j\in\mathbb{N}}$ is less visible. An explanation could come from the fact that the wavelet coefficients associated to the most irregular points (i.e. the points with a Hölder exponent closer to 0) are disturbed because of the shuffling.

For $b = 0.1$, $a \in \{0.1, 0.2, \ldots, 0.8\}$ and $c = a + 0.1$, we have computed 20 simulations of the function $B_\cdot^H$ with H both shuffled by blocks and unshuffled. For each simulation and each admissible sequence $\sigma^{(\cdot)} \in \Sigma$, the smallest h for which $\nu_{c,\sigma^{(\cdot)}}(h) = 1$ has been computed. Figure 5.28 shows for each admissible

sequence $\sigma^{(.)}$, the boxplot of the distance between c and the detected h (i.e. the absolute value of their difference). In both cases, the method using the correction $\sigma_1^{(\alpha)} = (2^{-\alpha j}\sqrt{\log\log 2^j})_{j\in\mathbb{N}}$ clearly gives the best results.

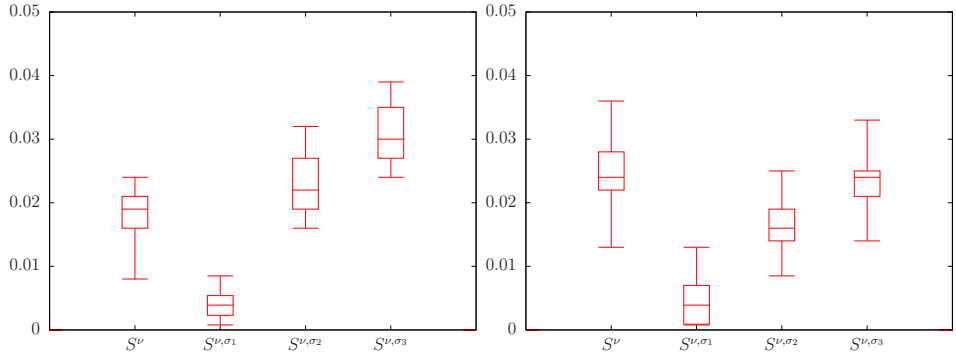

(a) Unshuffled H (b) Shuffled H

Figure 5.28.: Boxplot of the distance between c and the smallest h such that the profile evaluated in h equals 1 ($a = 0$ and $b = 0.1$). The left boxplot corresponds to the profile ν_f, and the three others correspond to the generalised profile $\nu_{f,\sigma^{(\cdot)}}$, with $\sigma_1^{(\alpha)} = (2^{-\alpha j}\sqrt{\log\log 2^j})_{j\in\mathbb{N}}$, $\sigma_2^{(\alpha)} = (2^{-\alpha j}\log\log 2^j)_{j\in\mathbb{N}}$ and $\sigma_3^{(\alpha)} = (2^{-\alpha j}\sqrt{\log 2^j})_{j\in\mathbb{N}}$.

5.4 Contributions of Profile-based Methods: Summary

In this chapter, contributions of profile-based methods are presented. The first part of this chapter uses the LPM. For a real-life signal f, the first main issue developed here is the detection of Hölder exponents h such that $d_f(h) = 1$. Let us recall that, for a fixed $h > 0$, the LPM uses two functions to approximate $d_f(h)$:

$$C \mapsto \tilde{\nu}_f^{-,C}(h) \quad \text{and} \quad C \mapsto \tilde{\nu}_f^{+,C}(h). \tag{76}$$

As already seen in the previous chapter, if several processes exist within the signal f, Functions (76) can contain information about these processes. For example, if f is the concatenation of two independent fractional Brownian motions of parameters H_1 and H_2, then if $h \in (H_1, H_2)$, within Functions (76), we have a first part which is increasing or decreasing and a second part with a stabilisation equal to 1. Consequently, in such cases, we can approximate two Hölder exponents such that $d_f(h) = 1$: a first one which is the greatest h such that the first function of (76) has all its value equal to 1, and a second one

which is the smallest h such that the second function of (76) has all its value equal to 1. If the distance between the approximation of these two Hölder exponents is significantly different from 0, then the signal has at least two Hölder exponents h such that $d_f(h) = 1$.

In the particular case of the concatenation of independent two fractional Brownian motions, the two Hurst indexes are well approximated: the smallest index is detected with the first function of (76), and the greatest one is detected with the second function of (76). The same detection is done on the concatenation of two independent log-normal cascades. The use of this method on these two examples highlights the link between the ability of the LPM to approximate $d_f(h)$ and the statistical behaviour of the histograms of wavelet coefficients on a fixed scale j. For signals for which it is statistically impossible to see two constituting processes from the wavelet coefficients, the LPM has difficulties to detect these processes. As a consequence, the precision in the approximation of the spectrum is negatively impacted.

This chapter also confirms the ability of the LPM to approximate non-concave spectra. For example, it can detect the non-concave part of the spectrum of the concatenation of two independent log-normal cascades. Moreover, this ability allows the LPM to approximate the Hausdorff dimension $\dim_{\mathcal{H}}$ of sets of points $E^f(h)$ sharing the same Hölder exponent h with $\dim_{\mathcal{H}} E^f(h) < 1$, when the signal is composed of a finite number of Hölder exponents h. However, it cannot approximate the value of these exponents. This fact is illustrated with the help of the Cantor set and its generalisations.

These results show that the LPM is a good method to study the kind of signals presented above, compared to the WLM which is unable to distinguish the two Hurst indexes in the concatenation of two independent fractional Brownian motions, the non-concave part of the concatenation of two independent log-normal cascades and to detect the Cantor set when it is related to the regularity of the function.

Moreover, it is usual in practice to perform two regressions when applying a multifractal formalism: one corresponding to the smallest scales and the second corresponding to higher scales (see Chapter 6). We show that the LPM can compute the exponents related to largest scales, with an approximation of the same order of magnitude as with the WLM. Let us notice that these exponents are less well approximated than those at smallest scales, and thus their interpretation on real-life signals must be done carefully.

The last part of this chapter presents a use of the generalised profile $\nu_{f,\sigma^{(\cdot)}}$, defined in the context of the spaces $S^{\nu,\sigma^{(\cdot)}}$ which are a generalisation of the spaces S^{ν} with the help of the admissible sequences. Let us recall that the asymptotic behaviour of $||f - P_{x_0}||_{L^\infty(B(x_0,2^{-j}))}$ is of the form

$$\sigma_j = 2^{-h_j(x_0)}\tau_j,$$

where $\tau = (\tau_j)_{j\in\mathbb{N}}$ is an admissible sequence which is negligible compared to $(2^j)_{j\in\mathbb{N}}$. On simulations of theoretical signals of size 2^{20}, we can detect the sequence τ within the Hölderian behaviour. More precisely, comparing the obtained approximation of the Hölder exponent with the generalised profiles associated to the sequences σ whose correction τ belongs to $\{(\sqrt{\log\log 2^j})_{j\in\mathbb{N}}, (\log\log 2^j)_{j\in}, (\sqrt{\log 2^j})_{j\in\mathbb{N}}\}$, we see that the profile associated with the corresponding correction of the Hölderian behaviour gives the best approximation. This allows to detect the Khintchin Law on simulations of the Brownian motion. Let us notice that, for real-life signals, it is very difficult to distinguish a noise from the sequence τ. Nevertheless, the method associated to the generalised profile $\nu_{f,\sigma^{(\cdot)}}$ should help to detect an unknown Hölderian behaviour in theoretical signals for which the noise can be minimised. A second application could be found in the study of processes for which one can obtain many realisations.

Chapter 6

Study of the Fractal Structure of Mars' Topography (< 15 km)

This chapter studies the fractal structure of Mars' topography. The surface roughness of Mars is an intensively studied subject within the scientific community (see [3, 85, 87, 95, 112, 113, 123, 125, 118, 114, 5] for example). Identifying the best possible landing sites for rovers or future manned missions and finding out the geophysical processes that shape the face of the planet are among the most common reasons to analyse Mars' topography.

These studies usually reveal two distinct scaling regimes in the topography of Mars (one at small scales, the other at larger scales), while the scale break varies from one work to another. The Hölder exponents (usually called in physics the power-law exponents or Hurst exponents) associated with these scaling laws, appear to differ according to the region considered for the study (cratered terrains, smoother plains, ice cap, etc.) but some common features can still be noticed among the different works. These exponents are sometimes used to claim that Mars' topography is a monofractal or multifractal field, which may depend on the definition of mono- or multifractality adopted by the authors.

Moreover, the studies mentioned above examine one-dimensional (1D) along-track series following North-South trajectories or some different regions that display distinct features (craters, plain, ice cap, etc.) but without an analysis of the whole surface of Mars. This implies that the two-dimensional (2D) nature of the topographic field has not been taken into account. For this reason, we began in 2016 a complete study of the roughness of Mars in 1D and 2D, published in [42]. More precisely, we took global longitudinal and latitudinal topographic profiles into account, and perform a thorough local two-dimensional analysis which keeps the 2D aspect of the data. We also showed that such an analysis allows to recover the main features of the surface of Mars. So far as we know, this was the first complete study of the planet Mars in 2D. The method used was the WLM; at that time, the LPM was not yet fully operational. Moreover, one of our goals was also to convince researchers that the wavelet-based methods are suitable candidates for the study of scaling properties of planetary surfaces. Before publishing this article, we have presented a preliminary 1D study in the conference [41].

The goal of this chapter is to complement this previous study with the LPM, and to show that the simultaneous use of the WLM and the LPM allows to get additional information about the fractal nature of signals. The complete study of the roughness of Mars at small scales with the WLM is presented and we do a similar study with the LPM. We have shown in [42] that a scale break occurs at $\approx$ 15 kilometers; this is in good agreement with [3, 87, 95]. This implies that, in order to study the roughness of Mars at small scales, the first five scales j are sufficient to perform the study with a wavelet-based method. A study at larger scales is presented in [42] with the WLM. Such a study has not been performed yet with the LPM. The main reason is, as already mentioned in Section 5.1.3, that this kind of study is more delicate, since the exponents detected at larger scales are less well approximated than those at smallest scales. Before using the LPM at larger scales on real-life signals, it is necessary to further investigate the efficiency of this method for such scales, by looking at the influence of the size of the signal on the approximation of the exponents. Section 5.1.3 shows however that the first results are promising.

The first section presents a state of the arts on the study of the planet Mars, and the data used for our analysis. The second section presents the complete study done with the WLM at small scales. As mentioned above, each method uses a different criterion to sort the mono- and multifractal signals. In [42], the criterion used is the linear correlation coefficient of the points of the function $q \mapsto \eta_f(q)$ (see Section 1.7). However, following a talk with A. Arneodo, it has become clear that this criterion is not optimal for several reasons: it is strongly influenced by the interval in which q varies, and by a few extreme values of the wavelet coefficients. It has been shown in Section 4.5 that these extreme values, that are present in the signals related to the topography of Mars [40], modify the behaviour of $\eta_f(q)$. Moreover, we have seen in Section 5.1.1 that the WLM tends to not see the multifractality in some cases. Consequently, it is more difficult to know if the value of the linear correlation coefficient of the points $(q, \eta_f(q))$ reflects the fractal behaviour of f, or the presence of extreme values of wavelet coefficients. For the same reasons, the coefficient c_2 of the Taylor expansion of η_f is not necessarily a better choice; in the case of the planet Mars, it gives similar results as the linear correlation coefficient. For these reasons, this section presents the correlation as a parameter of the WLM allowing another classification of signals than the usual mono- and multifractal distinction. Indeed, this coefficient remains important, since we can link it to some physical properties of the topography of Mars.

It is possible to refine the computation of the function η_f, for example by removing the extreme values of the wavelet coefficients, but this requires a preprocessing before using the WLM. We prefer an approach requiring fewer manipulations of the data. The LPM allows precisely to proceed without this kind of manipulations, given its robustness (see Section 4.5). Therefore Section 6.3 gives a methodology to study real-life signals with the LPM, and

more precisely a criterion to distinguish the mono- and multifractality. This method is applied on the longitudes and the latitudes of the planet Mars. In addition to present an answer to A. Arneodo's issue, this section shows that the LPM can be successfully applied to real-life signals, and it is thus a suitable candidate for the study of scaling properties of planetary surfaces. This section ends with presenting a 2D study of the roughness of Mars with the LPM. This analysis allows to have additional information about the local properties of the regularity of Mars.

The results presented in Section 6.2 are a collaboration with A. Deliège and S. Nicolay and have been published in [42]. The results presented in Section 6.3 are a collaboration with S. Nicolay and L. Reynaerts, and they are a part of a work in progress that will be the subject of a forthcoming article. Computational resources have been provided by the "Consortium des Équipements de Calcul Intensif" (CÉCI), funded by the "Fonds de la Recherche Scientifique de Belgique" (F.R.S.-FNRS) under Grant No. 2.5020.11.

This chapter is structured as follows:

6.1 State of the Arts and Data

In this section, a short review is given concerning the scaling properties of Mars' topography, obtained during the past two decades. Numerous works about the scaling properties of Mars' topography have been conducted using several tools, such as median differential slopes [85, 118], root mean square

(RMS) slope and deviation [114], wavelets [95], power spectral density (PSD) [3] and statistical moments [87] [123]. Let us first note that the power-law exponent β obtained with the PSD method is related to the Hurst (scaling) exponent H obtained with other methods as $\beta = 2H + 1$ [87, 114]. From now on, β will be automatically replaced by $H = (\beta - 1)/2$, so that only H is used to facilitate comparisons.

The value of the exponent H obviously depends on the scales chosen and these scales vary from one work to another. The first study using the PSD method [3] displays two different regions of Mars: a cratered one and a smooth one. The power spectrum of both sites display a power-law with $H \approx 1.2$ (< 10 km). Such results are in agreement with those obtained in [95] on the analysis of Mars polar topography. Using the variance of a wavelet transform of the data, it appears that $H \approx 1.25$ (< 24 km). A study of the whole gridded surface of Mars using the PSD was later carried out in [112], where statistical confirmation of the different scaling regimes is brought. It is suggested that $H \approx 1.4$ (< 3.3 km). One can see that, even tough there are common features between these works, there seems to be no consensus on the value of H.

Slightly different results are found when other methods are used. For example, authors in [114] use the RMS deviation to compute the Hurst exponent of 30-kilometers long profiles and so covering the planet with small grids. It appears that the distribution of the exponents H follows a Weibull distribution with mean 0.7. In the same spirit, authors in [113] computed generalised structure functions (based on surface elevation increments) of order 1 to 12 related to nine distinct sites on Mars which led to exponents $H \approx 0.75 - 0.9$. More recently, in [87], a multifractal formalism based on the statistical moments of several orders relying on Haar fluctuations was used. It turns out that this computation of H gives $H \approx 0.76$ (< 10 km).

Consequently, drawing on these works on the surface roughness of Mars, it seems that PSD-based and wavelet-based methods and those relying on (some kinds of) statistical moments of fluctuations display an exponent $H \approx 1.2 - 1.4$ with the former methods and $H \approx 0.7 - 0.9$ with the latter (< 25 km).

In this chapter, we use one of the topographic maps generated from the Mars Orbiter Laser Altimeter (MOLA) Mission Experiment Gridded Data Records (MEGDRs) [124], which are global topographic maps of Mars created by combining altimetry values from the PEDR data acquired over the entire MGS mission (about 600 million measurements). These data are collected during the Mars Global Surveyor mission from 1997 to 2001. MEGDRs are available at 4, 16, 32, 64 and 128 pixels per degree and are available at

`http://pds-geosciences.wustl.edu/missions/mgs/megdr.html`.

In order to have as many scales as possible at our disposal, the 128-pixel-per-degree map is naturally chosen. Let us note that this map almost represents the whole planet; the latitude ranges from 88° S to 88° N. More details about

the mission, the data and the MOLA experiment can be found in [124, 125] and on the website mentioned above. These data are already used in [3] and [95].

6.2 A Complete Study of the Roughness of Mars in 1D and 2D with the WLM (< 15 km)

This section presents a complete study of the roughness of Mars with the WLM at the scales j taken between 0 and 4. This choice is justified in [42, 40]. We first recall the implementation of the WLM and some key values to sort the signals. The results for both the $1D$ and $2D$ signals are presented. We finish by showing that the value of the Hölder exponent in 2D allows to detect major surface features of Mars.

6.2.1 WLM in Practice

Let us briefly explain how to implement the WLM (the method is presented in Section 1.7) on a real-life signal f. For a fixed q, the value $\eta_f(q)$ is approximated by the slope of the function

$$j \mapsto \frac{\log S_f(j,q)}{\log 2}.$$

In practice, we have only access to a finite number of the scale j and this function is not necessarily linear; it is often a piecewise linear function. This implies the existence of two (or more) distinct scaling regimes. These kind of signals is met in the study of the roughness of Mars (e.g. Figure 2 in [87], Figure 3 in [113] and Figure 1 and 5 in [42]). Consequently, the scales chosen to compute the slope is a crucial point of the algorithm, and influence the approximation of the Hölder spectrum. In this work, we choose the scales $j = 0, \ldots, 4$. This choice is justified in [42, 40].

If the function

$$q \in \mathbb{R} \mapsto \eta_f(q)$$

displays a linear behaviour, the signal is said *monofractal* at the scales used to build η_f; otherwise it is *multifractal* at those scales. In practice, we must choose an interval for the values of q, and this choice strongly influences this distinction. There exists several methods to determine if a function is linear or not. Moreover, the values of η_f can also be also strongly influenced by some extreme values of the wavelet coefficients (see Section 4.5). For all these reasons, we prefer not to set up all the parameters needed to develop a method making a clear distinction between the mono and multifractality using the WLM. We propose in Section 6.3.1 a new method for such a distinction, with

the help of the LPM, which requires a minimum of parameters and which is more robust than the WLM.

However, we still study the linear behaviour of η_f on a chosen interval centred at the origin, because it can be relied with some physical properties of the planet Mars. We take the simplest approach: the linear correlation coefficient c. From numerical experiments on Mars, we set that η_f is "linear enough", if the associated linear correlation coefficient c is greater than 0.98 in the 1D case and 0.97 in the 2D case, due to the fewer number of wavelet coefficients available in this context. In this case, the Hurst exponent characterising the irregularity of the surface is assimilated to the slope of η_f. Otherwise, when η_f "is not linear enough", the slope of the best-fit (in the least square sense) linear regression of η_f gives a scaling exponent which does not fully represent the irregularity of the surface, but gives a criterion to sort the signals.

Let us note that, in order to limit the influence of anomalously large coefficients in the computations, the values of q range from -2 to 2 for the one-dimensional study and from -1.5 to 1.5 in the two-dimensional case. The difference comes again from the fact that we grid the map in the latter case (see next section) and we thus have less wavelet coefficients due to shorter signals. In this work, we use again the third-order Daubechies wavelet [39] and the 2D analysis uses a tensor product-based technique (see Section 1.5.3).

6.2.2 Results for the One-Dimensional Analysis

We perform the WLM on one-dimensional latitudinal and longitudinal bands: in this framework, 22528 latitudinal and 46080 longitudinal topographic profiles are analysed.

As far as the longitudinal signals f are concerned, more than 99.7% of them have an associated function η_f "linear enough", with respect to the criterion set in the previous section, i.e. the corresponding η_f has a linear correlation coefficient c greater than 0.98. This can be seen on the top left histogram in Figure 6.1. The exponents H extracted as function of the longitude and the histogram of their distribution are also represented in Figure 6.1 (middle left and bottom left). The mean value of H is 1.15 with a standard deviation of 0.06. As expected, such results are in agreement with PSD- and other wavelet-based methods [3, 95].

Regarding the latitudinal signals, it appears that 92.1% have an associated function η_f "linear enough". Such a drop in the proportion with the longitudes may seem surprising at first, but a few reasons may contribute to explain it: the crustal dichotomy of Mars, the presence of polar caps, the fact that the map is actually a projection of the planet, the North/South trajectory of the orbiter, among others. Moreover, if we only keep latitudes between $80°S$ and $80°N$, then more than 96.7% of the signals have a function η_f "linear enough", and this percentage rises above 99.9% if we allow $c > 0.975$; this can be noted

on the top right histogram in Figure 6.1 (with latitudes kept from $80°S$ to $80°N$). Considering only these restricted latitudes, the mean value of H is 1.05 with standard deviation 0.13. The influence of latitude can be clearly seen in Figure 6.1 and such a latitudinal pattern is in agreement with [114]. Besides, a clear difference appears between the two hemispheres: the mean value of H is 0.98 in the North and 1.12 in the South.

Let us note that the results of the longitudinal case remain almost unchanged when poles are removed and that the clear difference of shape in the histograms of Figure 6.1 and the differences in the values of H may indicate a slight anisotropy of the surface roughness (< 15 km), as mentioned in [5].

6.2.3 Results for the One-Dimensional Analysis: Localisation of the Values with Strong Correlation Coefficients

To complete the study of the 1D analysis of Mars' topography, we briefly discuss the spatial distribution of the bands with a function η_f, "linear enough or not". For that purpose, Figure 6.2 shows a topographic map of Mars in false colours. On the top of the map (resp. on the right), red lines indicate the few longitudinal (resp. latitudinal) bands exhibiting a linear correlation coefficients $c < 0.98$. The analysis carried out on a band is somehow a "global" analysis, compared to the more "local" 2D analysis performed in the next section.

That being said, it appears in Figure 6.2 that a large part of the Northern hemisphere displays a function η_f "not linear". This could be the result of the fact that the topographic profiles at these latitudes are smooth and, from time to time, interrupted by a crater or an anomalously irregular pattern. Therefore, both the wavelet coefficients related to the smooth behaviour and those associated with the rougher one are present, which globally results, quite logically, to a function η_f "not linear". Moreover, some sites of Mars seem to have an impact on the global characterisation of the fractal nature of a band. Indeed, regions such as Hellas Planitia ($50°S$ $70°E$), Elysium Mons ($25°N$ $174°E$), Olympus Mons ($20°N$ $225°E$) and the Tharsis region ($0°N$ $250°E$) probably influence both longitudinal and latitudinal analyses. These explanations should be investigated in more details in future works, since the influence of possible artefacts cannot be completely excluded.

6.2.4 Results for the Two-Dimensional Analysis

Let us now examine the results of the two-dimensional WLM performed on the topographic map of Mars. Such a study is, to our knowledge, the first of its kind. Contrary to [5] and [54] where the two-dimensional multifractal detrended fluctuation analysis is used to study a grayscale image of a relatively

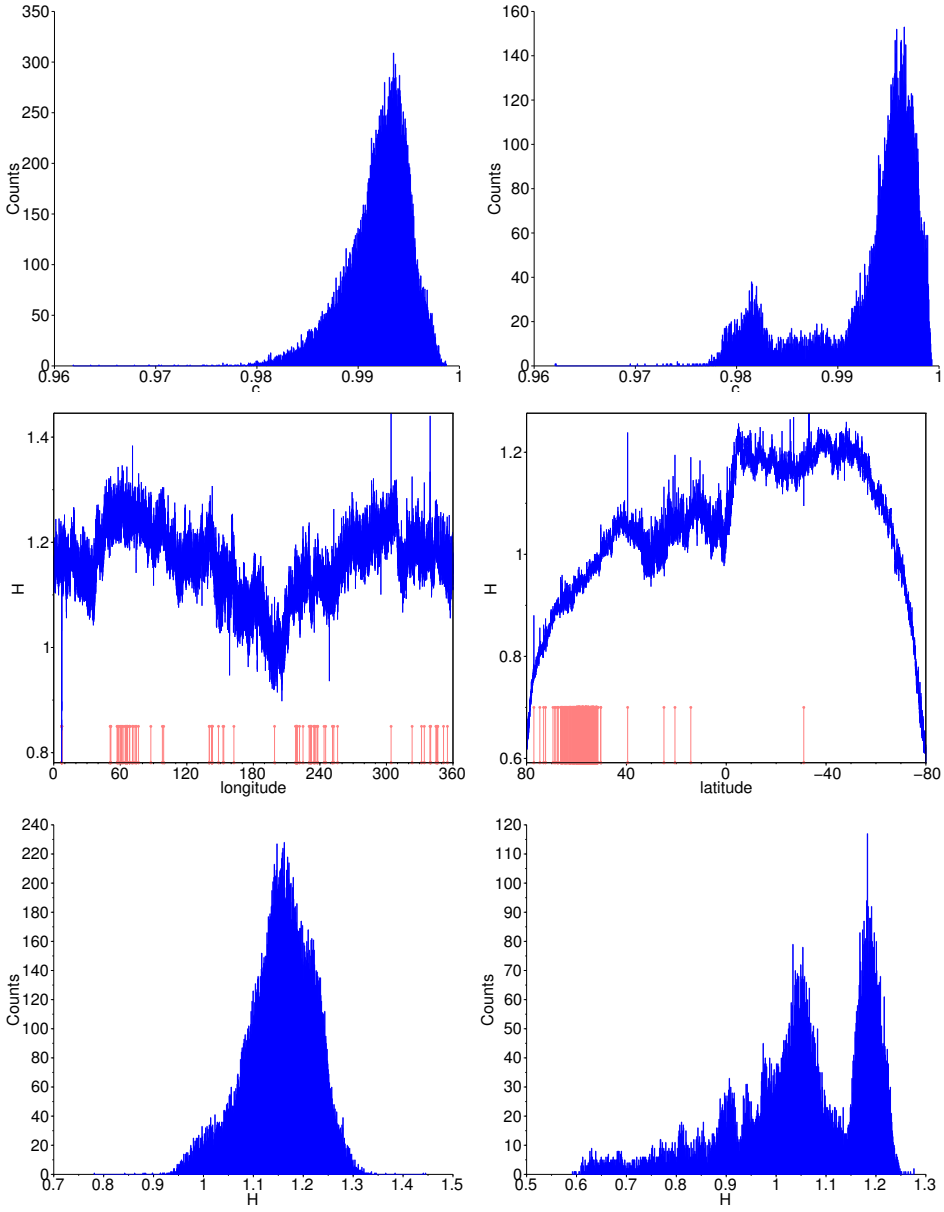

Figure 6.1.: Top: Histograms of the distribution of the linear correlation coefficients c (related to the functions η_f, see text) for the longitudinal (left) and latitudinal (right) analyses. The data are subdivided into 1000 equally spaced bins. Middle: Exponent H as a function of longitude (left) and latitude (right). The red lines indicate the topographic profiles with $c < 0.98$. Bottom: the corresponding histograms of the distributions of H.

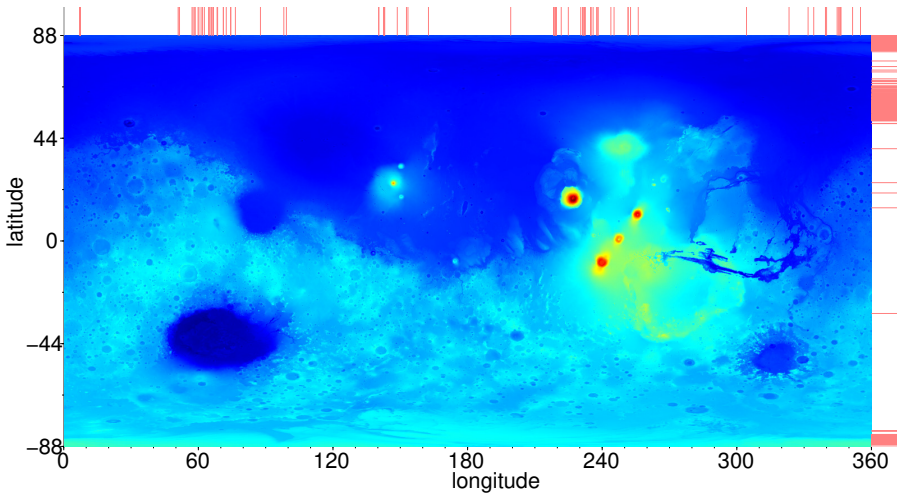

Figure 6.2.: Topographic map of Mars in false colours (dark blue corresponds to an altitude of roughly -8100 meters and dark red to 21200 meters). On the top of the map (resp. on the right), red lines indicate the few longitudinal (resp. latitudinal) bands having a linear correlation coefficients $c < 0.98$.

small part of Mars, we aim at examining the whole surface, where data are actual topographic measurements. For that purpose, the map used in the one-dimensional case is first gridded into squares of 1024×1024 pixels (which will be called tiles in the following) thus giving ≈ 1000 tiles to analyse. Such tiles correspond to windows of $8° \times 8°$ on Mars. The choice of the tile size is rather subjective but is a good compromise between a local analysis (size not too large) and the statistical meaning of the results (size not too small). In a different approach, a similar resolution ($5° \times 5°$) is used in [112], where a more detailed justification of such a choice is provided. In order to increase the statistical significance of the following results, the grid is also shifted 512 pixels rightward, then downward and finally both rightward and downward, giving us a total number of 3696 tiles to work with. Let us recall that, due to the restricted number of data available in such tiles, the parameter q now ranges from -1.5 to 1.5 and the threshold for the coefficient c for the function η_f to be considered as "linear enough" is now 0.97.

Not surprisingly, the two-dimensional analysis of Mars' topography reveals that the function η_f has a behaviour "linear enough". Indeed, 96.1% of the considered tiles have a function η_f with a linear correlation coefficient c greater than 0.97, as shown in Figure 6.3. As seen in the spatial distribution of these coefficients (Figure 6.3), the regions with a function η_f with a behaviour "not linear enough" are mostly located around Hellas Planitia ($50°S$ $70°E$), Amazonis Planitia ($25°N$ $180°E$) and Acidalia Planitia ($25°N$ $330°E$).

The mean of the exponents H is 1.12, with standard deviation 0.13, which is consistent with the one-dimensional analysis; their distribution is represented in Figure 6.3. One can note that this histogram is somehow bimodal as the one corresponding to the latitudinal study, suggesting that the latitudinal pattern previously observed has some influence in this case. This is confirmed in Figure 6.4, which shows the longitudinal and latitudinal average of H of the 2D analysis. It can also be noted that these curves display a similar behaviour as those obtained by averaging the exponents of the 1D case by blocks of 1024 longitudinal and latitudinal bands. Besides, the difference between the two hemispheres is similar to the 1D case: the mean value of H is 1.07 in the North and 1.17 in the South.

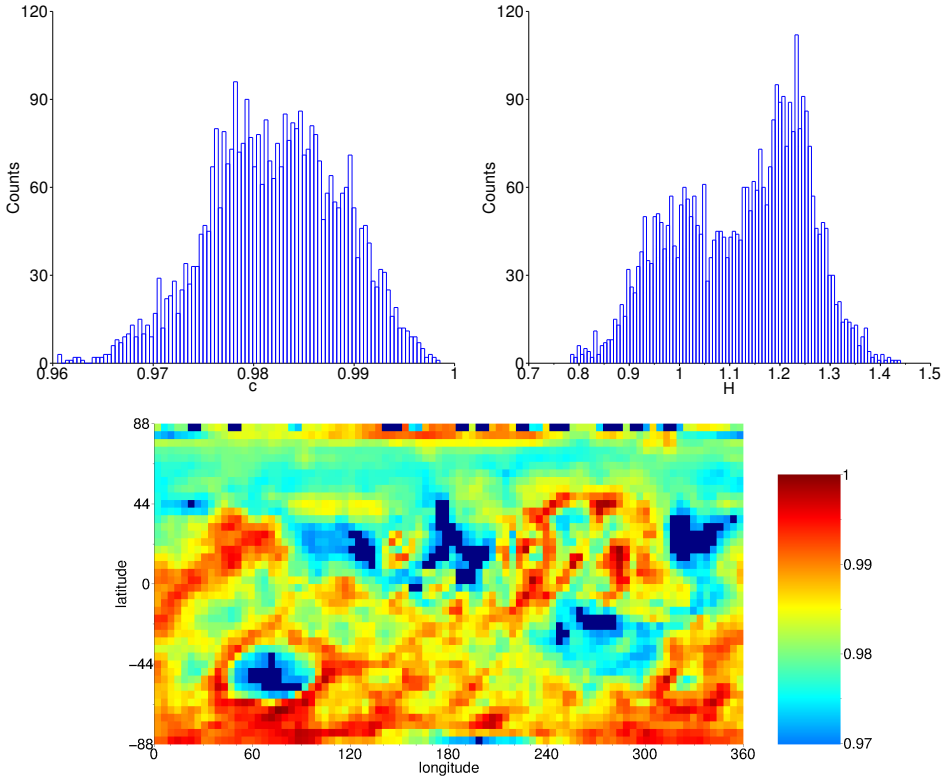

Figure 6.3.: Top: Histograms of the distribution of the linear correlation coefficients c (related to the functions η_f, see text) and the exponents H for the 2D analysis with the WLM. The data are subdivided into 100 equally spaced bins. Bottom: The spatial distribution of the coefficients c, where the tiles with $c < 0.97$ are all coloured in dark blue.

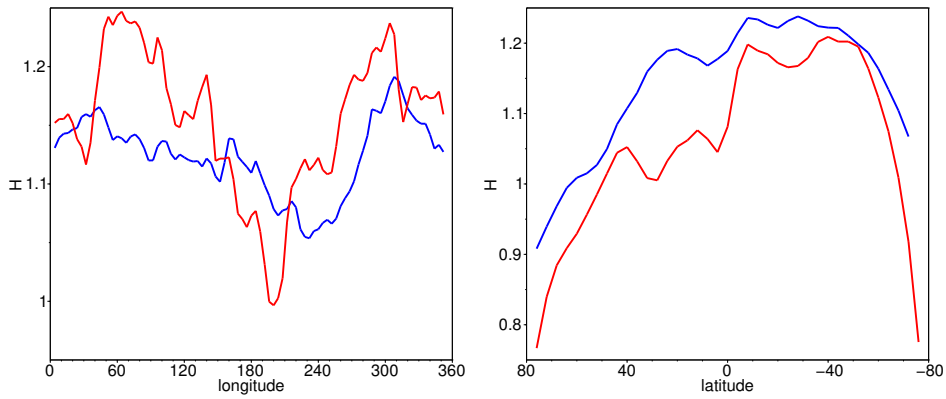

Figure 6.4.: Left (resp. right): the blue line indicates the mean of the exponents H longitudinally (resp. latitudinally) in the 2D case. The red line represents the mean of the exponents H of the 1D case by blocks of 1024 longitudinal (resp. latitudinal) bands. In both cases, the blue and red curves display a similar behaviour.

6.2.5 Results for the Two-Dimensional Analysis: Detection of Major Surface Features

In this last section, we show that the spatial distribution of the scaling exponents H obtained from the two-dimensional analysis of Mars is not "random". Indeed, it is possible to detect major surface features of Mars in the spatial distribution of these exponents, which is an extra argument in favour of the effectiveness of the WLM. The identification of a particular feature is merely qualitative and subjective. In other words, we do not use any algorithm to determine whether a pattern is detected or not; such a decision may depend on the expectations of the reader for a feature to be detected. Nevertheless, as shown below, there is often no point denying that some characteristics are clearly identified.

For that purpose, we consider 9 of the most famous sites of the Red Planet: Hellas Planitia (A), Isidis Planitia (B), Elysium Mons (C), Vestitas Borealis - Northern plains (D), Olympus Mons (E), Tharsis (F), Valles Marineris (G), Argyre Planitia (H) and Acidalia Planitia (I). These regions are represented in Figure 6.5. Let us recall that the analysis carried out in the previous section was only performed on a sample of tiles of 1024×1024 pixels, not all the possible ones. The value of H corresponding to a tile is associated to the central pixel of the tile and, in order to fill in the gaps, the missing values are interpolated using a 2D cubic spline. Let us note that the interpolation method used is not of primary importance; it is only used for more comfortable visual results and the interpolated values are not used in any statistical analysis

in this paper. The maps representing the spatial distribution of the scaling exponents H are displayed in Figure 6.5.

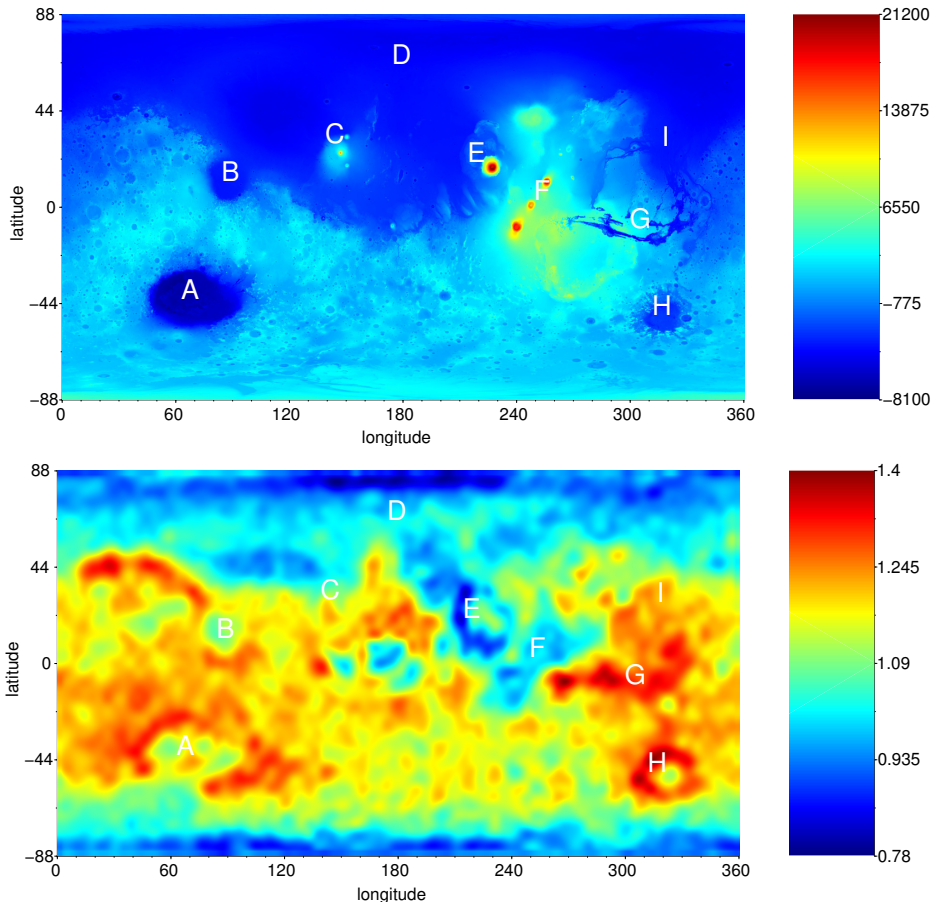

Figure 6.5.: Top: the topographic map of Mars in false colours. Bottom: the map representing the spatial distribution of the exponents H computed with the WLM. The regions of interest are Hellas Planitia (A), Isidis Planitia (B), Elysium Mons (C), Vestitas Borealis - Northern plains (D), Olympus Mons (E), Tharsis (F), Valles Marineris (G), Argyre Planitia (H) and Acidalia Planitia (I). It can be noted that most of these regions are clearly detected.

Among the 9 features of interest, it seems reasonable to say that sites A, B, D, F, G and H can be identified on the map, whereas regions C and E are more difficult to see and the site I is less visible. However, this last site can be detected thanks to the linear correlation coefficients (see Figure 6.3), as the sites A, C and D. Let us note that, as already mentioned, poles appear to behave differently than their surroundings but this may be due to some

artefacts such as the projection used to generate the maps. Also, the typical crustal dichotomy and the border of that feature (the vast Vestitas Borealis and Northern plains in a broad sense) are detected on the map.

6.3 A Complete Study of the Roughness of Mars in 1D and 2D with the LPM (< 15 km)

This section presents the first results obtained with the LPM on real-life signals. These results have not been published yet. The goal of this study is twofold: first to show that the LPM is a suitable candidate for studying the fractality of real-life signals, and more particularly, the properties of planetary surfaces, and secondly, to show that the LPM allows to obtain additional information compared to the WLM.

Section 6.3.1 gives a methodology to study real-life signals with the LPM. More precisely, we propose a method to distinguish the mono- and the multifractality. This approach is applied on the 1D and 2D analysis of Mars' topography. We first show that we obtain similar results concerning the values of the Hurst exponent compared to previous studies, and we also discuss about the multifractality of the bands of Mars. Finally, Section 6.3.3 presents the results about the two-dimensional study and shows that some additional information about the roughness of Mars' topography is obtained, comparing with the WLM.

6.3.1 A Method to Distinguish the Mono- and Multifractality with the Help of the LPM

This section presents a method based on the LPM to determine if a real-life signal f is monofractal or multifractal. More precisely, this method allows two detections: the first one detects if there exists an exponent h such that $d_f(h)$ is strictly smaller than n, n being the dimension of the domain of f, and the second one detects if f has several Hölder exponents whose associated iso-Hölder sets have a full-Lebesgue measure.

Let us begin with the first detection. From Chapter 4, it suffices to find a real h (with a bisection method for example), such that the function

$$C > 0 \mapsto \tilde{\nu}_f^C(h) \tag{77}$$

has a stabilisation with a value strictly smaller than n.

Let us recall that, it is possible to detect some values strictly smaller than n on numerical simulations of monofractal signals (see Section 4.1 for the case of fractional Brownian motions). We must thus define a threshold M close to n for which, if there exists h such that the value of the stabilisation of the

function (77) is smaller than M, then the signal is considered *multifractal*. From Figure 4.7, which shows the smallest value obtained for a stabilisation on fractional Brownian motions, it seems reasonable to take $M = n - 0.05$.

Let us notice that for the LPM, we compute separately the increasing part and the decreasing part of the spectrum, with the help of the functions $\tilde{\nu}_f^+$ and $\tilde{\nu}_f^-$ respectively. Consequently, the method also allows to know if the spectrum d_f has an increasing part or not, and a decreasing part or not.

The second detection presented in this section allows to know if f has several Hölder exponents whose associated iso-Hölder sets have a full-Lebesgue measure. This kind of signals is studied in Section 5.1. Let us recall how to detect these Hölder exponents: the smallest (resp. the greatest) Hölder exponent $H_{\min}$ (resp. $H_{\max}$) such that $d_f(H_{\min})$ (resp. $d_f(H_{\max})$) is equal to n, is approximated as the greatest (resp. the smallest) h such that the function

$$C > 0 \mapsto \tilde{\nu}_f^{-,C}(h) \quad (\text{resp. } C > 0 \mapsto \tilde{\nu}_f^{+,C}(h))$$

has all its value equal to n. In the case of a monofractal signal, the approximation of $H_{\min}$ is close to $H_{\max}$ (see Section 4.3). We must thus give a threshold N for which if $|H_{\min} - H_{\max}|$ is greater than N, then the signal is considered having (at least) two Hölder exponents, whose associated iso-Hölder sets have a full-Lebesgue measure. In view of Chapter 4 and Chapter 5, it seems reasonable to take $N = 0.05$.

In conclusion, a real-life signal f is considered as *monofractal* if the two following conditions are satisfied:

1. there does not exist an exponent h such that the functions

$$C > 0 \mapsto \tilde{\nu}_f^{-,C}(h) \quad \text{and} \quad C > 0 \mapsto \tilde{\nu}_f^{+,C}(h)$$

   have a stabilisation with a value smaller than $M = 0.95$,

2. the distance $|H_{\min} - H_{\max}|$ is smaller than $N = 0.05$.

If one condition is not satisfied, f is considered as *multifractal*. In this case, several scenarios are possible:

1. if there exists h such that the function $C > 0 \mapsto \tilde{\nu}_f^{+,C}(h)$ has a stabilisation with a value smaller than $M = 0.95$, then f has a spectrum with an increasing part,

2. if there exists h such that the function $C > 0 \mapsto \tilde{\nu}_f^{-,C}(h)$ has a stabilisation with a value smaller than $M = 0.95$, then f has a spectrum with an decreasing part,

3. if the distance $|H_{\min} - H_{\max}|$ is greater than $N = 0.05$, then f has (at least) two Hölder exponents whose the associated iso-Hölder sets have a full-Lebesgue measure.

The next sections apply these methods on one-dimensional latitudinal and longitudinal bands of the planet Mars and on the tiles that grid the map of mars.

Remark 6.3.1. If $|H_{\min} - H_{\max}| < 0.05$, f has only one Hölder exponent $H^{\tilde{\nu}}$ such that $d_f(H^{\tilde{\nu}}) = n$. In this case, this exponent is approximated by

$$H^{\tilde{\nu}} = \frac{H_{\min} + H_{\max}}{2}. \tag{78}$$

Let us recall that to sort the signals with the WLM, we have decided to compute the slope of the function

$$q \in [-2, 2] \mapsto \eta_f(q),$$

for all signals f, even if η_f is not linear (see Section 6.2.1). In Section 5.1.1, we have seen that this slope is close to $H^{\tilde{\nu}}$, in some cases. Consequently, we also compute $H^{\tilde{\nu}}$ for all signals, even if $|H_{\min} - H_{\max}| > 0.05$. This value allows to sort the signals and also to compare the results obtained with those of the WLM.

6.3.2 Results for the One-Dimensional Analysis

In this section, we compute the exponent $H^{\tilde{\nu}}$ defined in (78), for each one-dimensional latitudinal and longitudinal bands. Figure 6.6 shows $H^{\tilde{\nu}}$ extracted as the functions of longitude and latitude. These functions are similar to their equivalent obtained with the WLM (see Figure 6.1). The mean value of the exponent for the longitudinal signals is 1.18, with a standard deviation of 0.08. Regarding the latitudinal signals, the mean value of the exponent is 1.06, with a standard deviation of 0.14. Moreover, the influence of the latitude is clear: the mean value is 0.99 in the North and 1.13 in the South. Such results are in agreement with the WLM (see Section 6.2.2) and other wavelet-based methods (see [3, 95]). It confirms a slight anisotropy of the surface roughness.

Let us now look at the histograms of these exponents on Figure 6.7. Regarding the latitudinal signals, the histogram is similar to its equivalent obtained with the WLM (see Figure 6.1): there is a main peak close to 1.2 and a second close to 1.05. The case of the longitudinal signals is more interesting: as for the WLM, we have the main peak close to 1.2, but we have a second peak close to 0.98, which is not present in the case of the WLM.

Figure 6.8 shows on the topographic map of Mars, the location of the few longitudinal bands having $H^{\tilde{\nu}}$ between 0.95 and 1, i.e. those forming the second peak of the histogram obtained with the LPM. We clearly see that most of the bands are located at the same place: between longitudes 190° and 220°. To explain this specific location of these bands, one way to look at the criterion related to the distance $|H_{\min} - H_{\max}|$.

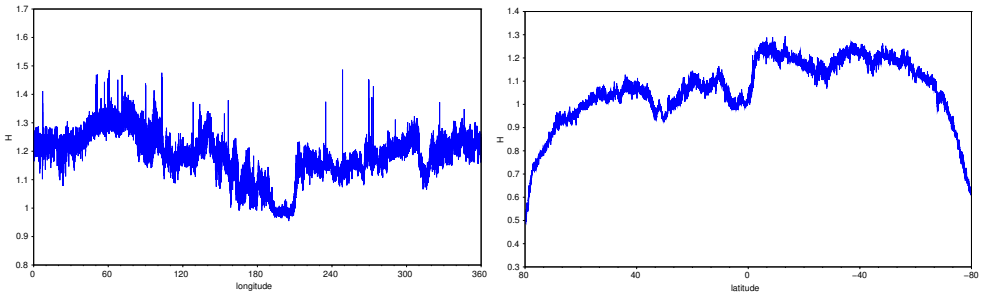

(a) function of longitude (b) function of latitude

Figure 6.6.: Approximation of the exponent $H^{\tilde{\nu}}$ defined in (78) for each longitude and latitude. As for the WLM, we keep the latitudes from 80°S to 80°N.

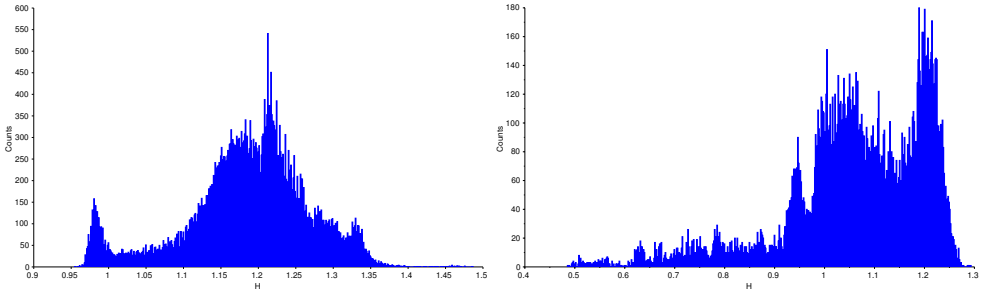

(a) longitude (b) latitude

Figure 6.7.: Histograms of the distributions of the Hölder exponent defined in (78) on one-dimensional longitudinal and latitudinal (with latitudes kept from 80°S to 80°N) bands with the LPM.

Figure 6.9 shows the longitudinal and latitudinal bands where

$$|H_{\min} - H_{\max}| < N,$$

with $N = 0.05$, i.e. the bands f considered as having only one Hölder exponent h such that $d_f(h) = 1$. We notice that for the longitudes, the bands located between 190° and 220° (i.e. those that stand out in Figure 6.8) seem to have (at least) two Hölder exponents whose the associated iso-Hölder sets have a full-Lebesgue measure. Moreover, when we look the values $|H_{\min} - H_{\max}|$ for these bands, we see that they are greater than 0.25.

We notice that almost 50 percents of the longitudinal bands have values for $|H_{\min} - H_{\max}|$ smaller than $N = 0.05$ and this percentage rises to 70 if $N = 0.08$. Regarding the latitudinal bands, we have some 35 percent for $N = 0.05$, and this percentage rises to 60 if $N = 0.08$. This difference between

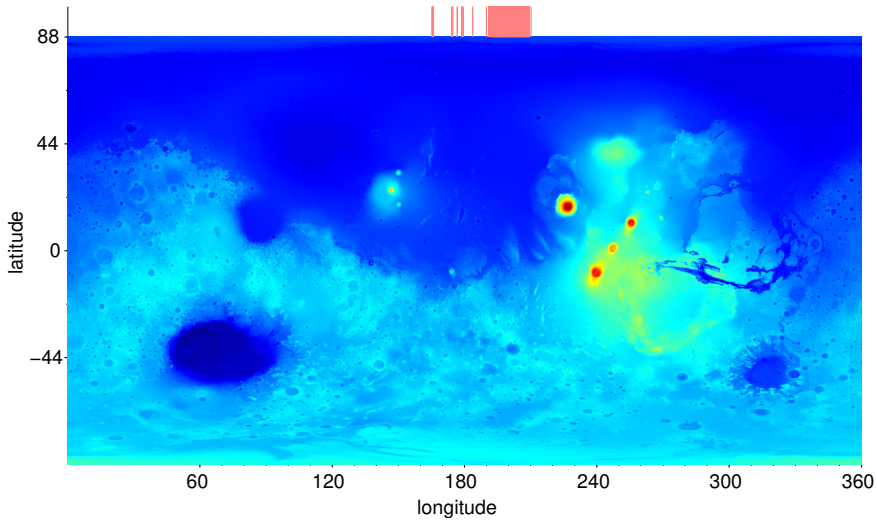

Figure 6.8.: Topographic map of Mars in false colours. On the top of the map, red lines indicate the few longitudinal bands exhibiting a dominant Hölder exponent between 0.95 and 1

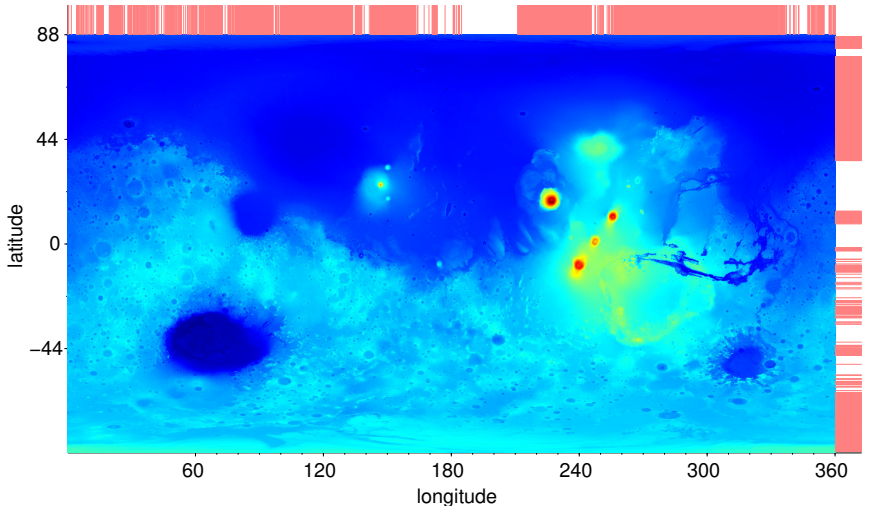

Figure 6.9.: Topographic map of Mars in false colours. On the top of the map (resp. on the right), red lines indicate the longitudinal bands (resp. latitudinal) whose the value of $|H_{\min} - H_{\max}|$ is smaller than 0.05, meaning that there exists exactly one Hölder exponent whose the associated iso-Hölder set has a full-Lebesgue measure.

the longitudinal and latitudinal bands confirms again the slight anisotropy in the topographic field.

Remark 6.3.2. Let us go back to the longitudinal bands located between 190° and 220°. There remains an important question: why are these bands, satisfying $|H_{\min} - H_{\max}| > 0.05$, highlighted when comparing the LPM's and the WLM's histograms, while other signals satisfying the same condition are not?

Let us recall that the slope of the function

$$q \mapsto \eta_f(q)$$

seems to give the average value between $H_{\min}$ and $H_{\max}$, when we have two processes, one is associated to $H_{\min}$ and the other one to $H_{\max}$. This fact seems true when the processes have the same weight in the signal considered (see the end of Section 5.1.1). It seems reasonable to think that the slope does not give the average value between $H_{\min}$ and $H_{\max}$ when, within the same signal, the two processes have different weights. This could be an explanation for what happens for the longitudinal bands located between 190° and 220°.

To end this section, let us study a last parameter presented in the previous section: the detection of an exponent having a value smaller than $M = 0.95$, for the stabilisation of the functions

$$C > 0 \mapsto \tilde{\nu}_f^{-,C}(h) \quad \text{and} \quad C > 0 \mapsto \tilde{\nu}_f^{+,C}(h).$$

Figure 6.10 shows the longitudinal and latitudinal bands for which the method does not detect an exponent h with a value of the stabilisation smaller than $M = 0.95$. More than 99 percent (resp. 95 percent) of the longitudinal bands (resp. latitudinal) have a spectrum with an increasing part, and there are 72 percent (resp. 62) which have a spectrum with an decreasing part. If we take $M = 0.8$, we have 95 percent (resp. 70 percent) of the longitudinal bands (resp. latitudinal) whose the spectrum has an increasing part, and there are 51 percent (resp. 44) whose the spectrum has an decreasing part. This difference between the longitudes and the latitudes may come from that the crustal dichotomy of Mars, the presence of polar caps, the fact that map is a projection of the planet, the North/South trajectory of the orbiter, among others.

The multifractality may seem surprising, because it goes against most studies done in the field. Here are some elements to justify these results. First, we have seen in the previous chapters that the WLM (and consequently, similar methods based on a structure function such as the DFA), may not detect the multifractality of a signal: either the scaling function does not contain the information about the multifractality (as the concatenation of two Brownian motions), either the criterion of mono/multifractality is hardly reliable to a

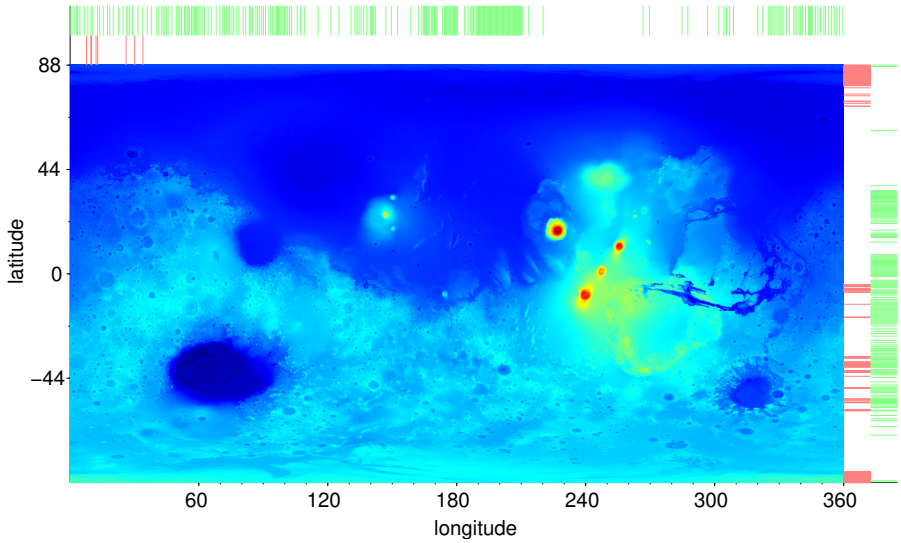

Figure 6.10.: Topographic map of Mars in false colours. On the top of the map (resp. on the right), red lines indicate the longitudinal bands (resp. latitudinal) for which the method does not detect an exponent h with a value of the stabilisation of the function $C > 0 \mapsto \tilde{\nu}_f^{+,C}(h)$ smaller than 0.95, while the green ones correspond to a stabilisation of the function $C > 0 \mapsto \tilde{\nu}_f^{-,C}(h)$ smaller than 0.95.

physical property of the signal. Consequently, there is no consensus on the efficiency of these methods to distinguish the mono- and the multifractality. On the other hand, these methods are well-known to correctly approximate the (dominant) Hurst exponent, and in this case, our method gives similar results (this Hurst exponent is defined as $H^{\tilde{\nu}}$ with the LPM). Consequently, the LPM seems a suitable candidate for the study of scaling properties of planetary surfaces. This method is radically different than the other ones (since it is not based on a structure function), and we think that it allows to override certain defect of the previous methods.

These results give a positive answer to the question of A. Arneodo, for who it seemed that our study with the WLM does not support the hypothesis of the monofractality in these signals. We confirm his intuition: most of the longitudinal and latitudinal bands on the planet Mars have a multifractal behaviour (< 15 km).

6.3.3 Results for the Two-Dimensional Analysis

Let us now analyse the Mars' topography with the LPM, keeping the 2D aspect of the data. The same strategy as for the WLM is used: the map is gridded into tiles of 1024×1024 pixels with a shift of 512 pixels (more detail at the beginning of Section 6.2.4) and the two-dimensional LPM is performed on each tile. Let us notice that the LPM does not require modifications in its algorithm when passing in two dimensions, compared to the WLM for which the range of the parameter q has been modified.

To begin with, Figure 6.11 shows the map of the spatial distribution of the exponents $H^{\tilde{\nu}}$ computed with the LPM. Let us recall that the identification of a particular feature is merely qualitative and subjective. We will later see a first objective criterion, deduced from the histograms of the exponents, to sort the roughness of Mars' topography.

As for the WLM, this map allows to identify some major surface features of Mars, such as Hellas Planitia (A), Isidis Planitia (B), Vestitas Borealis - Northern plains (D), Tharsis (F), Valles Marineris (G) and Argyre Planitia (H). The identification of the two regions Elysium Mons (C) and Olympus Mons (E) is less obvious, but (C) seems more visible compared to the map obtained with the WLM.

This map also shows that the distribution of the values of the exponents seems to be different between the WLM and the LPM. Indeed, the values are between 0.78 and 1.4 for the WLM, while they are between 0.74 and 1.6 for the LPM. The mean of the exponents $H^{\tilde{\nu}}$ is 1.16, with standard deviation 0.14. This mean is slightly larger than the one obtained with the WLM. The difference between the two hemispheres is still present: the mean value of $H^{\tilde{\nu}}$ is 1.11 in the North and 1.2 in the South.

Figure 6.12 shows the histograms of the distributions of the exponents $H_{\min}$, $H_{\max}$ and $H^{\tilde{\nu}}$. Let us recall that the exponent $H^{\tilde{\nu}}$ is the equivalent of the exponent H of the WLM, in the sense that it is used to characterise the regularity of the signal and allows to sort the signals. The distribution of $H^{\tilde{\nu}}$ has a main peak located on the left, and a second peak on the right. This is the opposite of the WLM (see Figure 6.3).

Let us now explore the results in further detail to give an explanation of the difference between the distribution of the exponents H and $H^{\tilde{\nu}}$. Let us recall that this last one is defined as

$$H^{\tilde{\nu}} = \frac{H_{\min} + H_{\max}}{2}.$$

The histograms of $H_{\min}$ and $H_{\max}$ also have two peaks, where the main peak is on the left. This implies that the difference is not due to a different behaviour of the functions $\tilde{\nu}_f^-$ and $\tilde{\nu}_f^+$. However, the main peak for the histogram of $H_{\min}$ is located in the interval $[0.9, 1]$, while that of $H_{\max}$ is in $[1.1, 1.2]$. This therefore suggests the presence of signals that do not have only one dominant

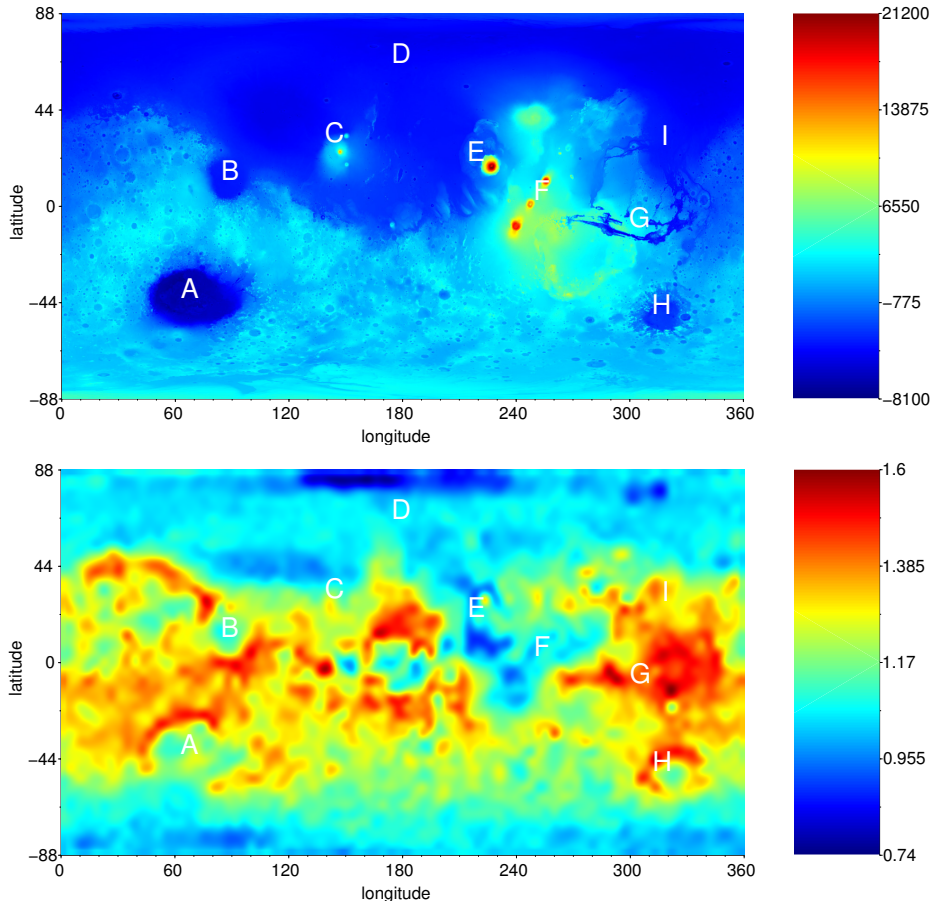

Figure 6.11.: Top: the topographic map of Mars in false colours. Bottom: the map representing the spatial distribution of the exponents $H^{\tilde{\nu}}$ computed with the LPM. The regions of interest are Hellas Planitia (A), Isidis Planitia (B), Elysium Mons (C), Vestitas Borealis - Northern plains (D), Olympus Mons (E), Tharsis (F), Valles Marineris (G), Argyre Planitia (H) and Acidalia Planitia (I). It can be noted that most of these regions are clearly detected.

exponent, but at least two. This will be confirmed later in the study of the distance $|H_{\min} - H_{\max}|$, which is thus a first explanation of the difference obtained between the WLM and the LPM.

To complete the study of the spatial distribution of the values of the exponents, Figure 6.13 shows two maps of Mars, one with the help of the WLM and the other with the help of the LPM, each divided into three zones: a first zone corresponding to the exponents smaller than 1, a second zone to the

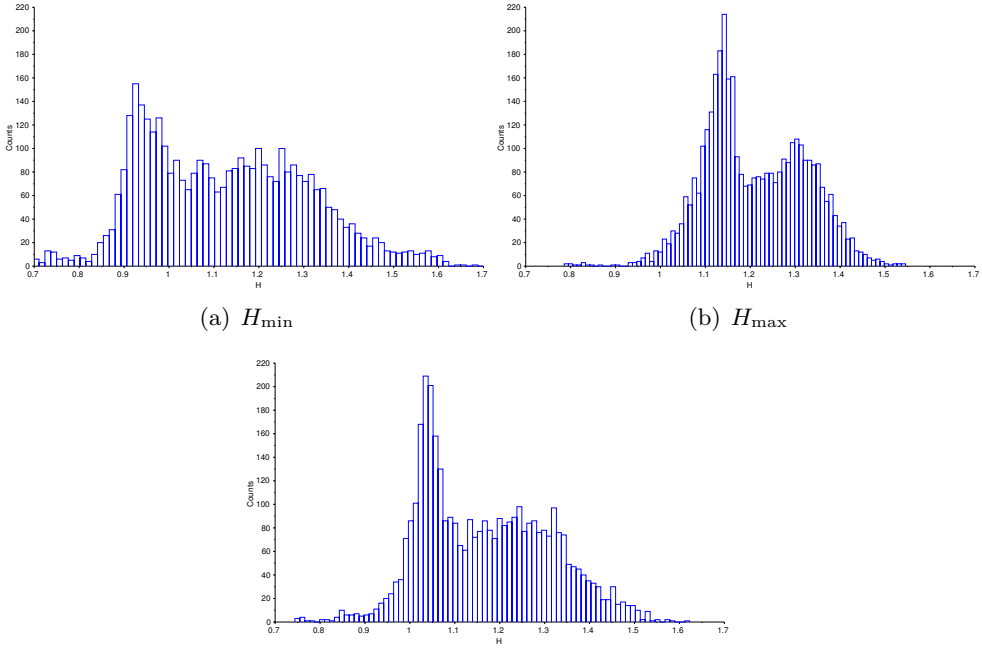

(a) $H_{\min}$ (b) $H_{\max}$

(c) $H^{\tilde{\nu}}$

Figure 6.12.: Histograms of the distribution of the exponents $H_{\min}$, $H_{\max}$ and $H^{\tilde{\nu}}$.

exponents belonging to the interval $[1, 1.1]$ (that is corresponding to the tiles belonging to the main peak of the histogram of $H^{\tilde{\nu}}$) and a third zone to the exponents larger than 1.1.

The threshold 1.1, which corresponds to the value separating the two peaks of the exponents' distributions for each method, seems to play an important role in the characterisation of Mars' topography. For both of the methods, the boundary separating the exponents with a value smaller and larger than 1.1 is the same.

The exponents with a value smaller than 1.1 correspond to a site containing the poles and, in the North, an area extending to the crustal dichotomy, its boundary and the zones (E) and (F). However, this site behaves differently for each method: the WLM tends to give exponents smaller than 1, while the LPM gives exponents larger than 1. Let us recall that, as already mentioned, the analysis of poles is more delicate, due to some artefacts such as the projection used to generate the maps. However, we can not explain this difference only by these artefacts, because this difference extends beyond the poles.

To understand this difference, let us now look at the distances $|H_{\min} - H_{\max}|$. Figure 6.14 gives the map representing the spatial distribution of these distances. This map shows that the majority of the tiles having an exponent

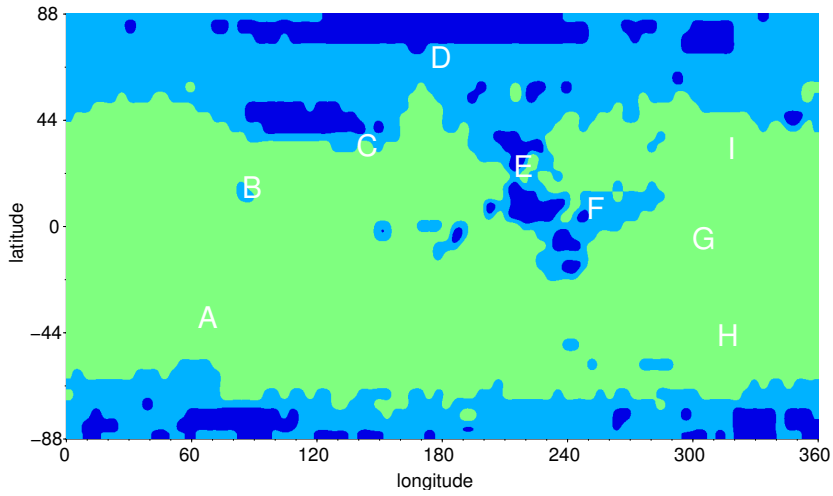

(a) LPM

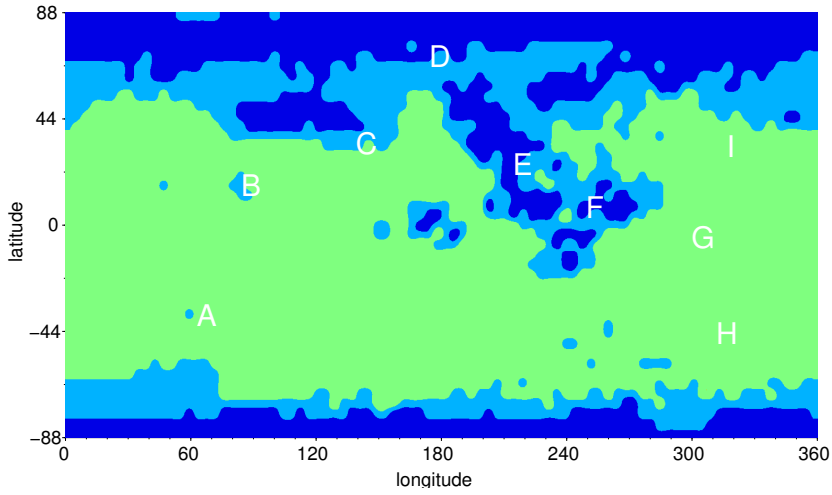

(b) WLM

Figure 6.13.: Map of Mars divided into three zones: a first zone corresponding to the exponents smaller than 1 (dark blue), a second zone to the exponents belonging to the interval $[1, 1.1]$ (light blue) and a third zone to the exponents larger than 1.1 (green).

smaller than 1.1 have a distance $|H_{\min} - H_{\max}| > 0.15$. These tiles seem to have (at least) two dominant exponents. In this case, neither $H^{\tilde{\nu}}$ nor the exponent H obtained with the WLM correspond to the Hölder exponent (from a theoretical point of view). As already mentioned in the previous sections, there thus exist (at least) two different phenomena, which do not necessarily

occurs in the same proportion. This can explain the difference between the WLM and the LPM on this site. The majority of the tiles having $H^{\tilde{\nu}} > 1.1$ seems to have only one dominant exponent, for which $H^{\tilde{\nu}}$ approximates this exponent.

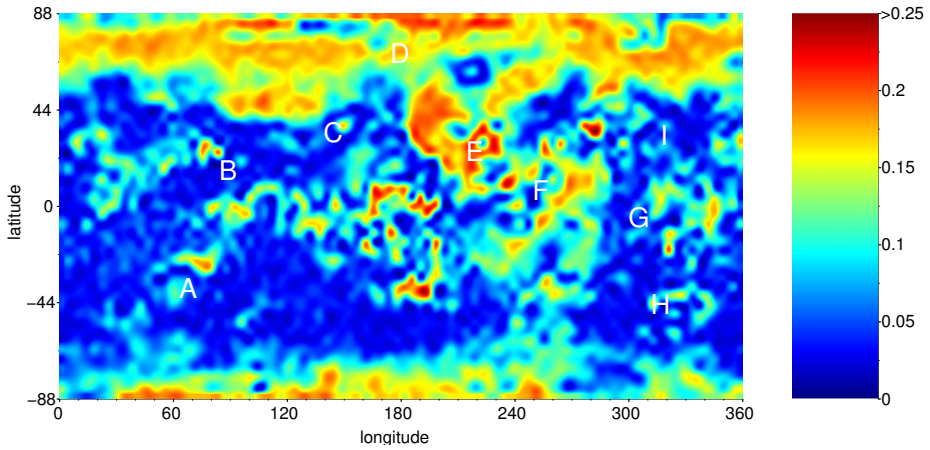

Figure 6.14.: Map representing the spatial distribution of the distances $|H_{\min} - H_{\max}|$.

To complete the study of the distance $|H_{\min} - H_{\max}|$, let us notice that 36% of the tiles have a distance smaller than 0.05, 55% have a distance smaller than 0.1 and 2% have a distance larger than 0.25.

To conclude the analysis with the LPM, it remains to check the existence of an increasing and a decreasing part of the spectra of the tiles. Figure 6.15 shows the map representing the spatial distribution of the smaller stabilisation detected for the functions $C \mapsto \tilde{\nu}_f^{+,C}(h)$ and $C \mapsto \tilde{\nu}_f^{-,C}(h)$.

We clearly see that the site corresponding to the exponents smaller than 1.1 tends to have a spectrum without increasing and decreasing part. Moreover, the other site (with the exponents larger than 1.1) contains some tiles having spectra without increasing and decreasing part, but it also has some tiles with a spectrum having an increasing or a decreasing part.

Let us recall that the WLM shows the existence of the tiles with a correlation coefficient c smaller than 0.97. When we look the map giving the spatial distribution of c (Figure 6.3), we see that when $c < 0.97$, the LPM indicates that the spectrum has an increasing or a decreasing part. This confirms that when c is small, the signal is indeed multifractal but if c is close to 1, the signal is not necessarily monofractal; this can be explained by the fact that the regression is performed on a small number of scales. Moreover, when the signal is multifractal, the slope of the linear regression of η_f does not necessarily correspond to the dominant Hölder exponent (from a theoretical point of view), while H^{ν} does, as soon as there exists only one dominant Hölder

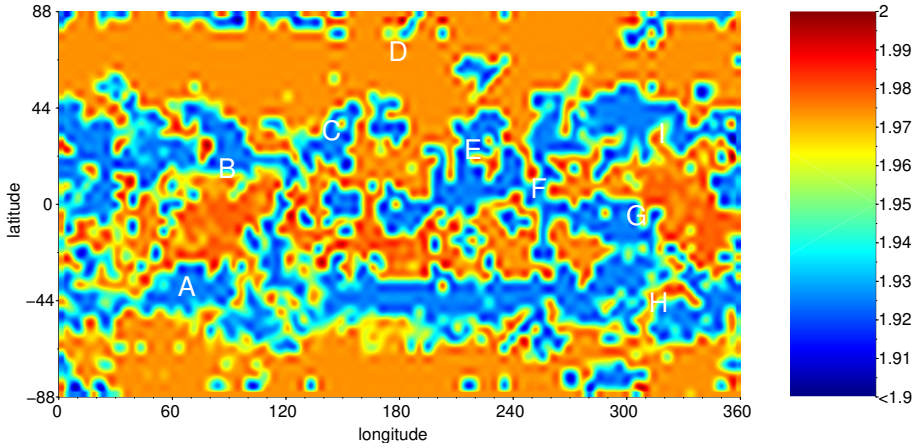

(a) $\tilde{\nu}^+$

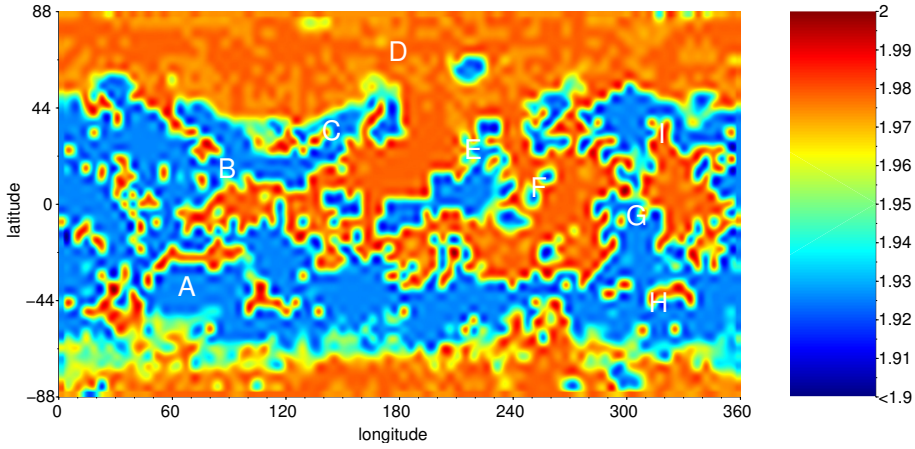

(b) $\tilde{\nu}^-$

Figure 6.15.: Map representing the spatial distribution of the smaller stabilisation detected for the functions $C \mapsto \tilde{\nu}_f^{+,C}(h)$ and $C \mapsto \tilde{\nu}_f^{-,C}(h)$.

exponent. Let us notice that this last hypothesis is not always verified in this zone (see Figure 6.14). All these reasons can explain the difference between the histograms of exponents obtained with the WLM and the LPM, when the exponent is larger than 1.1.

Finally, let us notice that 62% (resp. 58%) of the tiles have all the stabilisations of their functions $C \mapsto \tilde{\nu}_f^{+,C}(h)$ (resp. $C \mapsto \tilde{\nu}_f^{-,C}(h)$) larger than the threshold 1.95, and this percent rises to 72% (resp. 67%) if the threshold becomes 1.9. This result is very different compared to these obtained for the one-dimensional analysis done with the LPM, where we have more than 95% of the signals with a spectrum having some stabilisation smaller than 0.95. This

is not surprising, because the two-dimensional analysis is done on local signals (tiles of size 1024×1024 pixels), while the one-dimensional analysis is done on signals extending along the whole planet (latitudes and longitudes). It seems reasonable to think that these last signals have a multifractal behaviour, while local signals have spectra with a discrete support.

6.4 Conclusion

We use the MOLA data from the Mars Global Surveyor mission to study the surface roughness of Mars at small scales (< 15 km) with the WLM and the LPM. For each methods, we first focus on the one-dimensional latitudinal and longitudinal topographic profiles of the complete 128-pixels-per-degree map of the planet. In these scales, the two methods give similar results for the mean scaling exponent: with the WLM (resp. the LPM), $H \approx 1.05$ (resp. $H^{\tilde{\nu}} \approx 1.06$) for the latitude, and $H \approx 1.15$ (resp. $H^{\tilde{\nu}} \approx 1.18$) for the longitude. Moreover, a latitudinal trend also appears with each method, as well as indications of a slight anisotropy in the topographic field, though such statements have to be confirmed via several analyses. Regardless the values of the scaling exponents, we also show that our results are in agreement with previous seminal studies, thus confirming that the wavelet-based methods are well-suited to study the irregularity of celestial bodies. The comparison between the WLM and the LPM allow to highlight some sites and to make assumptions about the roughness of the planet: for example, the analysis suggest the existence of two processes with different weights for the longitudinal bands located between 190° and 220°. Moreover, the one-dimensional analysis does with the LPM gives a positive answer to the question of A. Arneodo, by confirming the multifractal behaviour of most of longitudinal and latitudinal bands on the planet Mars.

The results obtained in the 2D analysis allow to show the importance of analysing the data with two radically different methods: the WLM, which is based on a structure function, and the LPM which is not. The mean scaling exponent obtains with the WLM is $H \approx 1.12$, while the exponent provides by the LPM is $H^{\tilde{\nu}} \approx 1.16$. The analysis of the histograms of the exponents obtained with the two methods has highlighted several phenomena. First, the threshold 1.1 for the value of the exponents seems to be an invariant between the two methods: the tiles having an exponents with a value smaller than 1.1 correspond to the poles and in the North, it extends roughly to the crustal dichotomy. Secondly, the analysis suggests that the roughness of this last site contains several monofractal processes with different weights. Contrariwise, the roughness of the other site (with the exponents larger than 1.1) contains some mono- and multifractal processes having only one dominant exponent.

The 2D analysis also gives information of the scaling law at a “local” level, which allows us to show that the spatial distribution of the exponents recovers

some of the most characteristic features of the surface of Mars. To our knowledge, such a complete 2D analysis on the fractal nature of Mars' topography was made for the first time in [42], which has been partly transcribed in this chapter. The analysis with the LPM confirms these results.

Further investigations are needed to fully understand the Martian topography. Nevertheless, it appears that the WLM and the LPM are useful tools in the present framework and that the comparison between these two methods gives some additional information about the roughness of Mars' topography. The results provided in this chapter could be used as a solid basis for further investigation on the scaling properties of the surface roughness of Mars. The topography of other celestial bodies could be systematically studied in future works.

Finally, this chapter also shows that the LPM is a wavelet-based method able to characterise the regularity of real-life signals. It is not based on a structure function (unlike the WLM and the DFA for example), and hence allows to obtain results interesting to compare to the results of the others. Moreover, it is robust and allows to have some criteria to study the multifractality of the signal, not requiring a lot of additional parameters, unlike the WLM.

Index

Bibliography

[1] Abry, P., Flandrin, P., Taqqu, M. S., and Veitch, D. Self-similarity and long-range dependence through the wavelet lens, 2000.

[2] Abry, P., Wendt, H., Jaffard, S., Helgason, H., Goncalves, P., Pereira, E., Charib, C., Gaucherand, P., and Doret, M. Methodology for multifractal analysis of heart rate variability: From lf/hf ratio to wavelet leaders. In *Nonlinear Dynamic Analysis of Biomedical Signals EMBC conference (IEEE Engineering in Medicine and Biology Conferences)* (2010).

[3] Aharonson, O., Zuber, M., and Rothman, D. Statistics of mars' topography from the mars orbiter laser altimeter: Slopes, correlations, and physical models. *Journal of Geophysical Research 106*, E10 (2001), 23723–23735.

[4] Almeida, A. Wavelet bases in generalized besov spaces. *J. Math. Anal. Appl. 304* (2005), 198–211.

[5] Alvarez-Ramirez, J., Rodriguez, E., Cervantes, I., and Echeverria, J. Scaling properties of image textures: A detrending fluctuation analysis approach. *Physica A 361* (2006), 677–698.

[6] Ampère, A.-M. Recherche sur quelques points de la théorie des fonctions dérivées qui conduisent à une nouvelle démonstration du théorème de taylor, et à l'expression finie des termes qu'on néglige lorsqu'on arrête cette série à un terme quelconque. *Journal de l'Ecole Polytechnique* (1806), 148–181.

[7] Arneodo, A., Bacry, E., Manneville, S., and Muzy, J. F. Analysis of random cascades using space-scale correlation functions. *Phys. Rev. Lett. 80* (Jan 1998), 708–711.

[8] Arneodo, A., Bacry, E., and Muzy, J. F. Random cascades on wavelet dyadic trees. *Journal of Mathematical Physics 39* (1998), 4142–4164.

[9] Arneodo, A., Grasseau, G., and Holschneider, M. Wavelet transform of multifractals. *Phys. Rev. Lett. 61* (1988), 2281–2284.

[10] Arneodo, A., Vaillant, C., Audit, B., Argoul, F., d'Aubenton Carafa, Y., and Thermes, C. Multi-scale coding of genomic information: From dna sequence to genome structure and function. *Physics Reports 498*, 2 (2011), 45 – 188.

[11] Athreya, K., and Lahiri, S. *Measure Theory and Probability Theory.* Springer, 2006.

[12] Aubry, J.-M., Bastin, F., Dispa, S., and Jaffard, S. Topological properties of the sequence spaces S^ν. *J. Math. Anal. Appl. 1* (2006), 364–387.

[13] Aubry, J.-M., Bastin, F., Dispa, S., and Jaffard, S. Prevalence of multifractal functions in S^ν spaces. *J. Fourier Anal. Appl. 13* (2007), 175–185.

[14] Aubry, J.-M., and Jaffard, S. Random wavelet series. *Comm. Math. Phys. 227* (2002), 483–514.

[15] Audit, B., Thermes, C., Vaillant, C., d'Aubenton Carafa, Y., Muzy, J.-F., and Arneodo, A. Long-range correlations in genomic DNA: A signature of the nucleosomal structure. *Phys. Rev. Lett. 86* (2001), 2471.

[16] Ayache, A., Esser, C., and Kleyntssens, T. Different possible behaviors of wavelet leaders of the brownian motion. *Statistics and Probability Letters* (2019).

[17] Ayache, A., Shieh, N.-R., and Xiao, Y. Multiparameter multifractional brownian motion : local nondeterminism and joint continuity of the local times. *Annales de l'I.H.P. Probabilités et statistiques 47*, 4 (2011), 1029–1054.

[18] Ayache, A., and Taqqu, M. S. Multifractional processes with random exponent. *Publicacions Matemàtiques 49*, 2 (2005), 459–486.

[19] Bacry, E., Gloter, A., Hoffmann, M., and Muzy, J. F. Multifractal analysis in a mixed asymptotic framework. *Ann. Appl. Probab. 20*, 5 (10 2010), 1729–1760.

[20] Barndorff-Nielsen, O., and Shephard, N. *Continuous Time Approach to Financial Volatility.* Mathematics, Finance and Risk Series. Cambridge University Press, 2005.

[21] Barral, J., and Seuret, S. From multifractal measures to multifractal wavelet series. *J. Fourier Anal. Appl. 11*, 5 (2005), 589–614.

[22] Bastin, F., Esser, C., and Jaffard, S. Large deviation spectra based on wavelet leaders. *Revista Matemática Iberoamericana 32* (2016), 859–890.

[23] Bastin, F., Esser, C., and Simons, L. Topology on new sequence spaces defined with wavelet leaders. *Journal of Mathematical Analysis and Applications 431*, 1 (2015), 317 – 341.

[24] Benassi, A., Jaffard, S., and Roux, D. Elliptic gaussian random processes. *Revista Matemática Iberoamericana 13*, 1 (1997), 19–90.

[25] Besov, O. On a certain family of functional spaces. Embedding and extension theorems. *Dokl. Akad. Nauk. SSR 126* (1959), 1163–1165.

[26] Besov, O., Il'in, V., and Nikol'skij, S. Integral representations of functions and embedding theorems. *Moskva, Nauka* (1975).

[27] Besov, O., Kudryavtzev, L., Lizorkin, P., and Nikol'skij, S. Studies on the theory of spaces of differentiable functions of several variables. *Proc. Steklov Inst. Math. 182* (1990), 73–140.

[28] Bhattacharya, R., and Waymire, E. C. *Kolmogorov's Extension Theorem and Brownian Motion*. Springer International Publishing, 2016, pp. 167–178.

[29] Blumenthal, R., and Getoor, R. Sample functions of stochastic processes with stationary independent increments. *J. Math. Mech. 10* (1961), 493–516.

[30] Bogachev, V. *Measure Theory*. No. vol. 1 in Measure Theory. Springer Berlin Heidelberg, 2007.

[31] Boyarchenko, S., and Levendorski?, S. *Non-Gaussian Merton-Black-Scholes Theory*. Advanced series on statistical science & applied probability. World Scientific, 2002.

[32] Burke Hubbard, B. *Ondes et Ondelettes. La saga d'un outil mathématique*. Pour la Science, 1995.

[33] CARDO, R., and CORVALAN, A. Non-concave multifractal spectra with wavelet leaders projection of signals with and without chirps. *Fractals 17*, 3 (2009), 311–322.

[34] Clausel, M. *Quelques notions d'irrégularité uniforme et ponctuelle : le point de vue ondelettes*. PhD thesis, University of Paris XII, 2008.

[35] Clausel, M., and Nicolay, S. Wavelets techniques for pointwise anti-hölderian irregularity. *Constructive Approximation 33*, 1 (Feb 2011), 41–75.

[36] Comte, F., and Renault, E. Long memory in continuous-time stochastic volatility models. *Math. Finance 8* (1998), 291–323.

[37] Dahmen, W., Prössdorf, S., and Schneider, R. Wavelet approximation methods for pseudodifferential equations ii: Matrix compression and fast solution. *Advances in Computational Mathematics 1*, 3 (Oct 1993), 259–335.

[38] Daoudi, K., Lévy Véhel, J., and Meyer, Y. Construction of continuous functions with prescribed local regularity. *Constructive Approximation 14*, 3 (1998), 349–385.

[39] Daubechies, I. *Ten lectures on wavelets*. CBMS-NSF Regional Conference Series in Applied Mathematics, 1992.

[40] Deliège, A. *Application of wavelet transforms to geosciences: Extraction of functional and frequential information*. PhD thesis, University of Liege, 2017.

[41] Deliège, A., Kleyntssens, T., and Nicolay, S. Mars topography analyzed via the Wavelet Leaders Method. In *ITNG 2016 - New Trends in Wavelet and Numerical Analysis* (2016).

[42] Deliège, A., Kleyntssens, T., and Nicolay, S. Mars topography investigated through the wavelet leaders method: A multidimensional study of its fractal structure. *Planetary and Space Science 136* (2017), 46 – 58.

[43] Delour, J., Muzy, J., and Arnéodo, A. Intermittency of 1d velocity spatial profiles in turbulence: a magnitude cumulant analysis. *The European Physical Journal B 23*, 2 (Sep 2001), 243–248.

[44] Einstein, A. über die von der molekularkinetischen theorie der wärme geforderte bewegung von in ruhenden flüssigkeiten suspendierten teilchen. *Annalen der Physik 322*, 8 (1905), 549–560.

[45] Einstein, A., and Hopf, L. über einen satz der wahrscheinlichkeitsrechnung und seine anwendung in der strahlungstheorie. *Annalen der Physik 338*, 16 (1910), 1096–1104.

[46] Esser, C., Kleyntssens, T., and Nicolay, S. A multifractal formalism for non-concave and non-increasing spectra: The leaders profile method. *Applied and Computational Harmonic Analysis 43*, 2 (2017), 269 – 291.

[47] Falconer, K. *Fractal Geometry: Mathematical Foundations and Applications*. Wiley, 2004.

[48] Falconer, K. J. *The Geometry of Fractal Sets*. Cambridge Tracts in Mathematics. Cambridge University Press, 1985.

[49] Farkas, W., and Leopold, H.-G. Characterisations of function spaces of generalised smoothness. *Annalo Di Matematica Pura Ed Applicata 185* (2006), 1–62.

[50] Fleron, J. F. A note on the history of the cantor set and cantor function. *Mathematics Magazine 67*, 2 (1994), 136–140.

[51] Fraysse, A. Generic validity of the multifractal formalism. *SIAM Journal on Mathematical Analysis 39*, 2 (2007), 593–607.

[52] Frish, U. Turbulence. *Cambridge University Press* (1995).

[53] Grossmann, A., and Morlet, J. Decomposition of hardy functions into square integrable wavelets of constant shape. *SIAM Journal on Mathematical Analysis 15* (07 1984), 723–736.

[54] Gu, G.-F., and Zhou, W.-X. Detrended fluctuation analysis for fractals and multifractals in higher dimensions. *Physical Review E: Statistical, Nonlinear, and Soft Matter Physics 74*, 6 (2006), 061104.

[55] Haar, A. Zur Theorie der orthogonalen Funktionensysteme. *Mathematische Annalen 69*, 3 (1910), 331–371.

[56] Hardy, G. Weierstraß's non-differentiable function. *Trans. Amer. Math. Soc. 17* (1916), 301–325.

[57] Heurteaux, Y. Weierstraß functions in zygmund's class. *American Mathematical Society 133* (2005), 2711–2720.

[58] Hunt, B. R. The Hausdorff dimension of graphs of Weierstrass functions. *Proc. Amer. Math. Soc. 126*, 3 (1998), 791–800.

[59] Itô, K. On stochastic processes (infinitely divisible laws of probability). *Jpn. J. Math. 18* (1942), 884–901.

[60] Jaffard, S. Pointwise smoothness, two-microlocalization and wavelet coefficients. *Publicacions Matemàtiques 35*, 1 (1991), 155–168.

[61] Jaffard, S. Multifractal formalism for functions part I: Results valid for all functions. *SIAM J. Math. Anal. 28* (1997), 944–970.

[62] Jaffard, S. Oscillation spaces: Properties and applications to fractal and multifractal functions. *J. Math. Anal. 28* (1998), 4129–4141.

[63] Jaffard, S. Sur la dimension de boîte des graphes. *Comptes Rendus de l'Académie des Sciences - Series I - Mathematics 326*, 5 (1998), 555 – 560.

[64] Jaffard, S. The multifractal nature of Lévy processes. *Probab. Theory Relat. Fields 114* (1999), 207–227.

[65] Jaffard, S. On the Frisch–Parisi conjecture. *J. Math. Pures Appl. 79* (2000), 525–552.

[66] Jaffard, S. Beyond Besov spaces part 1: Distributions of wavelet coefficients. *J. Fourier Anal. Appl. 10* (2004), 221–246.

[67] Jaffard, S. Wavelet techniques in multifractal analysis, fractal geometry and applications: A jubilee of Benoit Mandelbrot. *Proceedings of Symposia in Pure Mathematics 72* (2004), 91–151.

[68] Jaffard, S. Beyond Besov spaces part 2: Oscillation spaces. *Constr. Approx. 21* (2005), 29–61.

[69] Jaffard, S., Lashermes, B., and Abry, P. *Wavelet Leaders in Multifractal Analysis*. Birkhäuser Basel, Basel, 2007, pp. 201–246.

[70] Jaffard, S., and Meyer, Y. Wavelet methods for pointwise regularity and local oscillations of functions. *Memoirs of the American Mathematical Society 587* (09 1996).

[71] Jaffard, S., and Nicolay, S. Pointwise smoothness of space-filling functions. *Appl. Comput. Harmon. Anal. 26* (2009), 181–199.

[72] Jeanblanc, M., and Simon, T. Elements de calcul stochastique. IRBID.

[73] Kahane, J. *Some Random Series of Functions*, 2nd ed. Cambridge Studies in Advanced Mathematics 5, Cambridge University Press, 1985.

[74] Kahane, J., Lemarié, P., and Lemarié-Rieusset, P. *Fourier series and wavelets*. No. vol. 3 in Studies in the development of modern mathematics. Gordon and Breach Publishers, 1995.

[75] Karatzas, I., and Shreve, S. *Brownian Motion and Stochastic Calculus*. Graduate Texts in Mathematics. Springer New York, 2012.

[76] Khintchine, A. über einen satz der wahrscheinlichkeitsrechnung. *Fund. Math. 6* (1924), 9–20.

[77] Klenke, A. *Probability Theory: A Comprehensive Course*. Springer London, 2007.

[78] Kleyntssens, T., Esser, C., and Nicolay, S. An algorithm for computing non-concave multifractal spectra using the S^ν spaces. *Communications in Nonlinear Science and Numerical Simulation 56*, Supplement C (2018), 526 – 543.

[79] Kleyntssens, T., and Nicolay, S. A refinement of the S^ν-based multifractal formalism: Toward the detection of the law of the iterated logarithm. *Submitted*.

[80] Krantz, S. Lipschitz spaces, smoothness of functions, and approximation theory. *Expositiones Mathematicae 3* (1983), 193–260.

[81] Kreit, D. *On generalized Hölder-Zygmund spaces*. University of Liege, 2016.

[82] Kreit, D., and Nicolay, S. Some characterizations of generalized Hölder spaces. *Math. Nachr. 285* (2012), 2157–2172.

[83] Kreit, D., and Nicolay, S. Characterizations of the elements of generalized hölder–zygmund spaces by means of their representation. *J. Approx. Theory 172* (2013), 23–36.

[84] Kreit, D., and Nicolay, S. Generalized pointwise hölder spaces defined via admissible sequences. *Journal of Function Spaces* (2018).

[85] Kreslavsky, M., and Head, J. Kilometer-scale roughness of mars: Results from mola data analysis. *Journal of Geophysical Research 105*, E11 (2000), 26695–26711.

[86] Kuratowski, K. *Topology*. Topology. Academic Press, 1968.

[87] Landais, F., Schmidt, F., and Lovejoy, S. Universal multifractal martian topography. *Nonlinear Processes in Geophysics Discussions 2* (2015), 1007–1031.

[88] Lashermes, B., Roux, S., Abry, P., and Jaffard, S. Comprehensive multifractal analysis of turbulent velocity using wavelet leaders. *Eur. Phys. J. B. 61 (2)* (2008), 201–215.

[89] Lemarié, P. G., and Meyer, Y. Ondelettes et bases hilbertiennes. *Revista Matemática Iberoamericana 2*, 1-2 (1986), 1–18.

[90] Leonarduzzi, R., Abry, P., Wendt, H., Jaffard, S., and Touchette, H. A generalized multifractal formalism for the estimation of nonconcave multifractal spectra. In *IEEE transactions on signal processing* (november 2018).

[91] Leonarduzzi, R., Touchette, H., Wendt, H., Abry, P., and Jaffard, S. Generalized legendre transform multifractal formalism for nonconcave spectrum estimation. In *2016 IEEE Statistical Signal Processing Workshop (SSP)* (June 2016), pp. 1–5.

[92] Lévy, P. *Théorie de l'addition des variables aléatoires.* Monographies des probabilités. Gauthier-Villars, 1954.

[93] Lévy, P. *Processus stochastiques et mouvement brownien.* Paris, 1965.

[94] Liggett, T. *Continuous Time Markov Processes: An Introduction.* Graduate studies in mathematics. American Mathematical Soc., 2010.

[95] Malamud, B., and Turcotte, D. Wavelet analyses of mars polar topography. *Journal of Geophysical Research 106*, E8 (2001), 17497–17504.

[96] Mallat, G. A theory for multiresolution signal decomposition : the wavelet representation. *IEEE Transaction on Pattern Analysis and Machine Intelligence* (1989).

[97] Mallat, S. Multiresolution approximations and wavelet orthonormal bases of l 2 (r). *Transactions of the American Mathematical Society 315* (09 1989), 69–87.

[98] Mallat, S. *A Wavelet Tour of Signal Processing, Third Edition: The Sparse Way*, 3rd ed. Academic Press, 2008.

[99] Maman, D., and Stéphane, S. Fixed points for the multifractal spectrum map. *Constructive Approximation 43*, 3 (Jun 2016), 337–356.

[100] Mandelbrot, B. Intermittent turbulence in self-similar cascades: divergence of high moments and dimension of the carrier. *J. Fluid Mech. 62* (1974), 351–358.

[101] Mandelbrot, B., and van Ness, J. Fractional Brownian motions, fractional noises and applications. *SIAM Review 10* (1968), 422–437.

[102] Mantegna, R. N. Fast, accurate algorithm for numerical simulation of Lévy stable stochastic processes. *Phys. Rev. E 49* (1994), 4677–4683.

[103] Meneveau, C., and Sreenivasan, K. R. Simple multifractal cascade model for fully developed turbulence. *Phys. Rev. Lett. 59* (Sep 1987), 1424–1427.

[104] Meyer, Y. *Wavelets, Vibrations and Scalings.* CRM monograph series. American mathematical society, 1998.

[105] Meyer, Y., and Salinger, D. *Wavelets and operators*, vol. 1. Cambridge university press, 1995.

[106] Mörters, P., and Peres, Y. *Brownian Motion*. Cambridge Series in Statistical and Probabilistic Mathematics. Cambridge University Press, 2010.

[107] Moura, S. D. On some characterizations of besov spaces of generalized smoothness. *Mathematische Nachrichten 280*, 9-10 (2007), 1190–1199.

[108] Muzy, J. F., Bacry, E., and Arneodo, A. Wavelets and multifractal formalism for singular signals: Application to turbulence data. *Phys. Rev. Lett. 67* (Dec 1991), 3515–3518.

[109] Muzy, J.-F., Bacry, E., and Arneodo, A. Multifractal formalism for fractal signals: The structure function approach versus the wavelet-transform mudulus-maxima method. *Phys. Rev. E 47* (1993), 875–884.

[110] Nicolay, S. *Analyse de Séquences ADN par la Transformée en ondelettes : extraction d'informations structurelles, dynamiques et fonctionnelles*. PhD thesis, University of Liege, 2006.

[111] Nicolay, S., Touchon, M., Audit, B., d'Aubenton Carafa, Y., Thermes, C., Arneodo, A., et al. Bifractality of human DNA strand-asymmetry profiles results from transcription. *Phys. Rev. E 75* (2007).

[112] Nikora, V., and Goring, D. Mars topography: bulk statistics and spectral scaling. *Chaos, Solitons and Fractals 19* (2004), 427–439.

[113] Nikora, V., and Goring, D. Martian topography: Scaling, craters, and high-order statistics. *Mathematical Geology 37*, 4 (2005), 337–355.

[114] Orosei, R., Bianchi, R., Coradini, A., Espinasse, S., Federico, C., Ferriccioni, A., and Gavrishin, A. Self-affine behavior of martian topography at kilometer scale from mars orbiter laser altimeter data. *Journal of Geophysical Research 108*, E4 (2003), 8023.

[115] Parisi, G., and Frisch, U. On the singularity structure of fully developed turbulence. *Turbulence and predictability in geophysical fluid dynamics* (1985), 84–87.

[116] Peltier, R.-F., and Lévy Véhel, J. Multifractional Brownian Motion : Definition and Preliminary Results. Research Report RR-2645, INRIA, 1995. Projet FRACTALES.

[117] Poincareé, H. *Science et Méthode*. Flammarion, 1908.

[118] Pommerol, A., Chakraborty, S., and Thomas, N. Comparative study of the surface roughness of the moon, mars and mercury. *Planetary and Space Science 73* (2012), 287–293.

[119] Raible, S. *Lévy Processes in Finance: Theory, Numerics, and Empirical Facts*. PhD thesis, University of Freiburg, 2000.

[120] Rudin, W. *Real and complex analysis*. Mathematics series. McGraw-Hill, 1987.

[121] Schoutens, W. *Levy Processes in Finance: Pricing Financial Derivatives*. Wiley Series in Probability and Statistics. Wiley, 2003.

[122] Seuret, S. Multifractal analysis and wavelets. In *Lecture notes from the CIMPA school* (2013), New trends in harmonic analysis.

[123] Shepard, M., Campbell, B., Bulmer, M., Farr, T., Gaddis, L., and Plaut, J. The roughness of natural terrain: A planetary and remote sensing perspective. *Journal of Geophysical Research 106*, E12 (2001), 32777–32795.

[124] Smith, D., Neumann, G., Arvidson, R. E., Guinness, E. A., and Slavney, S. Mars global surveyor laser altimeter mission experiment gridded data record, mgs-m-mola-5-megdr-l3-v1.0. Tech. rep., NASA Planetary Data System, 2003.

[125] Smith, D., Zuber, M., Frey, H., Garvin, J., Head, J., et al. Mars orbiter laser altimeter: Experiment summary after the first year of global mapping of mars. *Journal of Geophysical Research 106*, E10 (2001), 23689–23722.

[126] Tankov, P., and Cont, R. *Financial Modelling with Jump Processes, Second Edition*. Chapman and Hall/CRC Financial Mathematics Series. Taylor & Francis, 2015.

[127] Testud, B. *Étude d'une classe de mesures autosimilaires : calculs de dimensions et analyse multifractale*. PhD thesis, Université Blaise Pascal, 2004.

[128] Triebel, H. Interpolation theory function spaces differential operators. *North-Holland Publishing company* (1978).

[129] Triebel, H. Theory of function spaces. *Birkhäuser Verlag* (1983).

[130] Triebel, H. Theory of function spaces ii. *Birkhäuser Verlag* (1992).

[131] Triebel, H. A note on wavelet bases in function spaces. *Proc. Orlicz Centenary Conference "Function Spaces 7"* (2003).

[132] Triebel, H. Theory of function spaces iii. *Birkhäuser Verlag* (2006).

[133] Triebel, H. Bases in function spaces, sampling, discrepancy, numerical integration. *European Mathematical Society* (2010).

[134] Weierstrass, K. *Über Continuirliche Functionen Eines Reellen Arguments, die für Keinen Werth des Letzteren Einen Bestimmten Differentialquotienten Besitzen.* Springer Vienna, 1988, pp. 190–193.

[135] Wendt, H., Abry, P., Jaffard, S., Ji, H., and Shen, Z. Wavelet leader multifractal analysis for texture classification. In *Proc IEEE conf. ICIP* (2009).

[136] Wendt, H., Roux, S. G., Jaffard, S., and Abry, P. Wavelet leaders and bootstrap for multifractal analysis of images. *Signal Processing 89*, 6 (2009), 1100 – 1114.

[137] Wiener, N. Differential-space. *Journal of Mathematics and Physics 2*, 1-4 (1923), 131–174.

[138] Wood, A., and Chan, G. Simulation of stationary Gaussian processes in $[0,1]^d$. *J. Comput. Graph. Statist. 3* (1994), 409–432.

[139] Zygmund, A. Smooth functions. *Duke Math. J. 12* (1945), 47–76.